UNIVERSITY OF SOUTHAMPTON

FACULTY OF NATURAL & ENVIRONMENTAL SCIENCES

SCHOOL OF OCEAN AND EARTH SCIENCES

THE ROLE OF BIOMINERALS IN ENHANCING THE FLUX OF ORGANIC CARBON INTO THE DEEP OCEAN

by

Frédéric André Corentin Le Moigne

Thesis for the degree of Doctor of Philosophy

February 2009 - May 2012

UNIVERSITY OF SOUTHAMPTON

Abstract

FACULTY OF NATURAL & ENVIRONMENTAL SCIENCES

SCHOOL OF OCEAN AND EARTH SCIENCES

Doctor of Philosophy

THE ROLE OF BIOMINERALS IN ENHANCING THE FLUX OF ORGANIC CARBON INTO THE DEEP OCEAN

by Frédéric André Corentin Le Moigne

The biological carbon pump (BCP) is the mechanism by which atmospheric CO_2 is stored over long time scales in the ocean and over geological time scales in the seabed. It has been suggested that there may be some causal effect between biomineral (opal and calcite) and organic carbon (POC) fluxes. Biominerals may increase the density of organic aggregates while they may also provide chemical or physical protection from remineralisation. However, the scarcity of coupled POC and biominerals export data from the upper ocean prevents a thorough understanding of the so called 'ballast effect'. Further uncertainties exist in the way in which biominerals affect particles aggregation and degradation in the upper ocean. This project addresses these two issues using $^{234}Th/^{238}U$ disequilibria from a range of settings and lab experiments in which aggregation -degradation and remineralization processes acting on sinking aggregates are simulated using roller tables

It is shown using data from the Porcupine Abyssal Plain that export is appropriately estimated using the C/Th ratio of the total particulate pool, which at this site approximated that of the >53 μm POC pool. Also, are reported results from one of the first attempt to measure POC, PIC and BSi downward fluxes from the surface ocean using ^{234}Th-^{238}U, ^{210}Po-^{210}Pb disequilibria and drifting sediments trap synchronously at the Porcupine Abyssal Plain time-series site during summer 2009. The differences between techniques are ascribed to their biogeochemical behaviour more than integration time. Further, a compilation of ^{234}Th derived surface POC, BSi, PIC and lithogenic material export fluxes is presented. The proportion of non-mineral associated sinking POC was highly variable and ranged from 0 to 73% of the total POC flux. It is possible that persistent pool of non-mineral associated sinking POC may feature at depth conversely to what was previously ascertained. It is proposed that the occurrence of an important proportion of non-ballast associated sinking POC in high latitude diatom dominated areas could explain the low transfer efficiencies observed in those environments. Finally, phytoplankton incubation in cylindrical rolling tanks in the presence and absence of added calcite minerals and microzooplankton to observe the resulting effects on losses of OM, and regeneration of nutrients was performed. Generally the presence of zooplankton and/or added calcite had little effect in losses of POM. It is concluded that the factors influencing the proportion of POC incorporated into aggregates seems to be the most important determinant of export.

Table of contents

Table of Figures

Table of Tables

Abbreviations

AOU: Apparent oxygen utilization

BSi: Biogenic silica

CC: Carrying coefficient

Chl-a: Chlorophyll-a

CTD: Conductivity, Temperature, Depth; sensors pack used on the rosette

dpm: Disintegration per minute (=1/60Th Becquerel); units in which ^{234}Th activity is expressed

DOC: Dissolved organic carbon

DOM: Dissolved organic matter

DON: Dissolved organic carbon

DOP: Dissolved organic phosphorus

GEOTRACES An International Study of Marine Biogeochemical Cycles of Trace Elements and their Isotopes

ICP-MS: Inductively-coupled plasma mass spectrometer

ICP-OES: Inductively-coupled plasma optical emission spectrometer

MilliQ: Deionised and UV sterilized water with a conductivity of 18.2 MΩcm^{-1}

MLD: Mixed layer depth

MLRA: Multiple linear regression analysis

PCS: Phytoplankton community structure

PIC: Particulate inorganic carbon

POC: Particulate organic carbon

PP: Primary productivity

PON: Particulate organic nitrogen

RSD: Residual standard deviation

SAPS: Standing alone pump system

SS: steady state

SD or σ: Standard deviation

TDN: Total dissolved nitrogen

TPP: Total particulate phosphorus

TEP: Transparent exopolymer particles

US-JGOFS United States- Joint Global Ocean Fluxes Studies

^{234}Th: Thorium-234

^{230}Th: Thorium-230

^{229}Th: Thorium-229

^{238}U: Uranium-238

^{210}Po: Polonium-210

^{210}Pb: Lead-210

Declaration of Authorship

I, Frédéric André Corentin Le Moigne declare that the thesis entitled

The Role of Biominerals in Enhancing the Flux of Organic Carbon into the Deep Ocean.

and the work presented in it are my own. I confirm that:

- this work was done wholly or mainly in candidature for a research degree at this University;
- where any part of this thesis has been previously been submitted for a degree or any other qualification at this University or any other institution, this has been clearly stated;
- where I have consulted the published work of others, this is always clearly attributed;
- where I have quoted from the work of others, the source is always given. With the exception of such quotations, this thesis is entirely my own work;
- I have acknowledged all main sources of help;
- Where the thesis is based on work done by myself and others, I have made clear exactly what was done by others and what I have contributed myself;

Signed:……..

Date:…….

Acknowledgments

First, I would like to thank my supervisor, ***Richard Sanders.*** *During those three years,* ***Richard*** *has provided advices, an indefectible support, and as much freedom to pursue my own ideas than any student could wish for.*

Maria Villa *provided an incredible guidance for the accomplishment of this work. I'm thankful to her for all the advice, motivation, inspiration, help she gave me, for all the many things she has taught me over those past three years and overall for her immense kindness.*

At the start of my PhD ***Paul Morris*** *played an invaluable role in first welcoming me in what was for me a new institution but also in a new country; and secondly teaching me all the specificities of the thorium technique.* ***Paul*** *put me on good tracks for the completion of my PhD.*

Thanks to ***Christina de La Rocha*** *for guiding me in a challenging experiment undertaken during this PhD.* ***Christina*** *has provided me with a lot ideas and insightful comments in a scientific field I was not familiar with.*

Also, I would like to thank the reviewers who accepted to examine this part work and gave insightful comments that improved this thesis.

I am very grateful to people I have been working closely with on different subjects and tasks during my PhD: ***Emmanuel Laurenceau, Chris Marsay, Patrick Martin,, Stephanie Henson,, Katsia Paborstava, Morgane Gallinari, Peter Statham, Richard Lampitt,, Adrian Martin,*** *and* ***Hélène Planquette.***

Thanks to, ***Richard Sanders****,* ***Eric Achterberg*** *and* ***Mark Moore*** *for their great leaderships on cruises D341, D350 and D354. I am thankful to the captains and NMF crews of the R.R.S Discovery for their assistance during those cruises.*

Also, and in no particular order, I would like to thank people that help me in different manner by providing help and/or advices of all sorts: ***Mehdi Boutrif, Christian Tamburini , Kostas Kiriakoulakis, Eithne Tynan, Dougal Montyfiled, Kev Saw, Sam Ward , Joe Stewart, Anya Cricker, Helen Griffin, Thanos Gritzalis Papadopoulos, Stuart Painter, Ian Salter, Alex Poulton, Mark Stinchcombe,, Mike Lucas, Ana Borerro Santiago, Elise Van meersche, Sebastian Steinberger, Bob Head, Darryl Green, Laure Resplandy, Oceanopolis Brest, Sari Geiring, Jessica Klar,, Ross Holland,, Victoire Rerrolle, Cynthia Dumousseaud, Sandy Thomalla, Annick Masson, Rudolph Corvaisier, Andy Milton, Emilie Grosstefan,, Péré Masqué, Elisabet Verdeny Philippe Pondaven, Herwig Stibor, Céline Liourzou, Claire Labry, Zia. Chowdhury, Ranji Goddart, Jennifer Riley, Debbie Yarow, The NMF "stores" team, Universidad de Sevilla team and the CalMarO team***

,

To all my friends from home and Southampton," mention speciale" to ***Belmont Road, Bath Street*** *and* ***Kent Road crews***

And finally to my family

GRADUATE SCHOOL OF THE NATIONAL OCEANOGRAPHY CENTRE, SOUTHAMPTON

This PhD thesis by

Frédéric André Corentin Le Moigne

has been produced under supervision of the following persons

Supervisors:

Dr. Richard Sanders

Prof. Richard Lampitt

Chair of the Advisory Panel:

Prof Peter Statham

« Dans la vie, rien n'est à craindre, tout est à comprendre »

Marie Sklodowska-Curie (1867-1934)

1. General Introduction

1.1 The Ocean in the Global Carbon Cycle

The exchange of carbon between environmental reservoirs known as the global carbon cycle is driven by a range of geophysical, chemical and biological processes. The geological part of the carbon cycle operates over large time-scales (millions of years) whilst the biological - chemical - physical components of the global carbon cycle function over shorter time scales (hours to thousands of years). The global carbon cycle is commonly represented as four major carbon reservoirs interconnected by exchange pathways (Figure 1.1). These reservoirs are: the continental biosphere (terrestrial ecosystems, lakes, rivers and non-living organic material such as soil carbon), the sediment (which includes fossil fuels), the atmosphere and the ocean (which includes different carbon pools presented in section below). In the remainder of this introduction, emphasis will put on the latter.

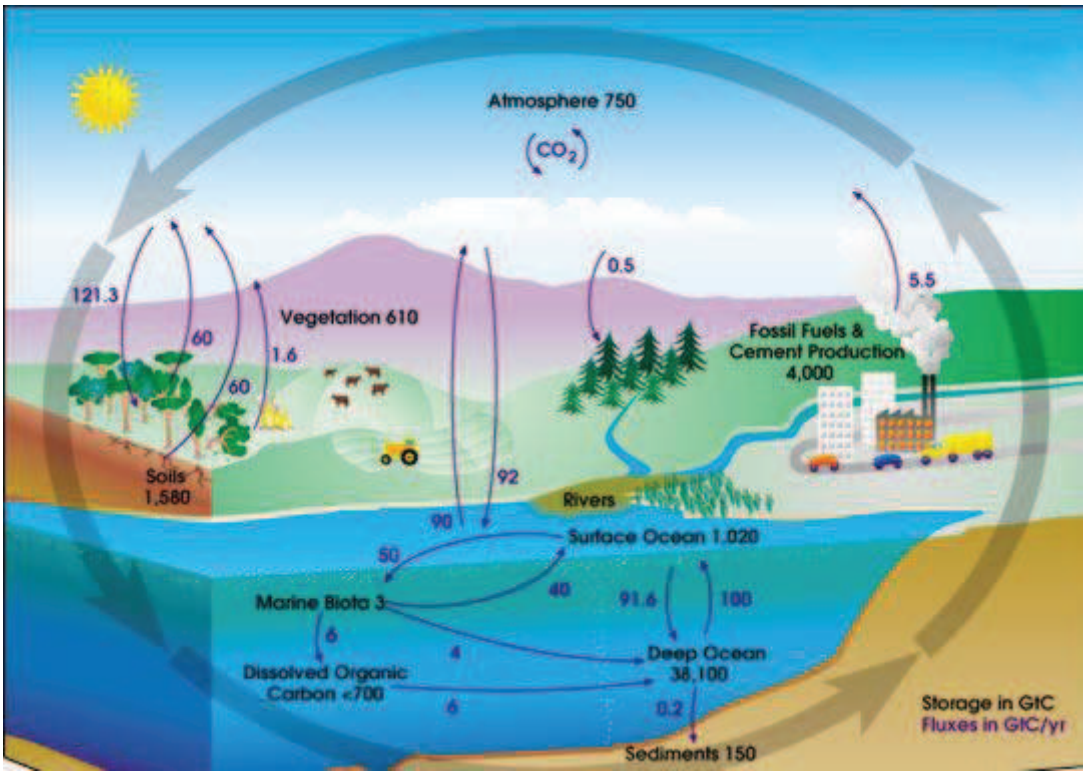

Figure 1.1: Global carbon cycle. Source: http://www.global-greenhouse-warming.com/global-carbon-cycle.html

Carbon dioxide (CO_2) gas is the primary form of carbon in the atmosphere. Despite being a very small part of the atmosphere overall (approximately 0.04%; http://www.esrl.noaa.gov/gmd/ccgg/trends/), it plays an important role in supporting life on planet Earth by regulating global temperature due to its role in absorbing radiation emitted by the planet. Since the industrial revolution, the atmospheric concentration of CO_2 has increased from 280 ppm to 380 ppm as a result of anthropogenic inputs of CO_2 to the atmosphere driven by changes in cement production, patterns of land usage and fossil fuel combustion (Keeling and Whorf, 1997). This has been accompanied (and likely caused) by a rise in average global surface temperature (Brown and Heim, 1998). Currently, the atmospheric concentration of CO_2 is of 395ppm (June 2012; co2now.org).

In the ocean, carbon is present in various chemical forms. These forms can be classified into four different compartments: dissolved inorganic carbon (DIC), dissolved organic carbon (DOC), particulate inorganic carbon (PIC) and particulate organic carbon (POC). DIC is the most abundant form of carbon in the ocean, in several forms including HCO_3^- and CO_3^{2-} which occur as a result of CO_2 dissociation in the water (see below). DOC is a broad classification for organic molecules of varied origin and composition within marine systems. PIC includes calcium carbonate in various polymorphs including calcite and aragonite. Finally POC is formed by biological processes in the upper layers in the ocean (Figure 1.2, (Sabine and Feely, 2007)).

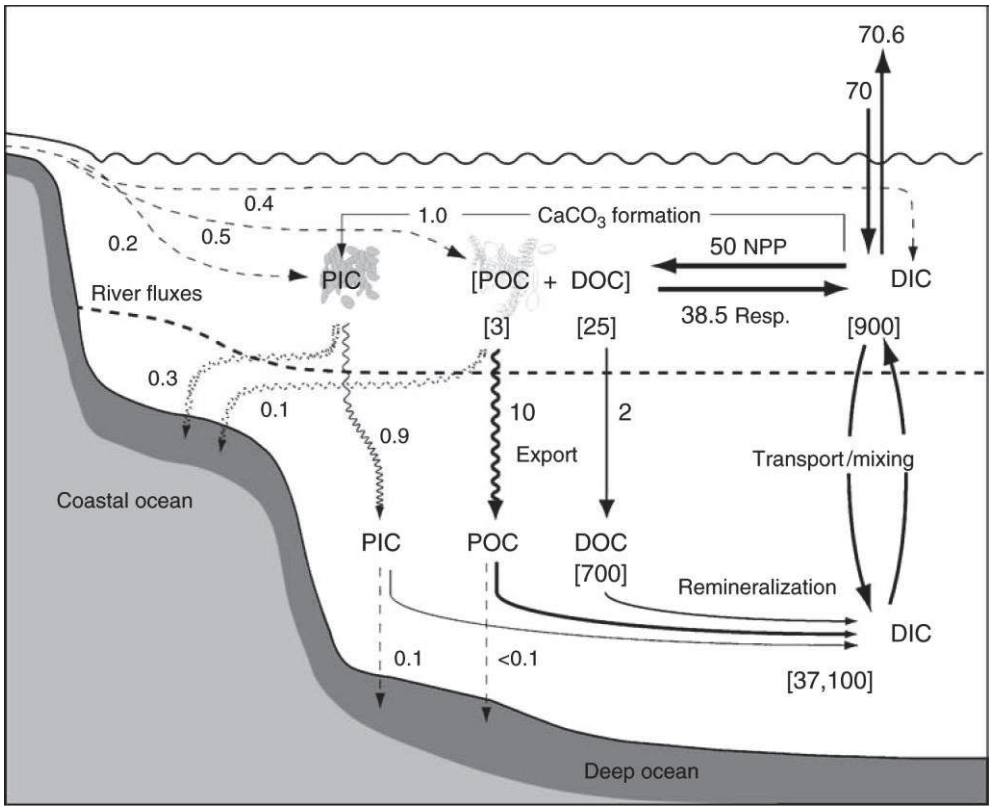

Figure 1.2: Schematic representation of the marine carbon cycle. Fluxes (arrows) are in Pg C/year and reservoir sizes (numbers in square brackets) are in Pg C. (Modified from (Sabine and Feely, 2007))

The atmospheric carbon reservoir is connected to the surface ocean via a simple equilibration of the CO_2 concentrations, a process known as the solubility pump (e.g. Figure 1.3). When atmospheric CO_2 diffuses across the ocean atmosphere interface, dissolution reactions ($CO_2(g) \leftrightarrow CO_2(aq) + H_2O \leftrightarrow HCO_3^- + CO_3^{2-} \leftrightarrow H_2CO_3^-$) redistribute dissolved CO_2 (DIC) into the various inorganic compartments of surface waters. Once in the sunlit layer, this DIC becomes available for autotrophic photosynthetic organisms to assimilate into organic material, via photosynthesis. At high latitudes where seawater is cooler and CO_2 is more soluble, the uptake of atmospheric CO_2 is enhanced, this is known as the physical carbon pump. However, at low latitudes, warm temperatures can cause the ocean surface to release carbon dioxide. This dissolved CO_2 can then be used in the biological process of photosynthesis.

Photosynthesis is the chemical reaction which transforms, under good light conditions, CO_2 and H_2O into organic molecules (a sugar) according to the simplified equation ($6CO_2 + 6H_2O + \text{light energy} \rightarrow C_6H_{12}O_6 + 6O_2$). As soon as these sugars are synthesised and with a good supply of macronutrients (nitrogen, phosphorus and silicon) and micronutrients (metals), the phytoplankton lives and grows. A lack of any of these macro or micronutrient results in a cessation of phytoplankton growth (Liebig, 1847).

Once fixed by photoautotrophic organisms, the organic carbon can follow various pathways with their relative importance depending on geographical variations in biological and chemical features of the ocean. Most organic carbon (DOC and POC, Figure 1.2) is transferred back to DIC by respiration processes that occur throughout the whole water column. The DIC formed by dissolution and respiration processes in the ocean interior is returned to the upper layers (where the

photosynthesis takes place) by physical transport mechanisms. Only a small fraction of the carbon fixed by plankton settles out of the photic zone as sinking organic particles (POC) with a minor fraction being further buried in deep sea sediments over geological time scales. The “biological side” of atmospheric carbon uptake driven by export from the uppers layer to the deep ocean is known as the biological carbon pump.

A further important process is the biological precipitation of calcium carbonate by algae such as coccolithophores. The calcification process consumes alkalinity, while the dissolution of this calcium carbonate produces alkalinity and thus modifies the DIC system ($Ca^{2+} + 2HCO_3^- \leftrightarrow CaCO_3 + CO_{2(g)} + H_2O$). This process is know as the carbonate counter pump (see Figure 1.3)(Heinze *et al.*, 1991). The relative magnitudes of both organic and carbonate counter pump can be represented by the so-called rain ratio (the ratio of particulate inorganic to organic carbon in the exported biogenic matter. This rain ratio measured as POC/PIC ratio in sediment traps ranges from 0.7 to 0.8 (Klaas and Archer, 2002)The remainder of this thesis will focus on the biological organic carbon pump.

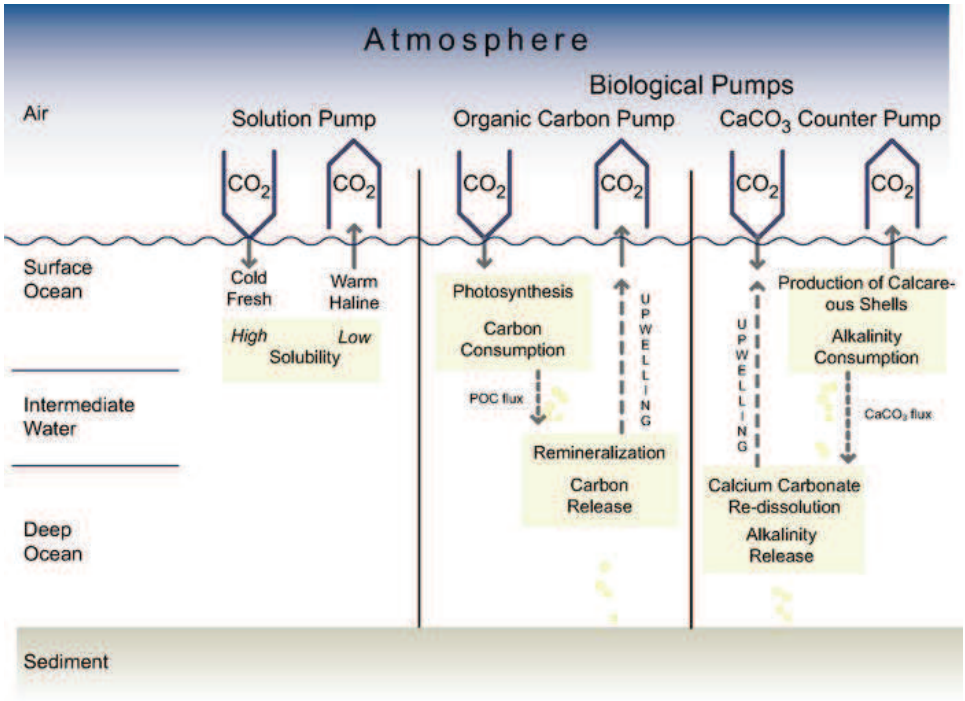

Figure 1.3: The three main ocean carbon pumps (the solubility pump, the organic carbon pump and the carbonate counter pump) acting as sources and sinks of atmospheric CO_2 in the ocean (Heinze *et al.*, 1991): Figure taken from http://www.ipcc.ch

1.2 The Biological Carbon Pump

The concept of the biological carbon pump from the late 70's (Eppley and Peterson, 1979) quantifies the importance of oceanic primary production in the global carbon cycle. The biological carbon pump can be divided into three steps: the production of organic matter (and biominerals) in surface waters, the sinking of these particles into the deep ocean, and the decomposition of the settling (or settled) particles in the water column or the seabed. As described in the section above, phytoplankton, *via* photosynthesis, transform DIC and nutrients into particulate organic matter (POC) and biominerals compounds (calcite or biogenic opal synthetised by diatoms). Most of this

organic matter enters the upper ocean food web composed of zooplankton, bacteria and higher trophic levels and is degraded /remineralised by their respiration, excretion or dissolution processes.

In this way the coupling of production and export processes allows the ocean to store CO_2 away from the atmosphere and contributes to the buffering of the global climate system. Without the oceanic biological carbon pump, atmospheric CO_2 concentrations would be almost twice their current levels (Sarmiento and Toggweiler, 1984). Recent studies have highlighted the challenge of quantifying the magnitude of the biological carbon pump. The most widely used quantification of global carbon export is derived from a linear relationship between observed *f*-ratio (defined below)and sea surface temperature (SST) (Laws *et al.*, 2000).

Total primary productivity (PP) includes production fuelled by both 'new' and 'regenerated' nitrogen (Dugdale and Goering, 1967). New production (NP) is assumed to be principally fuelled by nitrate supplied from depth by vertical mixing, whilst regenerated production (RP) is supported by the uptake of nitrogen derived from the recycling of organic matter in the euphotic zone. Over sufficiently large time and space scales, export production is equivalent to new production (Eppley and Peterson, 1979), so that the fraction of PP that is exported can be expressed as NP/(NP+RP), known as the *f*-ratio (Dugdale and Goering, 1967).

Applying this to satellite-derived (PP) and sea surface temperature (SST) fields yields an estimate of global carbon export of ~ 12 GtC yr^{-1}. This is comparable to the 10 GtC yr^{-1} obtained from a food-web model (Schlitzer, 2004), but substantially lower than a global application of the earliest export algorithm (21 GtC yr^{-1}) (Eppley and Peterson, 1979). Using a large database of thorium-derived export measurements (see section below for introduction to thorium-derived export measurements) compiled and

extrapolated to the global scale by correlation with satellite sea surface temperature fields (Henson et al, 2011) estimate global integrated carbon export to be ~ 5 GtC yr^{-1}, lower than most current estimates.

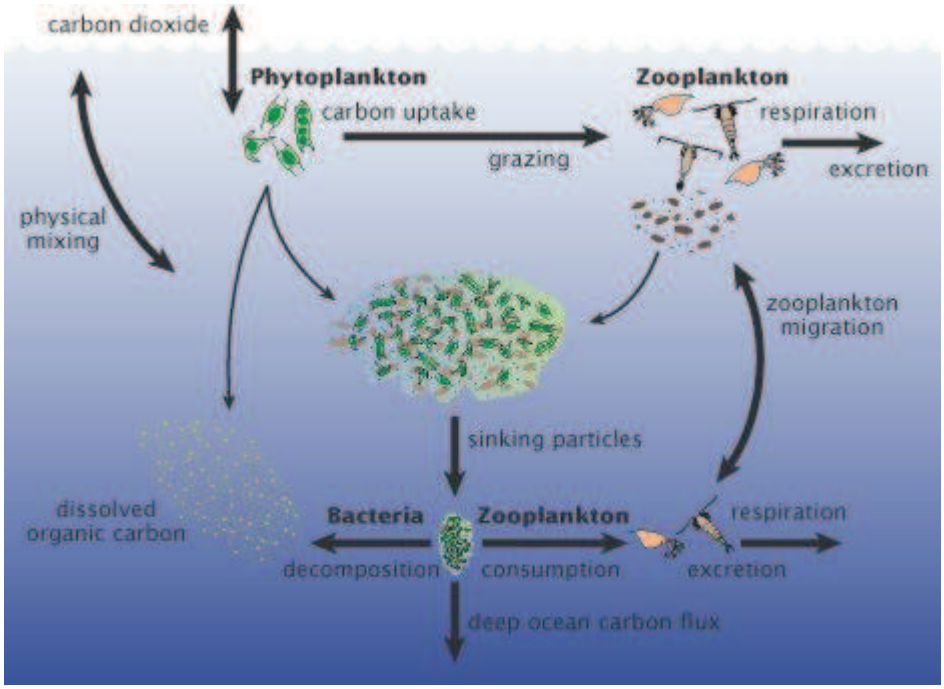

Figure 1.4: Schematic representation of the biological carbon pump in the ocean. http://earthobservatory.nasa.gov/

Qualitatively, the exported particulate organic carbon has mixed origins including dead phytoplankton cells, both contained in aggregates and in isolation, and zooplankton faecal pellets. The composition of this flux shows great variation from one oceanic area to another. Early studies suggested that the amount of material produced by phytoplankton (primary productivity) in the euphotic zone was the predominant factor over the strength of the carbon export in the ocean. However, the Joint Global Ocean Flux Study (JGOFS) which was conceived in the late 1980s to study the ocean carbon cycle and to understand the controls on the concentrations and

fluxes of carbon in the ocean showed that a major process in the the surface ocean is the production of large marine particles (also known as marine snow or aggregates). Understanding the production of these is as critical as understanding primary production if one wishes to understand the export flux of carbon from the surface ocean.

The major processes affecting the efficiency of carbon export can be summarised as follows (Banse, 1990; De La Rocha and Passow, 2007): (1) the amount of primary production in the euphotic zone; (2) the speed with which the marine snow sinks and (3) the rate of POC decomposition. The amount of primary production in the euphotic zone depends mostly on ecological conditions such as nutrient and light availability and/or the biological cycle of phytoplanktonic organisms.

The speed with which marine snow sinks depends on the formation processes and features of marine particles. To effectively sequester carbon into the deep ocean, marine particles must be exported to depths below that of winter mixing, therefore, the sinking pool of organic carbon aggregated into particles, has to be large and dense enough to attain high sinking velocities.

Particle sizes and densities are thus important to consider. For example, the sinking velocity of a solitary phytoplankton cells is about 1 m d^{-1} (Smayda, 1971) while large particles have sinking velocities of about 100 m d^{-1} (Shanks and Trent, 1980; Alldredge, 1998). As a result, the particle organic carbon flux is probably controlled more by particle sinking rates (2) than carbon fixation by phytoplankton and primary productivity (1) (Boyd and Newton, 1999).

The rate of POC decomposition is a function of microbial activity. Bacterial hydrolysis plays a major role in the decomposition of sinking and suspended matter in the ocean. Marine aggregates have been shown to contain high concentrations of

hydrolytic enzymes, such as proteases, polysaccharidases, and glucosidases (Azam, 1998). More than 50% of the primary production in the euphotic zone is grazed and/or attacked by microbes whereas only about 1 % actually settles down to the seabed (Martin *et al.*, 1987; Lutz *et al.*, 2007). Following its formation, organic matter in the ocean rapidly decomposes and there is intense recycling of elements even within the euphotic zone.

The flux of POC in the ocean decreases more or less exponentially with depth below the euphotic zone (Martin *et al.*, 1987; Buesseler *et al.*, 2007) (Figure 1.5). The depth to which POC exported from the euphotic zone is transported must be determined by the balance between the carbon content of the particle, the rate of microbial hydrolysis, and the sinking rate of the particle. This balance is obviously subject to a very high variability in space and time leading to a very wide range in carbon export flux occuring globally.

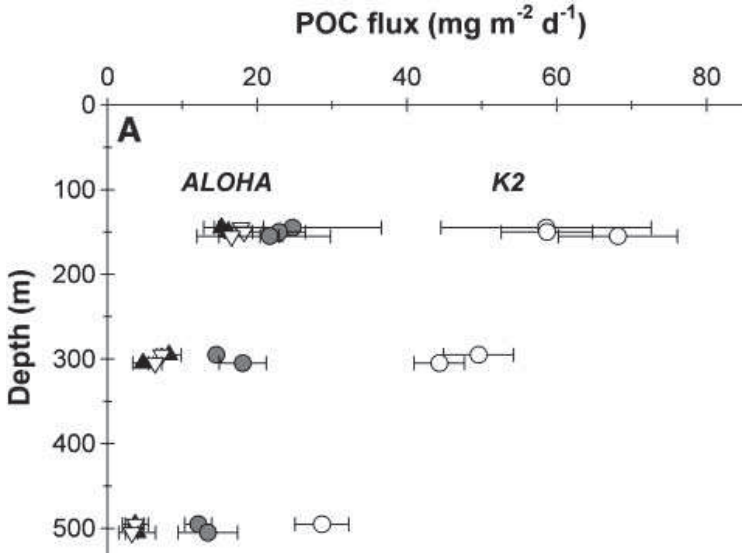

Figure 1.5: POC flux versus depth at ALOHA (22° 45′ N, 158° W) and K2 (47° N 160° E) taken from (Buesseler et al., 2007).

1.3 How can carbon export flux be enhanced from the surface ocean?

The ratio of deep POC flux measured via sediment traps to primary production shows variability from one place to another, ranging from 0.08 to 0.38 in the Atlantic Ocean alone (Antia, 2001). There are many reasons that an increased downward transport of POC out of the euphotic zone does not directly occur following an increase in surface productivity. This decoupling between production and particulate export in the surface ocean (Buesseler, 1998) occurs due to a variety of reasons.

1.3.1 Aggregation and repackaging processes

The magnitude of the downward carbon flux is partially controlled by the aggregation (or flocculation) of smaller more numerous particles into larger less numerous aggregates and by the rate at which the resulting aggregates sink. The sinking velocity of POC in the ocean is mainly constrained by the size of the sinking material. The POC sinks efficiently when it is composed of large particles (sinking rate of 50m d^{-1}) and is able to reach the seabed within weeks (Billett *et al.*, 1980 and 1983), whereas individual phytoplankton cells (sinking rate of 2 m d^{-1}) with very low sinking velocities are unlikely to reach the deep ocean. Marine snow, a pool of combined particles with diameters greater than 0.5mm (Alldredge and Jackson, 1995), consists of a variety of mostly organic matter, including dead or dying animals, plankton, protists, faecal matter, sand, impure carbon particles resulting from incomplete combustion of a hydrocarbon and other inorganic dust. Marine snow can accumulate additional particles as they sink to the deep and other aggregates formed by the physical coagulation of smaller particles (McCave, 1984; Jackson and Burd, 1998).

The formation of those particles by coagulation processes is triggered by the presence of transparent exopolymer particles (TEP). These are acidic polysaccharide particles formed from dissolved precursors released by phytoplankton. TEP are very sticky and form the matrix of all marine snow (Passow, 2002). TEP are probably necessary as a trigger for phytoplankton aggregates to form, and hence for their sedimentation, but when other particle types are sinking TEP may constitute a smaller fraction of flux (Martin *et al.*, 2011). The rate of aggregate formation through coagulation furthermore depends on the size and concentration of particles (e.g., diatoms, feces, and detritus) in the water (Logan *et al*., 1995).

POC may also be repackaged into zooplankton faecal pellets (Bishop *et al*., 1978, 1980; Honjo and Roman, 1978) that may be large and dense enough to sink rapidly on their own but also may become incorporated into aggregates. Zooplankton faecal pellets may contribute significantly to large particle fluxes when euphausiids are present. Diel vertically migrating zooplankton feed at night in the surface waters and migrate to depth during the day. The carbon ingested at the surface is metabolized at depth and thereby 'actively' transported into the deep-sea, a key mechanism by which carbon export is enhanced (Steinberg *et al*., 2008).

1.3.2 The role of Biominerals in enhancing the Carbon Export: A Potential Ballast Effect? Theory and debate.

The regional variability of deep POC export is significantly reduced when normalised to the total mass flux. This observation has inspired a theory suggesting that mineral fluxes (such as calcite, opal, and lithogenic material) drives deep POC flux (Armstrong *et al.*, 2002). This result was interpreted as reflecting the physical protection of a fraction of the POC by the minerals. They concluded that their POC-

mineral export model could explain deep sediment trap data better than the famous VERTEX curve by Martin *et al.*, (1987). At the same time, two global deep sediment trap studies were published. Francois *et al.*(2002) presented a dataset showing a close relationship between the penetration of POC and PIC into the deep ocean with a less tight relationship in opal dominated environment. They suggested that PIC, a dense mineral, may increase particle sinking rate when incorporated into aggregates; also, the (re)packaging of particles in faecal pellets may lead to fast sinking of particles in non-siliceous areas. Finally, Klaas and Archer (2002) sugggested that high latitude diatom blooms may have a higher lability of the organic matter produced. Klaas and Archer, (2002) argued that in the deep ocean, minerals drive POC export with PIC having a predominance in driving the global downward POC flux. Fluxes of calcium carbonate and POC from deep sediment traps are correlated (Klaas and Archer, 2002)(Figure 1.6). There was also a significant correlation between opal fluxes and POC fluxes. They proposed that the particulate organic carbon flux was primarly driven by calcite because it is denser than opal and more abundant than clays.

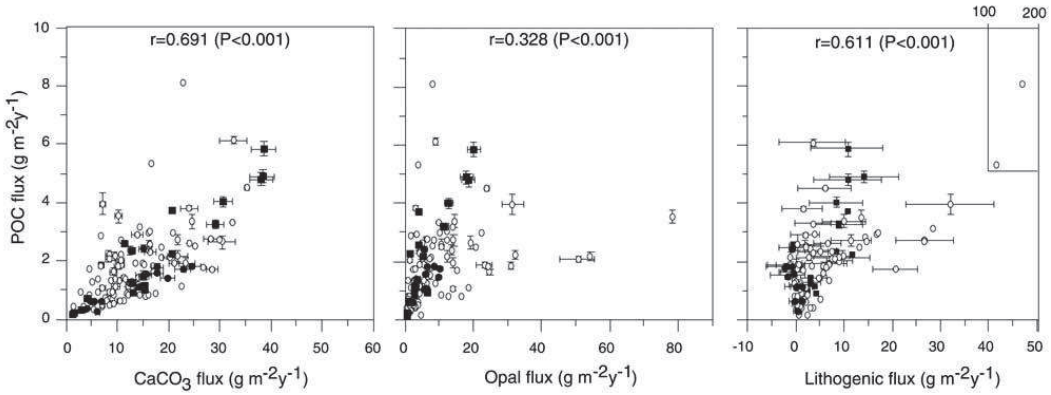

Figure 1.6: Relationship between POC flux versus $CaCO_3$, opal and lithogenic material fluxes for annual trap experiments below 1000 m depth. (Figures from Klaas and Archer, 2002).

Subsequent interpretation has focused on whether or not “a ballast effect” enhancing the flux of POC featured in the deep ocean in fact operates. First of all, the regressions (Francois *et al.*, 2002; Klaas and Archer, 2002) do not reveal whether it is biomineral fluxes which are responsible for POC fluxes or whether the reverse process occurs (Passow *et al.*, 2003; Passow and De la Rocha, 2006). Indeed, the organic snow formed in the surface could collect minerals thanks to their sticky carrying capacity (organic glue: TEP). Moreover, the incorporation of minerals into artificially nade organic aggregates causes aggregates to fragment into smaller particles (Passow and De la Rocha, 2006) with lower sinking rates potentially exporting less POC if extrapolated to the real conditions and reaching a saturation state of 5% in the POC/biomineral ratio (De La Rocha *et al.*, 2008) as found in the deep sediment trap studies shown in Armstrong et al., (2001) (e.g. in the Equatorial Pacific and Arabian Sea).

The competing processes of density addition and size reduction means that the relationship between sinking rates and the accumulation of minerals on aggregates is not straightforward (Hamm, 2002). On the other hand, the correlation obtained by Klaas and Archer (2002) could be an artefact of too much averaging (Passow *et al.*, 2003) and the greater importance of calcite as main ballast agent concluded by Klaas and Archer (2002) could be the result of the dominance of mid latitudes sites in their dataset. Another possible explanation for the apparent predominance of calcite as a ballast for POC is that the fate of dead diatoms cells and dead coccolithophorids cells are not the same. Coccoliths are separated from the cell (and thus from the POC) while diatom frustules trap POC within themselves (Passow and De la Rocha, 2006). In addition, the regional variability of Si:C in primary productivity in the ocean is deemed to be high (Ragueneau *et al.*, 2000), bringing a high variability in the POC

export to opal export ratio. Indeed, diatom blooms are known to export a large fraction of the primary productivity (Treguer and Pondaven, 2000) and when the approach of Klaas and Archer, (2002) was adopted on a regional scale in an opal dominated environment, opal appeared to be the most efficient "ballast agent" in the mesopelagic zone (Honda and Wanatabe, 2010; Buesseler *et al.*, 2007).

More recently, several studies have investigated the potential ballast effect in the surface ocean. Trull *et al.*, (2008) found limited evidence for a 'ballast effect' using an Indented Rotating Sphere (IRS) sediment trap during the VERTIGO program (Buesseler *et al.*, 2007) whereas Lee *et al.*(2009b) found a significant ballast effect during the MEDFLUX voyages (Lee *et al.* 2009a). Trull *et al.* (2008) recorded weak trends of decreasing POC/biomineral with decreasing sinking rate, the opposite of the expected tendancy that biominerals increase particles sinking rates. Lee *et al.*(2009b) show temporal and depth-related trends in POC and ballast content. Calcite was consistently the dominant mineral phase in sinking particles, but its relative abundance was lower when the diatom-bloom-driven opal flux was strong. They concluded that phytoplankton succession over the productive season could drive the efficiency of each biomineral to potentially drive POC export.

Thomalla *et al.*, (2008) and Sanders *et al.*, (2010) used ^{234}Th derived fluxes to obtain simultaneous measurements of the downward flux of POC and both calcite and opal. They used their datasets to test whether or not similar relationships to those found by Klaas and Archer, (2002) exists in the upper ocean. They found strong, statistically robust relationships between POC and biomineral fluxes from the euphotic zone including subpolar, subtropical and tropical environments. Slopes obtained from the relationships are significantly steeper than those reported by Klaas and Archer (2002) consistent with the known loss of POC as material sinks, relative to

the lower fraction of exported biomineral which is lost (Poulton *et al.*, 2006; Thomalla *et al.*, 2008; Sanders *et al.*, 2010).

There is a need to go beyond the simple correlation analysis used to date with more regional process studies of POC and biomineral export. Sanders *et al.* (2010) proposed a new approach defining two criteria to assess whether a ballast effect occurs. The first one is that it is an explicit requirement for export to occur that biominerals are exported in parallel with organic carbon and the second one is that exported particles are richer in biomineral (and therefore probably denser) than suspended particles. They found that negligible POC export can happen without biomineral export implying that biominerals are not required for POC export to occur. However, by considering whether exported material is stoichiometrically similar to the suspended particulate pool in the upper ocean, they found that most of the exported particles had a higher density than the upper ocean standing stock, a factor which may lead to their export.

Interestingly, Honda and Watanabe (2010) found that in the North Pacific, opal has a greater importance as a ballast agent than calcite. Also, they reported that in surface layers most of the sinking POC (78%) was not associated with any mineral. Using global compilations of particle export efficiency Henson *et al.*, (2012) found that the efficiency with which POC is transported to the deep ocean is negatively correlated with opal flux and not correlated with calcite flux. They conclude that the efficiency with which POC is transported to the deep ocean is primairly driven by the magnitude of recycling in the upper ocean rather than the availability of calite constrating with conclusions from Klaas and Archer (2002).

Interactions between biominerals and POC are important in the surface. However, the basic theory has to be improved and tested over different depth and

biogeochemical settings. The relative paucity of consistent flux data from the upper ocean and the lack of knowledge of aggregation processes mean that the potential ballasting mechanisms that may promote particle export from upper ocean are poorly understood. This therefore prevents the determination of potential interactions between POC and biominerals and further interpretation on the role of biominerals in enhancing the flux of organic carbon into the deep ocean. In addition, latitudinal and seasonal variability have to be carefully considered in this mechanism. Understanding the nature of this ballast effect in the upper ocean is a high priority area (Boyd and Trull, 2007).

1.3.3 Future implications

Ocean acidification is the name given to the ongoing decrease in the pH of the Earth's oceans, caused by their uptake of anthropogenic carbon dioxide from the atmosphere. Most carbon dioxide released into the atmosphere as a result of the burning of fossil fuels will eventually be absorbed by the ocean, with potentially adverse consequences for marine biota (Caldeira and Wickett, 2003). Laboratory and field studies reveal that acidification of sea water will hamper biogenic calcification in marine organisms such as coccolithophorids (Riebesell, 2004) which produce of great amount of calcite (PIC) in the ocean. What about the effect of acidification on ballast effect?

Recent modelling studies based on the conclusions of Klaas and Archer, (2002) about the ballast effect show that a decrease in calcite production result in an upward shift in the locus of POC remineralisation (Heinze, 2004; Hoffmann *et al*., 2009) thereby lowering the flux of POC to the deep sea which is equivalent to a weakening of the marine biological carbon pump (Hoffmann *et al*., 2009). Moreover, according to Hoffmann *et al*. (2009), a reduced ballast effect could expand hypoxia

zones in the ocean in the future 1000 years due to accelerated remineralisation processes of POC in the upper ocean.

1.4 Estimating the particle export flux with emphasis on the radionuclides-derived export estimates.

There are several ways by which downward export fluxes can be measured. We can divide techniques in two groups : (1) indirect measurements based on nutrient uptake (Sanders *et al.*, 2005; Eppley and Peterson, 1979; Henson *et al*., 2006; Pondaven *et al.*, 2000), on oxygen utilization (Jenkins, 1982), on radioisotopes (Rutgers van der Loeff *et al*.,2006; Buesseler *et al*.,1992; Verdeny *et al.*, 2008) and by synthesising numerous biological rate processes (Boyd *et al.*, 1999). (2) the direct measurements from sediments traps (Lampitt *et al.*, 2008).

1.4.1 Radionuclides disequilibrium

The Radioactive short-lived Thorium-234 (^{234}Th, $t_{1/2}$=24,1d) (Bath *et al*., 1969) has been used as a tracer of several transport processes and particle cycling in aquatic systems by different techniques (Rutgers van der Loeff *et al*.,2006). It can be used to estimate how much POC is exported into the deep ocean (Buesseler *et al*.,1992; Cochran et Masqué, 2003; Rutgers van der Loeff, 2001) and this is the most widespread application of ^{234}Th approach (Waples *et al*.,2006). ^{234}Th is the daughter isotope of naturally occurring 238-Uranium (^{238}U, $t_{1/2}$=4,47.10^9y) which is conservative in seawater and proportional to salinity in well oxygenated environments (Ku et al.,1977; Chen et al.,1986). Unlike ^{238}U, ^{234}Th is insoluble in seawater and is particle reactive in the water column. As particles with ^{234}Th sinks through the water

column, a radioactive disequilibrium is formed between ^{238}U and ^{234}Th , which can be used to quantify the rate of particle export from the surface ocean.

An additional radionuclide pair is Lead-210 ($t_{1/2}$=22.3y) and Polonium-210 ($t_{1/2}$=138,4) pair, which are particle reactive radioisotopes in the ^{238}U decay series. This pair can be used as a tracer of particle cycling in the surface ocean (Cochran and Masqué, 2003). ^{210}Pb and the ^{210}Po have opposing behaviour regarding the mechanisms by which they bind to particles in the ocean (Verdeny *et al.*, 2008). ^{210}Pb adsorbs onto particle surfaces whereas ^{210}Po is biologically incorporated into the intracellular compartments of some phytoplankton and bacteria (Fisher *et al*., 1983; Cherrier *et al*.,1995; La Rock *et al*., 1996). As a result, cells containing ^{210}Po can be assimilated by zooplankton and excreted in sinking particles (faecal pellets). Thus, when biological activity is strong, disequilibrium between the ^{210}Pb/^{210}Po pair appears and can be used to estimate particle export as with the ^{234}Th/^{238}U disequilibrium. The ^{210}Pb/^{210}Po can assess particle carbon export on timescales from several months to a year, constrained by the half-life of ^{210}Po, which is a usefull time scale to estimate the carbon biogeochemical dynamics of mesoscale structures such as eddies (Verdeny *et al*., 2008). An important conceptual limitation and unknown in these radionuclides-derived export estimates.underlies in the molecular basis of interaction between radionuclides and biogenic/lithogenic matter as well as the speciation of these radionuclides in seawater. A better understanding of the molecular mechanisms of ^{234}Th “scavenging” is needed requiring examination of Th complexation to colloids, large particles, aggregation (Santschi *et al.*, (2006) and particle of different composition and origin.

1.4.2 C/Th ratios and POC export

The accuracy of the Th method relies critically on estimating the C/Th ratio of material sinking from the upper ocean (Buesseler et al., 2006). This estimate is most frequently achieved by assuming that sinking carbon (and mineral) is contained within large particles, often greater than 53 μm in size, whereas organic carbon within small particles is suspended in the water column, and small particles are assumed to be insufficiently large and/or dense to sink (Bishop et al., 1977; Fowler and Knauer, 1986). If significant material smaller than 53 μm is sinking, then this material is not taken into account by the Thorium technique unless the C/Th ratio measured on smaller particles is included in the calculation of POC export.

There is a considerable body of literature on how and why C/Th ratios vary with particle size and depth (see review in Buesseler et al., 2006), however there is little consensus on the most appropriate ratio to use. Numerous processes can impact C/Th ratios in the ocean including particle surface area to volume ratios (Santschi et al., 2006), solution chemistry issues (Guo et al., 2002; Hung et al., 2004), the chemical composition of particles and their affinity for ^{234}Th (Szlosek et al., 2009), POC assimilation by foodwebs (Buesseler et al., 2009), particle aggregation (Burd et al., 2000) and fragmentation (Maiti et al., 2010b) and Th decay (Cai et al., 2006). In most studies, C/Th is either constant or increases with particle size suggesting that surface to volume ratios and particle aggregation processes are likely to be the dominant processes affecting C/Th in the upper ocean (Buesseler et al., 2006).

The great attraction of the ^{234}Th technique is that its fundamental operation (diagnosis of thorium deficit, application of model to derive thorium flux, conversion to POC units using POC/^{234}Th ratio) allows a downward flux rate to be determined from a single water column profile of thorium coupled to an estimate of the

POC/^{234}Th (hereafter abbreviated as C/Th) ratio in sinking matter (Buesseler et al., 1992). This is highly advantageous in that it removes the complications associated with sediment trap deployments and provides an integrated estimate of export (over a timescale of weeks) rather than a snapshot of export rates (Lampitt et al., 2008). This approach is detailed below.

1.4.3 ^{234}Th derived estimate of the global biological carbon pump

Recently Henson *et al.*, (2011) compiled a global database of ^{234}Th derived estimates of particle flux and combined this with satellite derived estimates of sea surface temperature and primary production to estimate globally integrated export from the surface ocean. Their estimate of globally integrated carbon export including that component driven by dissolved organic carbon was ~ 5 GtC yr^{-1}, significantly lower than many other estimates (Henson *et al.*, 2011) including critically that made by Schlitzer (2004) using inverse modelling techniques. Henson *et al*. (2011) explored a range of possible reasons for this offset including uncertainties in nitrogen fixation and nitrification (which would bias *f*-ratio based estimates) or dissolved organic carbon cycling in the upper ocean. One potential explanation could be that the ^{234}Th approach excludes certain categories of particles from its calculation such as slow and potentially small sinking particles.

This suggestion is based on recent observations that state that particulate organic carbon (POC) can be clustered in three bio geochemically distinct pools: fast sinking particles, slowly sinking particles and the suspended pool (Alonso-Gonzalez *et al.*, 2010; Sanders *et al.*, 2010; Riley *et al.*, 2012). While the suspended and fast sinking pools are well described and represented (Alldredge and Gotschalk, 1988; Turner, 2002), little is known about the characteristics of the recently recognised slow

sinking pool which under some circumstances contribute significantly to carbon export (Alonso-Gonzalez *et al*., 2010; Riley *et al*., 2012).

When one looks at the Stoke's Law describing variation of sinking rates versus size of a marine particle, it is likely that the slow pool may be constituted of relatively small particles. Also recent work clearly suggests that aggregates and cells smaller than 53 µm may comprise a significant fraction of POC export (Waite *et al.*, 2000; Richardson and Jackson, 2007; Brew *et al.*, 2009; Stewart *et al.*, 2010).

1.5 Objectives

This thesis aims to study the strength of the biological carbon pump and more specifically the contribution of biominerals to enhancing the flux of organic carbon into the deep ocean. To address these issues, I used several complementary approaches. The first is understanding the limitations of the ^{234}Th method as a tracer of particle export, the second is building up a dataset of ^{234}Th derived carbon and biominerals export fluxes from various areas in the ocean and the third is simulating marine aggregate formation and degradation processes in the presence of biominerals and zooplankton grazing.

I will specifically address the following questions:

- What can be learned about the origin of the slow sinking pool from size fractionated C/Th ratios and what are the implications for globally estimated Th derived POC export?
- What is the ability of the ^{234}Th and ^{210}Po techniques to estimate fluxes of POC, and biominerals from the surface ocean and do they produce coherent estimates when considering integration time scale and particle affinity?

- What is the regional variability of the proportion of ballast associated versus non-ballast associated sinking POC in the surface ocean?
- What is the influence of calcite and microzooplankton on the degradation of marine aggregates?

1.6 Overview of Thesis Structure

This PhD thesis is organized as follows: a general introduction that puts in larger and more detailed context the rationale of this thesis is presented in ***Chapter 1.*** This chapter includes the carbon cycle, the biological carbon pump concept, how carbon export can be enhanced and the state of the debate over the "ballast theory".

In ***Chapters 2 and 3*** are described the results of a cruise undertaken to build up a dataset of POC, biominerals export fluxes. D341 (P.S.O.: Richard Sanders) took place from the 13th July to the 11th August 2009 on board the *R.R.S. Discovery* at the Porcupine Abyssal Plain (49W; 16.5W) where nine stations were occupied for $^{234}Th/^{238}U$ using the ^{234}Th "large volume technique" (Rutgers Van Der Loeff *et al.*, 1997) coupled with $^{210}Po/^{210}Pb$ (realised by Maria Villa, Universidad de Sevilla) and seven deployments of *in situ* pumps were undertaken with the content analysed for POC, PIC, BSi, ^{234}Th, ^{210}Po. This has lead to two pieces of work.

The first part, presented in ***Chapter 2***, explores the use of size fractionated C/Th ratios to sample the slow sinking pool of POC in the surface ocean and what size fractionated C/Th ratios tell us about the dynamic of this slowly settling POC pool. Also, ***Chapter 2*** explores origin of the slow sinking particles using size fractionated C/Th ratios and implications for global Th derived POC integrated export studies.

The second part, ***Chapter 3***, is presented as a publication entitled "Insights from a POC and biominerals radionuclide derived export study at the Porcupine

Abyssal Plain: implications for the ballast effect theory" under review in ***Deep Sea Research part I***.

In ***Chapter 4*** are presented informations on two others cruises undertaken to expand the dataset of POC, biominerals export fluxes. D350 (P.S.O.: C. Mark Moore) and D354 (P.S.O.: Eric Achterberg) took place from the 24th April to the 10th May 2010 and from the 4th July to the 13th August 2010 respectively on board the *R.R.S. Discovery* in the Iceland and Irminger basins where 20 stations were occupied for $^{234}Th/^{238}U$ using the "^{234}Th small volume technique" (Pike *et al.*, 2005) and 24 deployments of *in situ* pumps were undertaken with the content analysed for POC, PIC, BSi, ^{234}Th. The D350 and D354 datasets were combined with previous work from the Iceland basin (Morris, 2008; Sanders *et al.*, 2010) in order to assess the importance of calcite and opal in promoting the flux of POC from the surface ocean. This work based on the previous study by Klaas and Archer (2002), examines stations of ^{234}Th derived POC, calcite and opal export fluxes over the Atlantic and the Southern Ocean. ***Chapter 4*** is presented as a publication entitled "On the proportion of ballast versus non-ballast associated sinking POC in the surface ocean" accepted in ***Geophysical Research Letters***.

Chapter 5 presents experiments done between January 2011 and August 2011 at the LEMAR (UMR 6539 UBO/CNRS/IRD), European Institute of Marine Studies in Brest, France, in collaboration with Christina De La Rocha (Pr Université de Bretagne Occidentale), Emmanuel Laurenceau (Master student, Master Sciences Biologiques Marines, IUEM, Brest). This experimental work was carried out in rolling tanks to observe the influence of suspended calcite over the phytoplankton aggregation mechanisms. In addition, the results were further examined in terms of implications for the "ballast theory". This experimental work is presented as a

publication entitled “The Influence of Calcite and Microzooplankton on the Remineralisation of Sinking Aggregates” to be submitted to ***Global Biogeochemical Cycles***.

Finally, in ***Chapter 6***, conclusions will be put forward in a broader context. Future work that will be undertaken in the framework of the author’s post doctoral project (Seas*FX*, funded by NERC-GEOTRACES UK), supervised by Stephanie Henson, NOC, will be presented at the end of this chapter.

2. Origin and representation of the slowly sinking particles in the ^{234}Th derived POC export estimates

Data contribution: All samples were taken and analysed by the author during D341 (P.S.O.: Richard Sanders), except for POC (samples prepared by the author, then analysed by Bob Head, PML). Maria Villa (U. of Sevilla) helped with ^{234}Th processing at sea. Chris Marsay (NOC) helped with *in situ pumps* deployment. Paul Morris (WHOI) helped with ^{234}Th analysis and cruise mobilization.

Abstract The importance of the slow sinking pool of organic carbon (i.e settling velocity lower than 10 m d^{-1}) has recently been highlighted. At the Porcupine Abyssal Plain (PAP site), in summer 2009, the contribution of the slow sinking pool of carbon was on average 60% of the total export (Riley *et al*., 2012). While the exact origin and dynamic of this pool is still unclear, it is quite clear that it can represent a significant contribution to total carbon export on some occasions. Here, I attempt to better understand the origin and dynamics of the slow sinking pool. I use size fractionated C/Th ratios; we first explore to what extent the slow and fast sinking pools can be assumed to correspond to the small and large size fractions sampled with *in situ* pumps (e.g. 1-53µm and >53µm) based on theoretical relationship between particle size and sinking velocities and using the respective sinking speed of slow and fast pools measured at the PAP. I find that 1-53µm and >53µm size fractions represent slow and fast sinking pools respectively although we recommend a 10-53µm as size fraction to sample the slow sinking pool. Size fractionated C/Th ratios were invariant at depth at the PAP site suggesting a predominance of aggregation/disaggregation

processes. Hence, I propose that at the PAP site, the slow sinking pool may have resulted from *in situ* disaggregation of larger particles. Finally we attempt to implement the slowly settling pool of carbon into the commonly used ^{234}Th technique POC export approach.

2.1. Introduction

The biological carbon pump (BCP) is the biological mechanism by which CO_2 is stored on geological time scales in the deep ocean. It consists predominantly of the sinking of biogenic particles from the surface ocean to its interior (Falkowski *et al.*, 1998; Falkowski *et al.*, 2000; Sabine *et al.*, 2004) followed by their recycling. It has been suggested that without the BCP, atmospheric CO_2 levels would be almost twice as high as they are now (Sarmiento and Toggweiler, 1984). The mode by which carbon is transferred downwards is therefore a key issue in the context of global climate change.

The Particulate organic carbon (POC) is clustered in three bio geochemically distinct pools: fast sinking particles, slowly sinking particles and suspended pool (Alonso-Gonzalez *et al.*, 2010; Sanders *et al.*, 2010; Riley *et al.*, 2012). While the suspended and fast sinking pools are well described and represented (Alldredge and Gotschalk, 1988; Turner, 2002), little is known about the characteristics of the recently highlighted slow sinking pool despite substantial contribution to total carbon export (Alonso-Gonzalez *et al*., 2010; Riley *et al*., 2012). When one looks at the Stoke's law describing variation of sinking rates versus size of a marine particle, it is likely that the slow may be constituted of relatively small particles. Also recent work clearly suggests that aggregates and cells smaller than 53 µm may comprise a significant fraction of POC export (Waite *et al.*, 2000; Richardson and Jackson, 2007;

Brew *et al.*, 2009; Stewart *et al.*, 2010) The origin and nature of the slow sinking remains unclear. Alonso-Gonzalez *et al*., (2010) found that when it significantly contributes to total export the slow sinking pool was fresher than the rapidly settling pool based on limited biomarker dataset.

One commonly used technique to estimate particulate organic carbon (POC) export relies on the particle reactivity and short half life of the ^{234}Th isotope which create a deficit in ^{234}Th concentrations in the upper ocean when particles are exported. The thorium flux out of the upper ocean required to sustain the observed deficit is then computed using a steady state model and this is then combined with POC:^{234}Th ratios to estimate POC export (Buesseler *et al.*, 1992). The great attraction of the ^{234}Th technique is that its fundamental operation (diagnosis of thorium deficit, application of model to derive thorium flux, conversion to POC units using POC/^{234}Th ratio) allows a downward flux rate to be determined from a single water column profile of thorium coupled to an estimate of the POC/^{234}Th (hereafter abbreviated as C/Th) ratio in sinking matter (Buesseler *et al*., 1992). This is highly advantageous in that it removes the complications associated with sediment trap deployments and provides an integrated estimate of export over time scale of weeks (Lampitt *et al.*, 2008; Le Moigne *et al.*, in review-b).

However, the accuracy of the method relies critically on estimating the C/Th ratio of material sinking from the upper ocean (Buesseler *et al*., 2006). This estimate is most frequently achieved by assuming that sinking carbon is contained within large particles, often greater than 53 μm in size, whereas organic carbon within small particles is suspended in the water column, as they are assumed to be insufficiently large and/or dense to sink (Bishop *et al*., 1977; Fowler and Knauer, 1986).

Numerous processes can impact C/Th ratios in the ocean including particle surface area to volume ratios (Santschi *et al*., 2006), solution chemistry issues (Guo *et al.*, 2002; Hung *et al.*, 2004), the chemical composition of particles and their affinity for ^{234}Th (Szlosek *et al.*, 2009), POC assimilation in food web (Buesseler *et al*., 2009), particle aggregation (Burd *et al*., 2000) and fragmentation (Maiti *et al.*, 2010a) and Th decay Cai *et al*, (2006). In a review on the use C/Th, Buesseler *et al.*, (2006) concluded that C/Th increases or is approximately constant suggesting that particle surface area to volume ratios and aggregation process explain most of the C/Th variations with size.Thus, size fractionated C/Th ratios have abilities in providing information about the processes driving source and fate of particle in the ocean such as particle aggregation or disaggregation.

Recently we have estimated the relative contributions to total flux of the fast and potentially large sinking pools as being approximately 60/40 % in favour of the slow sinking and potentially small pool (Riley *et al*., 2012). In parallel, we measured size fractionated C/Th at several depth. Here, we first examine the relationship between slow/fast sinking particles with particles caught in both small/large (1-53 μm and >53 μm). Thus, variations of size fractionated C/Th potentially corresponding to the slow and fast sinking pool should lend insights into the possible sources and dynamic of the slow sinking pool in the ocean.

Also, if significant material smaller than 53 μm is sinking, then this material is not taken into account by the thorium technique as it is most commonly used unless the C/Th ratio measured on smaller particles is included in the calculation of POC export. Therefore, estimating export using a ^{234}Th deficit coupled to the C/Th ratio on large particles may underestimate total export and hence contribute to explaining the

discrepancy found between the ^{234}Th based global POC export estimates presented in Henson et al.(2011) and others.

2.2. Methods

In 2009 we measured size fractionated C/Th ratios, and total thorium depletions around the PAP time series site. Methodologies on both studies followed our published protocols (Thomalla *et al.*, 2006; Morris, 2008; Pollard *et al.*, 2009; Sanders *et al.*, 2010; Le Moigne *et al.*, in review-b). In brief, water samples were taken from 10 depths within the upper water column using a CTD rosette. Total ^{234}Th was extracted from solution by precipitation with MnO_2 for 8 hours (Van der Loeff *et al.*, 2006). The precipitate was filtered and ^{234}Th activity measured using a low level beta GM multicounter system (model Risø GM-25-5). Vertical profiles of ^{234}Th activity were converted to estimates of downward ^{234}Th flux using a one dimensional steady-state model (Cochran *et al.*, 1997; Buesseler, 1998).

Large (>53 μm) and small (1-53 μm) particulate matter was collected using *in situ* Stand Alone Pumping System (SAPS) deployed for 1.5 hrs beneath the mixed layer and 100 m beneath it. Approximately 1000–2000 L of seawater was filtered sequentially onto a 53 μm Nitex screen followed by a 1 μm Nitex screen. Particles were then rinsed off the screen using thorium-free seawater and the particle suspension quantitatively split into subsamples using a Folsom splitter. One split was then analysed for each of ^{234}Th or POC concentrations. POC samples were filtered onto precombusted GF/F filters, fumed and analysed using a Thermo Finnegan Flash EA1112 Elemental Analyser (Lorrain et al., 2003). ^{234}Th samples were filtered onto 142mm diameter (0.8 mm pore size) polycarbonate filters for subsequent direct analysis using a low level beta GM multicounter system (model Risø GM-25-5).

Hence the C/Th obtained is not impacted by collecting the two terms using different techniques. POC measured using *in situ* pumps differs from bottle collected POC for several reasons including bottles collecting more zooplankton; pumps inlet designs affecting the collection efficiency of certain type of particles (Liu *et al.*, 2005; Liu *et al.*, 2009); the exclusion of large particles in Niskin bottles (Bishop, 1994); pumping pressure (Gardner *et al.*, 2003); DOC adsorption onto filters (Turnewitsch *et al*., 2007); and the use of different filters in the two methods (Liu *et al*., 2009).

Concentrations of POC in suspended matter (referred as standing stock) were measured at 50m only by filtering 1 to 2 litres of seawater through pre-combusted 0.42µm GFF filter. Filters were dried and stored before acid fuming and analysis using an elemental analyser (Thermo Finnegan Flash EA1112) as described above.

2.3. Results and discussion

2.3.1. Can the 1-53µm size fraction particles be representative of the slow sinking pool? Insights from particle size versus particle sinking velocity relationships

Recent studies have suggested that in the surface waters (above 300m), slow sinking particles may occasionally contribute up to 50-60% of total export (Trull *et al.*, 2008; Alonso-Gonzalez *et al.*, 2010; Riley *et al.*, 2012). Alonso-Gonzalez *et al*. (2010) showed a bimodal distribution of total carbon flux with a significant contribution of the slow sinking pool to total POC fluxes (Periods I and III in the deployments from the Canary Islands described in their paper). On these occasions 62% and 25% of the total POC flux was carried by sinking velocity classes of 0.7-11m d^{-1} and >326 m d^{-1}

respectively. In Riley *et al.*, (2012) sinking velocity classes of slow and fast sinking pool were respectively of 9 m d^{-1} and 181 m d^{-1} respectively.

Given this, there is an opportunity to verify whether or not the small particles can be reasonably assumed as representing the slow sinking pool described in Riley *et al*., (2012). Then slow sinking particles could potentially be assumed as being representative of our small size fraction for the remainder of this manuscript before eventually implementing the contribution of the slow sinking within the ^{234}Th derived POC export model. We use Riley *et al.* (2012) values given above to verify whether our small size fraction theoretically corresponds to particle sinking speed lower than 9 m d^{-1} and whether our large size fraction theoretically correspond to particle sinking speed greater than 181 m d^{-1}. In order to address this, we need to understand how sinking velocity varies with particle size for a given density. We used one theoretical equations relating size and density to sinking speed for this purpose the Stoke's law (equation 1),

$$U = \frac{2}{9}\frac{g\left(\frac{d}{2}\right)^2(\Delta\rho)}{k\nu} \qquad \text{Equation 2.1}$$

Where *g* is acceleration due to gravity, kν is the dynamic viscosity of seawater, d the diameter of a particle and Δρ is the density difference between the aggregate and seawater, (0.1 and 0.2 for the dominant class of aggregate found on D341, J. Riley, personal communication. The density of particles was estimated from its morphology and assumed composition. Marine snow Aggreagtes, the dominant class of particles were assigned a literature value of 1.23 g cm^{-3} (Alldredge and Gotschalk, 1988)). the Stoke's law eqution has been as we believe it accurately describes the relationship

between particle size and speed. The great advantage of the equation is that it allows to test the size/speed relationships using different particles densities.

Using equations 2.1 we can see how sinking velocity of a particle varies as a function of particle size (Figure 2.1). Figure 2.1 presents sinking velocity as a function of particle size for a particles of density 1.1 and 1.2 (the density of the dominant class of aggregate found throughout D341, J. Riley, personal communication) using Stoke's equations.

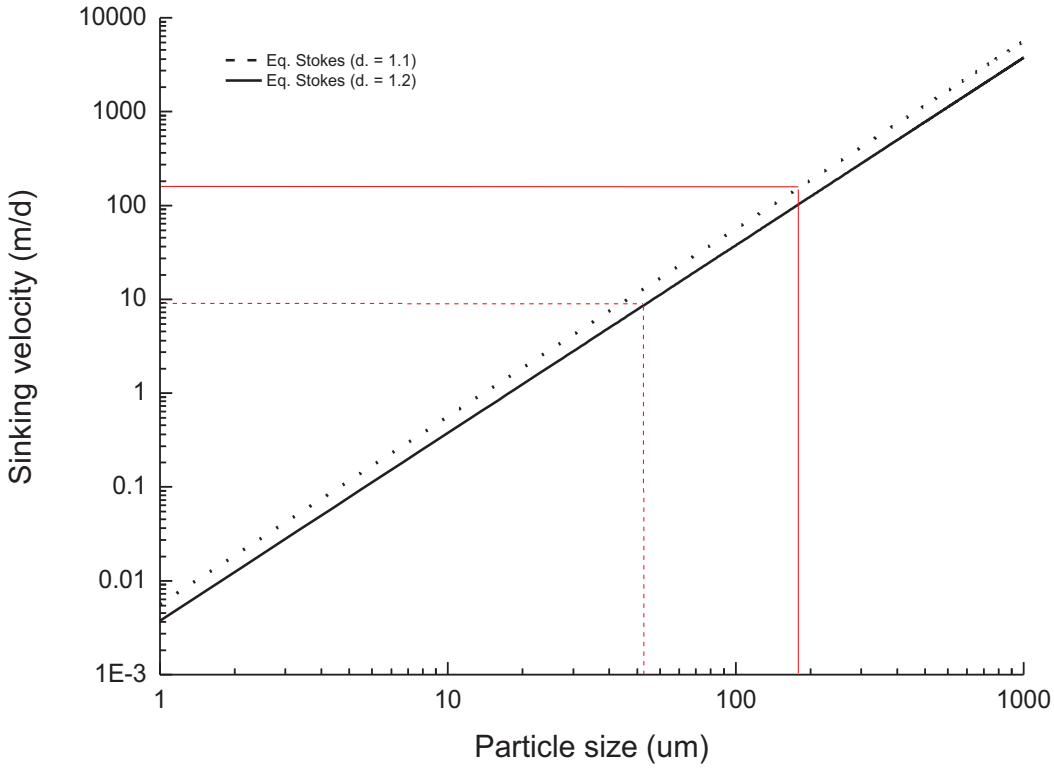

Figure 2.1: Variation of particle sinking speed as a function of particle size for given densities using equation from Stoke's law (equation 2.1). Red lines indicated the sinking velocity of both slow and fast sinking pool presented in Riley *et al.*,(2012)(dashed line = 9 m d^{-1}; plain line 181 m d^{-1})

If this equation accurately describes sinking velocity as a function of size, then it is impossible for a particle sinking slower than 9 m $d^{-1}$to be much larger than 53 µm. Similarly, particles sinking at a velocity equal or greater than 181 m d^{-1} are larger than 53 µm. At a first sight, this supports our assumption that small size fractions are representative of the slow sinking particles. Nevertheless, on one hand, we cannot exclude the possibility of a large particle (>53µm) falling at velocities down to 7-10 m d^{-1}. This should however not prevent us of assuming small(large) particles represent the slow(fast) sinking pool for the following reasons. The contribution to total carbon export of numerous settling velocities classes have not been measured in Riley *et al.*, (2012), however, it has been in Alonso-Gonzalez *et al.*, (2010) and they considered that 60% of total POC flux is contained in particles sinking at rates comprised between 0.7 and 11 m d^{-1}, the greater part of the slow sinking pool has sinking velocities that range between 0.7 and 5.4 m d^{-1} (See Figure 2 in (Alonso-Gonzalez *et al.*, 2010)). Therefore if the distribution of POC export is strongly bimodal with respect to size (Alonso-Gonzalez *et al.*, 2010) (most flux is carried by either slow or fast sinking particles with little flux carried by particles of intermediate sinking rate), the amount of large particles (>53µm) falling at velocities falling down to 7-10 m d^{-1} should be reduced.

On the other hand, if a minimum sinking velocity of 0.7 m d^{-1} is taken as the threshold below which a particle is considered as suspended, then there is a chance for particles sinking slower than 0.7 m d^{-1} to be caught in our 1-53 µm size fraction as the corresponding particle size for a sinking speed of 0.7 m d^{-1} is roughly 10 µm. When one examines the concentration of POC in particles >1µm (from added 1-53µm and >53µm size fractions) and standing stock POC concentration (0.42µm), it seems that not less than 70% of the POC standing stock was comprised between 0.42 and 1 µm

(Table 2.1). Therefore, in the worse case, only 30% of suspended matter would be caught in our 1-53µm size fraction.

Hence, the assumption that small particles represent the slow sinking pool and large particles represent the fast sinking pool is, we believe, reasonably acceptable. However, we suggest that using a 10-53µm size fraction would give a better representation of the slow sinking particles. Consequently, in the remainder of this manuscript, it will be assumed that slow sinking equals small size fraction and fast sinking equals large size fraction.

Table 2.1: POC standing stocks and POC in SAPS concentration at 50m (beneath the MLD)

	POC standing stocks 50m >0.42 µm	POC SAPS µmol l^{-1} >1 µm	POCstocks - POCSAPS 0.42-1µm	Percentage of suspended matter smaller than 1µm
16477	4.12	0.20	3.92	95.15
16523	4.04	0.65	3.39	83.91
16544	4.04	0.65	3.39	83.91
16559	4.04	0.65	3.39	83.91
16583	1.88	0.55	1.33	70.74
16592	9.98	0.33	9.65	96.69
16659	7.51	0.57	6.94	92.41

2.3.2 Origin of the slow sinking pool, importance of aggregation disaggregation processes.

If the presence of the slow sinking carbon pool features undoubtly, its origin remain obscure. Alonso-Gonzalez *et al*. (2010) concluded that when significantly contributing to the total export the slow sinking pool was fresher than the rapidly settling pool based on the reduced dataset of biomarkers. This trend was confirmed in the Pacific

by Trull *et al*., (2008). However, microbial activity (defined GABA, microbial decomposition marker) does not covary with the sinking speed in any systematic way (Alonso-Gonzalez *et al.*, 2010). Also, Riley *et al*., (2012) were unable to determine whether fast sinking alone or a combination of fast and slow particles supply POC to the deep ocean. Therefore the origin and formation of this slow sinking pool (when it is significant) is not clear. Two scenarios could be proposed: (1) the slow sinking pool sinks as it is until it gets remineralised in the mesopelagic zone; (2), that the slow sinking pool is constantly produced from *in situ* disaggregation of fast and large sinking particles throughout the water column. Here we further test the two options using size fractionated C/Th ratios at occasions where the contribution of the slow sinking pool has been deemed to be significant.

1) If the slow sinks as it is from the surface ocean, C/Th ratios at depth as will significantly differ. Indeed with increasing depth, particles from the slow sinking pool (small particles) would experience a much longer time in the water column relative to the fast sinking particles (large particles). At a given depth, as the slow sinking pool would spend more time in the water column and the loss of ^{234}Th via decay (Cai *et al.*, 2006) over C would likely be more important as most of the C remineralization happens between 50 and 150m (Maiti *et al.*, 2010a). At depth, this would result in increasing C/Th in the slow sinking pool (small size fractions) and therefore, greater C/Th ratios in the small size fraction.

2) If the slow sinking pool is produced *in situ* from the disaggregation of larger particles, the C/Th ratios would not significantly differ in both types of particles as indicated in (Buesseler et al., 2006).

In Figure 2.2 are presented C/Th ratios in the 1-53 and >53 μm size fractions. At both depth 50 and 150m, the C/Th ratios do not display significant variations in the two size fractions considered (Figure 2.2). Invariant C/Th ratios with size imply that large particles caught in the >53μm likely resulted from the aggregation/disaggregation of the small particles caught in the 1-53 μm as shown in Buesseler *et al*. (2006) their Figure 2. At 150m aggregation of particles is less likely to happen compared to disaggregation as at those depths the remineralization of particles is likely to be important (Maiti *et al.*, 2010a). Also, disaggregation processes, despite of being one of the greatest unknowns that affect marine particles, is deemed to be more important at depth because collision rates between particles decreases with depth (as particle concentrations do) (Burd and Jackson, 2009). Hence, our results suggest that large and small particles were mainly driven by aggregation/disaggregation processes. This has implications for the origin and the dynamics of the slow sinking pool at the PAP site and support hypothesis 2) that the slow sinking pool is rather produced *in situ* from the disaggregation of larger particles.

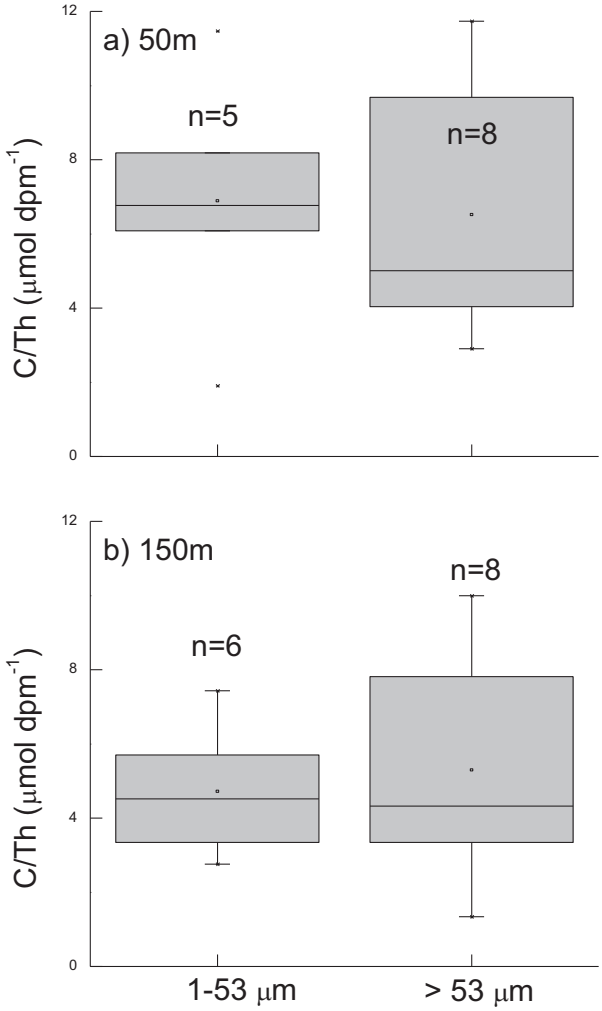

Figure 2.2: Variability of the size fractionated C/Th ratios at a) 50 m and b) 150m depth during D341.

2.3.3 Are size fractionated C/Th ratios always equal at depth when the contribution of the slow sinking pool is important?

Here we test this hypothesis with other published datasets as we did not extensively sample C/Th ratio as a function of depth at the PAP site during D341. As far as we are aware the sites where the relative contributions of slow and fast sinking particles to total POC export have been estimated include the Canaries (Alonso-Gonzalez *et al*., 2010) during the RODA cruises, the North pacific (Aloha and K2 stations) during the

VERTIGO voyages (Buesseler and Lampitt, 2008), at the Dyfamed station in the Mediterranean during the MEDFLUX program (Lee *et al.*, 2009a) and at the PAP site during the D341 cruise (this study). The contribution of the slow sinking pool was important on several occasions, more precisely during sampling periods I and III in the Canaries (June-December 2005 and May-November 2006, respectively) (Alonso-Gonzales *et al*., 2010), at station K2-2 (August 2006, (Trull *et al*., 2008) and at the PAP site during D341 (July 2009, (Riley *et al*., 2012)).

If our hypothesis is true (e.g. the slow sinking pool is produced *in situ* from the disaggregation of larger particles resulting in similar size fractionated C/Th at depth where slow sinking is important), then no clear trend in either size fractionated C/Th ratios should be present. At sites and periods where and when the contribution of slow sinking particles was important (e.g. PI, PIII, and K2-2), the only information on size fractionated C/Th ratios split at 53 µm is that presented here and in Buesseler *et al*., (2009) also examined size fractionation of C/Th ratios in the North Pacific using 51-1 µm (similar to our 1-53 µm size fraction) and 51-350 µm size fraction. Similarly, they did not find clear changes in size fractionated C/Th ratios at each depth sampled. One caveat to this comparison holds in the fact that Buesseler *et al*., (2009) did not used the same size fraction as done in this study. This demonstrates that when the contribution of the slow sinking pool is significant size fractionated C/Th are similar and hence further suggests that the slow sinking pool is rather produced *in situ* from the disaggregation of larger particles.

2.3.4 Weighting for the contribution of small particles to export within the ^{234}Th export model and implications ^{234}Th based global estimate of POC export.

As mentioned in Buesseler *et al*., (2006), particle sinking speed, particles POC concentrations and C/Th ratios are required to obtain a flux weighted estimate of POC. The contribution of each pool of POC is calculated using sinking velocities and POC concentration in each pool as described in Riley *et al.* (2012). We assume that the proportion of the deficit attributable to each size fraction scales with the contribution that each size fraction makes to total flux (see Section 3.2). The rates of the contribution of small and large particles to the flux from Riley *et al*., (2012) are presented in table 2.2 and implemented in the ^{234}Th model to give (equation 2.2):

$$POC\,export_{total} = P\left(FP\left(POC/_{^{234}Th}\right)_{>53} + SP\left(POC/_{^{234}Th}\right)_{53\square 1}\right) \quad (2.2)$$

Where *P* is the ^{234}Th flux (in dpm m^{-2} d^{-1}), and *FP* and *SP* are the contribution fast and slow sinking particles to the total flux respectively (see Table 2.2). Are only used values of C/Th ratios measured at 50 m as contribution to the flux of the slow and fast particles have only been estimated at 50m Riley *et al*., (2012). The results of these calculations are presented in Table 2.2 As expected from equal ratios on both size fractions presented, this method of partitioning flux between two pools gives a mean value of 10.1 ± 3.31 mmol m^{-2} d^{-1} which is not significantly different from that calculated using the method in which the thorium deficit is simply multiplied by a C/Th ratio from the entire pool (>1µm) or by a C/Th ratio from the large and fast particles (Table 2.2). Using the three different methods has thus a limited impact on the overall POC export during D341.

Table 2.2: Export at 50m estimated by partitioning observed deficit into that associated with fast and slow sinking pools (using numbers from Riley *et al*., (2012)). C/Th ratios used are representative of the total pool. These ratios are calculated by summing POC and thorium values from two size fractions summed prior to multiplying by deficit.. Final column is estimate of total export from C/Th >1 µm (e.g $[(POC_{>53} + POC_{1\text{-}53}) / (Th_{>53} + Th_{1\text{-}53})]$).

Station	^{234}Th flux dpm m^{-2} day^{-1}	Relative Contribution to the total flux[a]	Relative Contribution to the total flux[a]	^{234}Th flux dpm m^{-2} day^{-1}	^{234}Th flux dpm m^{-2} day^{-1}	
		fast	slow	fast	slow	
16477	1169	37	63	438.0	731.0	
16523	1048	37	63	392.6	655.4	
16544	1048	37	63	392.6	655.4	
16559	1264	37	63	473.6	790.4	
16583	1009	41	59	413.1	595.9	
16592	2130	19	81	410.2	1719.8	
16659	1394	49	51	688.9)	705.1	
Mean	1295	37	63			
Standard deviation	393	9	9			
	^{234}Th dpm l^{-1}	POC µmol l^{-1}	POC / ^{234}Th µmol dpm^{-1}	^{234}Th dpm l^{-1}	POC µmol l^{-1}	POC / ^{234}Th µmol dpm^{-1}
Station	>53 µm	>53 µm	>53 µm	1-53 µm	1-53 µm	1-53 µm
16477	0.01	0.13	8.9	0.04	0.07	1.91
16523	0.04	0.47	11.74	0.02	0.18	11.47
16544	0.04	0.47	11.74	0.02	0.18	11.47
16559	0.04	0.47	11.74	0.02	0.18	11.47
16583	0.03	0.16	4.91	0.05	0.39	8.19
16592	0.04	0.15	4	0.03	0.18	6.08
16659	0.02	0.09	4.07	0.07	0.48	6.77
Mean	0.03	0.28	8.16	0.04	0.24	8.19
Standard deviation	0.01	0.18	3.73	0.02	0.14	3.61

Table 2.2 (continued)

	POC export >53 µm mmol C m^{-2} day^{-1}	POC export >1 µm mmol C m^{-2} day^{-1}	POC export from weighted thorium mmol C m^{-2} day^{-1}
Station			
16477	2.23	4.64	5.5
16523	12.02	12.22	12.13
16544	12.02	12.22	12.13
16559	14.5	14.74	14.63
16583	8.26	6.93	6.91
16592	12.95	10.49	12.1
16659	9.43	8.56	7.57
Mean	10.2	10.1	10.1
Standard deviation	4.09	3.31	3.42

Based on our results it appears that using only the C/Th of large particles give satisfactory estimates of carbon export during D341. This is not consistent with the expectation of small (and slowly sinking) having surface area and hence high ^{234}Th activities (Buesseler *et al*., 2006). This would have higher C/Th ratios in the large particles. We demonstrate that during D341, small (slow) and large (fast) particles interactions were primarily driven by aggregation/disaggregation processes leading to invariant C/Th ratios in both fractions. Consequently we believe aggregation disaggregation played an important role in setting the size and sinking speed of particles collected beneath the mixed layer during D341.

Also, this has implications for globally integrated ^{234}Th derived POC export estimate. Henson *et al*., (2011) used ^{234}Th derived estimate to build a global estimate of the carbon export. This estimate is approximately twice lower than other (e.g Schlitzer (2004) and Laws et al., (2000)). Laws et al., (2000), used estimate of global carbon export is derived from a linear relationship between observed *f*-ratio and sea surface temperature (SST) (see introduction) while Schlitzer (2004) used an inverse

model matching the strength of the BCP with global nutrients distribution data. One could argue that their result is due to much of the database is based on ignoring export associated with small and slow particles that we now believe to be significant locally (Trull *et al.*, 2008; Alonso-Gonzalez *et al.*, 2010; Riley *et al.*, 2012). However, our attempt to include the contributions of both slow and fast sinking particles yielded to similar results between non-weighted and weighted Th derived POC flux. Furthermore, based on the limited dataset of coupled size fractionated C/Th and contribution of slow and fast sinking pool available, it looks like size fractionated C/Th ratios are invariant with respect to size where the contribution of the slow sinking pool has been deemed to be significant (see section 3.3). On balance we therefore feel that the difference between the large scale estimate of export which Henson *et al*., (2011) made and the other estimates cannot be readily explained by the thorium methodology ignoring the small size fraction, i.e. although the particles sampled for their C/Th ratio may have only been the large ones their C/Th ratios were probably similar to the total pool. The discrepancy between the Henson *et al*. (2011) and Schlitzer (2004) result is probably real. Possible explanations include decoupling of C and N in the upper ocean (Christian *et al*., 1997) since the Schlitzer (2004) result relies on a Redfield ratio to calculate carbon from nitrogen. One potential explanation that in our view merits further investigation is the fate of organic matter which accumulates in the upper ocean over seasonal timescales in both the particulate and dissolved form (Morris and Sanders, 2011). This material (which can account for up to 50% of new production) is clearly new production in the sense that it has not been recycled at the time of sampling, has not been gravitationally exported and which therefore the thorium calculation does not track. Finally the active transport of POC

by zooplankton diel migration (Steinberg *et al*., 2008) that is not taken into account in the Th methodology could also be another possibility.

2.4. Conclusion

We have attempted to better understand the dynamics of the slow sinking pool. We found that the PAP site 1-53µm and >53µm size fractions could represent slow and fast sinking pools respectively, although at the PAP site the use of 10-53µm size fraction to sample the pool of slow sinking particles would have been preferable. Size fractionated C/Th ratios were invariant at the PAP site suggesting a predominance of aggregation/disaggregation processes. Hence, we propose that at the PAP site, the slow sinking pool may have resulted of *in situ* disaggregation of larger sinking particles. In an attempt to implement the slowly settling pool of carbon in the commonly used ^{234}Th technique approach we found that a weighted flux method was not significantly different from that calculated using the method in which the thorium deficit is simply multiplied by a C/Th ratio from the entire pool (>1µm) or by a C/Th ratio from the large and fast particles. Also, this has implications for globally integrated ^{234}Th derived POC export estimate discrepancy berween ^{234}Th derived estimate to build a global estimate of the carbon export and other may not be explained by the exclusion of small and slow particles which we now believe to be significant locally.

Acknowledgements

We are grateful to thank Chris Marsay (NOC) and Bob Head (PML) for sampling and technical support. This research was supported by the CalMarO program (a FP7 Marie Curie initial training network, www.calmaro.eu, European Community, Grant

agreement no. 215157), the NERC programme OCEAN 2025 and project P07-RNM-02567 by Junta de Andalucía (Spain).

3. Insights from a POC and Biominerals Radionuclide Derived Export Study at the Porcupine Abyssal Plain: Implications for the Ballast Effect Theory.

The following chapter has been reproduced from a manuscript currently under review in Deep Sea Research Part I. F.A.C. Le Moigne, M. Villa, R.J. Sanders, C. Marsay, S. Henson and R. García-Tenorio, "Insights from a POC and Biominerals Radionuclide Derived Export Study at the Porcupine Abyssal Plain: Implications for the Ballast Effect Theory".

Data contribution: All samples were taken and analysed by the author during D341 (P.S.O.: Richard Sanders). ^{234}Th analysis, *in situ* pumps processing and BSi analysis were undertaken by the author. ^{210}Po and ^{210}Pb analysis was processed by Maria Villa. PELAGRA were deployed and processed by Chris Marsay (NOC). POC and PIC samples were prepared by the author, then respectively measured by Bob Head (PML) and Darryl Green (NOC). Paul Morris (WHOI) helped with ^{234}Th analysis and cruise mobilization. Stephanie Henson produced the remote sensing data.

Abstract

The simultaneous estimation of particulate organic carbon (POC), particulate inorganic carbon (PIC) and biogenic silica (BSi) export fluxes has proven to be essential in the study of carbon export due to the hypothesized role of biominerals in the sinking of organic particles. This paper presents results from one of the first attempts to measure POC, PIC and BSi downward fluxes from the surface ocean using

^{234}Th-^{238}U, ^{210}Po-^{210}Pb disequilibria and drifting sediments trap synchronously at the Porcupine Abyssal Plain time-series site during summer 2009. The combined use of the three techniques allowed us to analyze their suitability not only for POC flux estimation, but also for PIC and BSi fluxes. POC and PIC export based on Th was higher than POC and PIC export based on Po, whilst the drifting sediment traps produced the lowest export estimates. This emphasizes that the integration time of each technique relative to the seasonal cycle of primary production must be taken into account when estimating export fluxes. To better understand differences between ^{234}Th derived POC (biomineral) export and ^{210}Po derived POC (PIC) export, the ratios POC (PIC)/radionuclide in small and large particles were studied. The differences are ascribed to their biogeochemical behaviour. In addition, the contribution of smaller (1-53µm) particles to flux is also considered in order to explain the differences in derived fluxes, as we find that slow sinking particles may also have contributed to the export flux. When ratios in small particles are used, differences between ^{234}Th and ^{210}Po derived POC (PIC) fluxes are reduced. Notwithstanding this, further analyses are required to determine the actual implication of slow sinking particles in ^{234}Th and ^{210}Po-derived fluxes. On the contrary, BSi fluxes were low and the differences between methods were reduced whichever particle size fraction was used. Finally, we contribute to the on-going refinement of the ballast hypothesis, by confirming recent observations that link ballasting with the fast sinking pools in the surface ocean.

3.1 Introduction

The concept of the biological carbon pump (Eppley and Peterson, 1979) emphasises the importance of oceanic primary production in the global carbon cycle. Approximately 5 to 10 GTC.yr^{-1} are exported from the surface ocean into the deep

ocean interior (Falkowski *et al.*, 1998; Henson *et al.*, 2011). This coupling of oceanic production and export removes CO_2 from the atmosphere and contributes to the buffering of the global climate system. Without the oceanic biological carbon pump, atmospheric CO_2 levels would be almost twice as high as current concentrations (Sarmiento and Toggweiler, 1984). The mode by which carbon is transferred downwards is therefore a key issue in the context of global climate change.

Carbon export occurs via diverse processes including the sinking of dead phytoplankton cells, aggregates and zooplankton faecal pellets, with considerable spatial variability in the relative importance of these processes. The major processes affecting the efficiency of carbon export can be summarised as follows (Banse, 1990; De La Rocha and Passow, 2007): (1) the level of primary production; (2) the speed at which organic carbon containing particles (marine snow) sink and (3) the rate of particulate organic carbon (POC) decomposition. Of specific relevance to (2) is the potential increase in settling velocity mediated by the incorporation of biominerals including calcium carbonate and opal into aggregates which may increase their density - the so-called ballast effect (Klaas and Archer, 2002; Sanders *et al.*, 2010). Numerous techniques have been used to address the rate of POC export and the processes which control it. Here we focus on the application of two radiotracer pairs and drifting neutrally buoyant sediment traps to examine particle export processes at the Porcupine Abyssal Plain (PAP) site in summer 2009.

^{234}Th and ^{210}Po

The short-lived, radioactive isotope Thorium-234 (^{234}Th, half-life: $T_{1/2}$=24.1d) has been widely used as a tracer of particle export in aquatic systems (Buesseler *et al.*, 1992; Van der Loeff *et al.*, 2006; Waples *et al.*, 2006). The ^{234}Th technique is based

on measuring the deficit between ^{234}Th and ^{238}U ($T_{1/2}$=4.47.10^{9}y). Naturally occurring ^{238}U is conserved in seawater and occurs in proportion to salinity in well oxygenated environments (Ku *et al.*, 1977; Chen *et al.*, 1986). Its daughter, ^{234}Th, is particle reactive and is scavenged from surface waters as particles sink. It creates a deficit as the secular equilibrium, that occurs between thorium and uranium in a closed system, is disturbed. The measured deficit of ^{234}Th is often combined with the ratios of POC to particulate ^{234}Th (Tsunogai and Minagawa, 1976) to estimate POC export to the deep ocean (Buesseler *et al.*, 1992; Rutgers Van Der Loeff *et al.*, 1997; Cochran and Masque, 2003; Buesseler *et al.*, 2006).

Alternatively, particle reactive Lead-210 (^{210}Pb, $T_{1/2}$=22.3y) and Polonium-210 (^{210}Po, $T_{1/2}$=138.4d) can be used as tracers of particle cycling in the surface ocean (e.g. (Cochran and Masque, 2003)). The ^{210}Pb/^{210}Po pair has a different behaviour compared to ^{234}Th/^{238}U in terms of the mechanisms by which they bind to particles in the ocean. ^{210}Pb only adsorbs to particle surfaces, whereas ^{210}Po is additionally biologically incorporated intracellularly by some species of phytoplankton and bacteria entering the biological cycle of living organisms in a manner similar to sulphur. (Fisher *et al.*, 1983; Cherrier *et al.*, 1995; La Rock *et al.*, 1996; Stewart and Fisher, 2003a, b). As a result, ^{210}Po can be accumulated within the food web and thus is also assimilated by zooplankton (Heyraud *et al.*, 1976; Fowler and Knauer, 1986). Thus, when biological activity is strong a disequilibrium between the ^{210}Pb/^{210}Po pair occurs which can be used to estimate particle export in a similar way to the usage of the ^{234}Th/^{238}U disequilibrium.

Several studies have used both ^{234}Th and ^{210}Po to estimate particle flux (see reviews by Verdeny *et al.*,(2009) and Stewart *et al.*, (2010)). These reviews focus on the combined and synchronous use of both tracer pairs to derive better estimates of

POC export by improving understanding of particle flux, remineralization and also discuss the advantages and limitations of natural radionuclide tracers (Stewart *et al.*, 2010). Due to their different half-lives, particle affinity, formation processes and upper ocean residence times the combined use of both tracers offers great advantages for studying downward carbon, biomineral and total mass fluxes (Verdeny *et al.*, 2009).

There is a trend for ^{234}Th based estimates of POC flux to be higher than ^{210}Po derived POC fluxes when flux is high (Verdeny *et al.*, 2009). This is likely due to the differences in residence time and the amounts of lithogenic material present (Friedrich and van der Loeff, 2002; Verdeny *et al.*, 2009). In mid to low flux regions, the differences between fluxes obtained with both tracers decrease to near zero (Verdeny *et al.*, 2009).

The major difference between the ^{210}Pb/^{210}Po and ^{234}Th/^{238}U techniques are the timescales over which they integrate particle export: approximately 1 month for ^{234}Th, whilst ^{210}Pb/^{210}Po can assess particulate carbon export on timescales from several months to a year. The latter is set by the half-life of ^{210}Po, 138.4 days, which is similar to the time scale over which carbon biogeochemistry turnover occurs of mesoscale eddies for instance (Verdeny *et al.*, 2008; Verdeny *et al.*, 2009).

The second main difference between those two tracers is their particle affinities and biogeochemical behaviour (Verdeny *et al.*, 2009) as discussed above. These differences mean that ^{210}Po has a longer residence time in the upper ocean than ^{234}Th as it is more efficiently recycled than organic matter (Stewart *et al.*, 2007b). In addition ^{234}Th traces the total mass flux well whereas the strong biological affinity of Po implies that ^{210}Po is recycled more efficiently and it traces POC export well. This divergent behaviour provides insights into the nature of the particles being exported

(Friedrich and van der Loeff, 2002; Cochran and Masque, 2003; Verdeny *et al.*, 2009; Stewart *et al.*, 2010). Large (>50 μm) particles are often considered to dominate rapidly settling particles (Bishop *et al.*, 1977). However, slow sinking particles may also contribute significantly to export (Alonso-Gonzalez *et al.*, 2010).

Here we present POC and biomineral export fluxes from the PAP site in the North Atlantic (49N; 16.5W). We *i*) estimate C export using ^{210}Po, ^{234}Th, tracers and sediment traps to better understand the differences in the biogeochemical behaviour of the two radionuclides pairs; *ii*) address the suitability of the ^{210}Po/^{210}Pb method to estimate biomineral fluxes. Also, we examine the association of ^{234}Th, ^{210}Po and ^{210}Pb with POC, PIC and BSi content and its implications for understanding the differences between the two methods (e.g. contribution of slow sinking particles) and finally *iii*) to discuss the implications of this dataset for our current understanding of the ballast effect.

3.2 Material and methods

3.2.1 Study area

The PAP time-series site is approximately 900 km west of Brest, France and 600 km southwest of the Fastnet Rock, Ireland (Figure 3 1). The PAP site is considered to be representative of the open North-East Atlantic ocean and is not influenced by coastal and shelf processes (Lampitt *et al.*, 2008). Much important research has been conducted at or close to the PAP site since 1989 when the North Atlantic Bloom Experiment (Ducklow and Harris, 1993) was conducted nearby (approximately 350 km to the southwest). The PAP station falls within the North Atlantic Drift province identified by Longhurst, (1991).

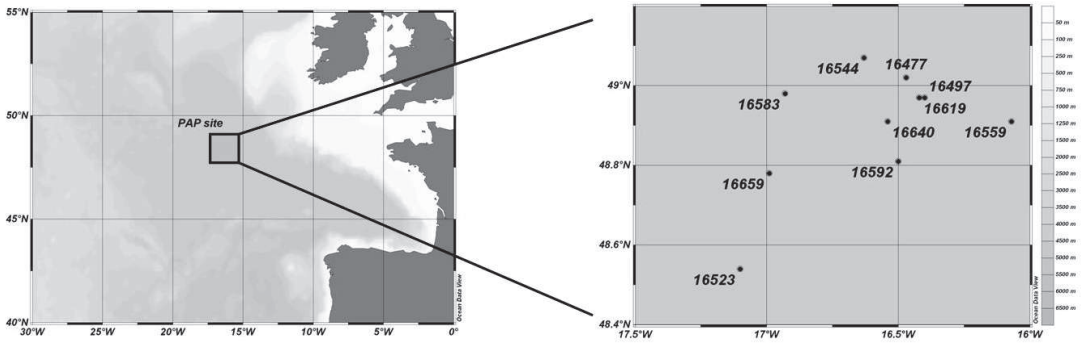

Figure 3.1: PAP site position and bathymetry map of the sampling area showing the major process stations sampled for radionuclides. Station 16559 was not sampled for $^{210}Po/^{210}Pb$.

3.2.2 Sampling strategy

Sampling took place from 13th July to 10th August 2009 on board *RRS Discovery* cruise D341. Figure 3.1 shows the study area and the station locations, with station numbers referring to the *RRS Discovery* station numbering system. Discrete water samples were collected using a stainless steel sampling rosette equipped with 24x20L Niskin® bottles and a CTD Seabird® sensor package. Samples for total ^{234}Th were taken from 10 depths between 0 and 500 m, with the highest resolution in the upper 100m. 10 L water samples were collected into carboys previously cleaned with MilliQ water and rinsed with sample. To check the accuracy of the method, triplicate samples were taken from 2000 m.

For total ^{210}Po and ^{210}Pb analysis, samples were taken from 10-15 depths from 0 to 800 m, with the highest resolution in the upper 150 m of the water column. 5L of water was collected in previously acid-rinsed, MilliQ-cleaned carboys that were pre-rinsed with sample. Duplicate samples were taken at various depths to check the reproducibility of the procedure.

3.2.3 Total ^{234}Th analysis

Total ^{234}Th was extracted from water samples using a medium-volume technique based on (Rutgers Van Der Loeff *et al.*, 1997). Three drops of 25% NH_3 and 125 µL of 60 $g.L^{-1}$ $KMnO_4$ were added and mixed, followed by 50 µL of 400 $g.L^{-1}$ $MnCl_2.4H_2O$ to form a MnO_2 precipitate, which scavenges ^{234}Th and other radionuclides while leaving its parent ^{238}U in the dissolved phase. Before adding reagents, samples were rendered alkaline with three drops of NH_3, the MnO_2 precipitate being stable only at alkaline pH. The precipitate was allowed to accumulate and settle for about 8 h before being filtered onto 142-mm diameter polycarbonate (Millipore) 0.8 mm pore size filters. The extraction yield (Van der Loeff *et al*., 2006) was checked by a second precipitation made with 10 samples processed in the same way as normal samples. The difference of ^{234}Th activity measured on the first and second precipitation was used to work out the extraction yield (98 ± 3 % during D341, so 100% extraction yield can be assumed within the uncertainty). This procedures has been successfully tested and compared to some of others institutions as presented by Maiti *et al.*, (2010b).

Filters were dried for 24 - 48 hours in Petri dishes, folded in a reproducible and consistent way into squares of 18×18mm, wrapped in Mylar foil and then counted for ß activity on a low level beta GM multicounter system (Model RisØ GM-25-5A) for ^{234}Th activity. The first counts were made straight after folding on board the ship. The second counts took place 1 month after the first, and a third and final counting was undertaken after 6 months (>6 ^{234}Th half-lives) to allow background correction. More details of the procedure can be found in Morris *et al.*, (2007).

^{238}U activity (A_U, dpm kg^{-1}) was calculated as $A_U = 0.0686 \times$ salinity, based on the average uranium concentration in seawater (of 3.238 ng g^{-1}) normalised to a salinity of 35 (Chen *et al.*, 1986). The uncertainty in the ^{238}U-salinity relationship was estimated by Chen *et al.* (1986) to be 3.3%.

3.2.4 Total ^{210}Po and ^{210}Pb analysis.

The radiochemical procedure was described in detail elsewhere (Masque *et al.*, 2002; Verdeny *et al.*, 2008; Villa *et al.*, 2009; Cutter *et al.*, 2010). In brief, 5 liter seawater samples were acidified to pH ~ 2 with HNO_3 immediately after collection. They were then spiked with ^{209}Po ($T_{1/2}$=102 yr) and stable Pb^{2+}, as internal tracers, and carrier Fe^{3+}. After 8 hours, NH_3 is added to allow $Fe(OH)_3$ to precipitate and to scavenge ^{210}Po and ^{210}Pb. The precipitate was left to settle down to a final volume of 250ml in HDPE bottles. The radiochemical separation of ^{210}Po from ^{210}Pb and their measurement was undertaken at CITIUS (Centro de Investigación, Tecnología e Innovación, Universidad de Sevilla) laboratory at the Universidad de Sevilla. Iron hydroxide was dissolved in concentrated hydrochloric acid, heated to dryness and re-dissolved in 1M HCl. Ascorbic acid was added to reduce Fe^{+3} to Fe^{2+} and ^{210}Po self-deposited onto a silver disk while heating (80ºC) and stirring for at least eight hours. ^{210}Po Activity was measured on these disks, counting time lead to uncertainties lower than 7%, ^{210}Po was calculated from these counts after ^{210}Pb determination. Afterwards, a second plating was done to remove any traces of Po and to ensure that only ^{210}Pb remained in the solution. The solution was ^{209}Po-spiked a second time and the samples were stored to allow ^{210}Po in-growth from ^{210}Pb. After at least 6 months, ^{210}Po and ^{209}Po were self-deposited and ^{210}Po activity calculated. Counting was done using alpha detector PIPS type (Canberra) and background corrections were done.

^{210}Pb activity was inferred from this ^{210}Po concentration after the subsequent decay corrections to the sampling day. Recoveries for Pb were obtained by ICP-MS measurement. Once ^{210}Pb determined, the initially measured ^{210}Po can be corrected due to the subsequent decay of ^{210}Pb into additional ^{210}Po prior to ^{210}Po-^{210}Pb separations. ^{210}Po measurements were also decay corrected from the measurement to plating, as well as from plating to sampling. ^{210}Bi and ^{210}Po in-growth were both considered in the ^{210}Pb decay corrections. Contamination due to ^{210}Pb-^{210}Po present in the lead carrier was subtracted. Activity of the internal tracer ^{209}Po was decay corrected from the reference date to the measurement date. The second plating was performed to remove any traces of polonium before storage as some of the initial ^{209}Po tracer could remain in the solution. This possibility was tested and less than 5% of the initial tracer was found in the cleaning disk. Nevertheless, to neglect over estimation of the radiochemical yield in the measurement of the ^{210}Pb, the amount of ^{209}Po added after cleaning is an order of magnitude higher than the one added on board. The minimum detectable activity of ^{210}Po and ^{210}Pb measurement (5 days counting of sample) was 0.2 cpm/100L. Replicate samples were collected to ensure the precision of the results.

3.2.5 Sampling and analysis of particulate matter.

Small (1-53 μm) and large (>53 μm) particles were sampled by filtering large volumes of sea water (1000 - 2500 L) through 53 μm and 1 μm (293mm diameter) NITEX® nylon mesh filters, using *in situ* pumps (Stand Alone Pumping Systems– SAPS, Challenger Oceanic ®). The pumps were deployed at 50 m and 150 m, corresponding to 10 and 110 m below the seasonal thermocline. Samples recovered on the mesh were resuspended using thorium-free filtered seawater and split into

fractions for subsequent measurements using a Folsom® splitter. A split (corresponding to ¼ of the total) was filtered onto precombusted 25mm GF/F filters and stored frozen for subsequent POC/N analysis as described in (Poulton *et al.*, 2006). The second split (corresponding to ¼ of the total) was filtered onto 142mm diameter 0.8 mm pore size polycarbonate filters for direct ^{234}Th analysis. Splits (corresponding to ¼ of the total) for ^{210}Po analysis were filtered onto 25mm GF/F filters, while splits for PIC and BSi (corresponding to $^{1}/_{8}$ of the total) were filtered through 25mm polycarbonate membranes and frozen for analysis onshore. ^{210}Po and ^{210}Pb in the 53 µm and 1µm fractions filtered onto GF/F filters were analysed following the two deposition-steps method described above. In this case, filters were fully digested in a mix of HNO_3, HCl and HF acids. Procedurials blanks values are given in appendix A.1, A.2 and A.3.

3.2.6 ^{234}Th and ^{210}Po models for export fluxes

Export rates of both ^{234}Th and ^{210}Po from the surface ocean were calculated using a one-box model (Coale and Bruland, 1987; Buesseler *et al.*, 1992; Buesseler *et al.*, 1998; Cochran *et al.*, 2000; Benitez-Nelson *et al.*, 2001; Cochran and Masque, 2003; Savoye *et al.*, 2006; Verdeny *et al.*, 2008).

Assuming steady state condition, $\frac{\partial A_2}{\partial t} = 0$, and no supply of ^{234}Th(^{210}Po)

related to physical processes, the ^{234}Th(^{210}Po) flux (dpm m^{-2} d^{-1}), called *P* is calculated through the water column as in equation 3.1,

$$P = \lambda \sum_{z=0}^{z=h} (A_2 - A_1) \cdot dz \qquad \text{(Eq 3.1)}$$

A_1 is the total parent activity concentration (dpm m^{-3}) for ^{238}U or ^{210}Pb; A_2 is the total ^{234}Th or ^{210}Po activity concentration (dpm m^{-3}); λ is the decay constant of the daughter (d^{-1}); and P is the loss of the daughter due to sinking particles (dpm m^{-3} d^{-1}). Previous ^{234}Th studies at the same site have ignored the advection/diffusion term (Thomalla *et al.*, 2006; Lampitt *et al.*, 2008; Thomalla *et al.*, 2008) as I do here. The effects of advection in ^{210}Po flux calculations are more complex, because the longer half-life of ^{210}Po (138 days) means that measurements are more strongly impacted in areas influenced by lateral advection and upwelling of deep waters (Verdeny *et al.*, 2008). Advection effects have been neglected in this case because the nature and origin of the water bodies have to be thouroughly examined to satisfy a realistic representation of the "advection diffusion" parameter in the ^{210}Po export model. Unfortunately, these features have not been extensively studied during D341. POC, PIC and BSi export estimates use ratios of POC, PIC or BSi to particulate ^{234}Th (POC:Th, PIC:Th, BSi:Th), in µmol dpm^{-1}, (or ratios to Po) multiplied by the $^{234}Th(^{210}Po)$ flux at each station.

3.2.7 PELAGRA drifting sediment traps

The PELAGRA (Particle Export measurement using a LAGRAngian trap) sediment trap module is built around an APEX float (Webb Research Corporation, USA). It is a neutrally buoyant platform with active buoyancy control to maintain the instrument at a level of constant pressure or density. Horizontal flow across the collection funnels is presumed to be negligible owing to the fact that the trap is neutrally buoyant (Salter *et al.*, 2007; Lampitt *et al.*, 2008). During this cruise, PELAGRA traps were deployed between 50 and 200m at the PAP site. The sampling strategy is described in Table 3.1. Splits of trap samples were analyzed for POC, PIC and BSi as described above. A full

description of the deployment strategy and analysis procedures used during cruise D341 can be found in Marsay *et al.* (2011).

Table 3.1 : PELAGRA trap numbers, sampling time, depths and sampling duration during cruise D341.

PELAGRA trap numbers	Deployment depth (m)	Sampling date and time	Sampling duration (in hours)
P2-1	150	15/07/2009 06:30	48
P2-2	50	20/07/2009 01:00	132
P2-3	50	29/07/2009 09:00	76
P5-3	50	29/07/2009 09:50	76
P7-3	200	29/07/2009 10:40	76
P2-4	50	04/08/2009 12:00	48
P4-4	180	04/08/2009 12:24	48

3.3 Results

3.3.1 Biogeochemical conditions

During sampling, a total of 10 process stations were occupied and sampled for ^{234}Th and 9 for ^{210}Po/ ^{210}Pb (Figure 3.1, Table 3.1 and 3.2). Chlorophyll-*a* derived from satellite data (MODIS, 8 days composite data, averaged on a 1º box centred around the PAP site) displayed two peaks prior to the cruise, one in mid May (0.9 mg chl-*a* m^{-3}) followed by a second peak in mid June (0.6 mg chl-*a* m^{-3}) (Figure 3 2). Primary productivity (PP) calculated using the VGPM algorithm (Behrenfeld and Falkowski, 1997) showed a typical pattern of increasing PP over the productive season reaching a peak in late June (2000 mg C m^{-2} d^{-1}) (Figure 3.2). After this peak, PP decreased gradually until the end of the year. PIC concentrations (calculated using the algorithm described in Balch *et al.*, (2005) showed a peak in mid may (6×10^{-4} moles m^{-3}), matching the Chl-*a* trend (Figure 3 2). After May, PIC concentrations remained quite high but followed no particular trend throughout the summer. The offset in time observed between peaks the standing stocks in Chl-*a* (and PIC) and PP is explained by

the algorithm calculation method including Chl-*a*, sea surface temperature (SST) and light to estimate PP. The offset is due to interaction between these terms. The phytoplankton community was composed of a mix of silicifying and calcifying phytoplankton, comparable to previous cruises at the site (Painter *et al.*, 2010a; Painter *et al.*, 2010b). Aggregates were abundant at the site, and sinking particles included radiolarian, acantharian and foraminiferal test (Riley *et al.*, 2012).

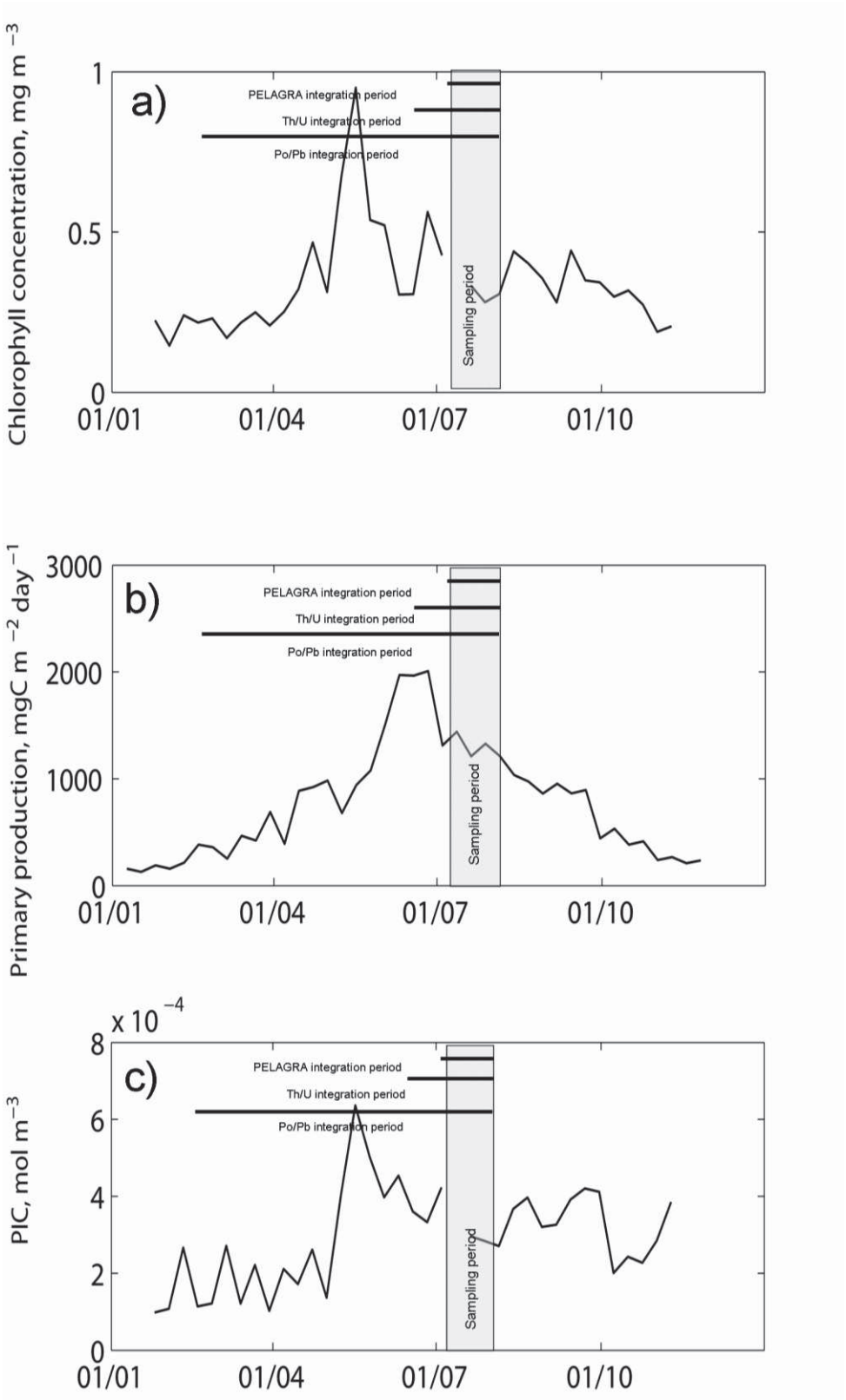

Figure 3.2: Chlorophyll-a concentration (MODIS, 8 day composite data, centered around the PAP site), primary productivity (PP: calculated using the VGPM algorithm

Behrenfeld and Falkowski, 1997) and PIC concentration (calculated using the algorithm described in Balch *et al.* 2005) in 2009

Table 3.2: Station ID, sampling time, position and samples taken for ^{234}Th and ^{210}Po/^{210}Pb during cruise D341.

Station ID	Date	Julian day	Latitude	Longitude	Depth range for ^{234}Th	Number of samples for ^{234}Th	Depth range for ^{210}Po/^{210}Pb	Number of samples for ^{210}Po/^{210}Pb
16477	13/07/2009	194	49.02 N	16.47 W	5-400m	7	5-1000m	13
16497	16/07/2009	197	48.97 N	16.40 W	5-750m	10	5-1000m	11
16523	20/07/2009	201	48.54 N	17.10 W	5-350m	10	5-1000m	15
16544	23/07/2009	204	49.07 N	16.63 W	5-400m	10	5-1000m	16
16559	24/07/2009	205	48.91 N	16.07 W	5-400m	10	-	-
16583	29/07/2009	210	48.98 N	16.93 W	5-400m	10	5-400m	10
16592	31/07/2009	212	48.81 N	16.51 W	5-600m	10	5-600m	10
16606	01/08/2009	213	48.67 N	16.57 W	2000m	3	-	-
16619	03/08/2009	215	48.97 N	16.40W	5-400m	9	5-1000m	16
16640	06/08/2009	218	48.91 N	16.54 W	5-400m	10	5-400m	10
16659	08/08/2009	220	48.78 N	16.99 W	5-400m	10	5-1000m	15

3.3.2 ^{234}Th and ^{210}Po export fluxes

Downward ^{234}Th and ^{210}Po fluxes (dpm m^{-2} d^{-1}) calculated at two depths (50 and 150m) using Eq. 3.1. for each station are shown in Table 3.3 and Figure 3.3. 50m and 150m were chosen as integration depths for ^{234}Th and ^{210}Po based on *in situ* pumps deployment depths based on the fact that total ^{234}Th activity profiles display lower limits of scavenging between those two depths (Figure 3 3). 150m ^{234}Th fluxes ranged from 440 dpm m^{-2} d^{-1} (at station 16640) up to 2035 dpm m^{-2} d^{-1} (at station 16544) while 50m-integrated ^{234}Th fluxes ranged from 309 dpm m^{-2} d^{-1} (at station 16640) to 2130 dpm m^{-2} d^{-1} (at station 16592) (Table 3.3).

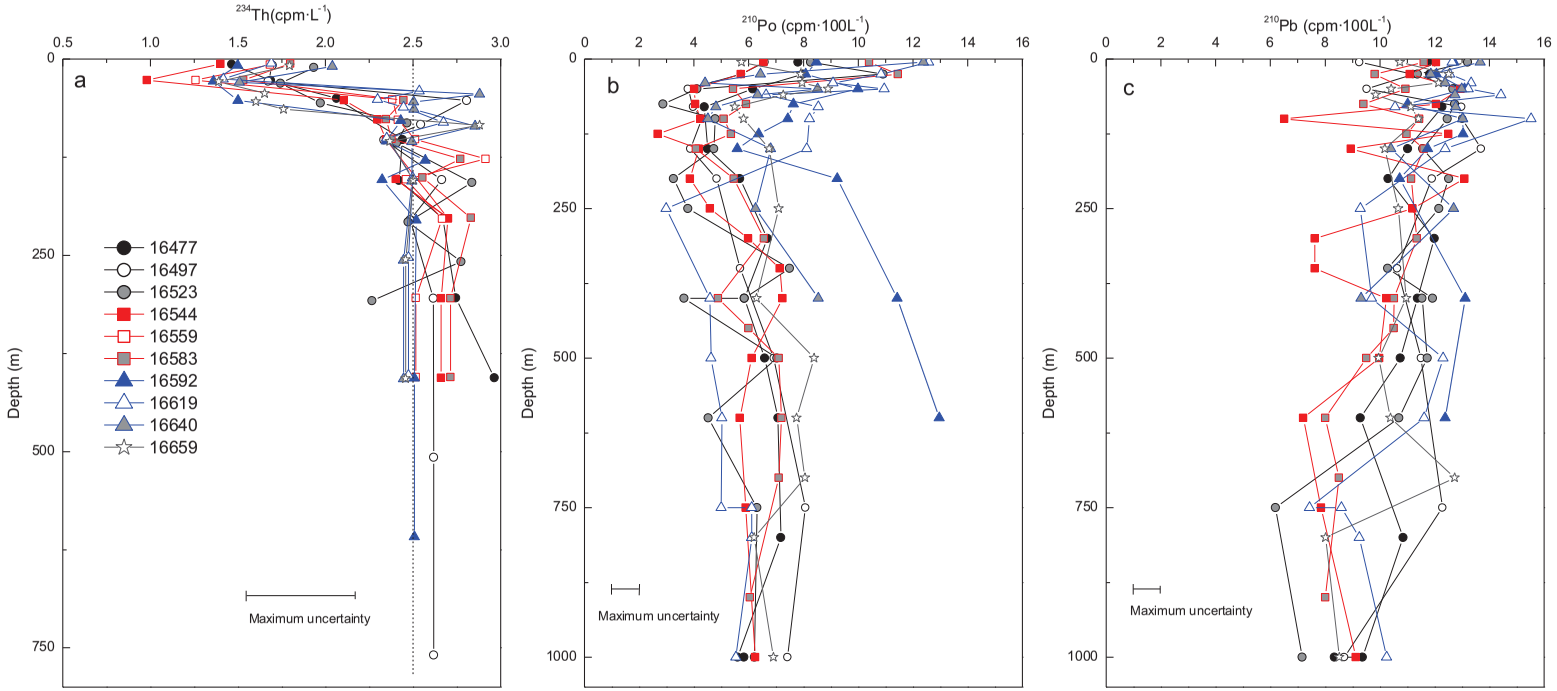

Figure 3.3: (a) ^{234}Th activity (in cpm l^{-1}), (b) ^{210}Po activity (in cpm 100 l^{-1}), (c) ^{210}Pb activity (in cpm 100l^{-1}), (d) ^{234}Th:^{238}U ratio, (e) ^{210}Po:^{210}Pb ratio versus depth. Symbols are given in panel (a) of the figure

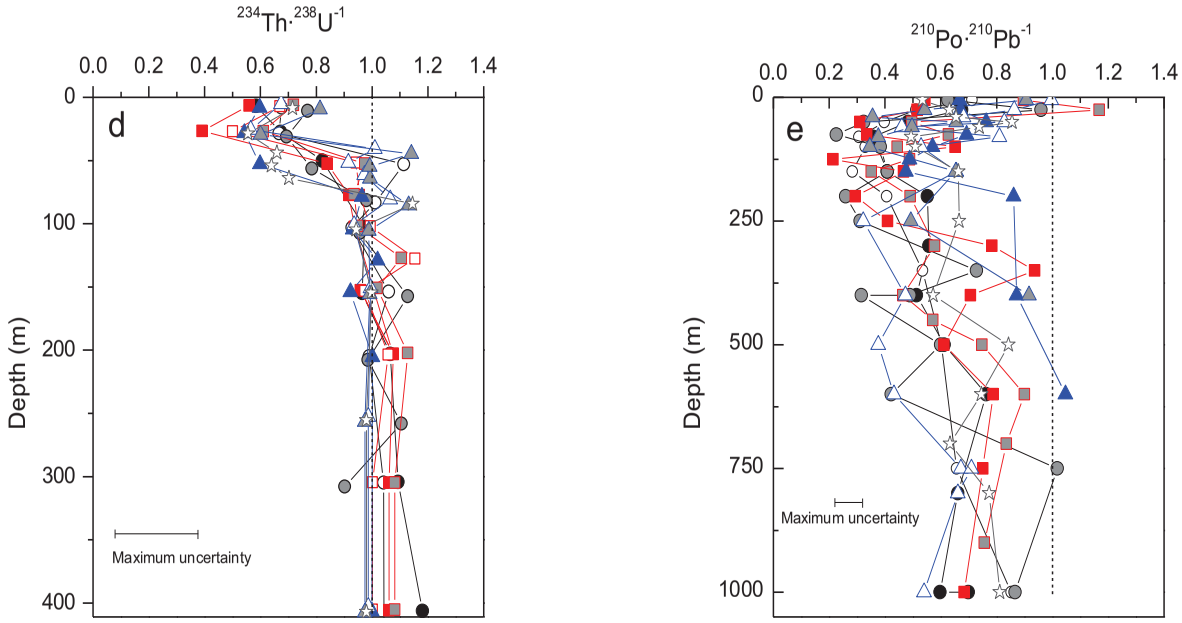

Figure 3.3: (continued)

Table 3.3: ^{234}Th and ^{210}Po export fluxes calculated with the steady state one-box model at two different integration depths. The error is the propagated analytical error.

Station ID	Latitude	Longitude	Integration depth (m)	^{234}Th flux (dpm m^{-2} d^{-1})	^{234}Th flux error	^{210}Po flux (dpm m^{-2} d^{-1})	^{210}Po flux error
16477	49.02 N	16.47 W	150	1560	234	54.9	5.4
16497	48.97 N	16.40 W	150	774	116	65.9	4.7
16523	48.54 N	17.10 W	150	1322	198	59.0	4.6
16544	49.07 N	16.63 W	150	2035	305	55.1	3.5
16559	48.91 N	16.07 W	150	1405	211	-	-
16583	48.98 N	16.93 W	150	1193	179	41.2	4.2
16592	48.81 N	16.51 W	150	1624	244	43.3	4.6
16619	48.97 N	16.42 W	150	1501	225	40.0	6.2
16640	48.91 N	16.54 W	150	440	66	58.1	6.1
16659	48.78 N	16.99 W	150	1676	251	43.8	4.7
16477	49.02 N	16.47 W	50	1169	175	16.1	2.7
16497	48.97 N	16.40 W	50	867	130	15.6	2.3
16523	48.54 N	17.10 W	50	1048	157	15.0	2.3
16544	49.07 N	16.63 W	50	1048	157	21.3	2.2
16559	48.91 N	16.07 W	50	1264	190	-	-
16583	48.98 N	16.93 W	50	1009	151	7.4	2.3
16592	48.81 N	16.51 W	50	2130	320	11.9	3.0
16619	48.97 N	16.42 W	50	1308	196	4.8	1.9
16640	48.91 N	16.54 W	50	309	46	14.0	2.1
16659	48.78 N	16.99 W	50	1394	209	12.1	1.7

150m-integrated ^{210}Po fluxes ranged from 40.03 dpm m^{-2} d^{-1} (at station 16619) up to 65.85 dpm m^{-2} d^{-1} (at station 16497), while 50m-integrated ^{210}Po fluxes ranged from 4.84 dpm m^{-2} d^{-1} (at station 16619) up to 21.30 dpm m^{-2} d^{-1} (at station 16544). At 150m, ^{234}Th fluxes averaged 1300 ± 500 dpm m^{-2} d^{-1}, while at 50m they averaged 1100 ± 460 dpm m^{-2} d^{-1}. For ^{210}Po, at 150m the average was 50 ± 10 dpm m^{-2} d^{-1}, and 13 ± 5 dpm m^{-2} d^{-1} at 50m. The standard deviation of thorium is larger indicating significant spatial variability despite the survey area being relatively small. On the contrary, for ^{210}Po, the low standard deviation of the averages emphasizes the low variability of ^{210}Po fluxes between stations.

3.3.3 Particulate matter to radionuclide ratios

Particle matter to radionuclide ratios are shown in Tables B.1, B.2,and B.3 (Appendix B). POC/^{234}Th ratios were between 1.34 (150 m, 53μm) and 11.74 (50 m, 53μm) μmol dpm^{-1}; PIC/^{234}Th ratios were between 0.01 (50 m, 53μm) and 1.37 (50 m, 1μm) μmol dpm^{-1} and BSi/^{234}Th ratios were between 0.005 (150 m, 53μm) and 0.087 (50 m, 53μm) μmol dpm^{-1}. POC/^{210}Po ratios were between 16.22 (50 m, 53μm) and 319.79 (50 m, 1μm) μmol dpm^{-1}; PIC/^{210}Po ratios were between 1.00 (150 m, 1μm) and 19.37 (150 m, 1μm) μmol dpm^{-1}; and BSi/^{210}Po ratios were between 0.001 (50 m, 53μm) and 0.089 (150 m, 1μm) μmol dpm^{-1}. Figure 3.4 shows the ratios of POC, PIC or BSi:radionuclide in particles >53μm versus those in particles 1-53 μm, collected at 150m and 50m depths.

Clear trends can be seen for ^{210}Po; at both depths the ratios of POC/^{210}Po, PIC/ ^{210}Po and BSi/ ^{210}Po are higher in particles 1-53 μm than in particles >53μm. The trend is not so clear for ^{234}Th. Regardless of depth and particle size, POC/^{234}Th values are scattered around the 1:1 line. We also studied these ratios for ^{210}Pb, also particle reactive. They generally followed the same trend as ^{234}Th for POC and BSi ratios and as ^{210}Po for PIC ratios (Table B.1, B.2, B.3 and Figure 3.4).

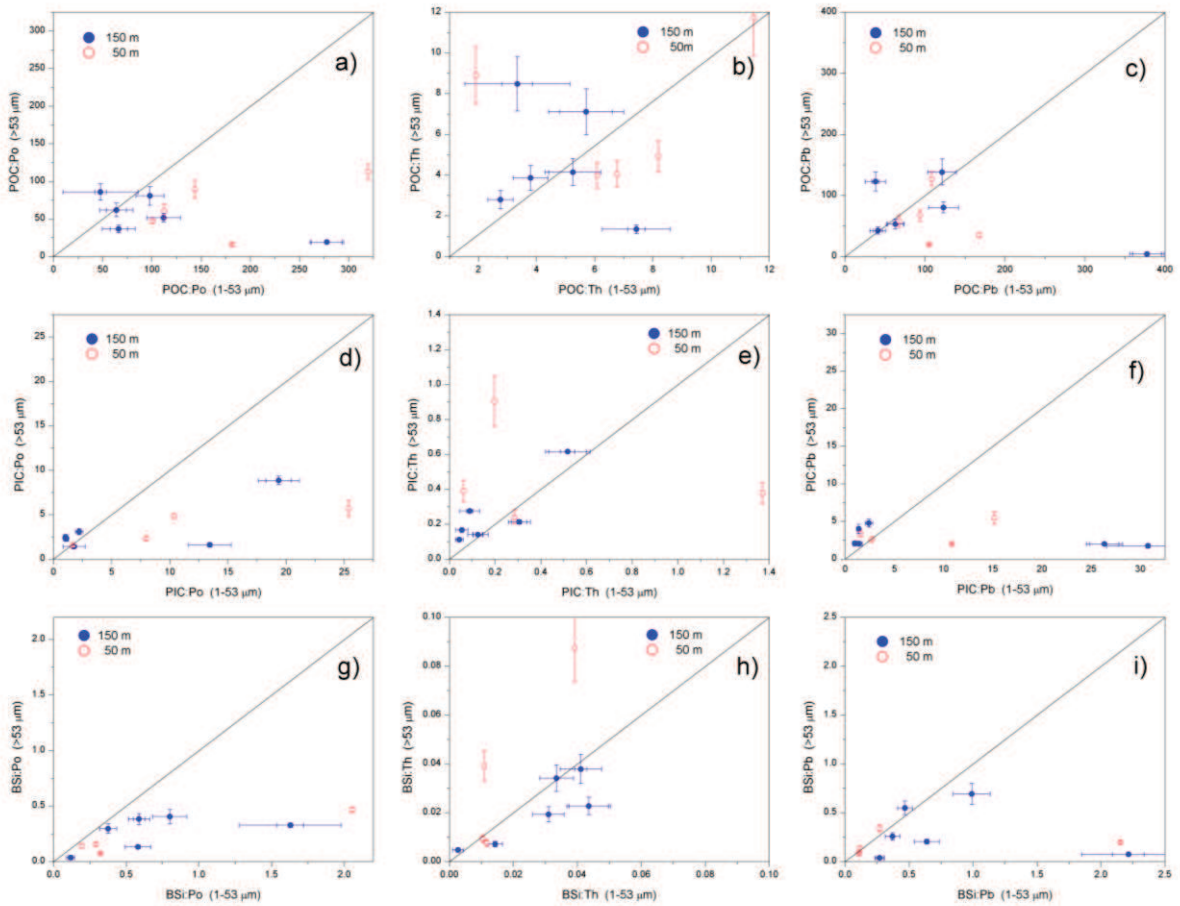

Figure 3.4: Particulate matter to radionuclide ratio (µmol:cpm) in >53 µm versus 1-53 µm particles collected at 50 and at 150 m (a) POC:Po (b) POC:Th (c) POC:Pb (d) PIC:Po (e) PIC:Th (f) PIC:Pb (g) BSi:Po (h) BSi:Th (i) BSi:Pb. The 1:1 line is depicted in the figure

3.3.4 Carbon fluxes.

To obtain POC, PIC and BSi fluxes, downward ^{234}Th (^{210}Po) fluxes are multiplied by the ratio of POC (or PIC, BSi) to ^{234}Th (^{210}Po). We measured this ratio in two size classes (1-53 μm and >53μm) and at two depths. The ^{234}Th-derived POC export (Th-POC export) at 150 m was between 1.69 mmol m^{-2} d^{-1} (at station 16640) and 17.27 mmol m^{-2} d^{-1} (station 16544) (Table B.1 and Figure 3.5). ^{234}Th-POC fluxes at 50m ranged from 3.8 mmol m^{-2} d^{-1} to 14.3 mmol m^{-2} d^{-1}.

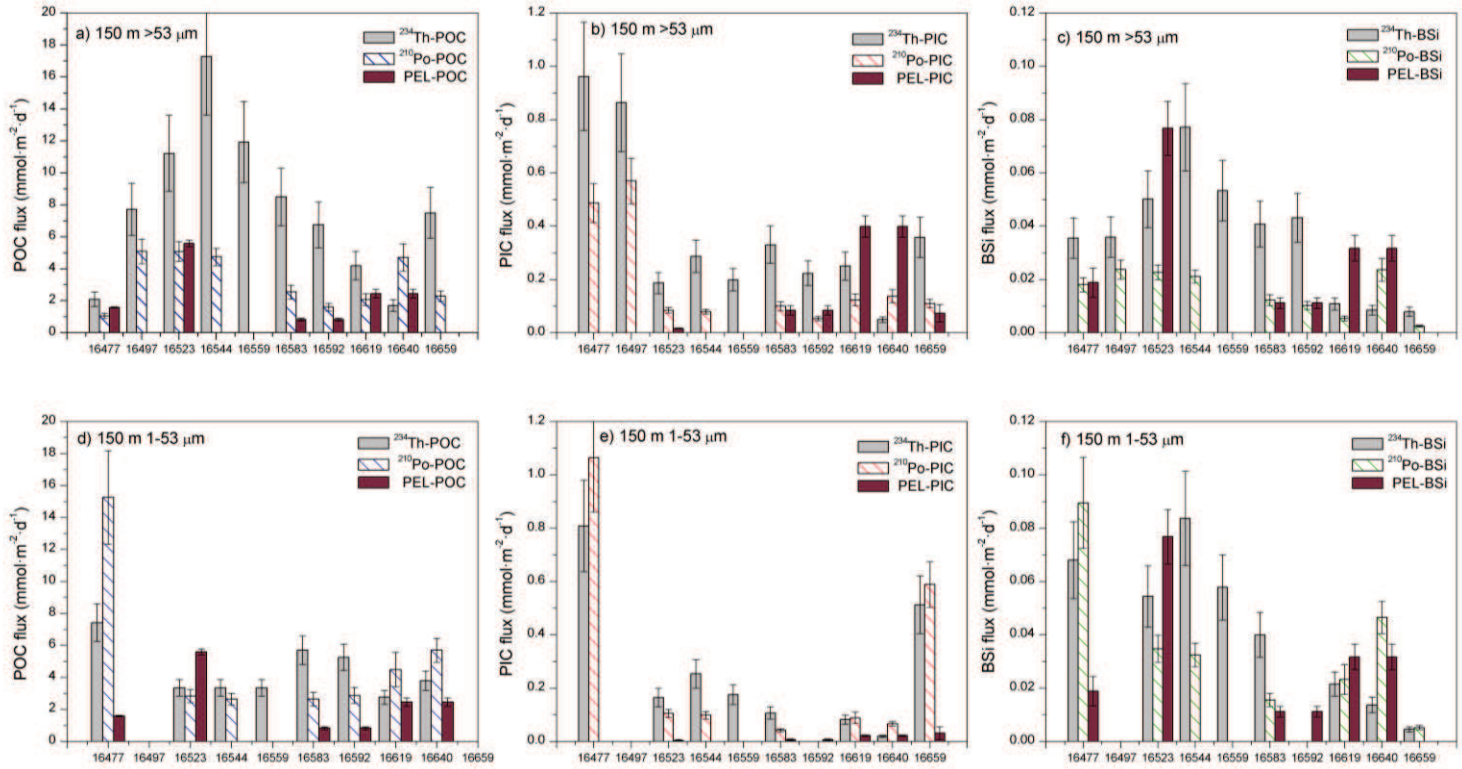

Figure 3.5: POC, PIC and BSi export fluxes obtained at each station at 50m and 150m and 50 m, using >53µm or 1-53µm particles. Derived from ^{234}Th, ^{210}Po fluxes or directly collected in drifting sediment traps (PELAGRA).

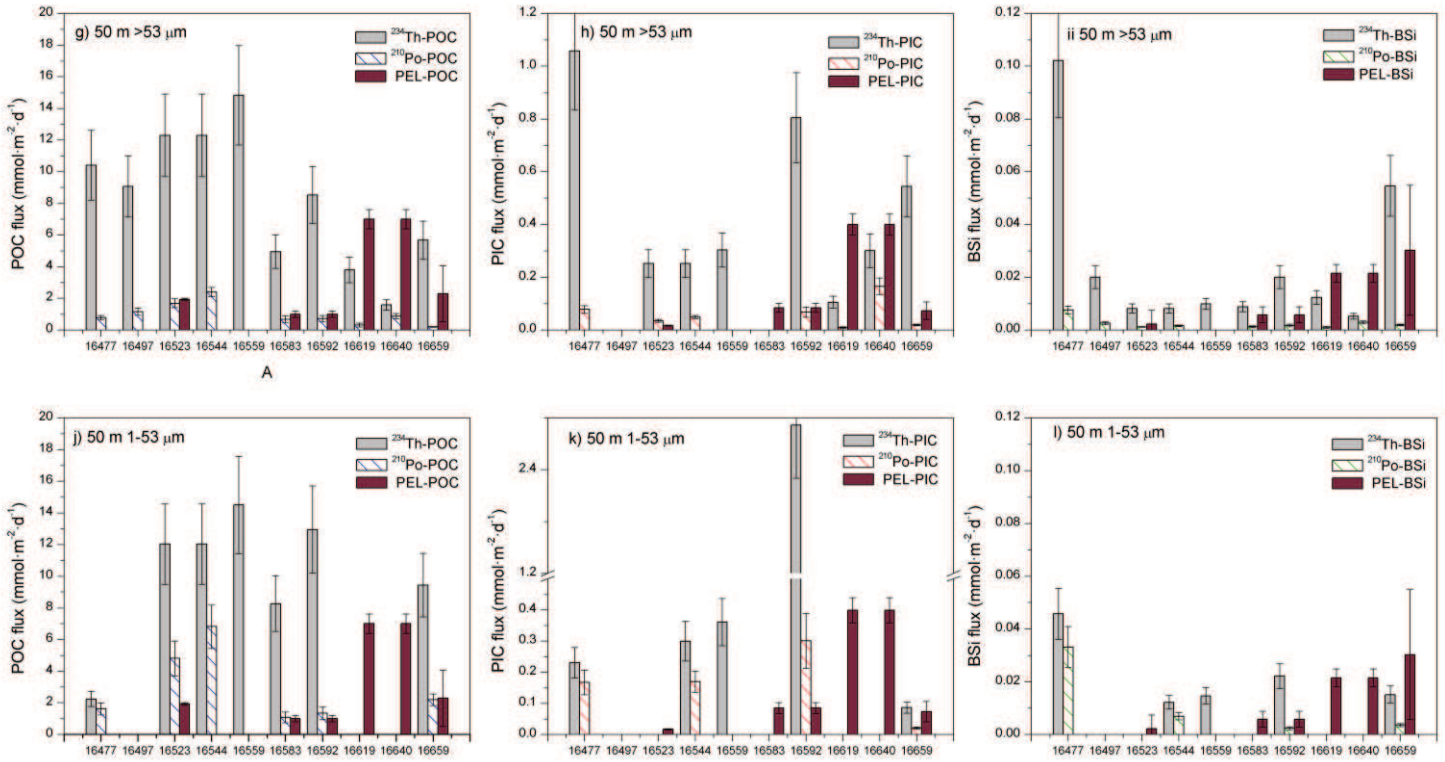

Figure 3 5: (continued)

The highest 150m-integrated ^{210}Po-derived POC export (Po-POC export) occurred at station 16497 (5.09 mmol m^{-2} d^{-1}) and the lowest at station 16477 (1.06 mmol m^{-2} d^{-1}). Fluxes at 150m were higher than fluxes at 50m, driven by higher ^{210}Po export at 150m than at 50m rather than by higher POC/^{210}Po ratios at 50m. POC fluxes from shallow (50-200m) drifting sediment traps (PELAGRA) fall between 0.92 mmol m^{-2} d^{-1} and 5.59 mmol m^{-2} d^{-1} at 150m and between 0.99 mmol m^{-2} d^{-1} and 7.0 mmol m^{-2} d^{-1} at 50m (Marsay *et al.*, 2011).

3.3.5 Biomineral fluxes.

Biomineral fluxes are given in Tables B.2, B.3 (supplementary material) and Figure 3.5 with average values being shown in Table 3.4. Stations 16477 and 16497 displayed the highest Th-PIC (0.96-0.86 mmol m^{-2} d^{-1}) and Po-PIC (0.49-0.57 mmol m^{-2} d^{-1}) export at 150m. Station 16640 presented the lowest Th-PIC export at 150m (0.05 mmol m^{-2} d^{-1}) and station 16592 had the lowest Po-PIC export (0.05 mmol m^{-2} d^{-1}). PELAGRA-PIC export was between 0.1 and 0.2 mmol m^{-2} d^{-1} at 150 m depth (Marsay *et al.*, 2011). Th-PIC values had, on average, similar values at 50 m and at 150 m. At 50m Th-PIC fluxes ranged from 0.1 to 1 mmol m^{-2} d^{-1}. Po-PIC values were slightly lower at 50m and ranged from 0.008 to 0.16 mmol m^{-2} d^{-1}. Th-PIC export was lower when ratios from the small size fraction were considered, whereas Po-PIC export increased with size fraction in most of the cases.

Table 3.4: Average ^{234}Th and ^{210}Po derived fluxes: POC, PIC and BSi, calculated as the average value from every station at 150 m and 50 m and for >1µm and>53 µm. Values are given in mmol m^{-2} d^{-1}. Uncertainties correspond to the standard deviation of the averages displayed. % corresponds to the relative uncertainty. PELAGRA values are from Marsay *et al*., (2011).

^{210}Po derived		POC flux	%	PIC flux	%	BSi flux	%
150m	53µm	3.2 ± 1.6	50	0.2 ± 0.2	99	0.02 ± 0.01	53
	1µm	5.2 ± 4.6	88	0.3 ± 0.4	133	0.04 ± 0.03	78
50m	53µm	1.0 ± 0.7	71	0.1 ± 0.1	87	0.00 ± 0.00	86
	1µm	3.0 ± 2.3	78	0.2 ± 0.1	70	0.01 ± 0.01	127
^{234}Th derived							
150m	53µm	7.9 ± 4.7	60	0.4 ± 0.3	81	0.04 ± 0.02	61
	1µm	6.1 ± 3.1	50	0.3 ± 0.3	100	0.04 ± 0.03	65
50m	53µm	8.3 ± 4.3	51	0.5 ± 0.3	72	0.02 ± 0.03	123
	1µm	10.2 ± 4.1	40	0.8 ± 1.2	154	0.02 ± 0.01	63
PELAGRA							
150m		2.3 ± 1.8	78	0.07 ± 0.03	45	0.03 ± 0.02	81
50m		3.6 ± 3.1	88	0.20 ± 0.19	95	0.011 ± 0.009	83

Th-BSi export at 150 m ranged from 0.008 to 0.077 mmol m^{-2} d^{-1}, and Po-BSi fluxes from 0.002 to 0.024 mmol m^{-2} d^{-1}. PELAGRA-BSi export displayed values between 0.005 and 0.02 mmol m^{-2} d^{-1} at 150 m depth (Marsay *et al.*, 2011). Fluxes at 50 m clearly decrease for Th-BSi and Po-BSi derived fluxes compared to 150m. Th-BSi and Po-BSi export showed values of similar magnitudes, when considering small and large particles.

3.3.6 Comparison between methods

A summary of the results displayed in Figures 3.5, 3.6 and Table 3.4 allows comparison of the methods. When calculated using particles >53μm, differences between ^{234}Th-POC export at 150m and 50m are not significant (ANOVA test, t = -0.022, p = 0.82), while ^{210}Po-POC fluxes are significantly depth dependent (t = 3.830, p = 0.002). PELAGRA-derived fluxes and ^{210}Po-POC fluxes are always lower than ^{234}Th-POC export. Assuming 100% of the ^{234}Th flux is carried by 1-53 μm particles, the differences between methods is reduced with Th-POC and Po-POC derived fluxes being similar (t = -0.154, p = 0.87) and also not different to the fluxes measured by PELAGRA (t = -1.739, p = 0.103).

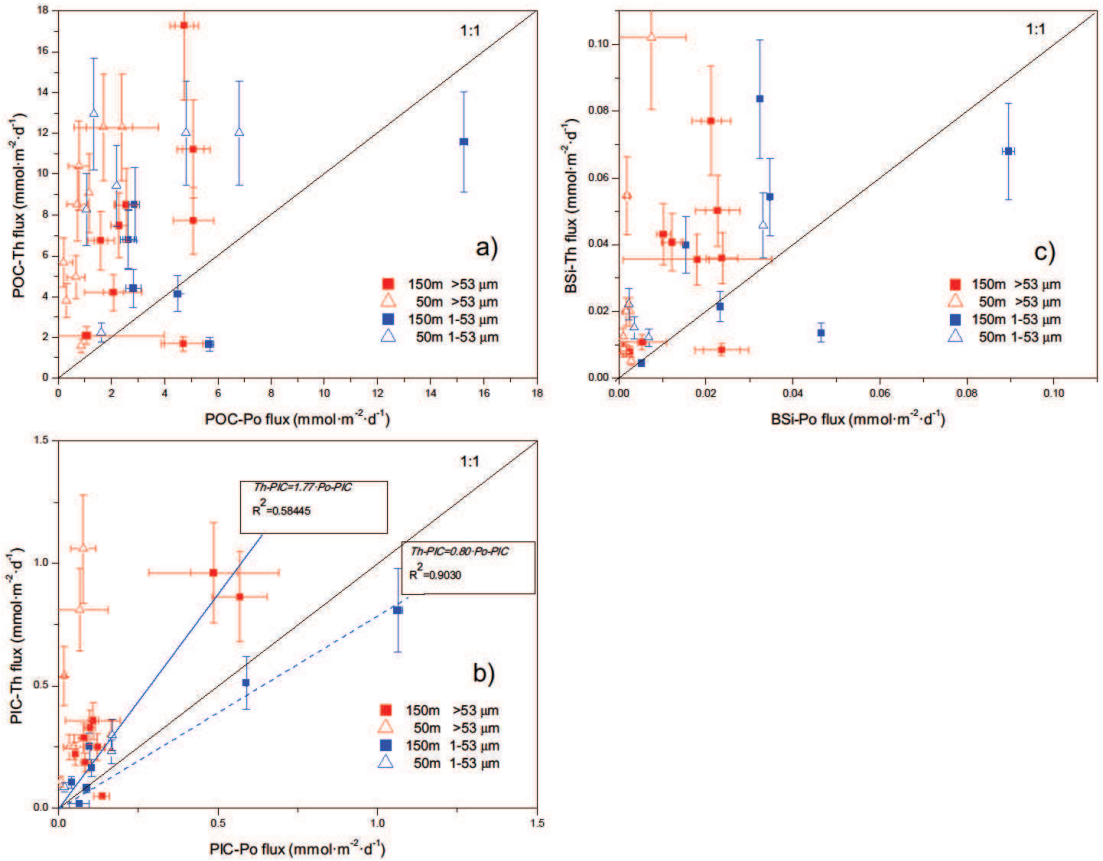

Figure 3.6. Th versus Po derived export fluxes. Values integrated at 50m and at 150m and considering 100% of the export due to >53µm particles and 1-53µm are presented. For (a) POC, (b) PIC and (c) BSi fluxes. The 1:1 line is depicted in the figure.

At 150m depth, stations 16477 and 16497 present the highest Th- and Po-derived PIC fluxes when large (>53 micron) particles are considered, with fluxes being higher than those from PELAGRA.

All other stations display similar trends in POC fluxes (i.e. highest values for Th-derived fluxes, followed by Po-derived fluxes and then fluxes measured by PELAGRA). At 50m the differences between Th-PIC and Po-PIC fluxes increased. As with the POC flux results, PIC fluxes derived from the 1-53 μm particles were statistically similar for the Th and Po methods ($t = -0.922$, $p = 0.37$), but in this case also to the PELAGRA fluxes ($t = -0.2927$, $p = 0.77$).

This trend changed with BSi fluxes as PELAGRA-BSi fluxes were sometimes in agreement with Th-BSi fluxes and sometimes with Po-BSi fluxes. At 50m, Po-BSi fluxes were extremely low, compared to Th-BSi and PELAGRA-BSi fluxes which were significantly similar to each other ($t = -3.561$, $p = 0.0029$).

Average values of BSi export are included in Table 3.4 to allow comparison between the three different methods. The minimum difference between methods is around 40%, increasing occasionally up to 100%, implying that opal export varies greatly between stations. For this reason, the comparison within methods, sizes and depths cannot be made for opal export using the average values, but only on a station by station basis.

Figure 3.6 depicts ^{234}Th- versus ^{210}Po-derived fluxes at 150m and 50m, and for each size fraction. Generally speaking, Th-derived fluxes were higher than Po-derived fluxes. For POC fluxes, some of the values coincide but the differences between ^{234}Th- and ^{210}Po-derived fluxes increased at 50m, since the ^{210}Po-POC fluxes at 50m were significantly lower than at 150m. No correlation between Th-POC and

Po-POC flux is apparent regardless particle size. On the contrary, PIC fluxes from the Po- and Th-methods show a certain correlation. At 150m, differences were smaller than the uncertainties and therefore not robust. ^{234}Th-derived versus ^{210}Po-derived fluxes show strong relationships (r^2=0.79 and r^2=0.9) when calculated using both small and large particles. BSi fluxes showed no particular correlation with depth or size, with the only general trend being that ^{234}Th gives higher fluxes than ^{210}Po. Again the differences between Th- and Po- derived fluxes increase for 50m integrated values.

3.4 Discussion

3.4.1 ^{234}Th-, ^{210}Po-derived and PELAGRA POC fluxes

As mentioned above, estimations of POC export fluxes can be performed through any of the three methods described (^{234}Th, ^{210}Po, PELAGRA). Since each method presents particular drawbacks, the combination of at least two of the three methods is preferred (e.g. Buesseler *et al.*, 2009 and 2008, Stewart *et al.*, 2007a, Verdeny *et al*., 2008 and 2009). Very few studies (already presented in the previous section) provide data from the three methods simultaneously. Of particular interest is the information provided by ^{210}Po-^{210}Pb disequilibria, since it is a relatively new method, and furthermore ^{210}Po biogeochemical behaviour is not well constrained. In the next section, I focus on the Th- and Po-POC fluxes calculated at 150m, assuming that 100% of the deficit of the flux is due to the export of large particles (>53μm). We follow this approach, as the vast majority of radionuclide export studies use only the large particle fraction to estimate export flux.

3.4.1.1. Relevance of integration times

My results show clear differences in POC fluxes calculated using the different methods. Averaged values from Table 3 4 decreased from 7.9 ± 4.7 mmol m^{-2} d^{-1} (Th-POC) to 3.2 ± 1.6 mmol m^{-2} d^{-1} (Po-POC) and 2.3 ± 1.8 mmol m^{-2} d^{-1} (PELAGRA-POC). In spite of the high variability, a general trend can be inferred where the Th-derived POC fluxes (integrated at 150m, >53μm particles) were sometimes more than twice the Po-POC fluxes, which in turn were equal to/or higher than PELAGRA fluxes (Figure 3.5). Figure 3.6 shows Th-POC fluxes versus Po-POC fluxes with most data points being above the 1:1 line representing equal Po-POC and Th-POC fluxes.

To analyse the origin of the systematic differences described above I focus on three main aspects: The integration times of the three methods, the biochemical behaviour of ^{234}Th and ^{210}Po and the exclusion of smaller particles in estimating export fluxes.

Figure 3.2 shows chlorophyll-*a* concentration derived from satellite data. A seasonal peak in mid-May is recorded, followed by a second peak in mid-June (0.6 mg Chl*a* m^{-3}). Primary productivity (PP) reached a peak (2g C m^{-2} d^{-1}) in late June (day 176 in Figure 3.2) and decreased afterwards. PELAGRA gives a Lagrangian snapshot of export over 48 to 72 hours prior to recovery date (4 PELAGRA deployments took place from 12 July to 13 August). According to Figure 3.2, the cruise occurred during a decrease in PP after its maximum peak on 26th June.

Th-POC flux integrates over about two half-lives of ^{234}Th (48 days), Th-POC fluxes obtained may therefore correspond to ^{234}Th deficits from particle export that may have occurred even two months prior to sampling. Hence, high values obtained from ^{234}Th export fluxes are probably caused by the particle export in late June/early July when productivity was largest and export was likely at its peak. ^{210}Po has a longer

half-life (134 days), which implies that this technique provides a seasonally averaged value of the export throughout the productive season. ^{210}Po approach can thus record particle export that happened about a year (two-half lives) prior to sampling, including the bloom observed in June (Figure 3 2).

Buesseler *et al.,* (2008) found that Po-POC flux > Th-POC fluxes > sediment trap fluxes in the oligotrophic Sargasso Sea. Differences between Th-POC and trap fluxes were assumed to be due to low collection efficiency of traps. Higher values for Po-POC fluxes found by Buesseler *et al.*, (2008) were ascribed to past events of higher export.

In this case, Th-POC > Po-POC > sediment trap fluxes and Th-POC values are up to three fold sediment trap values. As mentioned in the above section, Th-POC fluxes may be overestimated by the particle export subsequent to the bloom event in June (Figure 3 2), whereas PELAGRA has recorded export that occurred within the last 72 hours. This explanation was proposed by (Stewart *et al.*, 2007a) to explain similar results in the Mediterranean Sea during the MEDFLUX project. Nonetheless, it remains unclear why Po-POC fluxes do not account for the past bloom event at least at the same level as ^{234}Th, as would be expected because of its longer half-life. In the two following sections, I explore explanations related to the different affinities of particles and to size fractionated POC/radionuclides ratios to solve this discrepancy.

3.4.1.2 Particle affinity

The second main difference between ^{234}Th and ^{210}Po techniques is the higher affinity of ^{210}Po for POC relative to ^{234}Th, the latter being thus considered as a better tracer of total mass flux. As a result, the deficit created by the downward export of ^{234}Th specifically associated to the lithogenic material and not considered in POC/^{234}Th will

overestimate the Th-POC flux. The PAP site is located in an area where the annual dust deposition is relatively low (e.g. 0.5-1 g m^{-2} y^{-1}(Jickells *et al.*, 2005a)). Nonetheless, episodic dust events can occur and hence temporarily increase the total mass flux.

Similar results to what have been reported at BATS by Brew *et al.*,(2009); Stewart *et al.*, (2010) and Stewart *et al.*, (2011) where Th-POC flux> Po-POC fluxes ≥ sediment trap fluxes were specialfically found at 150 m in post bloom conditions. This suggests that Th-POC fluxes were higher (even in a non bloom period) due to an additional ^{234}Th export driven by lithogenic and detrital material. Likewise, as mentioned above, higher Th-POC fluxes were found in the Mediterranean Sea (MEDFLUX) compared to Po-POC and sediment traps fluxes (Stewart *et al.*, 2007a); this result was ascribed to the different biogeochemical behaviour of both radiotracers. Consistent with those results, in the global comparison of both radiotracers reviewed in (Verdeny *et al.*, 2009) Po-POC fluxes were in general lower than Th-POC fluxes. Potential explanations were i) the association of ^{234}Th with lithogenic material and/or ii) rapid removal of ^{234}Th on sinking particles in contrast to ^{210}Po, that will be more efficiently recycled.

A limitation to our approach of studying the particle affinity of ^{210}Po to particles remains in the fact that cells (within which ^{210}Po is incorporated) can potentially detached from particle and pass through the filter leading to underestimated ^{210}Po/POC ratios.

3.4.1.3 Size-fractionated POC/^{234}Th (^{210}Po) ratios

A final point to address is to which extent POC/^{234}Th and POC/^{210}Po size fractionated ratios influence Th-POC and Po-POC fluxes. The best method for collecting sinking

particles for the determination of POC/radionuclide ratios and the subsequent estimate of downward POC flux is still an open question (Burd *et al.*, 2000; Buesseler *et al.*, 2006; Stewart *et al.*, 2007a; Cochran *et al.*, 2009; Lepore *et al.*, 2009; Hung *et al.*, 2010; Xu *et al.*, 2011).

In our study case Po-POC fluxes are very sensitive to POC/^{210}Po ratios, since they drive temporal trends in Po-POC flux. Conversely, Th-POC values do not depend as much on POC/^{234}Th as on the variation of the ^{234}Th flux itself. Nevertheless, the POC/Th(Po) ratios that were collected during D341 cruise cannot be simply attributed to the present ^{234}Th-^{238}U and ^{210}Po-^{210}Pb disequilibria, because these deficits could have been produced during the June bloom. This temporal delay between the collection of particles for POC/Th(Po) evaluation and the moment where Th(Po) disequilibria were produced may lead to a bias in the results (Stewart *et al.*, 2007a; Buesseler *et al.*, 2008a).

Large (>50 μm) particles are often considered to dominate rapidly settling particles (Bishop *et al.*, 1977). Recent studies including some undertaken during this cruise (Riley *et al.*, 2012; Le Moigne *et al.*, in review-a), suggest that the export of small (typically <53μm) (Hung *et al.*, 2010; Hung and Gong, 2011) and/or slow particles (Alonso-Gonzalez *et al.*, 2010b; Riley *et al.*, 2012) can contribute more significantly to POC fluxes than previously thought. Le Moigne *et al.* (in review-a) addressed the issue of which is the most appropriate POC/Th ratio to use when "velocity fractionated" estimates of carbon flux are available, however (Le Moigne *et al.*, in review-a) use data (i.e. particle sinking speeds) that are not always accessible. It is worth mentioning that slow sinking particles are not ascribed to 1-53 um particles only and the inclusion of the total size fraction (> 1 μm) to calculate POC fluxes may not be the ideal option everywhere. Considering this, we believe that the contribution

of the size-fractionated ratios to our Po and Th POC derived fluxes must be analysed in our study. We achieved here an initial assessment of the implications of the contribution of slow sinking particles contribution to radionuclides derived POC fluxes. Further analysis are required to fully understand the processes in place.

First, if we assume that the POC flux is driven by large particles, the ratio that has to be used is the one measured from large particles $[POC/radionuclide]_{>53\mu m}$; equally, $[POC/radionuclide]_{1\text{-}53\mu m}$ should be used if we suspect a flux produced by small particles. If $[POC/radionuclide]_{>53\mu m} \sim [POC/radionuclide]_{1\text{-}53\mu m}$, POC (or biomineral) flux will not change regardless of which particles are contributing to export. When $[POC/radionuclide]_{>53\mu m} \neq [POC/radionuclide]_{1\text{-}53\mu m}$, the key question is how to obtain a realistic ratio if a significant contribution of small particles to export occurs (Hung and Gong, 2010). A spectrum of export estimates for any particular phase thus exists driven by the variability in the ratio of this phase to the relevant radionuclide in particles of varying sizes.

Figure 3.4a and 3.4b display $[POC/radionuclide]_{>53\mu m}$ versus $[POC/radionuclide]_{1\text{-}53\mu m}$ for ^{234}Th and ^{210}Po at 50m and 150m. For ^{210}Po it is clear that regardless of depth $[POC/radionuclide]_{>53\mu m} < [POC/radionuclide]_{1\text{-}53\mu m}$ at most of the stations. The implication is that if small particles contribute to flux and the ratio on the larger particles is used, Po-POC fluxes would be underestimated. On the contrary, POC/Th ratios from Figure 3.4 were equal, lower or higher for small versus large particles.

Figure 3.6a shows Th-POC fluxes versus Po-POC fluxes at 150m and 50m using $POC/^{234}Th$ and $POC/^{210}Po$ ratios from particles >53µm and in the 1-53 µm range. In the first case it is assumed that 100% of the export produced by ^{210}Po or ^{234}Th is driven by large particles, while in the second case, that the export is driven

only by small particles. In most cases, regardless of integration depth the points were over the 1:1 line, which represents equal Th-POC and Po-POC fluxes. When assuming 100% contribution of the small particles the points get closer to the 1:1 line: Po-POC values increase, whereas Th-POC slightly decreases.

Additionally, Villa *et al.* (2011) were able to estimate average settling velocities during the D341 cruise. Villa et al. (in prep) uses a one-box model to interpret ^{210}Po-^{210}Pb profiles and demonstrates that the present ^{210}Po-^{210}Pb disequilibria can be only interpreted if the contribution of slow sinking particles (< 10 m d^{-1}) is included. Consequently POC-Po fluxes obtained could be higher and decrease this offset with Th-POC fluxes (Figure 3 5 and 3 6). Nevertheless, what is the most suitable size fractionated or trap Th(Po)/POC ratio account for the slow sinking particle contribution is still an open question.

3.4.2 ^{234}Th-, ^{210}Po-derived and PELAGRA biomineral fluxes

Average values of biomineral fluxes are shown in Table 3.4. Figure 3.5 (b, e, h, k) shows the Th-PIC, Po-PIC fluxes and PIC fluxes measured by PELAGRA. Th-PIC fluxes are higher than Po-PIC and PELAGRA-PIC fluxes. Remarkably the spatial-temporal trend in PIC fluxes differs completely from the corresponding trend for POC fluxes at 150m using >53μm particles. Apart from the first two stations, the rest of the stations presented lower variability in PIC fluxes than in POC fluxes.

The trends in PELAGRA and PIC fluxes are similar with the range of values going again from Th-PIC>Po-PIC>PELAGRA-PIC. As observed for POC, PIC concentrations showed a peak at the PAP site during May 2009 (Figure 3.2), suggesting a PIC accumulation prior to our sampling in August. Like Th-POC, Th-PIC gives a higher average value of PIC export (Table 3.4). However, when small

particles are used to calculate fluxes Th-PIC and Po-PIC results tend to converge (e.g. Figure 3.6). It is worth recalling that, as for POC, particles collected in July might not represent the fluxes during the bloom and this might be also the origin of the discrepancies within results.

Figure 3.6 shows a strong correlation between Th-PIC and Po-PIC fluxes; this tight and constant affinity between both PIC and Th and also between PIC and Po is expected, since it is well know that the affinity of polonium and thorium for $CaCO_3$ is strong (Hull and Burnett, 1996; Geibert and Usbeck, 2004). Thus, the fact that, unlike POC, Th-PIC and Po-PIC are well correlated might be due to the fact that they associate similarly to PIC, but not to POC.

Th-BSi and PELAGRA-BSi fluxes (Figure 3.5, c, f, i, l) give similar values, within their uncertainties, whereas Po-BSi gives lower values. BSi export was low at the PAP site at this time of the season; however, a diatom bloom likely occurred earlier in the season (i.e. May) which could be expected to have been recorded by the Po approach. The absence of high Po-BSi export fluxes is likely due to BSi/^{210}Po ratios being measured in July/August when rapidly sinking and fresh material from a diatom bloom may already have sunk or been remineralized. This prevents us from a robust comparison of the ability of the three techniques to trace past opal export episodes. Unlike PIC, no relationship occurs between Th-BSi and Po-BSi in Figure 3. 6. Further studies in environments dominated by strong diatom blooms are needed to fully investigate the abilities of both tracers to estimate opal fluxes.

3.4.3 POC and biomineral to radionuclides ratios

The importance of radionuclide ratios for the calculation of POC and biomineral fluxes suggests further investigations are needed into the relationships between POC,

BSi and PIC and radionuclides on different size particles. This has been done previously for POC and BSi (Friedrich and van der Loeff, 2002; Stewart *et al.*, 2007b; Stewart *et al.*, 2010) but the relationship between radionuclides and PIC has not been thoroughly investigated so far.

POC(biomineral)/radionuclide ratios in 1–53μm and >53μm particles are shown in Figure 3.4. Ratios to ^{210}Pb were also studied because ^{210}Pb/^{210}Po is a useful biogeochemical tracer of particles (Friedrich and Rutgers van der Loeff, 2002) since ^{210}Pb has a high adsorption coefficient, similar to that of ^{234}Th. However, its particle affinity does not coincide exactly with that of ^{234}Th; furthermore, ^{210}Pb concentrations in seawater are continuously enhanced due to atmospheric deposition as an additional source. Thus a combined examination of the three radionuclides ratios should provide further information on the nature of the exported particles.

According to Buesseler *et al.*, (2006), if Th adsorption is a surface process then POC/^{234}Th ratios would increase as particle size increases due to a reduction in the volume:surface area (V:SA) ratio as particles increase in size during the seasonal progression of a biological community. The particle size spectrum is continuous and coagulation plays a strong role in the size spectrum of biogenic particulate matter (Moran and Moore, 1992). Buesseler *et al.*, (2006) state that a rapid aggregation (or coagulation) of small particles alone without loss of mass would probably yield no significant changes in V:SA ratios and hence no changes in POC/^{234}Th.

There would be a decrease of POC in large faecal pellets (assimilated by zooplankton), leading to them having smaller POC/^{234}Th ratios than non repackaged sinking particles. Smaller POC/^{234}Th ratios may also occur in large degraded particles as a preferential loss of POC occurs. Repackaging would lower POC/^{234}Th ratios, would increase particle size, whereas aggregation would not change (or only slightly

lower) the ratios. Riley *et al.* (2012) found that the particles we collected at the PAP site in 2009 were mainly aggregates, degraded material or faecal pellets in accordance with post-bloom conditions as described in section 3.1. However, measured ratios do not show any clear configuration in Figure.3.4. POC/^{234}Th ratios are scattered around the 1:1 line and furthermore, only two particle sizes are used. For this reason the dependence of POC/Th with particle size cannot be clearly observed in Figure 3.4.

PIC/^{234}Th shows clearer behaviour as PIC/^{234}Th is higher in large particles (Figure 3.4). The increase may be due to the increase of PIC in large particles formed by aggregation of smaller particles and biominerals, which is not followed by an increase in ^{234}Th. BSi/^{234}Th ratios do not follow the same pattern as PIC/^{234}Th ratios suggesting that aggregated particles were not significantly enriched in BSi. This implies that BSi sank quickly after the spring diatom bloom as explained above.

When studying POC/^{210}Po, PIC/^{210}Po and BSi/^{210}Po ratios in large versus small particles, small particles have higher ratios than > 53 μm particles (Figure 3.4). This result contrasts with those of Stewart *et al.*, (2010) who found no changes in POC/^{210}Po with size or depth. The increase of ^{210}Po in large particles compared to POC is probably due to i) the fact that ^{210}Po is bioaccumulated by the growing organism, and ii) the loss of organic carbon in degraded particles. ^{210}Po incorporated within organic carbon will also be lost, but ^{210}Po will remain bound to the surface.

A correlation with particle size cannot be established only using two particle sizes, but certain differences are observed. PIC/^{210}Po ratios decrease in all cases from 53 μm to 1-53 μm, either because particles and aggregates are enriched in ^{210}Po, or poor in PIC. A possible explanation is an enhancement of ^{210}Po in large particles via the incorporation of ^{210}Po into calcium carbonate, as a substitute for calcium (Matthews *et al.*, 2007). Since ^{210}Pb is only particle-surface reactive or incorporated

into the biomineral lattice and is not bound to organic carbon, ^{210}Pb behaviour has some similarities to the way ^{234}Th interacts with POC to regulate POC/^{210}Pb ratios, despite the fact that, unlike ^{234}Th, ^{210}Pb is continuously supplied by atmospheric deposition.

3.4.4 Ballast implications

The export of POC and biominerals are strongly correlated in both the deep (Francois *et al.*, 2002; Klaas and Archer, 2002) and the surface ocean (Sanders et al., 2010). These observations have prompted suggestions that these biominerals may enhance or cause organic C export by increasing the density of organic aggregates and thus acting as 'ballast'. Calcite and opal may also provide chemical or physical protection from remineralization (Armstrong *et al.*, 2002; Passow *et al.*, 2003). Recent studies have emphasized the importance of the slow sinking pool in the ocean (Alonso-Gonzalez *et al.*, 2010; Riley *et al.*, 2012). Also Riley *et al.*, (2012) concluded that the slow sinking pool may be unballasted while the fast sinking pool is mostly ballasted.

If it is considered that particles caught within the 1-53 µm size fraction particles are slowly sinking and those greater than 53 µm are fast sinking (Chapter 2), then using size fractionated POC to biomineral ratios in *in situ* pumps and POC to biomineral ratios from sediment traps should address the issue regarding a surface ocean ballast effect hypothesized in Riley *et al.* (2012).

Figure 3.6 presents POC to PIC ratios and POC to BSi ratios in particles greater than 53 µm, 1-53 µm particles and in particles caught by PELAGRA traps. The variability of POC:PIC ratios is greater in 1-53 µm particles while this variability is reduced in "large particles" (53 µm) and much lower in particles caught in PELAGRA traps (Figure 3.7). This suggests that POC and PIC export captured by

PELAGRA traps are strongly correlated, although the correlation is weaker in the large size fraction and even more so in the small size fraction. The trend is similar in the POC:BSi data. Strong correlations between POC and biomineral export fluxes have been deemed to be a relevant diagnostic of biomineral ballasting (Francois *et al.*, 2002; Klaas and Archer, 2002; Sanders *et al.*, 2010). Hence, as we found high variability in POC:biomineral ratio in 1-53 μm, the hypothesis that the slow sinking pool is largely unballasted (Riley *et al.*, 2012) is verified.

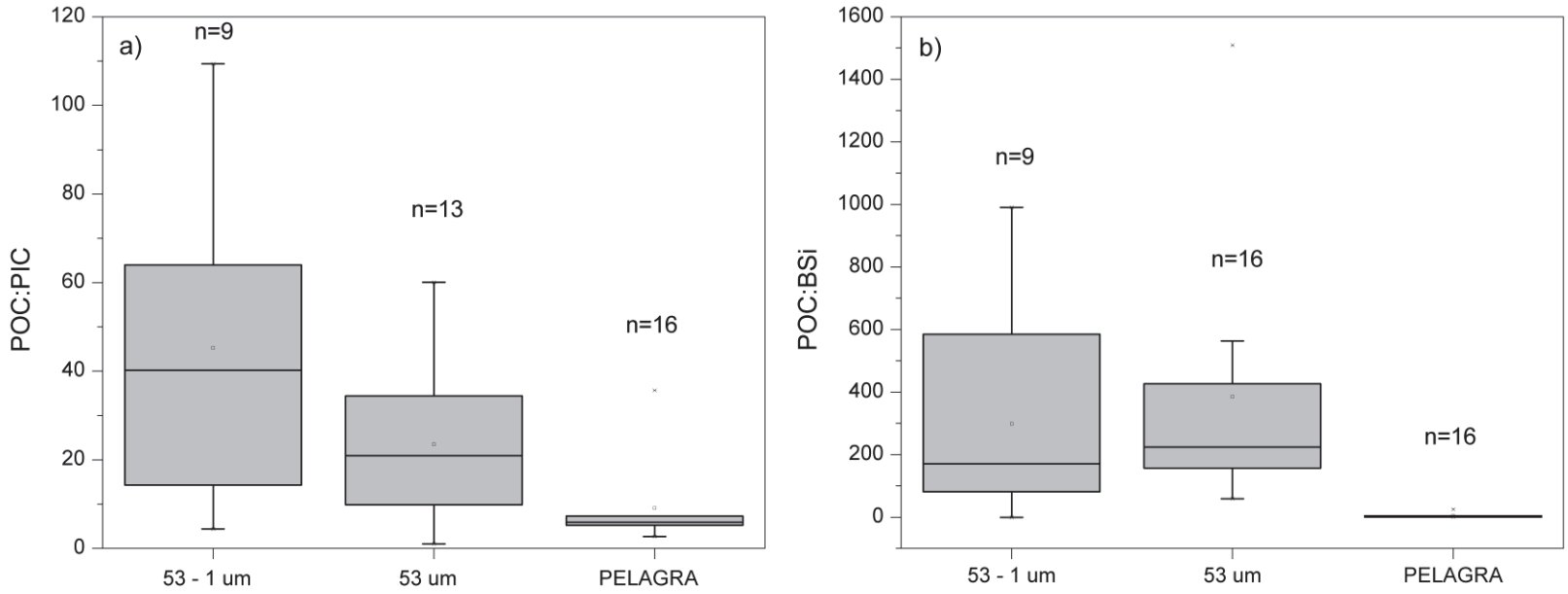

Figure 3.7: (a) POC:PIC and (b) POC:BSi ratios measured on large (>53µm) size fraction and small size fraction (53-1µm) from *in situ* pumps (SAPS) or PELAGRA traps. The area hilighted in grey represents the interquartile range

In order to improve our understanding of the physical and chemical mechanisms behind the ballast theory, further laboratory experiments in controlled investigations (i.e. measurements on artificially made marine particles) should be undertaken to link POC to biomineral ratio in marine particles to processes such as aggregation, disaggregation, degradation and respiration of sinking matter.

3.5 Conclusion

I have shown the ability of ^{234}Th and ^{210}Po to trace three major components of the mass flux in the surface ocean (POC, PIC and BSi export fluxes) at the Porcupine Abyssal Plain site in July 2009 and compared the results with fluxes obtained from free drifting sediment traps (PELAGRA). PELAGRAs provide the lowest values for POC and PIC fluxes. This is ascribed to the different integration times of the methods (days for sediment traps, 1-2 months for ^{234}Th and 6-12 months for ^{210}Po); also, PELAGRA traps measure a post bloom situation, whereas Po and Th derived fluxes are probably measuring deficits created one month ago, during the bloom. The ^{234}Th derived POC and PIC fluxes are higher than fluxes from the ^{210}Po approach, due to their different biogeochemical behaviours, previously reported in the literature. However, the results show that when using POC(PIC)/radionuclides ratio in small particles (1-53 μm), the discrepancies between the two methods tend to decrease. This is a relevant finding if the contribution of slow (potentially smaller) sinking particles to the flux is believed to be significant, as at the PAP site. We showed that conversely to Po, the Th deficit in the water column could have been overestimated due to lithogenic fluxes. Due to the reduced variability of POC(PIC)/radionuclide displayed in 1-53 μm relative > 53 μm particles, if small particles ratios are used to derive PIC

and POC fluxes, results from both methods tend to converge. This is an important finding if the contribution of slow (potentially smaller) sinking particles to the total flux is significant at the PAP site. Correlations between PIC-^{234}Th and PIC-^{210}Po fluxes indicate similar behaviour of both radioelements to PIC. BSi fluxes were relatively low resulting in similar values using the three methods. In addition to the on going ballast theory debate, the data suggest that the large (and potentially fast sinking) pool is mostly ballasted, whereas the small fraction is unballasted.

Acknowledgment

We would like to thank warmly Paul Morris (WHOI) for various advice as well as help with the D341 mobilisation on the *RRS Discovery*. We would like to thank the captain and crew of the *RRS Discovery* and the D341 scientific team. We also gratefully acknowledge Bob Head (PML) for processing POC samples and Darryl Green (NOC) for processing calcite samples. The improvements suggested four anonymous reviewers are gratefully acknowledged. This work is part of the lead author's doctoral research and was supported by the CalMarO program, a FP7 Marie Curie initial training network, www.calmaro.eu, European Community (Grant agreement no.: 215157), by the U.K. Ocean 2025 program and by Junta de Andalucía, project P07-RNM-02567, Spain.

4. On The Proportion of Ballast versus Non-Ballast Associated Carbon Export in the Surface Ocean.

The following chapter has been reproduced from a manuscript accepted with minor correction in Geophysical Research Letters. Frédéric A.C. Le Moigne, Richard J. Sanders, Maria Villa-Alfageme, Adrian P. Martin, Katsiaryna Pabortsava, Hélène Planquette, Paul J. Morris, Sandy J. Thomalla, " On the proportion of ballast versus non-ballast associated carbon export in the surface ocean".

Data contribution: All measurements were taken and analysed by the author during D341 (P.S.O.: Richard Sanders), D350, (P.S.O.: C. Mark Moore) and D354, (P.S.O.: Eric Archterberg). ^{234}Th analysis, *in situ* pumps processing and BSi analysis were undertaken by the author. Maria Villa (U. of Sevilla) helped with ^{234}Th processing on D354. Andy Milton, Patrick Martin and Katsia Paborsatva (NOC) helped the ^{234}Th analysis and recovery work back in our home lab. Mark Stinchcombe and Katsia Paborsatva processed the background counting on D350. Chris Marsay (NOC) helped with *in situ pumps* deployment. POC and PIC samples were prepared by the author, then respectively analysed by Bob Head (PML) and Darryl Green (NOC). Helene Planquette (NOC) took *in situ* pumps splits for calcite on D285 and D286 that were analysed by the author.

Abstract: The role of biominerals in driving carbon export from the surface ocean is unclear. We compiled surface particulate organic carbon (POC), and mineral ballast

export fluxes from 55 different locations in the Atlantic and Southern Oceans. Substantial surface POC export accompanied by negligible mineral export was recorded implying that association with mineral phases is not a precondition for organic export to occur. The proportion of non-mineral associated sinking POC ranged from 0 to 73% and was highest in areas dominated by diatoms. This is consistent with previous estimates showing that transfer efficiency in such regions is low, however we propose that rather than this being due to diatom blooms being inherently characterized by poorly packaged aggregates which are efficiently exported but which disintegrate readily in mid water it is due to such environments having very high levels of unballasted organic C export.

4.1 Introduction

The concept of the biological carbon pump emphasises the importance of oceanic primary production in the global carbon cycle. Approximately 5 to 10 GTC yr^{-1} are exported from the surface ocean into the deep ocean interior (Henson *et al.*, 2011) mainly in the form of settling organic particles derived from phytoplankton production in the sunlit upper ocean. The coupling of oceanic production and export removes CO_2 from the atmosphere and contributes to the buffering of the global climate system. Without the oceanic biological carbon pump, atmospheric CO_2 levels would be almost twice as high as current concentrations (Sarmiento and Toggweiler, 1984). The mode by which carbon is transferred downwards is therefore a key issue in the context of global climate change.

In the deep ocean, strong correlations are observed between downward fluxes of biominerals (opal and calcite) and particulate organic carbon (POC). This observation inspired the “ballast hypothesis” which suggests sinking fluxes of

minerals (such as biogenic calcite, biogenic opal, and lithogenic material such as clays) assist in driving the POC flux to the deep sea (Armstrong *et al.*, 2002b; François *et al.*, 2002; Klaas and Archer, 2002). Correlations based on multiple linear regression analysis (MLRA) between mineral and POC fluxes into deep sediments traps reflected both physical protection provided from remineralization provided by minerals and increasing aggregate density provided by denser minerals (François *et al.*, 2002; Klaas and Archer, 2002).

Whilst data from the deep ocean suggest that correlations between mineral and POC flux occur, even if the details are opaque, in the upper ocean a paucity of data means that we cannot even say whether such a relationship exists. This prevents an understanding of mechanisms that may promote particle export from the upper ocean (Honda and Watanabe, 2010; Sanders *et al.*, 2010). In addition, whilst the existence of non-ballast associated POC has been demonstrated in the surface (Armstrong *et al.*, 2002b; Honda and Watanabe, 2010), little is known about its variability in the surface ocean.

Klaas and Archer, (2002) assumed that non-ballast associated POC disappeared below 1000m contrasting with the findings of Honda and Watanabe, (2010) who show a persistent non-ballast associated POC flux at depth. If the contribution of the non-mineral ballast associated pool is important in the surface ocean, then significant non-ballast associated POC may be a general feature at depth. Hence, the exclusion of the latter pool could potentially affect the hypothetical predominance of POC fluxes associated with calcite suggested by Klaas and Archer, (2002) in the global ocean.

To explore this issue, we performed MLRA on estimations of ^{234}Th derived POC and biomineral fluxes in the Atlantic and Southern Ocean (Morris *et al.*, 2007;

Thomalla *et al.*, 2008; Sanders *et al.*, 2010; Le Moigne *et al.*, in review-b). We also examine the variability of surface carrying coefficients, the surface proportion of the non ballast associated fraction of POC flux and speculate on the implications for the ballast hypothesis.

4.2 Methods

We compiled 55 parralel POC and biomineral (calcite and opal) export data derived from ^{234}Th measurements from 7 cruises (AMT-14, D285, D286, D321, D341, D350, D354). Locations, period and references are given in Table C.1 (Appendix C) (Thomalla *et al.*, 2006; Morris *et al.*, 2007; Thomalla *et al.*, 2008; Sanders *et al.*, 2010; Le Moigne *et al.*, in review-b). During D285, 286, AMT-14, D321 and D341, total ^{234}Th was extracted and counted using methods described in Thomalla *et al.*, (2006). On D350 and D354 we used the ^{234}Th "small-volume" technique with ICP-MS assessment of recoveries for ^{234}Th extraction (Pike *et al.*, 2005) with recoveries 94.2 ± 3.4 % for D350 and 90.6 ± 6.7 % for D354. Vertical profiles of ^{234}Th activity were converted to estimates of downward ^{234}Th flux using a one dimensional steady-state model (Buesseler *et al.*, 1992). These fluxes were then converted to estimates of downward particle flux using the ^{234}Th:POC or ^{234}Th:biomineral ratio on large (>53 μm) particles collected using an *in situ* Stand Alone Pumping System (SAPS) deployed for 1.5 hrs at a single depth beneath the mixed layer (see Table C.1 Appendix C). Approximately 1500–2000 L of seawater was filtered onto a 53 μm Nitex screen. Particles were then rinsed off the screen using thorium free seawater, and the particle suspension evenly split into four subsamples using a Folsom splitter. Each split was then analyzed for one of the following: ^{234}Th, POC, calcite and opal. POC, BSi and PIC samples were analyzed as in Sanders *et al.*,(2010). On D285 and

D286, particles were rinsed off the 53um mesh and were digested using aqua-regia followed by HF/HNO_3 digestion solution. Calcium concentrations were determined using an ICP-MS quadrupole (Planquette *et al.*, 2009). Large particle aluminum concentrations were not measured during AMT-14, D321, D341, D350, D354, therefore literature values were taken from Lambert *et al.*, (1984) (AMT-14) and Kuss and Kremling, (1999) (AMT-14, D321, D341, D350 and D354). Al (Aluminium) fluxes for D285 and D286 are presented in Planquette *et al.*, (2009).

Export integration depths for each station are given in supplementary material (comprised between 50 and 265m) (Table C.1, Appendix C). Lithogenic fluxes were estimated as ((100/8)xAl) (Honda and Watanabe, 2010) assuming that most particulate Al is of lithogenic origin, although it can be present in diatom frustules (Gehlen *et al.*, 2002). This ratio is based on averaged elemental composition of the continental crust; the crustal abundance of Al being 8%(Wedepohl et al., 1995). The non-ballast fraction may be biased by applying a constant Al value to work out lithogenic fluxes (*via* $Al/^{234}Th$ ratio) for AMT-14, D321, D341, D350, D354.This is because we used averaged values from (Lambert *et al.*, 1984), who show average Al concentrations in particles are presented as a function of latitudinaly defined areas in the Atlantic. For AMT-14, three different Al concentrations in particles matching AMT-14 transect stations locations were taken based on proximity.

To examine correlations between mineral and POC fluxes, I adopt a MLRA approach similar to Klaas and Archer, (2002) and Honda and Watanabe, (2010). Total POC flux (POC_{total} flux) was divided into portions associated with or carried by BSi (POC_{BSi}), calcite (POC_{pic}), lithogenic material (POC_{lith}) and residual POC (POC_{res}). MLRA were used to fit the data to equation 4.1:

$$POC_{total} = POC_{PIC} + POC_{BSi} + POC_{lith} + POC_{residual} = a.PIC_{flux} + b.BSi_{flux} + c.Lith_{flux} + d \quad \text{(Eq.4.1)}$$

where *a*, *b* and *c* are defined as "carrying coefficients (CCs)" (Klaas and Archer, 2002) while *d* is the portion of POC that is not associated with any minerals. In order to study the regional variability of CCs, stations have been grouped according to their location and/or sampling time as presented in Table C.1 and C.2 (Appendix C).

4.3 Results and discussion

4.3.1 General considerations

Here I survey the magnitude of surface POC and biomineral export as a function of latitude. Latitudinal variations of POC, PIC and BSi show high export in polar and sub-polar regions (Figure 4.1). At mid latitudes, POC export still occurs while biomineral export is low. The latitudinal pattern of lithogenic material export seems to be correlated with the global pattern of aerosol deposition, the North Atlantic receiving most of the dust input relative to the South Atlantic and the Southern Ocean (respectively 43, 4 and 6% total dust inputs to the global ocean (Jickells *et al.*, 2005)).

The near-zero data points for PIC, BSi and lithogenic export plots, particularly relative to POC export (Figure 4.1) suggests that the minerals are not an absolute precondition for organic carbon flux to occur. This suggests that a non-protected or ballasted POC pool plays a significant role in the surface ocean as previously demonstrated by Honda and Watanabe, (2010) in the North Pacific.

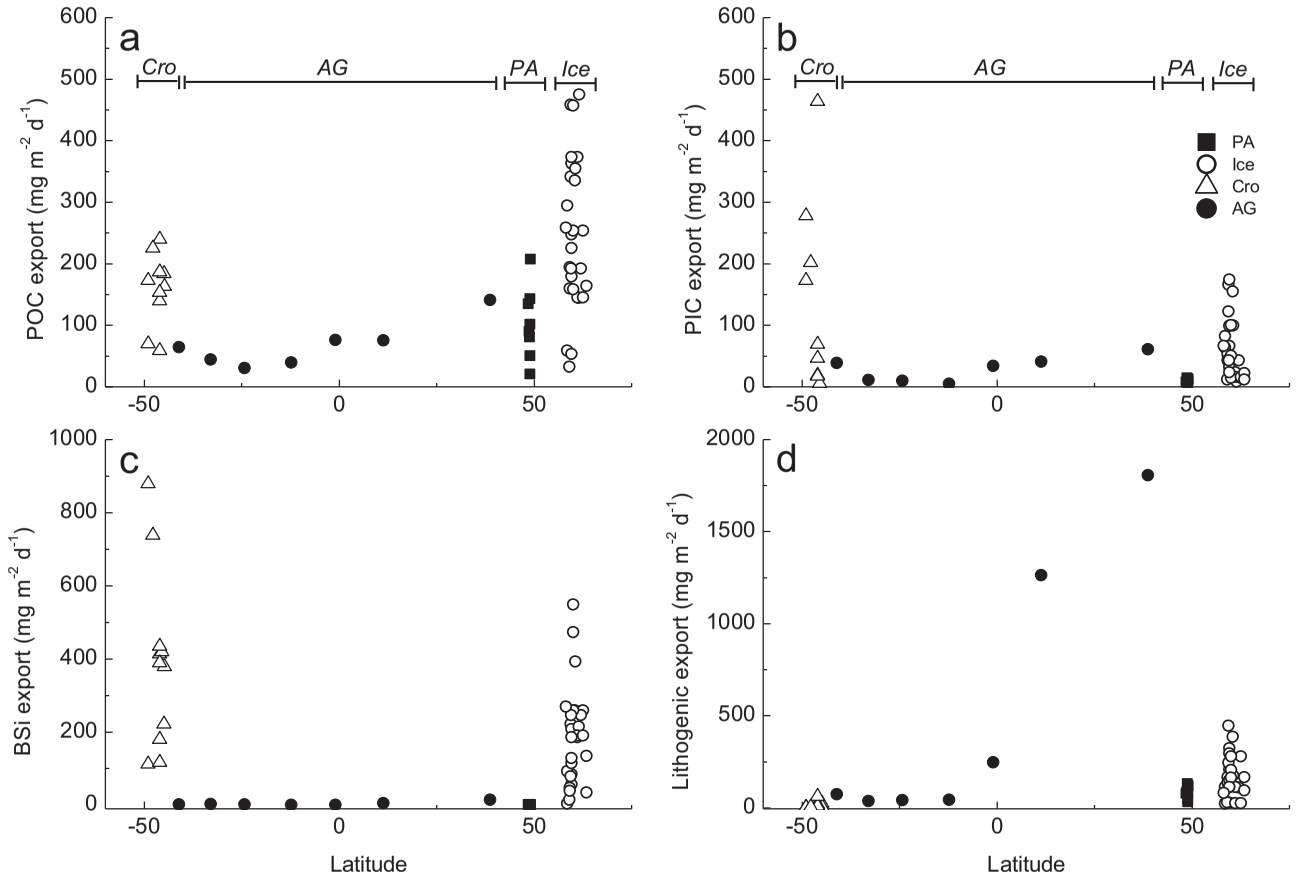

Figure 4.1: (a) POC, (b) PIC, (c) BSi and (d) lithogenic material export (in mg m^{-2} d^{-1}) as a function of latitude (º).

4.3.2 The variability of carrying coefficients in the surface ocean

In this section, I examine the variability of CCs and link it to phytoplankton community structure at time of sampling (Table 4.1). In the Iceland (*Ice*) group the calcite CC is larger than the CC for either opal or lithogenic material, which is somewhat surprising given previous observations that show opal as an important ballasting biomineral in the region (Martin *et al.*, 2011) during the spring bloom. This apparent larger contribution of calcite in the total flux can be explained by the fact that most of the *Ice* group stations were occupied in July-August 2007 (21 of 28 stations, see Appendix C, Table C.1), during which coccolithophores formed an increasingly important component of the plankton (Poulton *et al.*, 2010). The Porcupine Abyssal Plain (*PA)* and Atlantic gyres (*AG)* groups display higher carrying coefficients for opal than for both calcite and lithogenic material. This is quite an unexpected result because calcification rates are higher than silicification rates at these locations (Poulton *et al.*, 2006).

The Crozex (*Cro)* station group also showed a higher value for *b* suggesting that POC was more associated with BSi than with PIC. During the Crozex cruises (D285/286, see Appendix C, Table C.1 in supplementary material), plankton community structure shifted from a mixed *Phaeocystis*/diatom community to a microflagellate dominated community (Poulton *et al.*, 2007).

Therefore, the absence of the calcifying group of phytoplankton may explain the negligible calcite CC of the *Cro* station group. Honda and Watanabe (2010) concluded that 92% of sinking POC was associated with minerals (mainly opal) at 5000m. In the surface Honda and Watanabe, (2010) reported less than 20% of sinking

POC was associated with minerals (either opal, calcite or lithogenic) matching our findings in the Southern Ocean.

Table 4.1: Carrying coefficients (CCs) for each group station compared to previous studies. n is the sample number. Values in italics and brackets are CCs estimated using $POC_{total} = POC_{PIC} + POC_{BSi} + POC_{lith} = a.PIC_{flux} + b.BSi_{flux} + c.lith_{flux}$ as done in (Klaas and Archer, 2002) ignoring parameter *d* (e.g. forcing the intercept to zero). Surface CCs from previous study: * (Honda and Watanabe); † (Lam *et al.*, 2011). [1]The proportion of non mineral associated sinking POC is calculated as in (Honda and Watanabe, 2010) (parameter d in their Table 1). As the d parameter represents an absolute POC flux, it is expressed as mg POC m^{-2} d^{-1}.

		Carrying Coefficients (CCs)					
Station groups and locations	N	*a*	*b*	*c*	*d (inter-cept)*	R^2 (p value)	Proportion of non mineral associated sinking POC (%)[1]
Iceland (*Ice*)	28	0.69 *(0.85)*	0.32 *(0.47)*	0.17 *(0.49)*	76.00 *(0)*	0.50 (<0.001) *0.88 (<0.001)*	32.6
PAP group (*PA*)	8	5.13 *(4.99)*	79.67 *(79.59)*	-0.29 *(-0.30)*	-2.77 *(0)*	0.81 (0.020) *0.96 (<0.001)*	-2.6
Atlantic gyres (*AG*)	7	1.14 *(1.96)*	3.98 *(4.70)*	-0.01 *(-0.02)*	23.61 *(0)*	0.89 (0.019) *0.94 (0.002)*	37.5
Crozex (*Cro*)	12	-0.11 *(0.02)*	0.16 *(0.27)*	0.45 *(2.04)*	105.45 *(0)*	0.20 (0.020) *0.83 (<0.001)*	73.9
All sites	55	0.005 *(0.21)*	0.26 *(0.47)*	0.07 *(0.19)*	120.387 *(0)*	0.16 (0.006) *0.63 (<0.001)*	67.7
Western Pacific Subartic gyre (150m)*	21	0.05	0.35	0.17	0.41	0.58	81.6
Global surface (0-115m)†	165	0.73	0.17	not estimated	3.35	0.33	Not estimable
Global surface (115-265m)†	165	0.41	0.06	not estimated	0.79	0.28	Not estimable

Whilst calcite and opal concentrations appear to be related to downward POC flux rates, they are not the sole determinants of the flux. It is likely that an important additional factor is the detailed of the phytoplankton community structure (e.g.

silicifying vs calcifying vs non mineralizing groups) at the time of sampling reported elsewhere (Poulton *et al.*, 2006; Poulton *et al.*, 2007; Poulton *et al.*, 2010). Future studies looking at CCs should integrate normalized indices of phytoplankton community structure to address this issue.

4.3.3 The variability of non mineral associated sinking POC in the surface ocean

We followed the approach of Honda and Watanabe, (2010) using CCs which allows us to explore the variability of the proportion of non-mineral associated sinking POC. Results indicate that the non mineral associated sinking POC flux in the surface ocean ranges from 0 (we considered the small negative proportion of non-mineral associated POC at *PA* as 0) to 73% (*Cro*) of total POC flux.

The *Ice* and *AG* station groups have similar fractions of non-associated POC export (32 and 37% respectively, Table 4.1). At *Ice* stations, diatoms blooms are reported in spring (Martin *et al.*, 2011) with coccolithophores in the post bloom period (Poulton *et al.*, 2010).

In the *AG*, PIC and BSi producers represented ranges of 3-24% and 4-27% of the surface ocean POC fixation respectively (Poulton *et al.*, 2006). This continual production of biominerals likely leads to the relatively small fraction of POC export not associated with biominerals for both groups.

The *PA* group recorded the lowest fraction of unballasted export. Most of the *PA* data are from cruise D341 where I was able to divide the flux into a fast sinking ballasted pool and a slow sinking pool which my initial observations suggested was unballasted (Riley *et al.*, 2012; Le Moigne *et al.*, in review-b). Furthermore, the

dataset presented here suggests that the fast pools contained rather little non biomineral associated POC during D341.

The *Cro* station group displays the highest proportion of non-associated POC, which is unexpected given the known role of diatoms in regulating Southern Ocean carbon export (Treguer and Pondaven, 2000). This could be due to the presence of *Phaeocystis (*Poulton *et al., 2007)*, a non-mineralizing organism documented as playing an important role in carbon export elsewhere in the ocean (DiTullio *et al.*, 2000).

Honda and Watanabe (2010) estimated the proportion of non associated POC as being approximately 82% of the total POC export in the Western Subarctic Pacific (at 150m), a value which is close to that we found in the *Cro* group. In the Western Subarctic Pacific region the phytoplankton community is similar to the one found around the Crozet plateau, being composed mostly of pico and nanophytoplankton with a seasonal diatom peak in spring followed by picoeukaryotes and *Synechococcus* dominance in summer (Liu *et al.*, 2004). This similarity in PCS between the two regions, coupled to the rarity of coccolithophores south of the Subantartic front in the Indian sector of the Southern ocean (Mohan *et al.*, 2008), potentially explains the large proportion of non ballast-associated POC in both regions. Overall the occurrence of a non associated POC flux is not unique to the Western Subarctic Pacific as suggested by Honda and Watanabe (2010).

4.3.4 Implication for the ballast hypothesis

In this remainder of this section, I explore how the occurrence of an important non-ballast associated POC flux in surface could potentially affect the strong correlations between POC and minerals found by Klaas and Archer, (2002) at depth. Armstrong *et*

al., (2002) found that the flux of organic matter at depths >1800m is directly correlated with the fluxes of ballast minerals at these depths. They hypothesized that this represented the remnants of a ballasted exported pool with a surface non-mineral associated pool having been totally degraded in the upper ocean.

Our direct observations of surface non-associated flux support this concept. Surprisingly, the pool of non-associated sinking POC seems to be more important in high latitude provinces where opal is often thought to play an important role in the transport of POC (e.g.: the Southern Ocean or the Western Pacific Subarctic (Honda and Watanabe, 2010)).

This could find its origin in the dynamic of the export fluxes. Those areas are dominated by intense diatoms bloom in spring, however for the remainder of the year, a non blooming regime dominates during which opal represents a low fraction of the total flux (Lam *et al.*, 2011). For instance, *Cro* (November-January) sampled a declining bloom that peaked in October (Venables *et al.*, 2007). Therefore, *Cro* stations generally represent non blooming regime described in Lam *et al.*(2011).

Armstrong *et al.*, (2002) hypothesized that non-mineral associated POC disappears exponentially with depth based on sediment traps deployed along 140ºW at the Equatorial Pacific site (EqPac). The EqPac region has unique biogeochemical features such as the upwelling of nutrient-rich water, and a divergence zone, which supports a highly productive phytoplankton community that contributes significantly to global new production (Chavez and Barber, 1987) and thus to export. Despite this unique setting, the concepts developed from the deep trap data appear relatively applicable across larger spatial scales with differing ecosystem structures.

The proportion of non-associated sinking POC is highly variable in the surface ocean and represents an important fraction of the total POC flux. (Klaas and Archer,

2002) assumed that below 1000 m the non-associated sinking POC was negligible. This assumption is very likely to be valid in areas where the proportion of non-associated sinking POC is low. It is unclear however whether non-associated sinking POC is completely absent at depth in settings where the non-associated sinking POC in the surface is important (for instance in Honda and Watanabe (2010) and *Cro* station group in this study).

Ignoring non-associated sinking POC (e.g. forcing the intercept *d* to 0) forces extra variability into the CCs. On a statistical basis, removing the *d* parameter should improve the significance of MLRA. However, forcing the intercept *d* to 0 does not improve the statistical significance (Table 4.1). Other parameter assessing the statistical significance of the MLRA such as the Akaike information criteria could be attempted to solve this issue. For instance, at *Ice*, when d is ignored, CC for lithogenic material becomes more important than the CC for BSi. Similarly, the all sites CC (Table 4.1) for PIC becomes more important when *d* is ignored. Hence, the CCs could then be substantially distorted if the intercept is significant. Moreover, when d is ignored, the MLRA gains in statistical significance.

This could potentially bring new insights about the global predominance of POC flux associated with one or another mineral.

The most surprising result is that diatom dominated areas are characterized by the highest levels of non associated POC export both our study and that of Honda and Watanabe (2010). This is consistent with the results of François *et al.* (2002); Lam *et al.*(2011) and Henson *et al.* (2012) who show that transfer efficiency is low in high latitudes diatoms dominated areas. They argue that this is due to low levels of recycling and poorly packaged aggregates in such regions. However I suggest that an alternative hypothesis is that such regions have very high levels of non-mineral

associated POC export, which is readily remineralised in midwaters with a small export of mineral associated export which is efficiently transferred giving an overall low transfer efficiency.

4.4 Conclusions

Global compilation of surface POC and mineral export fluxes suggest that the proportion of POC associated with each mineral is driven by phytoplankton community structure more than latitude. In the surface ocean, the proportion of non-associated sinking POC is highly variable and may be important at high latitude regions. Adjustments in community composition and the mineral content of the sinking particles will alter the efficiency by which POC is transported to depth. For example, predicted shifts of biomineralizing species such as diatoms toward smaller species (Bopp *et al.*, 2005) may alter the partitioning of ballast vs non-ballast associated sinking POC in the surface ocean and potentially increase the proportion of free POC. If this happens, community composition and the mineral content of the sinking particles will be affected and thereby alter the efficiency by which the POC is transported to depth. This is a critical issue for the ocean atmosphere partitioning of CO_2 (Kwon *et al.*, 2009).

Acknowledgments

We would like to thank the captain and crew of the RRS *Discovery* and the D341-D350-D354 scientific teams. We also gratefully acknowledge Bob Head (PML), Darryl Green, Chris Marsay and Andy Milton (NOC) for assistance in analytical work. This work is part of the lead author's doctoral research and was supported by

the CalMarO program, (E.U, grant agreement no.: 215157) and by the U.K. Ocean 2025 program.

5. The Influence of Calcite and Microzooplankton on the Remineralization of Sinking Aggregates

The following chapter has been reproduced from a manuscript to be submitted in Global Biogeochemical Cycles. Frédéric A.C. Le Moigne, Morgane Gallinari, Emmanuel Laurenceau, Christina L. De La Rocha "The Influence of Calcite and Microzooplankton on the Remineralisation of Sinking Aggregates"

Data contribution: The rolling tanks were set up and prepared by the author, Morganne Gallinari (IUEM) and Emmanuel Laurenceau (Master student, IUEM, Plouzane, Brest, France. Chalk preparation, ammonium, POC, PON, DW, PIC, bacterial enumerations were performed by the author with help of respectively Annick Masson, Celine Liorzou and Anne-Clair Baudoux (IUEM). Sinking speeds, aggregates enumeration, size and cultures were undertaken by Emmanuel Laurenceau. Zooplankton cultures were provided by Oceanopolis Brest. Nitrates, nitrites and dissolved silicon were analysed by Morganne Gallinari (IUEM). DOC and TDN were analysed by Zia Chowdury and Cynthia Dumousseaud (both NOC). TPP, DOP, and phosphates were analysed by Claire Labry at IFREMER Plouzane. Christina de La Rocha analysed ectoenzymes activities. Philippe Pondaven and Herwig Stibor (IUEM) advised on microzooplankton handling.

Abstract: In the deep ocean, strong correlations observed between downward fluxes of minerals and particulate organic carbon (POC) have inspired the "ballast hypothesis" which posits that association with minerals provides POC physical

protection from remineralisation and excess density which increases sinking speeds, two factors which increase export efficiency. Many previous studies have confirmed the link between ballast and sinking speeds. We incubated phytoplankton in darkness in cylindrical rolling tanks in the presence and absence of added calcite minerals (coccoliths) and microzooplankton (rotifers) to observe the resulting effects on losses of POM, changes in DOM concentrations, losses of organic matter, and regeneration of nutrients. POM, measured as POC, particulate organic nitrogen (PON), and total particulate phosphorus (TPP), decreased by 20-60% over the 8 days of the experiment due to remineralisation and conversion to DOM. There were differences for the different elements (C, N, P, and Si), but generally the presence of zooplankton and/or added calcite had little effect in losses of POM. Microzooplankton drove greater production of ammonium and phosphate via remineralisation. In the experiment as a whole, net phosphorus remineralisation occurred, but not net nitrogen remineralisation, despite observed increases in ammonium concentrations. Overall, we conclude that the factors influencing the proportion of POC incorporated into aggregates such as the amount of POC that winds up in aggregates seems to be the most important determinant of export. However, it would be important to verify these results in experiments incorporating a more complex food web (i.e., including bacterivores, a variety of microzooplankton, and perhaps mesozooplankton as well).

5.1 Introduction

Through the processes of the biological pump, 5 to10 Gt C per year are exported to the deep ocean in the form of dissolved and particulate organic matter (Falkowski *et al.*, 1998; Henson *et al.*, 2011). Without such transfer of carbon to the deep ocean, pre-Industrial atmospheric CO_2 concentrations would have been almost twice as high

as they were (Broecker and Peng, 1982; Parekh *et al.*, 2006) and a greater portion of the current annual anthropogenic CO_2 emissions would remain in the atmosphere, exacerbating the current increase of atmospheric CO_2 (Sarmiento and Toggweiler, 1984; Le Quéré *et al.*, 2010). Having a predictive understanding of the amount of carbon exported to the deep ocean is therefore a key issue in the framework of global climate change.

In the deep ocean, strong correlations are observed between downward fluxes of biominerals (opal and calcite) and particulate organic carbon (POC). This observation has inspired the "ballast hypothesis" that suggests sinking fluxes of minerals (such as biogenic calcite, biogenic opal, and lithogenic material like clays) drive the POC flux to the deep sea (Armstrong *et al.*, 2002a; Francois *et al.*, 2002; Klaas and Archer, 2002). Correlations between mineral and POC fluxes into deeply deployed sediments traps (Deuser *et al.*, 1981; Klaas and Archer, 2002) have been interpreted to reflect both (1) physical protection provided from remineralisation provided by minerals (Francois *et al.*, 2002) and (2) the association of minerals with sinking POC, thereby increasing aggregate or fecal pellet density and therefore sinking velocity (Francois *et al.*, 2002; Klaas and Archer, 2002; Passow *et al.*, 2003; Ploug *et al.*, 2008a; Engel *et al.*, 2009b; Fischer and Karakas, 2009; Lee *et al.*, 2009b; Sanders *et al.*, 2010). Klaas and Archer (2002) argued that in the deep ocean, calcite is predominantly associated with POC because of calcite's greater abundance and density compared to opal and clay. However, it has also been shown that addition of minerals fragments aggregates into smaller, denser aggregates (De La Rocha *et al.*, 2008; Engel *et al.*, 2009b), potentially lowering aggregate sinking velocities.

Although the concept of a ballasting role of biominerals for the export of large aggregates is gaining support (Ploug *et al.*, 2008a; Thomalla *et al.*, 2008; Engel *et al.*,

2009b; Lee *et al.*, 2009b; Iversen and Ploug, 2010; Sanders *et al.*, 2010; Riley *et al.*, 2012; Le Moigne *et al.*, in review-b), very little evidence of minerals' ability to reduce rates of organic matter remineralisation has been gathered so far (Engel *et al.*, 2009a; Iversen and Ploug, 2010). Particulate organic matter (POM) in sediments can be protected from decomposition via their adsorption onto the surfaces of minerals (Mayer, 1994; Hedges and Keil, 1995), through the formation of stable, 3-D structures of organic matter and mineral that physically protect organic matter against degradation (Liu and Lee, 2007), and through the size the minerals add to the organic matter, retaining it in the particulate size fraction.

It is far from clear, however, that such processes occur or are important for the protection of POM in the water column, although minerals have been hypothesized to physically exclude bacteria and ectoenzymes from aggregates (Engel *et al.*, 2009a) or perhaps to hinder zooplankton grazing on aggregates. Confusing the issue is that the colonization of aggregates by bacterivorous zooplankton could reduce bacterial activity, decreasing rates of organic matter decomposition (Grossart and Ploug, 2001).

To begin to address these issues, I allowed phytoplankton to aggregate in the presence and absence of calcite minerals and microzooplankton, and the character, composition, and sinking velocity of the resulting aggregates was monitored several times over 8 days. The formation and sinking of the aggregates are detailed in a companion paper (Laurenceau *et al.*, in prep). This chapter concerns the composition, remineralisation, and solubilisation of material over the course of the experiment.

5.2 Materials and methods

5.2.1 Experimental Set-up

Experiments were carried out in cylindrical tanks kept in rotation on motorized tables to allow particles to sink freely throughout the duration of the experiment (Shanks and Trent, 1980; Passow and De la Rocha, 2006; De La Rocha *et al.*, 2008). More details about the set up and methods used in this chapter are described in appendix D. Twelve 4.5-liter tanks were set up, covering three replicates of four different treatments (Table 5.1): phytoplankton only, phytoplankton + minerals (1.5 mg/L), phytoplankton + microzooplankton (6200 rotifers l^{-1}) and phytoplankton + microzooplankton + minerals (coccoliths).The amount of rotifer inoculated in the tanks was driven by technical limitation and is fairly low relative to the amount of POM in suspension in the tanks. Calcite concentrations corresponds to the particles remaining in suspension after several minutes as explained in appendix D.5. This concentration corresponds to 10 fold the concentration of PIC in surface open ocean waters (Poulton *et al.*, 2006). Tanks were kept in darkness at 15ºC and held in rotation at speeds, generally between 1.5 and 3 revolutions per minute (RPM), that were adjusted during the experiment to maintain POM in suspension as it became incorporated into aggregates. Samples were taken on days 0, 2, 4, and 8.

Table 5.1. Experimental design

Phytoplankton only (P)		+ Zooplankton (*PZ*)		+ Minerals (*PM*)		+ Minerals and Zooplankton (*PZM*)	
tank 1 (T1)	day 2	tank 2 (T2)	day 2	tank 3 (T3)	day 2	tank 4 (T4)	day 2
tank 5 (T5)	day 4	tank 6 (T6)	day 4	tank 7 (T7)	day 4	tank 8 (T8)	day 4
tank 9 (T9)	day 8	tank 10 (T10)	day 8	tank 11 (T11)	day 8	tank 12 (T12)	day 8

All tanks were filled a mixture of seawater (salinity of 34.33; somlit-db.epoc.u-bordeaux1.fr) filtered through 0.6 μm polycarbonate filters to remove phytoplankton and microzooplankton but not bacteria and an equal volume mixture of two different diatom cultures, *Skeletonema marinoï* and *Chaetoceros gracilis*, grown in modified f/2 medium ($Si(OH)_4$ = 50 μM; PO_4 = 4 μM; NO_3 = 64 μM, and vitamins and trace elements in f/2 quantities). Two species of phytoplankton were used in order to obtain aggregates nearer to the oceanic conditions.

Microzooplankton (the marine rotifer, *Brachionus* sp.) were added to tanks 2, 6 and 10. Minerals were added to tanks 3, 7 and 11. Both microzooplankton and minerals were added to tanks 4, 8 and 12. Approximately 3 x 10^4 individual rotifers were added to the rotifer containing tanks, for an abundance of 6200 individuals per liter, with the exception of T10, which received only 2 x 10^4, translating into an abundance of 4400 rotifers per liter.

The solution of suspended calcium carbonate was prepared from Cretaceous (Maastrichtian) chalk from the cliffs of Rügen, Germany, on the Baltic Sea. The chalk was disaggregated, gently ground, soaked overnight in bleach, and then rinsed with deionized distilled water (Milli-Q). The calcite was then suspended in artificial sea water (1l made of 1.68g of $NaHCO_3$, 71.25g of $MgSO_4$ and 321.25g of NaCl) and only those particles remaining in suspension after several minutes were used in the experiment. A similarly prepared solution of chalk from Rügen used by De La Rocha et al. (2008) consisted largely of coccoliths and smaller calcium carbonate debris. Calcite was added to tanks 3, 7, 11, 4, 8 and 12.

The experiment lasted 8 days. Tanks 1, 2, 3 and 4 were sampled on day 2, tanks 5, 6, 7 and 8 on day 4, and tanks 9, 10, 11 and 12 on day 8. Aggregates were removed with a 10-ml disposable pipette with its tip cut off and concentrated in a

flask, allowing for separate samples of aggregates and of "background" water to be taken. Final volume of the total aggregates collected were recorded. Hereafter, treatments (summarized in Table 5.1) will be abbreviated as *P* for phytoplankton only, *PZ* for phytoplankton + zooplankton, *PM* for phytoplankton + mineral and *PZM* for phytoplankton + zooplankton + mineral.

5.2.2 Bacteria counts

4 mL of background water samples were fixed with formalin (2% v/v) and frozen at -80ºC until preparation for counting. A solution of Tween 80 was used to facilitate the detachment of bacteria from the particulate organic matter (Yoon and Rosson, 1990). This mixture was sonicated (3 X 10s) in an ice bath, filtered onto 0.2 μm filters and then stained with SYBR gold (Invitrogen) for 15 min in the dark. 1 mL of sample was filtered onto black polycarbonate filters (0.22 μm) and mounted with 30μL of phosphate buffer solution:glycerol (1:1). 0.01% v:v - p-phenylenediamine) was used to ensure good conservation during storage at -20 ºC until further counting. More than 200 bacteria were typically counted using an Olympus epifluorescence microscope.

5.2.3 Nutrients

Silicate, nitrate + nitrite, and phosphate were analysed by standard methods using a Bran+Luebbe AAIII auto-analyser as described by Aminot and Kerouel (2007). Ammonium was analysed manually by spectrophotometry (Shimatzu UV 1700) as described by Koroleff (1969).

5.2.4 Particulate matter analysis

50 to 250 mL of sample for particulate organic carbon (POC) was filtered (50 to 250 ml) onto pre-combusted (450ºC, 4h), pre-weighed Whatman GF/F filters, rinsed with a few mL of ultra pure water (MilliQ) to remove salts, and dried at 40ºC for 24h. Afterwards, filters were fumed to remove inorganic carbon and POC and PON were measured using a Flash 1112 series elemental NC analyser ThermoQuest as described in Lorrain *et al.*, (2003).

50 to 250 mL of sample for particulate inorganic carbon (PIC) were filtered onto 0.4 µm Millipore polycarbonate filters, rinsed with MilliQ water, and dried. Filters were digested in 0.4M nitric acid for 24 h. Concentrations of Ca and Na were determined using a PerkinElmer Optima 4300DV inductively coupled plasma optical emission spectrometer (ICP-OES) using a concentric glass nebulizer and a baffled, cyclonic spray chamber as described in Poulton *et al.*(2006). PIC was calculated assuming that all PIC was $CaCO_3$. The low Na concentrations in the digests indicated complete removal of sea-salt from the filters by the MilliQ water rinsing and therefore no calcium contribution from seawater.

5 to 50 mL of sample for biogenic silica ($bSiO_2$) were filtered onto 0.4µm polycarbonate filters (Millipore) and dried at 60ºC. $bSiO_2$ was dissolved in 4 mL of 0.2 M NaOH at 80ºC for 45 min (Nelson *et al.*, 1989), neutralized by addition of 1 mL of HCl and determined colorimetrically as dissolved silicon samples (see previous section).

5 to 50 mL of sample for total particulate phosphorus (TPP) were filtered onto pre-combusted (450ºC, 4h) Whatman GF/F filters and rinsed with filtered seawater. Filters were then dried at 60ºC for 24h and frozen for further analysis. Once defrosted, filters were rinsed with 2mL of 0.17M Na_2SO_4. The filters were then placed in 20 mL

precombusted borosilicate scintillation vials with 2mL of 17mM $MgSO_4$. The vials were covered with aluminium foil, dried at 95ºC, and stored in a desiccator until analysis. The vials were combusted at 450ºC for 2 h and, after cooling 5mL of 0.2NHCl were added to each vial. Vials were closed and heated at 80ºC for 30 min to digest TPP into phosphates. The digested TPP samples were analyzed with the standard molybdate colorimetric method for phosphates (Monaghan et al., 1999; Aminot and Kerouel, 2007).

5.2.5 Ectoenzyme activity: leucine hydrolysis

Aminopeptidase activity was measured using L-leucinemethyl coumarinyl amide (Leu-MCA) in methyl Cellosolve as substrate analogue (Hoppe *et al.*, 1988). Samples were incubated in duplicate across a range of leucine concentrations and with sterile-filtered and boiled seawater controls (Hoppe *et al.*, 1988). Fluorescence was measured in a FP-1520 spectrofluorometer (JASCO) at a 364 nm excitation wavelength and a 445nm emission wavelength. Final results are expressed in terms of maximal velocities (V_{max}) from fitting a Michealis-Menton curve through the resulting data.

5.2.6 Dissolved Organic Carbon, Nitrogen and Phosphorus

50ml were filtered through pre-combusted (450ºC, 4h), Whatman GF/F filters into 60 mL acid cleaned HDPE bottles and stored frozen (–20ºC) until analysis. Dissolved organic carbon (DOC) and total dissolved nitrogen (TDN) was measured using a Shimadzu TOC VCSH Total Organic Carbon Analyzer with the TNM-1 Total Nitrogen detector, according to methods of Pan *et al.*(2005). Dissolved organic nitrogen (DON) concentrations were calculated as the difference between TDN and

inorganic forms of dissolved nitrogen (e.g. nitrates, nitrite, and ammonium). 5 to 50 mL of sample for dissolved organic phosphorus (DOP) in the background water was filtered through a precombusted Whatman GFF. 15 mL of filtered samples were placed in precombusted borosilicate vials and frozen at –20ºC until analysis via a segmented flow automated method with on-line photo-oxidation (Aminot and Kerouel, 2001).

5.3 Results

5.3.1 Formation of aggregates

Aggregates formed overnight in all but the phytoplankton-only tank following the introduction of the phytoplankton, zooplankton, and minerals to the various rolling tanks. By the time of sampling on day 2, there were 75–220 aggregates >1mm in all but the phytoplankton-only tanks, which still contained no aggregates. By day 4, the phytoplankton-only tanks contained ~50 aggregates >1mm while the other tanks had reached their maximum numbers of aggregates of ~220.

This aggregation of the phytoplankton in the tanks drove a considerable amount of the decrease over time in POC, PON, TPP, and $bSiO_2$ that remained suspended in the water in the tanks after they had been removed from the roller table (Figure 3.1).

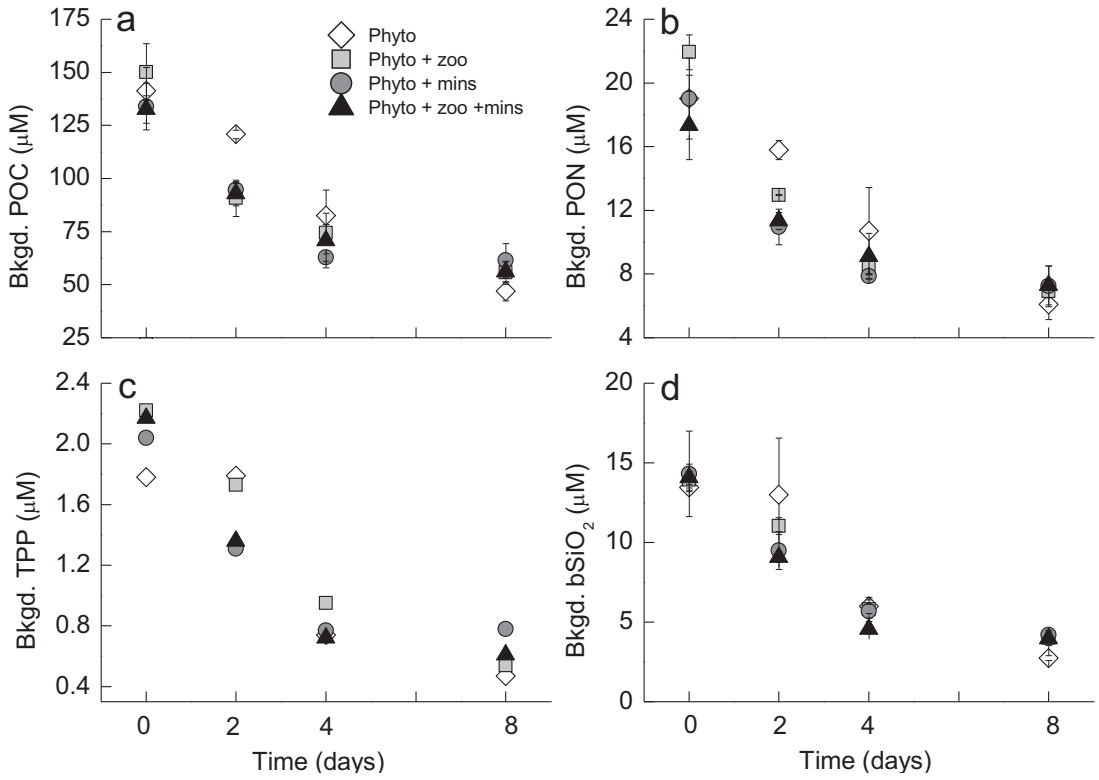

Figure 5.1: Concentrations of (a) POC, (b) PON, (c) TPP and (d) $bSiO_2$ remaining suspended in the background water after tanks were removed from the rolling table and sinking particles allowed to settle.

5.3.2 Photosynthetic efficiency

The quantum efficiency of photosystem II (F_v/F_m) of the phytoplankton in the experiment declined throughout the experiment from initial values of 0.6 (Figure 5.2). By day 2, quantum efficiencies were below 0.5 for both phytoplankton, both incorporated into aggregates and not, in all treatments. By day 4, they fell below 0.3 in all cases and were markedly lowest in aggregates in all but the treatments containing zooplankton but no added calcite.

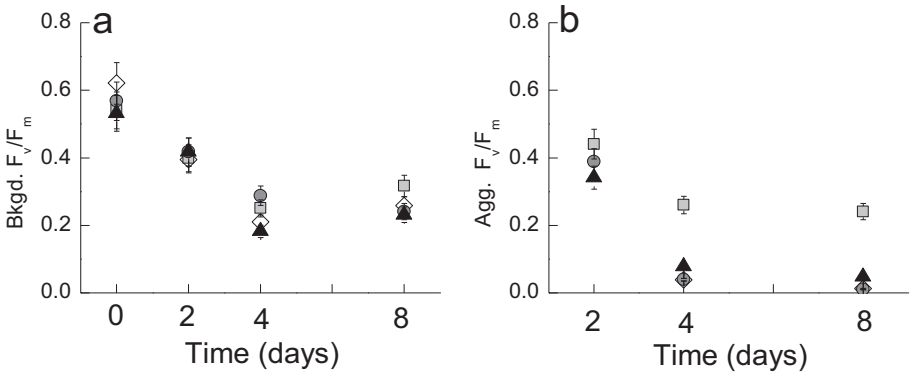

Figure 5.2: Photosynthetic efficiency (F_v/F_m) of phytoplankton in (a) the background water and (b) associated with aggregates. Symbols as in Figure 5.1.

5.3.3 Material in the dissolved phase, suspended particulate matter, and aggregates

The decrease in the photosynthetic efficiency of the diatoms in the experiment coincided with an increase in the concentrations of most nutrients (Figure 5.3) and other dissolved materials (Figure 5.4) and with a decrease in the amount of suspended POM (Figure 5.1) (Tables 5.2-5.6).

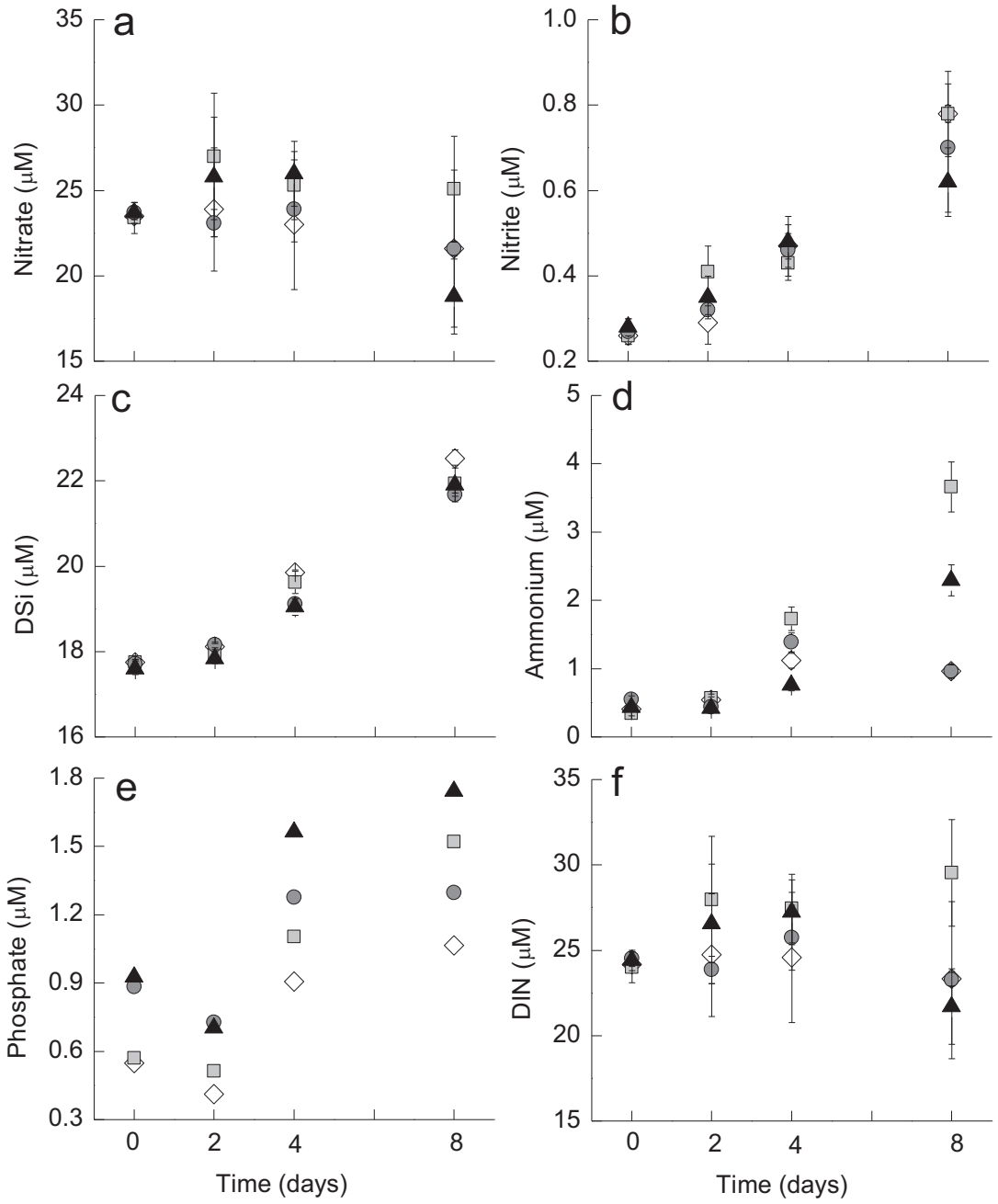

Figure 5.3: Concentrations of (a) nitrate, (b) nitrite, (c) ammonium, (d) DSi, (e) phosphate, and (f) DIN (nitrate + nitrite + ammonium) in the tanks. Symbols as in Figure 5.1.

Dissolved silicon (DSi) concentrations increased in all tanks from an initial concentration of 17.7 ± 0.1 µM to an average final concentration of 22.0 ± 0.4 µM (Table 5.5; Figure 5.3) (Table 5.6). Phosphate concentrations also increased by 0.4–

1.0 μM (Tables 5.4 & 5.6). Nitrite concentrations in all treatments increased between the beginning to the end of the experiment (from 0.27 ± 0.02 μM at day 0 to 0.70 ± 0.08 μM on day 8). Ammonium concentrations roughly doubled in the *P* and *PM* tanks and increased five- to tenfold in the tanks containing zooplankton (Table 5.3). The only nutrient not to show a general increase during the experiment was nitrate, which remained relatively close to 23 μM in the *P* and *PM* tanks and did not rise above 27, even in the zooplankton-containing tanks (Table 5.3; Figure 5.3).

Concentrations of DOM increased during the experiment. Between the beginning and end of the experiment, concentrations of DOC in the tanks rose from 130–160 μM to 170–180 μM in all but the phytoplankton-only tanks (Figure 5.4). Likewise, there was a notable increase in DOP in all but the phytoplankton-only tanks. DON concentrations also increased in all tanks between day 0 and day 8, with the greatest increase occurring in tanks containing zooplankton (P*Z* and *PZM*).

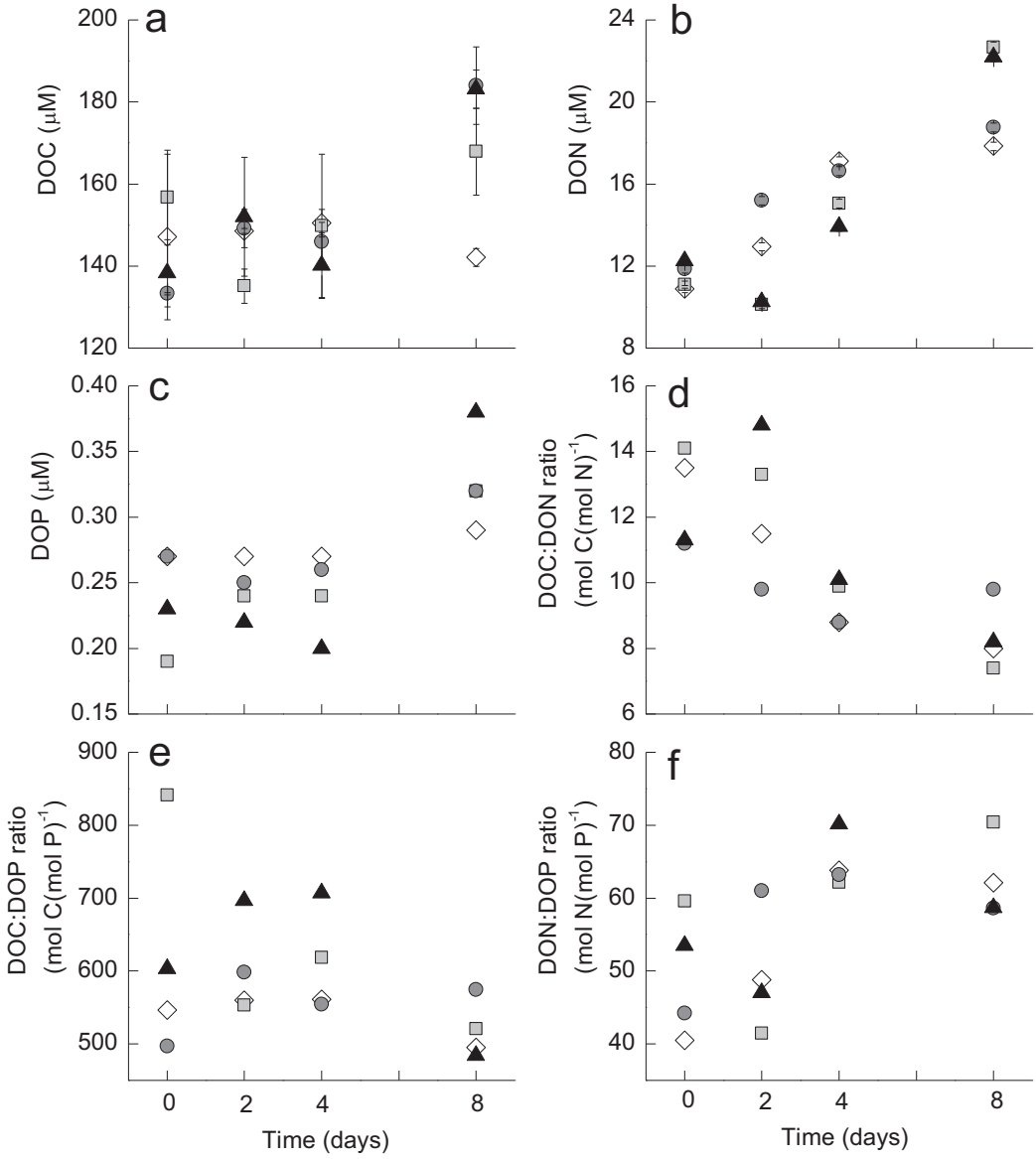

Figure 5.4: Background (a) DOC, (b) DON and (c) DOP concentrations and the molar elemental composition (C:N:P) of (d) DOC:DON, (e) DOC:DOP, (f) DON:DOP. Symbols as in Figure 5.1.

In contrast, the amount of particulate matter decreased during the experiment. Suspended particulate matter (POC, PON, TPP, and $bSiO_2$) in the tanks decreased from day to day during the experiment (Figure 5.1). This decrease in suspended matter, however, is due not only to the destruction of this material, but also to its incorporation into aggregates large and dense enough to sink (and therefore no long be

sampled as part of the suspended matter). The total amount of POC, PON and TPP in aggregates from *PZ*, *PM* and *PZM* tanks increased from day 2 to day 4 then decreased through to the end of the experiment (Table 2). In the phytoplankton-only tanks (where visible aggregates first appeared sometime between days 2 and 4, aggregate POC, PON and TPP increased through the end of the experiment.

Table 5.2. Dissolved and particulate organic carbon. Errors are from samples replication.

	Bkgd POC	Agg POC	Total POC	DOC	Total OC
P	µmol L^{-1}	µmol L^{-1}	µmol L^{-1}	µM	µmol L^{-1}
d0	141 ± 11	0	141 ± 11	147 ± 20	289 ± 23
d2	121 ± 2	0	121 ± 2	149 ± 1	269 ± 2
d4	83 ± 12	26 ± 5	109 ± 13	151 ± 3	259 ± 14
d8	47 ± 4	31 ± 1	78 ± 4	142 ± 2	220 ± 5
PZ					
d0	150 ± 13	0	150 ± 13	157 ± 12	307 ± 18
d2	91 ± 9	6	96 ± 9	135 ± 4	232 ± 10
d4	75 ± 4	50	124 ± 4	150 ± 18	273 ± 18
d8	56 ± 5	39 ± 2	95 ± 6	168 ± 11	263 ± 12
PM					
d0	134 ± 11	0	134 ± 11	144 ± 13	278 ± 17
d2	95 ± 3	21 ± 1	115 ± 3	149 ± 5	265 ± 6
d4	63 ± 2	43 ± 3	106 ± 3	146 ± 5	252 ± 6
d8	62 ± 8	41 ± 2	103 ± 8	184 ± 9	286 ± 13
PZM					
d0	133 ± 7	0	133 ± 7	144 ± 13	277 ± 15
d2	93 ± 6	28 ± 3	121 ± 6	152 ± 14	273 ± 16
d4	71 ± 13	50 ± 3	120 ± 13	140 ± 8	261 ± 15
d8	56 ± 5	38 ± 3	94 ± 5	183 ± 5	277 ± 7

5.3.4 Bacteria counts

Bacteria abundances in the background water did not significantly vary with time or treatment (Figure 5.5). The highest abundance recorded was in the *PM* treatment at day 0 ($3.32 \pm 1.21 \times 10^6$ cells mL^{-1}) whereas the lowest bacteria

abundance was observed in *PZM* at day 8 ($1.21 \pm 0.61 \times 10^6$ cells mL^{-1}). These counts are, however, within error of each other. On all days where there are data, bacterial abundances are the lowest in zooplankton containing tanks, although, again, the numbers are within error of the counts for the other tanks.

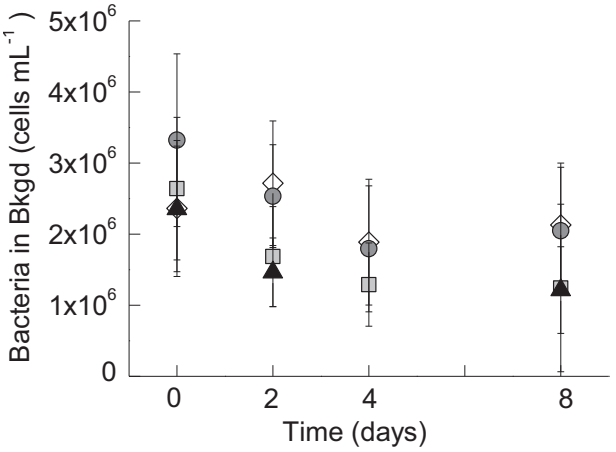

Figure 5.5: Abundance of bacteria in background water. Symbols are as in Figure 5.1.

5.3.5 Ectoenzyme activities

At the beginning of the experiment, rates of leucine hydrolysis were the same in the different treatments (Figure 5.6). However, at the end of the experiment, the V_{max} for the leucine hydrolysis was greater in the background water of the *PM* tanks ($V_{max} = 177.2 \pm 19.2$ h^{-1} for *PM*) than in the other treatments ($V_{max} = 108.3 \pm 23.1$ h^{-1} for *P;* $V_{max} = 103.3 \pm 13.6$ h^{-1} for *PZ;* $V_{max} = 119.3 \pm 13.8$ h^{-1} for *PZM*).

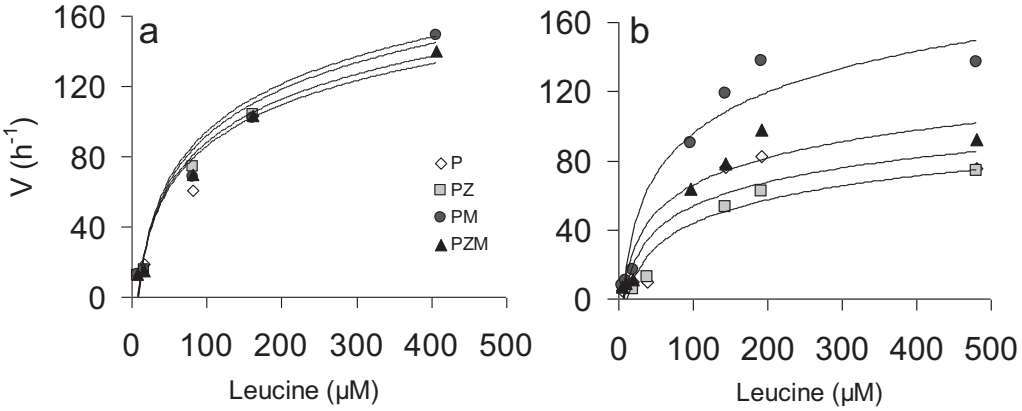

Figure 5.6: Aminopeptidase activity in the background water of the tanks on days 0 (a) and 8 (b) as determined from the hydrolysis of leucine. Filled circles represent *P* tanks, filled triangles represent *PZ* tanks, open circles represent *PM* tanks, and open triangles represent *PZM* tanks.

5.4 Discussion

5.4.1 POM losses versus remineralisation versus DOM production

POM that has been destroyed is generally no longer an active part of the biological pump, as in general dissolved material does not sink through the ocean. POM can be destroyed both through remineralisation (oxidation that results in the regeneration of dissolved inorganic nutrients) and through transformation into DOM (via excretion by phytoplankton, zooplankton, and bacteria, through "sloppy feeding" by zooplankton, and through solubilisation by ectohydrolases). Although DOM can be relatively labile and short-lived, this distinction between remineralisation and conversion to DOM is interesting because only remineralisation converts organic carbon to CO_2.

In this chapter, I therefore attempt to separate losses of POM, remineralisation of nutrients, and changes in concentrations of DOM.

5.4.2. Decline in the condition of the phytoplankton during the experiment

With respect to the destruction of POM and the potential regeneration of nutrients during the experiment, is important to know the state that the phytoplankton inoculated into the rolling tanks were in, because healthy cells should in principle be more resistant to destruction. The phytoplankton dispensed into the rolling tanks at the beginning of the experiment were indeed initially relatively healthy, as indicated by a quantum efficiency of photosystem II (F_v/F_m) around 0.6 (Parkhill *et al.*, 2001) (Figure 5.2). Values of F_v/F_m declined dramatically with time, not due to a lack of nutrients (all of which existed in abundance) (Figure 5.3), but likely to the dark conditions of the incubation. By day 2, quantum efficiencies of PSII had dropped 28% to about 0.4 in all treatments (Figure 5.2), indicating cells under stress. By day 4, values of F_v/F_m had dropped below 0.1 for cells associated with aggregates in the *P*, *PM*, and *PZM* tanks and remained there through day 8, indicating cells in extreme stress. Values of F_v/F_m, however, remained around 0.3 for non-aggregated cells in all tanks and in aggregates in the *PZ* tank, the ammonium regenerated by zooplankton in this tank perhaps sustaining the phytoplankton in a healthier condition than in the other tanks.

In short, the dark conditions of the incubation quickly drove the phytoplankton into stress, rendering them vulnerable to lysis and microbial attack.

5.4.3 The loss of POM

As the incubation in darkness progressed, the total amount of POC, PON, and TPP present in the tanks (i.e., the sum of that present in aggregates and as non-sinking particles in the background water) declined (Tables 5.2-5.4; Figure 5.7).

Table 5.3. Dissolved and particulate organic nitrogen, and DIN. * error calculated as the standard error of the 4 measurements at d0.

	Bkgd PON	Agg PON	Total PON	DON	Total ON
P	µmol L^{-1}	µmol L^{-1}	µmol L^{-1}	µmol L^{-1}	µmol L^{-1}
D0	19 ± 3	0	19.0 ± 2.6	10.9 ± 1.1	30.0 ± 2.8
D2	16 ± 1	0	15.8 ± 0.6	13.0 ± 3.7	28.8 ± 3.8
D4	11 ± 3	3.5 ± 0.6	14.2 ± 2.8	17.1 ±4.0	31.4 ± 4.9
D8	6 ± 1	4.8 ± 0.1	10.9 ± 1.0	17.9 ± 1.3	28.7 ± 1.6
PZ					
D0	22 ± 1	0	21.9 ± 1.1	11.1 ± 1.1	33.0 ± 1.5
D2	13 ± 0	1	13.9 ±0.0	10.1 ± 3.7	24.1 ± 3.8
D4	9 ± 1	6.6	15.2 ± 0.5	15.1 ± 4.0	30.2 ± 4.4
D8	7 ± 0	5.8 ± 0.2	12.7 ± 0.5	22.7 ± 1.6	35.4 ± 5.0
PM					
D0	19 ± 2	0	19.0 ± 1.5	11.9 ± 0.7	30.9 ± 1.6
D2	11 ± 1	3.2 ± 0.6	14.2 ± 1.3	15.2 ± 2.0	29.4 ± 2.4
D4	8 ± 0	6.2 ± 0.5	14.1 ± 0.5	16.6 ± 2.6	30.7 ± 2.6
D8	7 ± 1	5.7 ± 0.3	12.9 ± 1.3	18.8 ± 4.9	31.7 ± 5.0
PZM					
D0	17 ± 2	0	17.4 ± 2.2	12.2 ± 0.9	29.6 ± 2.3
D2	11 ± 1	4.4 ± 0.8	15.8 ± 0.9	10.3 ± 3.7	26.0 ± 3.8
D4	9 ± 1	7.4 ± 0.6	16.5 ± 1.6	13.9 ± 2.1	30.4 ± 2.6
D8	7 ± 1	5.5 ± 0.3	12.8 ± 1.3	22.2 ± 3.4	35.0 ± 3.6

Table 5.3 (continued)

	nitrate	nitrite	NH_4*	total DIN	Total N
P	µmol L^{-1}	µmol L^{-1}	µmol L^{-1}	µmol L^{-1}	µmol L-
D0	23.5 ± 0.1	0.26 ± 0.21	0.41 ± 0.07	24.2 ± 0.3	54.1 ± 2.7
D2	23.9 ± 3.6	0.29 ± 0.05	0.54 ± 0.07	24.7 ± 3.6	53.5 ± 1.0
D4	23.0 ± 3.8	0.47 ± 0.07	1.12 ± 0.07	24.6 ± 3.8	56.0 ± 2.8
D8	21.6 ± 0.4	0.78 ± 0.02	0.96 ± 0.07	23.4 ± 0.4	52.1 ± 1.6
PZ					
D0	23.4 ± 0.9	0.26 ± 0.02	0.35 ± 0.07	24.0 ± 0.9	57.0 ± 1.1
D2	27.0 ± 3.7	0.41 ± 0.06	0.57 ± 0.07	27.9 ± 3.7	52.0 ± 1.0
D4	25.3 ± 2.0	0.43 ± 0.04	1.73 ± 0.07	27.4 ± 2.0	57.7 ± 3.5
D8	25.1 ± 3.1	0.78 ± 0.10	3.66 ± 0.07	29.5 ± 3.1	64.9 ± 1.2
PM					
D0	23.7 ± 0.4	0.27 ± 0.03	0.55 ± 0.07	24.5 ± 0.4	55.5 ± 1.5
D2	23.1 ± 0.8	0.32 ± 0.01	0.44 ± 0.07	23.9 ± 0.8	53.2 ± 2.2
D4	23.9 ± 1.9	0.46 ± 0.04	1.39 ± 0.07	25.8 ± 1.9	56.5 ± 1.1
D8	21.6 ± 4.6	0.70 ± 0.15	0.96 ± 0.07	23.3 ± 4.6	55.0 ± 1.9
PZM					
D0	23.7 ± 0.6	0.28 ± 0.02	0.43 ± 0.07	24.4 ± 0.6	54.0 ± 2.2
D2	25.8 ± 3.5	0.35 ± 0.05	0.42 ± 0.07	26.6 ± 3.5	52.6 ± 1.5
D4	26.0 ± 1.9	0.48 ± 0.04	0.76 ± 0.07	27.2 ± 1.9	57.6 ± 1.7
D8	18.8 ± 2.2	0.62 ± 0.08	2.30 ± 0.07	21.7 ± 2.2	56.7 ± 1.7

Table 5.4. DOP, TPP, and dissolved inorganic phosphate.* error calculated as the standard error of the 4 measurements at d0

	Bkgd TPP*	Agg TPP*	Total TPP*	DOP*
P	µmol L^{-1}	µmol L^{-1}	µmol L^{-1}	µM
D0	1.78 ± 0.17	0	1.78 ± 0.17	0.27 ± 0.03
D2	1.79 ± 0.17	0	1.79 ± 0.17	0.27 ± 0.03
D4	0.74 ± 0.17	0.30 ± 0.17	1.04 ± 0.24	0.27 ± 0.03
D8	0.47 ± 0.17	0.45 ± 0.17	0.93 ± 0.24	0.29 ± 0.03
PZ				
D0	2.22 ± 0.17	0	2.22 ± 0.17	0.19 ± 0.03
D2	1.73 ± 0.17	0.10 ± 0.17	1.83 ± 0.24	0.24 ± 0.03
D4	0.95 ± 0.17	0.65 ± 0.17	1.60 ± 0.24	0.24 ± 0.03
D8	0.54 ± 0.17	0.47 ± 0.17	1.00 ± 0.24	0.32 ± 0.03
PM				
D0	2.04 ± 0.17	0	2.04 ± 0.17	0.27 ± 0.03
D2	1.31 ± 0.17	0.39 ± 0.17	1.70 ± 0.24	0.25 ± 0.03
D4	0.77 ± 0.17	0.62 ± 0.17	1.39 ± 0.24	0.26 ± 0.03
D8	0.78 ± 0.17	0.57 ± 0.17	1.34 ± 0.24	0.32 ± 0.03
4				
D0	2.17 ± 0.17	0	2.17 ± 0.17	0.23 ± 0.03
D2	1.36 ± 0.17	0.60 ± 0.17	1.96 ± 0.24	0.22 ± 0.03
D4	0.72 ± 0.17	0.77 ± 0.17	1.50 ± 0.24	0.20 ± 0.03
D8	0.61 ± 0.17	0.56 ± 0.17	1.17 ± 0.24	0.38 ± 0.03

Table 5.4 (continued)

P	Total OP µmol L^{-1}	PO_4^* µM	Total P µmol L^{-1}
D0	2.05 ± 0.17	0.55 ± 0.17	2.60 ± 0.25
D2	2.06 ± 0.17	0.41 ± 0.17	2.47 ± 0.25
D4	1.31 ± 0.24	0.91 ± 0.17	2.22 ± 0.30
D8	1.21 ± 0.24	1.07 ± 0.17	2.28 ± 0.30
PZ			
D0	2.41 ± 0.17	0.57 ± 0.17	2.98 ± 0.25
D2	2.07 ± 0.24	0.51 ± 0.17	2.59 ± 0.30
D4	1.84 ± 0.24	1.10 ± 0.17	2.94 ± 0.30
D8	1.32 ± 0.24	1.52 ± 0.17	2.85 ± 0.30
PM			
D0	2.31 ± 0.17	0.88 ± 0.17	3.19 ± 0.25
D2	1.95 ± 0.24	0.73 ± 0.17	2.68 ± 0.30
D4	1.66 ± 0.24	1.28 ± 0.17	2.93 ± 0.30
D8	1.66 ± 0.24	1.30 ± 0.17	2.96 ± 0.30
PZM			
D0	2.40 ± 0.17	0.93 ± 0.17	3.33 ± 0.25
D2	2.18 ± 0.24	0.70 ± 0.17	2.88 ± 0.30
D4	1.69 ± 0.24	1.56 ± 0.17	3.26 ± 0.30
D8	1.55 ± 0.24	1.74 ± 0.17	3.29 ± 0.30

Only 45% to 77% of the initial POC, PON, and TPP remained at the end of the experiment. Similar values (Table 5.5) were seen for the inorganic biomineral $bSiO_2$ associated with the diatoms inoculated into the tanks. The missing 23% to 55% of the POM and $bSiO_2$ had to have been either remineralized and/or converted into DOM.

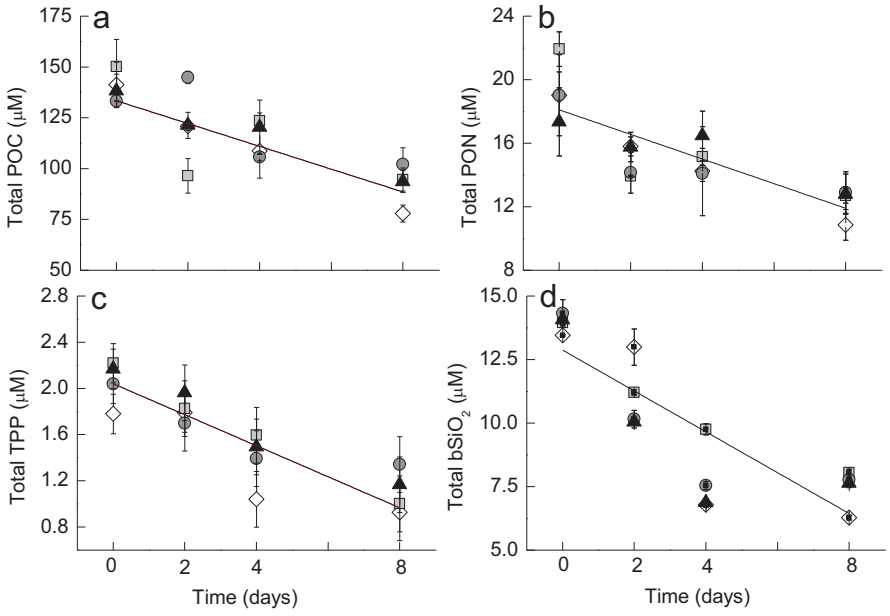

Figure 5.7: Total (background + aggregate) concentration of (a) POC, (b) PON, and (c) TPP versus day in the different treatments. The regression through all the data (except *PZ* on day 2) shown in panel (a) is POC = –9.1(d) + 134.9 (r^2 = 0.90). The regression through all the data shown in panel (b) is PON = –0.78(d) + 18.11 (r^2 = 0.69). The regression through all the data in panel (c) (except *PM* on day 8) is TPP = –0.13(d) + 2.03 (r^2 = 0.83). The regression through all the data in panel (d) is $bSiO_2$ = –0.80(d) + 12.9 (r^2 = 0.71).

Table 5.5. DSi and $bSiO_2$.

P	Bkgd $bSiO_2$ µmol L^{-1}	Agg $bSiO_2$ µmol L^{-1}	Total $bSiO_2$ µmol L^{-1}	DSi µmol L^{-1}	Total Si µmol L^{-1}
D0	13.5 ± 0.0	0	13.5 ± 0.0	17.8 ± 0.0	31.2 ± 0.0
D2	13.0 ± 0.7	0	13.0 ± 0.7	18.1 ± 0.1	31.1 ± 0.7
D4	6.0 ± 0.1	0.8 ± 0.1	6.8 ± 0.1	19.8 ± 0.1	26.6 ± 0.1
D8	2.8 ± 0.0	3.5 ± 0.1	6.3 ± 0.1	22.5 ± 0.2	28.8 ± 0.2
PZ					
D0	14.0 ± 0.1	0	14.0 ± 0.1	17.8 ± 0.1	31.7 ± 0.1
D2	11.0 ± 0.1	0.2	11.2 ± 0.1	17.9 ± 0.1	29.1 ± 0.1
D4	5.8 ± 0.2	3.9 ± 0.2	9.8 ± 0.2	19.6 ± 0.3	29.4 ± 0.3
D8	4.0 ± 0.1	4.0 ± 0.1	8.1 ± 0.1	21.9 ± 0.4	30.0 ± 0.5
PM					
D0	14.3 ± 0.5	0	14.3 ± 0.5	17.7 ± 0.1	32.0 ± 0.5
D2	9.5 ± 0.2	0.7 ± 0.2	10.2 ± 0.3	18.2 ± 0.1	28.3 ± 0.3
D4	5.7 ± 0.1	1.9 ± 0.1	7.6 ± 0.2	19.1 ± 0.1	26.7 ± 0.2
D8	4.2 ± 0.1	3.6 ± 0.2	7.8 ± 0.2	21.7 ± 0.0	29.5 ± 0.2
PZM					
D0	14.1 ± 0.2	0	14.1 ± 0.2	17.6 ± 0.1	31.7 ± 0.2
D2	9.1 ± 0.1	1.0 ± 0.0	10.0 ± 0.1	17.8 ± 0.1	27.9 ± 0.1
D4	4.6 ± 0.1	2.3 ± 0.0	6.9 ± 0.2	19.0 ± 0.2	25.9 ± 0.2
D8	4.0 ± 0.1	3.7 ± 0.2	7.6 ±0.1	21.9 ± 0.0	29.5 ± 0.2

Table 5.6. Estimates of remineralization. (values in parenthesis are possibly affected by contamination). Errors are from samples replication.

P	N remineralization est. From DIN µmol L^{-1}	P remineralization est from PO_4 µmol L^{-1}	Si remineralization est. from DSi µmol L^{-1}
D2	0.5 ± 3.6	–0.14 ± 0.25	0.4 ± 0.1
D4	0.4 ± 3.8	0.36 ± 0.25	2.1 ± 0.1
D8	–0.8 ± 0.4	0.52 ± 0.25	4.8 ± 0.2
PZ			
D2	3.9 ± 3.8	– 0.06 ± 0.25	0.2 ± 0.1
D4	3.4 ± 2.2	0.53 ± 0.25	1.9 ± 0.3
D8	5.5 ± 3.3	0.95 ± 0.25	4.2 ± 0.4
PM			
D2	–0.6 ± 0.9	–0.15 ± 0.25	0.4 ± 0.1
D4	1.2 ± 2.0	0.40 ± 0.25	1.4 ± 0.2
D8	–1.2 ± 4.6	0.42 ± 0.25	4.0 ± 0.1
PZM			
D2	2.2 ± 3.5	–0.23 ± 0.25	0.2 ± 0.2
D4	2.8 ± 2.0	0.63 ± 0.25	1.4 ± 0.2
D8	–2.7 ± 2.3	0.81 ± 0.25	4.3 ± 0.1

Table 5.6 (continued)

	C remineralization est. from OC	N remineralization est. from ON	P remineralization est from OP	Si remineralization est. from $bSiO_2$
P	µmol L^{-1}	µmol L^{-1}	µmol L^{-1}	µmol L^{-1}
D2	19 ± 23	1.2 ± 4.6	–0.01 ± 0.25	0.5 ± 0.5
D4	29 ± 26	–1.4 ± 5.5	0.74 ± 0.25	6.7 ± 0.0
D8	68 ± 24	1.2 ± 3.2	0.84 ± 0.25	7.2 ± 0.0
PZ				
D2	75 ± 20	9.0 ± 4.1	0.33 ± 0.25	2.7 ± 0.0
D4	33 ± 25	2.8 ± 4.3	0.57 ± 0.25	4.2 ± 0.1
D8	44 ± 21	–2.4 ± 3.7	1.08 ± 0.25	5.9 ± 0.0
PM				
D2	14 ± 18	1.6 ± 2.8	0.36 ± 0.25	4.2 ± 0.4
D4	26 ± 18	0.2 ± 2.7	0.65 ± 0.25	6.8 ± 0.3
D8	(-8 ± 21)	–0.7 ± 5.2	0.65 ± 0.25	6.5 ± 0.3
PZM				
D2	11 ± 22	3.6 ± 4.4	0.22 ± 0.25	4.0 ± 0.0
D4	50 ± 21	–0.8 ± 3.4	0.71 ± 0.25	7.2 ± 0.0
D8	(-0 ± 16)	–5.4 ± 3.6	0.85 ± 0.25	6.4 ± 0.1

This apparent decrease in POM and $bSiO_2$ reflects the destruction of particulate matter during the experiment, although the numbers are influenced to some extent by undersampling of sinking aggregates <1mm that were present in the tanks by days 2 to 4 (see discussion below). Relative to the total amount of C, N, P, and Si in the tanks, this undersampling was minor, while relative to the amount of particulate matter, it was, at times, significant.

Tabulation of the total amount of nitrogen (total dissolved nitrogen and total particulate nitrogen) in the sampled tanks during the experiment, suggests that under-sampling and tank to tank variability existed but relative to the total amount of nitrogen in the tanks were not a major source of error (Table 5.3).Excepting tank 10 (the *PZ* tank on day 8 which appears to contain an excessive quantity of N), the average amount of N accounted for when each tank was sampled was 54.9 ± 2.0 μmol L^{-1}, indicating that the amount of nitrogen in the tanks could be accounted for within ±4%. The average N-content of the tanks on each sampling day showed no trend over time (d0 = 55.2 ± 1.4, d2 = 52.8 ± 0.7, d4 = 56.9 ± 0.8, and d8 = 54.6 ± 2.3), again suggesting that relative to the total amount of material present, tanks were fairly quantitatively sampled. Similar patterns can be seen with total P and total Si (Tables 5.4-5.5), the two other elements for which there is a complete set of budget data, altogether lending confidence that the sampling was quantitative enough for the noted losses in POM and $bSiO_2$ to be meaningful. However, as will be discussed below, gains in dissolved silicon were considerably less than losses of $bSiO_2$ (Table 5.5), something which would indicate undersampling of the particulate matter during latter stages of the experiment.

Interestingly, the losses of total POC, total (aggregate plus background) PON, total TPP, and total $bSiO_2$ in the tanks (in terms of μmol L^{-1} per tank per day) were essentially linear with time (Table 5.7; Figure 5.7). Total POC decreased by 5.7 μmol L^{-1} per tank per day ($r^2 = 0.84$; $\alpha = 0.01$), total PON by 0.78 μmol L^{-1} per tank per day ($r^2 = 0.69$; $\alpha = 0.01$), total TPP by 0.13 μmol L^{-1} per tank per day ($r^2 = 0.83$; $\alpha = 0.01$), and total $bSiO_2$ by 0.80 μmol L^{-1} per tank per day ($r^2 = 0.71$; $\alpha = 0.01$). For the different treatments, the trends are similar, although the linear regressions are not always significant due to the small number of data points (Table 5.7). Decline in concentrations of total POC and total PON was the slowest in the *PM* and *PZM* treatments, but that pattern does not hold for total TPP or total $bSiO_2$. Had the experiment been longer and more particulate matter destroyed, it is likely that the daily loss rate would have declined.

Table 5.7: Loss of POM and $bSiO_2$ per day tabulated as the slope of linear regressions through the data on Figure 5.7. *not significant

	POC				PON			
	Slope (μmol L^{-1} d^{-1})	r^2	α	*n*	slope (μmol L^{-1} d^{-1})	r^2	α	*n*
P	–7.7	0.99	0.01	4	–0.98	0.97	0.05	4
PZ	–6.9	0.99	0.01	3	–0.94	0.99	0.01	4
PM	–3.6	0.78	n.s.*	3	–0.65	0.66	n.s.*	4
PZM	–5.3	0.95	0.05	4	–0.53	0.84	n.s.*	4
	TPP				$bSiO_2$			
	Slope (μmol L^{-1} d^{-1})	r^2	α	*n*	slope (μmol L^{-1} d^{-1})	r^2	α	*n*
P	–0.12	0.78	n.s.*	4	–1.00	0.77	n.s.*	4
PZ	–0.15	0.99	0.01	4	–0.70	0.92	n.s.*	4
PM	–0.16	0.99	0.05	3	–0.76	0.68	n.s.*	4
PZM	–0.13	0.96	0.05	4	–0.76	0.64	n.s.*	4

5.4.4 Production and destruction of DOM

In a general sense, concentrations of DOM increased during the experiment (Figure 5.4). There were, however, differences between treatments. The presence of zooplankton drove the largest gains in both DON and DOP (Tables 5.3 & 5.4). Added calcite minerals had little influence on the net increase in DON duringof the experiment (i.e. there was a rise of 6.9 μM in the both *P* and *PM* tanks and of ~11 μM in both the *PZ* and *PZM* tanks). However, the minerals were associated with a 3-fold greater increase in DOP in the *PM* compared to *P* tanks (0.018 versus 0.052 μM), although the increase in DOP in the *PZ* and *PZM* tanks was virtually the same (0.14 versus 0.15 μM). Accordingly, the change in DON divided by the change in DOP in the *P* tanks was 380 mol mol^{-1} compared to 131 mol mol^{-1} in the *PM* tanks, and it was 85 mol mol^{-1} compared to 184 mol mol^{-1} in the *PZ* and *PZM* tanks, respectively. Despite the differences, in all cases, the net production of DON severely outstripped that of DOP both in term of the Redfield ratio (16 mol mol^{-1}) and of the N/P ratio of the POM (which was approximately 10 mol mol^{-1}).

The increase in DON was also marked enough, relative to the increase in DOC, to drive the C:N ratio of the DOM in the tanks down from an average of 12.9 ± 1.1 mol mol^{-1} on day 0 to an average of 8.4 ± 1.0 mol mol^{-1} at the end of the experiment. This enrichment of the DOM in nitrogen relative to carbon is driven by both DOC loss and DON gain in the *P* tanks, by a net increase of DOC and DON at unity in the *PZ* tanks, and by a 4- to 6-fold greater net increase of DON than DOC in the mineral containing tanks. Thus in all cases, the DOC is failing to increase the roughly 7 times faster that it could potentially from the nearly Redfield value of POC/PON in the tanks.

As will be discussed later in the section on remineralisation, the significantly greater increase in DON than in DOC and DOP reflects that there was net remineralisation (i.e. destruction of the organic form) of phosphorus and carbon but not of nitrogen. Nitrogen limitation of the bacteria in the tanks, which is plausible given the DOC/DON ratios >10 mol mol^{-1} over most of the experiment (Caron *et al.*, 1988) could have resulted in retention of nitrogen within bacteria rather than its excretion as ammonium (although ammonium concentrations did increase slightly in all tanks, even the ones without added microzooplankton). Alternatively, in addition to or rather than utilizing DON, bacteria could have been taking up ammonium directly throughout the experiment and converting it to DON (Caron *et al.*, 1988).

In summary, remarkable relative gains in DON (compared to DOC and DOP) were observed in all treatments, with much greater increases in DON and DOP occurring in the tanks with zooplankton and with minerals having no discernible influence on net increase in DON. The *P* tanks were the only ones to show net loss of DOC between the beginning and the end of the experiment. It is not surprising that zooplankton might enhance the production of DOC. It is not clear if the minerals increased the rate of production of DOC or decreased its rate of destruction, or somehow interfered with the measurement of DOC concentrations (the *PM* and *PZM* treatments have notably high DOC concentration on day 8 and a perplexing increase in total organic matter content between days 4 and 8; Tables 5.2 & 5.6) (as discussed in the next section).

5.4.5 Destruction of organic matter

There are two ways that the amount of remineralisation that occurred during the experiment can be estimated: by the losses of organic matter and $bSiO_2$ and by the

increase in concentrations of dissolved inorganic nutrients (Table 5.6). Changes in dissolved inorganic carbon concentrations and pCO_2 were not monitored.Therefore losses of organic carbon were the only means of assessing carbon remineralisation during the experiment.

Judging from the total loss of organic carbon from the tanks, an indistinguishable amount of carbon remineralisation occurred between days 0 and 8 in the *P* and *PZ* treatments, 68 ± 24 μmol L^{-1} versus 44 ± 21 μmol L^{-1} (Table 5.6). In the *P* tank, the increase in C remineralisation was relatively uniform throughout the second part of the experiment, starting at 5 μmol L^{-1} d^{-1} for the first 2 days of the experiment, and stabilizing at 9.75 μmol L^{-1} d^{-1} between days 2 and 4 as well as days 4 and 8. Between days 4 and 8 in the *PZ* tank, a similar loss of organic carbon of 7.25 μmol L^{-1} d^{-1} occured.

What happened with carbon remineralisation in the mineral-containing tanks, however, is less clear. Until day 4, losses of organic carbon in the *PM* and *PZM* tanks were within the same range as those in the *P* tanks (Table 5.6). However, between days 4 and 8, organic carbon concentrations *increased* in the *PM* and *PZM* tanks (Tables 5.2 & 5.6). One explanation for this is that the DOC samples that were analyzed were somehow contaminated, perhaps during filtration or handling of the samples.

However, the N budget for these samples, which is based in part on DON measured at the same time as DOC and on the same aliquots of water, is reasonably sound (Table 5.3) as the measured DON concentrations do a good job of closing the N budget. It is also unlikely that net carbon fixation occurred in these mineral-containing tanks between days 4 and 8. The cells in these tanks were in clearly stressed condition based on the state of their photosynthetic apparatus (Figure 5.2) and were,

furthermore, kept in darkness. However, between days 4 and 8 *PM* and *PZM* tanks were placed within the same black tent, therefore, some carbon fixation in response to a light leak cannot be excluded as a possibility. Thirdly, it may be that the calcite provided additional surface for bacterial colonization, moving them up into the particle size range sampled by the GF/F filters used for POC analyses, causing an apparent increase in the amount of organic carbon in the tanks on some days (due to the bacteria not being taken into account by the day 0 sampling). A last and more likely possibility is that the error on the DOC measurement (Table 5.6) precludes us from drawing strong conclusions about carbon remineralisation from the losses of organic carbon in these tanks.

Likewise, the propagated errors of 2 to 5 μmol L^{-1} on the total amount of organic nitrogen in the tanks make it difficult to see if there was any net loss of organic nitrogen during the experiment (Table 5.6). However, that errors of this size all but obscure the signal is in itself suggestive that negligible amounts of nitrogen remineralisation back to nitrate during the 8 days of the experiment, even in the presence of microzooplankton.

In contrast to the situation for organic nitrogen, it appears that significant remineralisation of organic phosphorus to phosphate occurred during the experiment (Table 5.6). Likewise, the remineralisation of silicon was also clear from losses of $bSiO_2$ during the experiment (Table 5.6), with losses starting out slowly in the *P* tank, but catching up to the other three tanks by day 4 of the experiment.

5.4.6 Nutrient regeneration as an indicator for remineralisation

Given the difficulties included in sampling particulate matter and the large errors in some of the measurements of organic constituents in the tanks, it would be better to

determine net remineralisation directly from the change in concentrations of dissolved inorganic nutrients. Net remineralisation is specified because the decrease in phosphate concentrations between day 0 and day 2 in the *P* and *PZ* tanks (Figure 5.3) suggests that for the first 48 hours of the experiment, the phytoplankton retained enough energy stores to take up phosphate even though the experiment was conducted in darkness (although bacteria could also have taken up phosphate). This would presumably hold true for DIN uptake (and, for the diatoms, for DSi uptake as well), despite the lack of a visible decrease in their concentrations between days 0 and 2 (Figure 5.3).

Estimates of silicon remineralisation based on changes in DSi concentrations are smaller than the estimates based on $bSiO_2$, in this case, an entirely particulate quantity. In this case, it looks like the $bSiO_2$-based estimate overshot by an average of 51 ± 9 %, or roughly 2 μmol L^{-1}. Both estimates, however, suggested that the presence of zooplankton and/or added calcite had no detectable influence over $bSiO_2$ dissolution.

As with the remineralisation estimate based on losses of organic phosphorus, estimates based on increase in dissolved inorganic phosphate indicated that phosphate remineralisation occurred and that more of it occurred in the zooplankton-containing tanks (Table 5.6). However, the phosphate-concentration based estimates are roughly 0.2 μmol L^{-1} lower than the organic phosphorus-based estimates, suggesting the organic phosphorus-based estimates are overestimating phosphorus remineralisation by, on average, 33 ± 28 %. This could be blamed on under-sampling of the TPP, or it could be related to the drop in dissolved inorganic phosphate concentrations of up to 0.2 μM that occurred during the first two days of the experiment (Table 5.4), presumably due to uptake by the phytoplankton before they ran out of energy to do so.

To judge from the observed net change in DIN (nitrate + nitrite + ammonium) during the experiment (Tables 5.3 & 5.6; Figure 5.3), virtually no net nitrogen remineralisation occurred during the experiment, in accordance with the same suggestion from the organic nitrogen data discussed in the above section. The net change in DIN remained close to 0 between day 0 and day 8 in the *P* (–0.8 ± 0.4 μmol L^{-1}), *PM* (–1.3 ± 4.6 μmol L^{-1}); and *PZM* (–2.7 ± 2.3 μmol L^{-1}) treatments. Only in the *PZ* treatment did DIN concentrations increase during the experiment, doing so by 5.5 ± 3.3 μmol L^{-1} DIN between day 0 and day 8. Altogether, this could suggest that detectable net remineralisation of organic matter occurred only in the presence of zooplankton and even that was notably hindered in the presence of added calcite.

It is worth pointing out that while net remineralisation of nitrogen did not clearly occur during the 8 days of the experiment (with the possible exception of the *PZ* tank), nitrogen remineralisation was in fact happening. This can be seen in the several μM increase in ammonium concentrations (greatest in the two treatments containing zooplankton) (Figure 5.3). Nitrite concentrations also slightly increased in all tanks, indicating that nitrification had begun but was occurring relatively slowly. It is not unusual for there to be a several day lag between ammonium excretion and nitrite production and then between nitrite production and nitrate production (Von Brand *et al.*, 1942). The lack of coherent increase in nitrate concentrations during the 8 days of the experiment is unsurprising in light of this expected delay and in the relatively minor increases in ammonium and nitrite (Figure 5.3).

The POM, DOM, and dissolved inorganic nutrient data all suggest that there was notable decoupling of the remineralisation of organic C and P relative to organic N, with clearly observable remineralisation of C and P occurring, but virtually no N remineralisation. This might have been due to efficient retention of N by bacteria in

the experiment due to the high C:N ratio (i.e. >10 mol mol^{-1}) of DOM in the tanks, rendering it difficult for bacteria to obtain enough N relative to C to fuel growth (Caron *et al.*, 1988). Such nitrogen-limited bacteria may have even taken up and assimilated ammonium (Wheeler and Kirchman, 1986; Caron *et al.*, 1988), damping increase in ammonium concentrations, and preventing notable increase in DIN concentrations and detectable loss in total organic nitrogen in the rolling tanks (Table 5.3).

5.4.7 Evidence for health and activity of zooplankton and bacteria during the experiment

Given the complexity of the results and the lack of net N remineralisation, it is necessary to consider how "typical" the activities of the microzooplankton and bacteria were during the experiment and whether or not low concentrations of oxygen might have influenced the patterns observed for remineralisation.

Like large zooplankton species such as copepods, microzooplankton species such as *Brachionus* sp. are known to graze on coccolithophorids (Harris, 1994; Antia *et al.*, 2008) which, like the aggregates formed here in the *PM* and *PZM* treatments, contain coccoliths. Likewise, rotifers are known to be able to graze on whole aggregates (Zimmermann-Timm *et al.*, 1998) and were observed to do so during the experiment (Laurenceau *et al*, in prep).

The increase in ammonium concentrations in the zooplankton-containing tanks (Figure 5.3) can be ascribed to ammonium excretion by live rotifers feeding on phytoplankton during the experiment. This can be tested by determining whether the observed increase in ammonium concentrations could be supported given known rates of ammonium excretion for rotifers. As ammonium concentrations increased from day

2 onwards, ammonium excretion rates (E_{NH4} in µg of ammonium N per mg of zooplankton DW per h) were calculated between day 2 and day 8 during the experiment as:

$$E_{NH_4} = \frac{\frac{[NH_4]_{d8} - [NH_4]_{d2}}{DW_B}}{\Delta t} \qquad \text{Equation 5.1}$$

where $[NH_4]_{d8}$ and $[NH_4]_{d2}$ are concentrations of ammonium on days 8 and 2, Δt is the time between the two sampling points, DW_B is the dry weight per individual *Brachionus* (a value of 0.16 µg per individual (Theilacker and Mc Master, 1971)) . The resulting excretion rates of ammonium per rotifer biomass, ranging from 0.05 µg N mg^{-1} h^{-1} to 0.09 µg N mg^{-1} h^{-1}, although likely to be slight underestimates considering that some ammonium was converted to nitrite during the experiment (Figure 5.3) and that heterotrophic bacteria may have been taking up and assimilating ammonium, compare well with the theoretical maximum ammonium excretion rate of *Brachionus* at 15ºC of 0.11 µg N mg^{-1} h^{-1} (Ejsmont-Karabin, 1983). That the calculated excretion rates are realistic in terms of rotifer biomass supports there having been a significant grazing activity by the rotifers over the duration of the experiment. Moreover, observations were made prior to the experiment of rotifers from the culture used in the experiment feeding on diatom aggregates.

The estimated ammonium excretion rates of 0.05 to 0.09 µg N mg^{-1} h^{-1} (averaged to be 0.07 µg N mg^{-1} h^{-1}) may be used to estimate the (minimum) total amount of PON grazed by the rotifers during the experiment. Assuming no utilisation of DON and assuming a range of N assimilation efficiency of 61% (10ºC) to 85% (20ºC) for *Brachionus* sp. (Nagata, 1989), the total amount of PON ingested by rotifers needed to support the estimated (minimum) amount of ammonium excretion would range from 1.3 to 2.4 µmol L^{-1} of PON over 8 days. Most of this PON, of

course, remained as PON, but as rotifer PON instead of phytoplankton PON. Thus little of the 5-9 μmol L^{-1} loss in PON in the *PZ* and *PZM* tanks (Table 5.3) was related to grazing by the microzooplankton. This fits with the observation of similar levels of PON loss in the *P* and *PZ* treatments and in the *PM* and *PZM* treatments (Table 5.3). A longer experiment duration, a higher abundance of rotifers may have been needed to see significant losses of POM due to consumption by microzooplankton.

Just as it is useful to note that the activities of the microzooplankton (as evidenced from estimated rates of ammonium excretion above) during this remineralisation experiment were relatively "normal", it is useful to have evidence that heterotrophic bacteria were also present and functioning. Although, due to practical limitations, bacterial production was not measured, bacteria were observed in both the water in the tanks and in the aggregates that formed (Figure 5.5) at typical concentrations of between 1.5×10^6 and 3.5×10^6 cells per mL.

That these bacteria were also active can be seen from the measurement of ectoenzyme (aminopeptidase) activities in the water of the tanks (Figure 5.6). At the beginning the experiment, the pattern for aminopeptidase activity is the same in all of the treatments, with the maximum velocity (V_{max}) for leucine hydrolysis being 227 ± 10 h^{-1} and the half saturation constant (K_s) being 192 ± 18 μM ($r^2 = 0.99$). By the final day of the experiment, the values for both V_{max} and K_s had decreased in all tanks, with values ranging from 177 ± 19 h^{-1} and 87 ± 28 μM ($r^2 = 0.97$) in the PM treatment to 103 ± 14 h^{-1} and 157 ± 50 μM ($r^2 = 0.98$) in the PZ treatment. The decrease in V_{max} was smaller in the two mineral containing treatments, which also experienced the greater decrease in K_s (Figure 5.6). The overall drop in aminopeptidase activities may be related to the possible decrease in free-living bacterial abundances during the experiment (Figure 5.5). The divergence in the V_{max} and K_s values between the

different treatments may reflect shifts in the bacterial population dominating each tank or to the response of the bacterial community to changes in DOM concentrations and composition in the different treatments. In any regard, at least as assayed from leucine hydrolyis, the bacteria in the tanks remained active over the course of the experiment.

Lastly, aerobic respiration requires oxic conditions to occur. One could ask whether there was enough O_2 in the tanks for the aerobic oxidation of organic matter to occur throughout the duration of the experiment.

Although dissolved oxygen concentrations were not measured, it is unlikely that conditions in the tanks were either anoxic or suboxic at any point during the experiment. This is based on several observations. First, the tanks, when opened for sampling, did not smell of the H_2S that would have resulted from anoxic conditions. Likewise, the rotifers added to the *PZ* and *PZM* tanks were still visibly alive and swimming at the end of the experiment. Previous experiments in rolling tanks with comparable amount of organic matter in them (around 500 µmol of total POC), did not report suboxic or anoxic conditions even when their duration was longer (Engel *et al.*, 2009a). And lastly, the O_2 consumption calculated from the increase in phosphate concentrations by day 8 assuming Redfield stoichiometry (Anderson and Sarmiento, 1994) is 350 µmol O_2 in the phytoplankton tanks and almost twice that in the tanks with added zooplankton (Table 5.4). Based on loss of OC and OP, the O_2 consumption ranges from 0 µmol (*PZM,* likely contaminated in DOC, see section above) to 440 µmol (*P*) and from 500 (*PM*) to 830 (*PZ*) µmol of O_2 per tank respectively. If the tanks were saturated with O_2 at the beginning of the experiment, there would have been 1,400 µmol of O_2 per tank, leaving, in the very worst case, 580 µmol O_2 (130 µmol L^{-1}) at the end of the experiment. This is in excess of hypoxia (< 60-120 µM O_2)

(Stramma *et al.*, 2008) and should not have resulted in impaired rates of aerobic decomposition of the organic matter.

However, it is important to mention that oxygen concentration inside the aggregates could have differed from the concentrations in the background water. Balzano *et al.*, (2009); Ploug *et al*. (2010) among others, showed a gradient in oxygen concentration from the surface to the interior of aggregates. Oxygen concentrations were almost twice less inside the aggregate relative to the surface. This could explain the difficulties in the interpretation of the N cycling in our experiement as nitrification versus denitrification (conversion of N to volatile nitrous) in sub oxic aggregates leading to changes in N species difficult to resolve and budget to a process level.

5.4.8 A brief summary of the effects of minerals and microzooplankton

Overall, losses of POC, PON, TPP, and $bSiO_2$ of 20-60% by the end of the experiment related to remineralisation and production of DOM occurred linearly. The loss of POC and PON occurred slightly more slowly in the calcite-containing tanks than in the tanks lacking added calcite as previously observed (Engel *et al.*, 2009a). Concentrations of DOM, in contrast, were more variable, reflecting the simultaneous occurrence of DOM production and consumption. Although DON concentrations increased continuously throughout the experiment, especially in the tanks containing zooplankton, concentrations of DOC and DOP really only increased between days 4 and 8 (the end of the experiment).

Remineralisation during the experiment, tabulated from either losses of organic matter or increase in concentrations of dissolved inorganic nutrients, did not follow expected patterns of enhance remineralisation of N and P over C observed over longer periods of time (Martin *et al.*, 1987; Verity *et al.*, 2000). In general, C was

preferentially remineralized relative to N and P, indicative more of respiration than nutrient cycling. This might indicate an insufficiently complex food web within the rolling tanks (i.e. a lack of mesozooplankton, no microzooplankton in the *P* and *PM* tanks and too small an abundance of them in the others, and perhaps a lack of bacterivores in all tanks due to the pre-filtration of the seawater used through 0.6 μm filters). Such a thought is bolstered by the remineralisation of phosphorus and the increase in ammonium being greatest in the two zooplankton-containing treatments.

Neither the zooplankton nor the added calcite minerals had an impact on the increase in DSi concentrations due to the dissolution of $bSiO_2$.

5.4.9 Implications for the ballast hypothesis and future experiments with aggregates.

Strong relationships between sinking fluxes of POC and biominerals into sediment traps in the deep sea have been interpreted to reflect both (1) physical protection provided by minerals of a fraction of the POC against remineralisation and (2) the increase in sinking velocity of POM due to the ballasting effect of mineral particles adsorbed onto or otherwise associated with the POM (Francois *et al.*, 2002; Klaas and Archer, 2002; Passow *et al.*, 2003; Lee *et al.*, 2009b; Sanders *et al.*, 2010).

Although the idea that the association of organic matter with minerals could protect it from microbial attack has been dismissed as operating on the wrong scale to be important in the water column, this experiment suggests that the presence of calcite has an influence over both the solubilisation of POC and the remineralisation of DOC to CO_2. However, over the short duration of the experiment undertaken (8 days) and at the abundance of microzooplankton added (6200 L^{-1}), limited effects of either added calcite or microzooplankton on POM loss or organic matter remineralisation can be

inferred due to contamination and undersampling (as summarized in the above section). Still, it is worth considering briefly to what depth organic matter in the above experiment would have been exported under in the different treatments considering the POM loss rates reported here and aggregate sinking speeds measured by Laurenceau *et al*., (*in prep*).

By converting the estimates for POC losses per day in each treatment (Table 5.7) and converting them to POC-specific loss rates starting from day 4 of the experiment (Table 5.8), the first day for which there were aggregates present in all tanks, it is possible to estimate how much POC would have been exported to 1000m in each treatment, assuming no significant change in either sinking velocity or POC loss rate over that time. As can be seen from the results, the relatively low POC specific loss rates (between 0.009 and 0.021 d^{-1}) mean that a high fraction of the POC in aggregates is exported to 1000m (>89% in all cases, but with the higher sinking speeds associated with the additional ballast provided by the added calcite pushing the preservation of aggregates in the *PM* and *PZM* treatments to 97%). Also, a significant proportion of the POC on day 4 existed in the form of aggregates (24 to 41%) rather than as smaller, suspended particles. The POC reaching 1000m in aggregates from the two mineral containing treatments would have arrived about twice as fast as that in aggregates lacking the additional calcite ballast, although the difference is really only one of a few days. The estimated export efficiency at 1000m (calculated as the percentage of aggregate POC that would have reached 1000m divided by the average total POC at day 0) displays higher values in mineral and zooplankton containing tanks (33%, 30%, 34% in *PZ*, *PM* and *PZM* respectively), largely due to the higher sinking speeds of the aggregates in these tanks (Table 5.8).

Table 5.8 Estimated export of POC. *considering that suspended POC in background was not sinking

	P	*PZ*	*PM*	*PZM*
Sinking speed (m d^{-1}) on d4	181	240	350	365
POC loss rate in tanks (µmol L^{-1} d^{-1})	7.7	6.9	3.6	5.7
POC-specific loss rate (d^{-1}) d4 to d8	0.021	0.016	0.009	0.012
Agg. POC on day 4 (µmol L^{-1})	26.2	49.1	42.9	49.6
POC at 1000m (µmol L^{-1})	23.3	46.0	41.0	47.9
Percentage of aggregate POC reaching 1000 m	89%	94%	97%	97%
Percentage of initial total POCreaching1000m*	17%	33%	30%	34%
Days needed to reach 1000m	5.5	4.2	2.9	2.7

Thus while the results support the notion that additional ballast increases aggregate sinking velocities, helping them to escape the upper ocean more quickly than without it, the presence of suspended calcite minerals in the water at the time of aggregate formation does not appear to influence the amount of available POC that forms in aggregates. The amount of POC that forms in aggregates, however, is a vital component of export efficiency as can be seen by the 60% efficiency of incorporation of POC into aggregates turning an aggregate export efficiency of approximately 90% into a total POC export efficiency of approximately 30%, as described in the preceding paragraph.

The POC-specific loss rates observed here (0.009 to 0.021 d^{-1}; Table 5.8) are both relatively similar to results obtained in some similar experiments (0.012 to 0.050 d^{-1}) (Verity *et al.*, 2000; Engel *et al.*, 2009a; Moriceau *et al.*, 2009), and relatively low compared to the C-specific respiration rates of 0.08 to 0.21 d^{-1} observed in other studies based on oxygen gradients in aggregates (Ploug and Jorgensen, 1999; Ploug and Grossart, 2000; Ploug *et al.*, 2008b; Iversen and Ploug, 2010). Strictly speaking these are not two different ways of estimating the same thing. Our POC-specific loss rate includes losses to both the solubilisation and the oxidation of the POC, while the

oxygen gradients represent oxygen consumption during organic matter respiration, representing the loss of C from microbes associated with aggregates, many of whom would be subsisting on DOM as opposed to POM.

Nonetheless, the lower specific rates for POC loss and the relatively minor amount of remineralization observed during this experiment, with only bacteria and one species of microzooplankton for heterotrophs, and during the experiments of similarly simple design are of concern. They suggest that this simplified approach, utilized here and in studies such as (Verity *et al.*, 2000; Ploug, 2001; Passow *et al.*, 2003; Moriceau *et al.*, 2007; Ploug *et al.*, 2008b; Engel *et al.*, 2009a; Iversen and Ploug, 2010), which attempts to isolate the effects of one group or another on the destruction or remineralization of aggregates, does not truly accomplish this. Because feedbacks and interactions between different groups affect the activities of the different groups and the proportion of respiration against nutrient regeneration (Wang *et al.*, 2009), the whole is truly greater than just the sum of its different, isolated parts. It may be necessary to use a relatively diverse heterotrophic community (bacteria, ciliates, flagellates, other microzooplankton, etc) for notable oxidation of organic matter and recycling of nutrients to occur. Even when a slightly more complex food web has been established in experiments (e.g., as by Ploug and Grossart, (2000)), mesozooplankton have still been generally left out of such experiments. We know, however, they can both consume material in aggregates directly and alter aggregate size and number as a side effect of their swimming behaviour (Dilling *et al.*, 1998; Dilling and Alldredge, 2000; Goldthwait *et al.*, 2004; Goldthwait *et al.*, 2005).

5.5 Conclusion

I performed incubation of phytoplankton in darkness in cylindrical rolling tanks in the presence and absence of added calcite minerals (coccoliths) and microzooplankton (rotifers). There were differences for the elements C, N, P, and Si, but generally the presence of zooplankton and/or added calcite had little effect in losses of POM. Overall, we conclude that the factors influencing the proportion of POC incorporated into aggregates seems to be the most important determinant of export. There is one caveat to this conclusion, however, and that is the effects of macrozooplankton and bacterivores were not tested here. We suggest that further degradation and dissolution experiments should incorporate a complete heteretrophic food web.

Acknowledgments

We thank H. Stibor, Oceanopolis Brest , P. Pondaven, , A.C. Baudoux, R. Corvaisier, A. Masson, C. Liourzou (IUEM), E. Achterberg, C. Dumousseau, Z. Chowdhury, S. Giering (NOC), C. Labrie (IFREMER) for technical support, discussions, and/or advice. This work is part of the lead author's doctoral research and was supported by the CalMarO program (a FP7 Marie Curie initial training network, www.calmaro.eu, European Community, Grant agreement no. 215157), Region Bretagne and the EURO-BASIN program.

6. General conclusion

6.1 Major findings

Chapters 2 and 3 mainly focussed on gaining a better understanding of the capabilities and limitations of the use of radioisotopes as tracer of POC and biomineral downward fluxes from the surface ocean. The great attraction of the ^{234}Th technique is that its fundamental operation (diagnosis of thorium deficit, application of model to derive thorium flux, conversion to POC units using POC/^{234}Th ratio) allows a downward flux rate to be determined from a single water column profile of thorium coupled to an estimate of the POC/^{234}Th ratio in sinking matter.

Chapter 2 considers using different pools of sinking POC recently highlighted (e.g. slow and fast sinking POC pools) into the Th based POC export calculation model. It is shown using data from the Porcupine Abyssal Plain that export is appropriately estimated using the C/Th ratio of the total particulate pool, which at this site approximated that of the >53 μm POC pool. Hence, the existing flux estimates using C/Th ratios on large particles probably approximate total flux. Information regarding the contributions of slow and fast particles to total flux was available and after verifying the theoretical relationship of sinking speed versus particles size, it appears that small and large correspond to slow and fast particles respectively. This information shows that estimates of size fractionated export can be obtained from size fractionated C/Th ratios and the total thorium deficit. This in principle enables an estimation of the sinking velocity of fractionated export from C/Th data alone. Furthermore, it is suggested that the offset between the ^{234}Th derived estimate of the magnitude of the biological carbon pump and other estimates of biological carbon

pump strength is likely not due to the exclusion of small slowly sinking particles in the thorium calculation.

In Chapter 3 results are reported from one of the first attempts to measure POC, PIC and BSi downward fluxes from the surface ocean using ^{234}Th-^{238}U, ^{210}Po-^{210}Pb disequilibria and drifting sediments trap synchronously at the Porcupine Abyssal Plain time-series site during summer 2009. The combined usage of the three techniques allowed us to analyze their suitability not only for POC flux estimation, but also for PIC and BSi fluxes. POC and PIC export based on Th was higher than POC and PIC export based on Po, whilst the drifting sediment traps produced the lowest export estimate. This emphasizes that the integration time of each technique relative to the seasonal cycle of primary production must be taken into account when estimating export fluxes.

To better understand differences between ^{234}Th derived POC (biomineral) export and ^{210}Po derived POC (PIC) export, the ratios of POC (PIC)/radionuclide in small and large particles were studied. The differences are ascribed to their biogeochemical behaviour rather than integration time. However, a thorough knowledge of the phytoplankton community structure and lithogenic material deposition would be useful information to confirm this statement.

In addition, the contribution of smaller (1-53μm) particles to flux is also considered in order to explain the differences in derived fluxes, and it appears that slow sinking particles may also have contributed to the export flux as shown in Chapter 2. When ratios in small particles were used, differences between ^{234}Th and ^{210}Po derived POC (PIC) fluxes were reduced.

Finally, we contributed to the on-going refinement of the ballast hypothesis, by showing a decreasing variability of POC:biomineral with increasing particle size.

Using conclusions from the theoretical relationship between sinking speed and particle size presented in Chapter 2, this confirms the recent hypothesis that link ballasting with the fast sinking pools in the surface ocean.

In Chapter 4, ^{234}Th derived surface particulate organic carbon (POC), biogenic silica (BSi), particulate inorganic carbon (PIC) and lithogenic material export rates from different locations and export regimes in the North Atlantic, the Atlantic tropical and Southern Oceans are considered. Substantial surface POC export accompanied by negligible mineral export was recorded suggesting an important role of a non protected/ballasted sinking POC in the surface ocean.

Mineral ballast carrying coefficients (CCs) were estimated for each area using multiple linear regression analyses after grouping stations based on geographical considerations. Carrying coefficients (CCs) differed from one oceanic province to another and were likely linked to the phytoplankton community at sampling time described eslswhere. This approach confirms that at the Porcupine Abyssal plain (Chapter 3), POC and PIC were tightly associated. The proportion of non-mineral associated sinking POC was highly variable and ranged from 0 to 73% of the total POC flux with at “all sites” estimate of 66%. It is explored how the occurrence of an important non-ballast associated POC flux in the surface could potentially affect the strong correlation between POC and minerals found at depth. It is possible that a persistent pool of non-mineral associated sinking POC may feature at depth conversely to previous results.

Finally in Chapter 5, I undertook an experiment to monitor the remineralization and degradation of artificially made (e.g. in rolling tank) aggregates in the presence/absence of suspended calcite and microzooplankton. I observed a clear decrease of POM over the course of the experiment suggesting that either degradation

or remineralization back to inorganic nutrient occurred. Both microzooplankton and bacteria remained active throughout the duration of the experiment while clear evidences of degradation/remineralisation were recorded from day 4 onwards.

Notable differences arose between treatments. The presence of microzooplankton enhanced POM remineralization back to inorganic nutrients as expected. Also, the presence of calcite minerals enhanced the accumulation of DOC. Furthermore, the presence of calcite in aggregates seemed to have reduced the microzooplankton feeding behaviour resulting in less rotifer induced remineralisation. Elemental ratios (C:N:P) in DOM and POM did not show significant differences between treatments. However, the DOM gained in both N and P relative to C reflecting the complexity of DOM dynamics. Overall, I conclude that the factors influencing the proportion of POC incorporated into aggregates seems to be the most important determinant of export. However, it would be important to verify these results in experiments incorporating a more complex food web (i.e. including bacterivores, a variety of microzooplankton, and perhaps mesozooplankton as well).

6.2 Closing Statement

Studies investigating the magnitude and the processes behind the biological carbon pump have been numerous in the two past decades. Conceptual improvements in the methods (e.g. PELAGRA (Lampitt *et al.*, 2008), Marine Snow Catcher (Riley *et al.*, 2012), Indented Rotating Sphere (Trull *et al.*, 2008), Multiple Unit Large Volume Filtration Systems (Lam *et al.*, 2011), Rolling tanks (De La Rocha *et al.*, 2008)) and/or finer spatial and temporal resolution (e.g. ^{234}Th at low SST spots (Henson *et al.*, 2011), nutrients (Schlitzer, 2004)) now allow the construction of global climatology of the dynamics and magnitude of the biological carbon pump.

It has been proposed that mineral fluxes should be included into modelled representation of the particle export (Armstrong *et al.*, 2002). The inclusion of minerals seemed to better constrain the global pattern of POC export compared to empirical parameterization of POC fluxes that do not imply any a priori mechanism of particle sinking and degradation (Martin *et al.*, 1987). However, including the mineral component in sophisticated models of POC flux requires the use of numerous parameters that are less well constrained (e.g. global mineral fluxes, links between phytoplankton community structure and export) adding additional uncertainties than when adopting the "simple " Martin curve approach (Bianchi *et al.*, 2012). As a results, future work should focus on (1) expanding the database of mineral fluxes in the ocean, (2) define standards for phytoplankton community structure indicators and expanding the dataset of calibrated phytoplankton community structure, (3) better understanding of the link between PCS and export in the surface ocean (e.g. aggregation between minerals and POC, dissolution rate of mineral which is important in driving the ballast to POC ratios).

6.3 Future work

This proposal called "Seasonal variability in the efficiency of upper ocean carbon export" has been written by Stephanie Henson and funded by NERC and GEOTRACES-UK for 18 months period starting in April 2012 with Stephanie Henson (NOC) as PI and myself as PDRA.

6.3.1 Rationale

A key component of the global carbon cycle is the ocean's biological carbon pump (BCP), dominated by the sinking of organic particles from the euphotic zone to the deep ocean (Falkowski *et al.*, 2000). The efficiency of the BCP sets the rate at which carbon is sequestered in the ocean, away from further contact with the atmosphere on timescales of hundreds to thousands of years. Knowledge of the magnitude of the BCP is central to our understanding of the global carbon cycle, the partitioning of carbon storage between different pools, and how the fluxes may change under future global warming. However, currently there remains uncertainty about the strength of the BCP (e.g.(Henson *et al.*, 2011)) and substantially more uncertainty about what controls its variability on seasonal timescales (Buesseler *et al.*, 2008). Recently, a new parameterisation of the export ratio (which describes the efficiency of the upper ocean BCP) was developed that suggested integrated global carbon export was less than half of some previously published estimates (Henson *et al.*, 2011). The large range in estimates of global carbon export, from 5-20 Gt C yr^{-1}, implies that, despite > 30 years of study, no consensus on the magnitude of the BCP is imminent (e.g.(Eppley and Peterson, 1979; Laws *et al.*, 2000; Burd *et al.*, 2010)). This suggests, worryingly, that our knowledge of a major planetary carbon flux is incomplete. The export ratio (e-ratio) algorithm developed by Henson *et al.*, (2011), however, has relatively large uncertainty at cold sea surface temperature (SST) (Figure 6.1), compared to warmer waters. Our hypothesis is that the variability in e-ratio at low temperatures is due to strong seasonality in phytoplankton bloom evolution at high latitudes, driven by temporal shifts in phytoplankton community structure. This project aims to improve the current parameterisation of e-ratio in global integrations by incorporating relevant seasonal information, and thereby reduce uncertainty in the estimate of global BCP

magnitude. This project will assess how seasonal variability of the phytoplankton bloom alters the e-ratio in the sub-Arctic through a combination of *in situ* and satellite data based studies. We propose to collate measurements of particulate organic carbon (POC) flux from two high latitude regions that experience cold SST and strong variability in phytoplankton blooms. This project will use data to be collected on two UK Ocean Acidification Research Programme (OA) cruises to the Arctic and the Antarctic (work funded by NERC). We propose to participate those two existing cruises in 2012 to take measurements of export flux and phytoplankton community structure (PCS). The variability in bloom stage and PCS encountered during the cruises will be used to determine the impact of seasonal gradients in bloom conditions on the e-ratio. Guided by the outcome of the *in situ* studies, we will extrapolate our results to the global scale using an existing database of POC measurements (Henson *et al.*, 2011) and satellite data-derived estimates of bloom stage and PCS. This will be used to develop an improved parameterisation of e-ratio and ultimately a new estimate of the magnitude of the global BCP.

6.3.2 Objectives

The project has two overall objectives: 1). Assess the impact of seasonal variability in the phytoplankton bloom on the export ratio in the sub-Arctic 2). Incorporate relevant seasonal information into parameterisations of export to reduce uncertainty in estimates of the global magnitude of the biological carbon pump Achievements of this project will be: 1). Quantification of the seasonal variability observed in the e-ratio in the high latitude ocean 2). Evaluation of the parameters that drive seasonal variability in the e-ratio 3). Reduced uncertainty in parameterisation of the e-ratio, incorporating

seasonal information 4). A new estimate of the global magnitude of the ocean's biological carbon pump

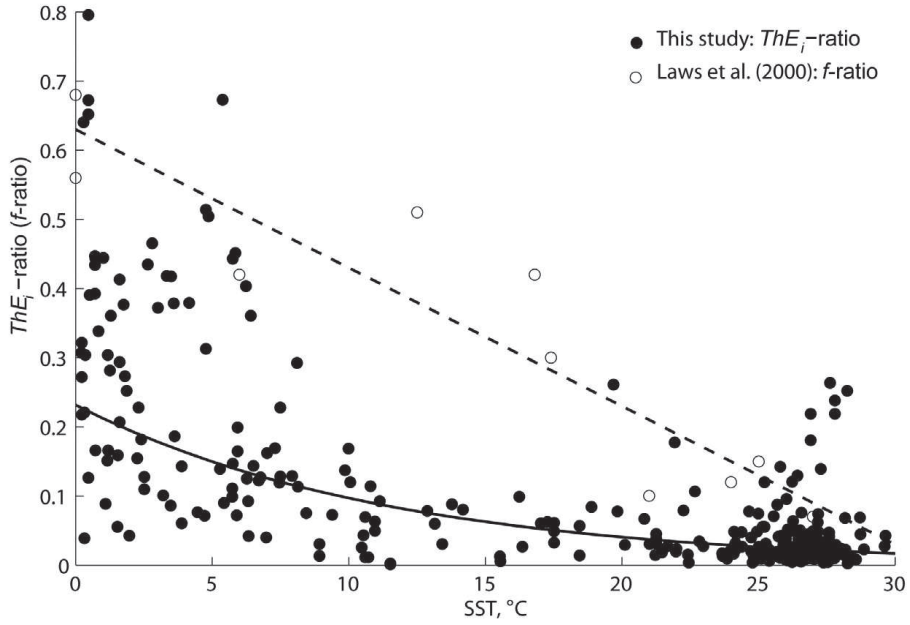

Figure 6.1: Relationship between e-ratio from thorium-based measurements and SST. Regression line is an exponential fit, e-ratio=0.23*exp$^{(-0.08*SST)}$, r2=0.5, p<0.01, n=306. Taken from (Henson *et al.*, 2011).

6.3.3 Our current parameterisation of e-ratio

In Henson *et al.*, (2011), a compilation of Th-export measurements gathered from the literature was used to estimate the global carbon export flux. To extrapolate from the ~ 300 measurements in the compilation to a global estimate, the relationship with SST was investigated. This was partly because the e-ratio is expected to co-vary with SST so that warm, subtropical locations have low e-ratio, and vice versa; partly to be consistent with previous global studies of export efficiency (e.g.(Laws *et al.*, 2000)); and finally as SST is a parameter readily obtained from satellite data, global estimates of carbon export are possible. The relationship between the Th-export based e-ratio and SST from (Henson *et al.*, 2011) is reproduced in Fig. 6.1. This algorithm was

applied to global maps of satellite-derived SST to estimate the globally integrated carbon export. The resulting estimate of 5 GtC yr^{-1} is significantly different from previous estimates using different methodologies that tend to cluster around 10-12 GtC yr^{-1} ((Laws *et al.*, 2000; Schlitzer, 2004; Dunne *et al.*, 2007)). It has been suggested that even these higher values are too low to balance the respiration by heterotrophic activity occurring in meso- and bathypelagic waters (del Giorgio and Duarte, 2002; Burd *et al.*, 2010). This range in estimates suggests that significant sources or sinks of carbon may have been overlooked, or that there are problems with one or more of the measurement methodologies. In our parameterisation of e-ratio, for example, there is clearly room for improvement. There is a large range of e-ratios at low SST, whilst the relationship is relatively well-constrained at moderate to high SST ($r^2 = 0.5$; Fig. E.1). Our hypothesis is that much of the scatter at low temperatures is due to strong seasonal variability in phytoplankton bloom evolution at high latitudes. Including appropriate seasonal information in the parameterisation of the e-ratio is likely to reduce the uncertainty in our estimate of global carbon export and further inform the debate on the magnitude of the global biological carbon pump.

6.3.4 How might seasonal variability in the phytoplankton bloom influence e-ratio?

Over sufficiently long time, and large spatial, scales export production is equivalent to new production (Eppley and Peterson, 1979). The e-ratio then is set by the relative proportion of new and regenerated production, with high e-ratios indicating systems dominated by new production, and low e-ratios indicating those dominated by recycled production. Seasonal variability in the e- ratio at high latitudes arises from the progression from primarily new production at the start of the phytoplankton

bloom, to regenerated production during later stages. This shift is reflected in the PCS, with large phytoplankton, usually diatoms, dominating new production in the early stages of the bloom, ceding to smaller plankton later in the season (e.g.(Barlow *et al.*, 1993)). Clearly, the point in the seasonal cycle at which an export measurement is taken will affect the estimated e- ratio. The e-ratio calculated from *in situ* measurements is generally assumed to be representative of the conditions during the year as a whole, despite data often having been collected during a single cruise. However, time series of POC flux to the deep ocean, as recorded in sediment traps, reveal distinct seasonal cycles (e.g.(Conte *et al.*, 2001; Lampitt *et al.*, 2001)), implying seasonal variability in upper ocean export efficiency. As diatoms have high growth rates and thrive at relatively low light levels (e.g.(Mann and Lazier, 2006)), they are able to increase their biomass very rapidly in spring as the mixed layer shoals. Large plankton tend to also be dense, and so may sink rapidly enough to avoid significant remineralisation in the surface ocean (Boyd and Trull, 2007). There is also evidence that certain species of diatoms can cause reproductive failure in copepods (Irigoien *et al.*, 2002), and are thus grazed less extensively than other primary producers. In addition, diatoms thrive in high nutrient, low light environments, which are associated with relatively weak stratification and an unstable mixed layer. This may facilitate sinking of large phytoplankton, reducing surface remineralisation and increasing export efficiency. After the peak of the high latitude bloom, as nutrients start to become scarce in the euphotic zone, smaller phytoplankton are able to out-compete the large plankton for the remaining resources. The summer period of the bloom is characterised by moderate biomass, dominated by small plankton, principally fuelled by regenerated nitrate (e.g.(Barlow *et al.*, 1993)). These small phytoplankton are generally insufficiently dense to sink rapidly, and also have a large surface area on

which dissolution can occur (Boyd and Trull, 2007). The strong stratification during summer likely also inhibits sinking of particles below the mixed layer, resulting in high remineralisation in the upper ocean and low export efficiency. The importance of the proportion of diatoms to determining the particle flux from the surface ocean, and their potential for high export efficiency, have been demonstrated in regional studies (Boyd and Newton, 1995; Buesseler, 1998; Boyd and Newton, 1999). Correlations between diatom abundance and thorium-derived POC flux have been noted in the Arabian Sea (Ducklow and Harris, 1993) and Baffin Bay (Amiel *et al.*, 2002). Nutrient drawdown, indicative of bloom stage, has also been shown to covary with Th-export in the North Atlantic (Buesseler *et al.*, 1992). In a North Pacific study, stations that had previously experienced greater diatom abundances had less particle remineralisation below the mixed layer, i.e. higher e-ratio (Buesseler *et al.*, 2009). A similar correspondence was noted in the Southern Ocean after the stimulation of a diatom bloom by iron fertilisation (Buesseler *et al.*, 2005). Another study in the Southern Ocean showed large spatial gradients in e-ratio along a transect from the ice-edge to north of the Polar Front, related to differing relative abundance of diatoms (Buesseler *et al.*, 2003). The seasonal differences in PCS and physical conditions outlined above imply that estimates of e-ratio made during the early stages of a bloom (high biomass, large plankton dominate) will likely be high relative to the annual mean, whereas measurements made in later phases (moderate biomass, small plankton dominate) may be low. By taking into account the bloom stage and PCS at the time of the measurement, these seasonal effects could be accounted for, resulting in more robust estimates of the e-ratio.

6.3.5 Research Plan

The challenge in determining the seasonal variability in e-ratio lies with the logistical difficulties of collecting export and PP data throughout the year. We propose a novel solution: to use spatial variability in bloom stage at the time of the measurement as an analogue for seasonal variability. Assessing the bloom stage for a particular location requires knowledge of the bloom evolution prior to measurements being taken, for which the optimal tool is satellite ocean colour data. Guided by the results from *in situ* studies in two high latitude regions, an analysis of the bloom stage for other published datasets will allow us to generalise our results for all seasonally variable regions. Finally, incorporating relevant seasonal information into the parameterisation of e-ratio will permit improved estimates of the magnitude of the biological carbon pump.

6.3.5.1 Objective 1: Assess the impact of seasonal variability in the phytoplankton bloom on the export ratio in the sub-Arctic and Antarctic

The first component of the project will collate measurements of Th-export and PCS collected on two high latitude cruises: an OA cruise to the Arctic (June-Jul 2012) and OA cruise to the Antarctic (Dec. 2012-Jan. 2013) on the RRS James Clark Ross. The locations were chosen to fulfil two criteria that must be met in order to investigate the controls on seasonal variability in the e-ratio. Firstly, to reduce uncertainty in our parameterisation of e-ratio, it needs to be better constrained at low SST (< 7 °C, based on Fig. 6.1). Secondly, in order to test our hypothesis that seasonal variability in bloom conditions alters the e-ratio, we need to sample in regions that have large variability in PCS, bloom stage and e-ratio, on the relatively short time and space scales of a single cruise. By considering data from both cruises we will increase the size of our dataset of simultaneous Th-export and PCS measurements, maximise the

variability in e-ratios and bloom stage, and finally leverage existing cruise programmes to our advantage. For both cruise datasets, e-ratio will be calculated following (Henson *et al.*, 2011), using the integrated satellite PP over the 16 days prior to the Th-export measurement. For each cruise, the bloom stage at the time of the thorium measurements will be assessed by 1) examination of the satellite chlorophyll (chl) record prior to the measurement and 2) PCS, in particular the abundance of diatoms relative to other phytoplankton functional groups. Using the satellite record, various criteria for 'bloom stage' will be evaluated, such as time elapsed since bloom start (e.g.(Henson *et al.*, 2009), or length of time before/after peak chl concentration, and considered in conjunction with the PCS data. Data from each cruise will be normalised (z-score) so that they are directly comparable. This will allow the stations to be ordered in terms, not of actual sampling date, but of bloom stage, thus creating a quasi-seasonal time series of e-ratio and PCS. The unique quasi-seasonal time series of coincident e-ratio and PCS for these high latitude regions will be used to quantify the seasonal variability in the e-ratio and its correlation with bloom stage and PCS. In particular, we will focus on time elapsed since the start of the bloom and since the peak, in order to classify each measurement as pre-bloom, during the peak of the bloom or post-bloom. In addition, the relative abundance of diatoms will be assessed, as their presence (absence) is an indicator of predominately new (regenerated) production and therefore high (low) e-ratio. A correlation analysis of the e-ratio versus bloom stage and PCS will be carried out to evaluate the potential for these parameters to influence the e-ratio. This analysis will allow us to 1) quantify the seasonal variability observed in e-ratio in the high-latitude ocean, and 2) evaluate the parameters that drive seasonal variability in the e-ratio.

6.3.5.2 Objective 2: Incorporate relevant seasonal information into parameterisations of export to reduce uncertainty in estimates of the global magnitude of the biological carbon pump

The second component of the project aims to develop an improved parameterisation of e- ratio. On the basis of the knowledge gained from the regional studies, we will incorporate relevant seasonal information into the e-ratio parameterisation, with the goal of reducing the scatter in the algorithm at low SST (Fig. 6.1). In its current form, SST explains 50 % of the variance (r^2=0.5) in e- ratio and so is obviously an important factor. We aim, however, to increase the variance explained by the algorithm, and hence to reduce uncertainty in our estimate of global carbon export. The parameters chosen to represent seasonal information (bloom stage and PCS) have been selected on the basis, primarily, of their expected correlation with e-ratio based on current understanding of processes controlling carbon export. However, they have another advantage: they can be derived from datasets with global coverage (either satellite or model-based). They can therefore be used, firstly, to define the bloom stage and PCS for other previously published measurements and secondly, to extrapolate from *in situ* measurements that represent a localised (in space and time) export estimate to globally-resolved estimates of carbon export. We have already collated a large number (> 300) of Th-export measurements from the literature (Henson *et al.*, 2011). The database will first be updated via a literature search for the latest reported Th- export measurements. Then, for every measurement in the database we will determine the bloom stage and relative abundance of diatoms at the time the measurement was taken. Bloom stage will be quantified by reference to the timing of the bloom start (Henson *et al.*, 2009) and bloom peak. For each location, an annual time series of satellite-derived chl will be analysed for timing of the bloom peak and bloom start

using the criterion established by Siegel *et al.*, (2002) and Henson *et al.*, (2006a). Characteristics of the PCS will be determined using three approaches: satellite-based estimates of dominant phytoplankton functional type (Alvain *et al.*, 2005) and size classes (Uitz *et al.*, 2006), and using output from a 3-D biogeochemical model (NASA Ocean Biogeochemistry Model;(Gregg *et al.*, 2003). Estimates of Th-export and *in situ* PCS are infrequently reported in the same paper, however we will attempt to trace published measurements from the same cruise. This will allow us to corroborate the satellite-derived estimates of PCS. Details of the satellite data and models to be used can be found in the 'Data & Methods' section. Indices of seasonality, such as time elapsed since bloom start, are meaningless in regions of weak seasonality, such as the oligotrophic gyres that don't experience a distinct bloom. These regions also have relatively little scatter in the e-ratio parameterisation shown in Fig.6.1. Therefore, this analysis will only be undertaken in regions of strong seasonality: principally high latitudes but also in seasonally variable upwelling or monsoonal regions. The majority of the scatter in our current e-ratio algorithm occurs at low temperatures (i.e. high latitudes), with the exception of some data with SST of 25-30 °C, that originates from the equatorial Atlantic region. High and low seasonality regions will be distinguished on the basis of the coefficient of variation of chl (annual standard deviation/annual mean). Equipped with this large database of e-ratios and coincident SST, bloom stage information and PCS, we will then refine the parameterisation of e-ratio shown in Fig. 6.1. Stepwise multiple linear regression will be carried out and the results assessed using correlation coefficients and the Akaike information criterion to determine the most appropriate model. We expect that including appropriate seasonal information in the algorithm for e-ratio will substantially improve our model over the original that considers SST alone. The initial analysis will be carried out using the climatological

mean seasonal cycle of chl and PCS, as many Th-export measurements were taken prior to the start of the satellite chl record (in September 1997). This approach will allow the maximum number of data points to be retained in the analysis and also alleviates the issue of missing ocean colour data due to cloudiness. This approach does however ignore interannual variability in phytoplankton seasonality, which can be substantial at mid-latitudes (e.g.(Henson *et al.*, 2009)). An additional multiple linear regression analysis will be undertaken using the subset of Th-export measurements that overlap with the satellite record and year-specific indices of seasonality. A comparison of the results using the subset of data and interannually varying explanatory variables versus climatological mean explanatory variables will give an indication of the importance (or otherwise) of including interannual information in the parameterisation of e-ratio, in addition to seasonal information. A revised estimate of global carbon export will be calculated based on our new e-ratio parameterisation and will further inform current efforts to find consensus among the different methodologies on the magnitude of the ocean's BCP. Outcomes from the 2nd stage of the project will be 1) reduced uncertainty in parameterisation of the e-ratio, incorporating seasonal information and 2) a new global estimate of the magnitude of the ocean's biological carbon pump.

6.3.6 Data and Methods

Measurements of Th-export made on both cruises will follow the same methodology well- established at NOC (Morris *et al.*, 2007; Thomalla *et al.*, 2008; Sanders *et al.*, 2010), which is briefly summarised here. Measurement of total ^{234}Th will be undertaken following the protocols for small-volume sampling described in (Pike *et al.*, 2005). Water samples of 4 litres are collected from multiple depths within the

upper water column using a CTD and the thorium is extracted from solution via precipitation with MnO_2. The activity of ^{234}Th is measured immediately on-board ship using a low-level beta counter, followed by repeated counts during the 6 months following sample collection. Vertical profiles of ^{234}Th activity are converted to estimates of downward ^{234}Th flux using a one dimensional steady-state model. An estimate of the ^{234}Th:POC ratio is needed to estimate the export flux, and so at each station large particulate matter will be collected using an *in situ* Stand Alone Pumping System (SAPS). Approximately 1500–2000 litres of seawater is filtered through a 53 μm Nitex screen, and the particle suspension quantitatively split into four subsamples using a Folsom splitter. Each split is then analyzed for either ^{234}Th, POC, calcite or biogenic silica. For determination of PCS, phytoplankton cells will be counted and identified from acidic Lugol's preserved water samples (2%, 250 ml) using an inverted microscope and camera system. Examination of filter samples (1 L, 0.8 μm pore-size polycarbonate filters) collected in parallel will allow further taxonomic information to be gathered, as well as accurate estimates of cell carbon. Our default source of satellite-derived chl will be the SeaWiFS instrument for two reasons. Firstly, it has the longest record (September 1997-present) of any ocean colour instrument, providing a consistent time series of data with maximum overlap with the *in situ* measurements for interannual analysis. Secondly, to be consistent with the (Alvain *et al.*, 2005), (Uitz *et al.*, 2006) and NOBM approaches to estimating PCS that all use SeaWiFS data as inputs. If it becomes necessary due to the failure of SeaWiFS, we will instead use data from MODIS, which would limit the interannual analysis to the period July 2002-present. Chl data at 8-day, 0.25° resolution will be used to estimate seasonal indices. The 8-day composites have proved to be a suitable compromise between accurately pinpointing timing of seasonal events and alleviating loss of data

due to cloudiness (e.g.(Siegel *et al.*, 2002; Henson *et al.*, 2006b)). The spatial scale over which the e-ratio varies, and which should therefore be compared with potential driving factors, remains an open question. A recent high resolution survey of thorium fluxes in the North Pacific and near Hawaii suggested that they vary on scales of 'tens to hundreds of kilometres (Buesseler and Boyd, 2009). We will perform our analyses using 0.25° resolution data, which will be a suitable compromise between reducing data loss due to cloudiness and resolving spatial variability. Global estimates of diatom presence will be obtained from two different satellite data-based algorithms and one biogeochemical model. The PHYSAT algorithm uses empirical relationships established between pigment markers of certain phytoplankton functional types (e.g. fucoxanthin indicates diatom presence) and water leaving irradiances at multiple wavelengths derived from the SeaWiFS satellite (Alvain *et al.*, 2005). The algorithm reports dominance of the phytoplankton community by diatoms, nanoeucaryotes, prochlorococcus, cyanobacteria and phaeocystis. The size-class based approach of (Uitz *et al.*, 2006) uses statistical relationships between satellite- derived chl concentration and phytoplankton size to estimate the euphotic zone integrated biomass of micro-, nano- and picoplankton. In their analysis, microplankton is assumed to comprise both diatoms and dinoflagellates. In a recent intercomparison study of multiple approaches to estimate PCS from satellite data (Brewin *et al.*, 2011), the Uitz algorithm performed very well, particularly in separating micro and nano/picoplankton classes. The PHYSAT algorithm performed less well, especially in detecting diatom dominance. The NOBM is an existing biogeochemical model, whose owners have provided open community access to the output. The NOBM explicitly models the abundances of 4 phytoplankton groups as contributions to total chl:diatoms, coccolithophores, chlorophytes and cyanobacteria (full details of the

model parameterisation can be found in (Gregg *et al.*, 2003; Gregg and Casey, 2007). Seasonal and spatial variability in chl is well-reproduced in the model, partly because it assimilates daily fields of SeaWiFS derived chl. These three approaches were selected because each provides a different metric of PCS: PHYSAT provides information on whether a population is dominated by diatoms, but is a binary function (dominance/non-dominance); the Uitz approach provides the biomass of size classes, but their microplankton class is not specific to diatoms; the NOBM produces diatom-specific chl concentrations, but relies on the model parameterisation of diatom growth. All approaches are expected to provide PCS estimates which can be meaningfully interpreted in the context of seasonal variability. Using all three methods will provide maximum flexibility in how PCS is parameterised in our statistical model of e-ratio and will also allow us to assess the confidence that can be placed on an individual estimate of PCS.

Appendix

A. Analytical methods

In this section, the analytical methods that were used by the author. Further information on other techniques used in the manuscript are presented in companion publications cited in the different chapters.

A.1 Dry weight, Particulate Organic Carbon and Particulate Organic Nitrogen

Particulate organic carbon samples were filtered onto pre-weighed, pre-combusted (450ºC for 12h) 25 mm Whatman GF/F filters. After filtration and rinsing, they were dried at 50ºC for 24h and weighed again to determine the dry weight. Once the re-weighing was done, the inorganic carbon was removed by placing filters in a dessicator and fuming them with HCl for 24h. Then, the filters were dried again before pelleting. Filters were wrapped in pre-combusted foil (450ºC for 12h) aluminium disks or silver capsules using a cleaned sample press.

Carbon and nitrogen contents of these pellets were determined on a Flash 1112 Elemental Analyser (Thermo Finnigan) based at the Plymouth Marine Laboratory (Chapter 2, 3 and 5) or at the LEMAR, Brest, France (chapter 4). The principle of the CHN analyser is as follows: the pelleted filter is combusted at very high temperature 1030ºC during a short time in presence of O_2. The C and N content of the samples are converted in the CO_2 and N_2 respectively by catalysis. Helium is used as carrier gas to transport the, CO_2 and N_2, through a chromatography column which separates CO_2 and N_2. Once detected, gases are converted as peak area and calibrated against known standards of acetanilide measured at the beginning of each run.

Blanks were prepared by rinsing a pre-combusted GF/F filters with MilliQ water using the filtration system used for the actual samples and by following the same process as for actual samples. 10 Blanks were prepared for each sets of POC/N analysis, and were then averaged and subtracted from the given values for each sample. For D341 (chapter 2 and 3) procedural blanks levels were 1.6 ± 0.8 µg of N and 19.9 ± 7.8 µg of C. For D350 and D354, blanks levels were 0.4 ± 0.1 µg of N and 5.9 ± 1.3 µg of C and finally for the aggregate experiment (Chapter 4) blanks levels were 0.2 ± 0.1 µg of N and 9.9 ± 2.3 µg of C.

A.2 Particulate Inorganic Carbon

Particulate inorganic carbon was estimated from Ca measurements made using an inductively coupled plasma optical emission spectrometry (ICP OES) PerkinElmer Optima 4300 ICP OES. PIC samples were filtered onto 25mm 0.4µm polycarbonate filters. Then, filters were digested during 24 hours in 0.4 M nitric acid. Acid addition and dilution were made gravimetrically on a high precision balance. The digests were then filtered with 0.4µm syringe filters and transferred into pre cleaned ICP OES auto sampler tubes. Ca and Na were then measured and calibrated against certified ICP standard solutions.

The sample was nebulised through a baffled, cyclonic spray chamber, and into the plasma torch. The plasma excites electrons of the atoms in the sample to higher energy levels, and as these transition back to their ground state, they emit photons at wavelengths characteristic of the atom. Electrons in any element may undergo a number of different such transitions, thus emitting photons at several characteristic wavelengths. Photons emitted from the plasma are separated according to wavelength, and the intensity of each beam is measured by appropriately positioned detectors. Na

was measured at only one wavelength, Ca was measured at several wavelengths and the results averaged.

The second-highest concentration standard was run every ten samples as a drift monitor preceded by an acid-blank (instrument drift was found to be negligible). For D341 (chapter 2 and 3) procedural blanks levels were 0.06 ± 0.04 ppm of Ca. For D350 and D354 (chapter 4), blanks levels were 0.02 ± 0.01 ppm of Ca and finally for the aggregate experiment (Chapter 4) blanks levels were 0.32 ± 0.04 ppm of Ca.

A.3 Biogenic Silica

Biogenic silica samples were filtered onto 25mm 0.4µm polycarbonate filters. BSi was dissolved in 10 ml of 0.2M NaOH at 60ºC for 3h and then shaken vigorously. Samples were then neutralised with 0.2 M HCl. The pH was checked on every sample. If the pH was not 8, 0.2 M NaOh or 0.2 M HCl was added. The resultant aqueous sample was run on the silicate channel of the nutrient analyser. The nutrient analyser used was a SEAL QuAATro autoanalyser for samples presented in chapters 2, 3 and 4 and on a Bran + Luebbe autoanalyser for the aggregates experiment (chapter 5)

The autoanalyser converts Si into a yellow silicomolybdate complex. Oxalic acid is then added to reduce excess molybdate. Silicomolybdate is then reduced with ascorbic acid to yield a more stable blue coloured compound, and the absorbance of the solution is then measured and quantified as peak height. Standards were prepared from solid sodium fluorosilicate (Na_2SiF_6) dissolved in a fixed volume of MilliQ, and further diluted in saline solution. The highest concentration standard was run every ten samples as a drift monitor followed by two saline solution blanks to assess carry-over. Both drift and carry-over were found to be negligible.

For D341 (chapter 2 and 3) procedural blanks levels were 0.89 ± 0.30 μM of BSi. For D350 and D354, blanks levels were 6.0 ± 0.1 μM of BSi and finally for the aggregate experiment (Chapter 4) blanks levels were 1.3 ± 0.6 μM of BSi.

A.4 Bacterial counts

On sampling, 5 ml of background water and 5 ml of aggregate solution were fixed with formalin (2% v/v) and directly frozen at -80ºC for further counting. Tween 80 was used (Yoon and Rosson, 1990) to detach bacteria from organic matter. Tween 80 was added to thawed samples to a final concentration of 10 μg/ml. This mixture was allowed to stand for 1 or 2 hours before being sonicated on ice. This procedure allowed time for the tween 80 to penetrate the detritus (Yoon and Rosson, 1990). During sonication, the tip of the probe was dipped 5 mm below the surface of the sample.

Samples were then subsequently diluted (up to 100-fold) with 0.2 μm filtered autoclaved MilliQ, and stained with SYBR gold (Invitrogen, final concentration of 1.0 $\times 10^{-4}$ of the commercial stock) for 15 min in the dark. Samples were then filtered onto black polycarbonate filters (0.22 μm) which were then mounted onto slides. A combined antifade and mountant (phosphate buffer solution:glycerol (1:1) and 0.01% v:v - p-phenylenediamine) was used to ensure good conservation during storage at -20 ºC until further counting. Slides were examined at 100x magnification under blue-light excitation using an Olympus epifluorescence microscope. Figure A.4 shows bacteria fluorescing under the microscope. More than 200 bacteria were typically counted in 20 fields (see Figure A.1 as illustration) of view as shown in table A.1

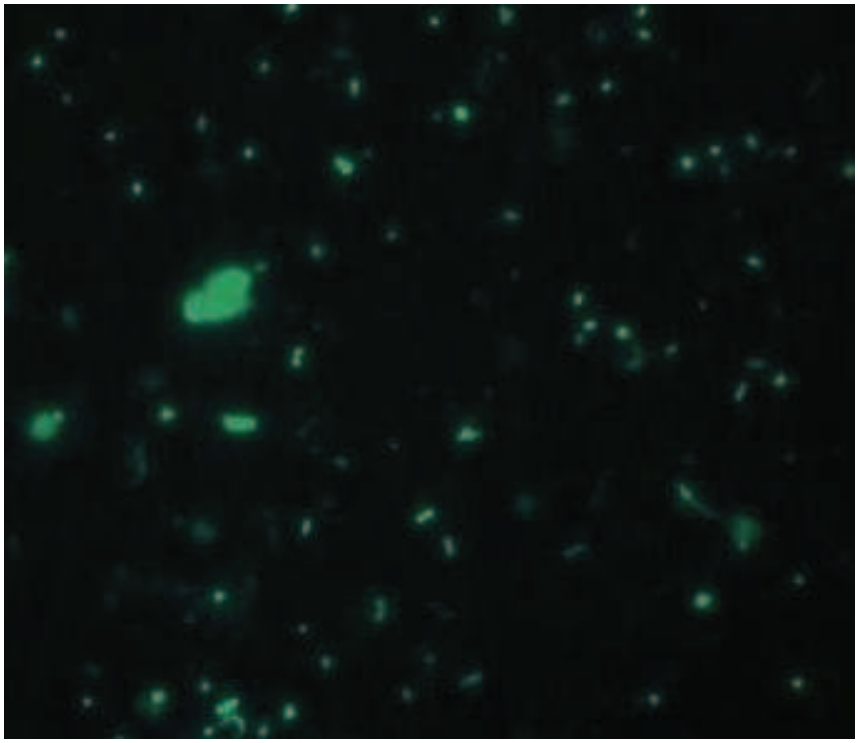

Figure A.1: Bacteria enumeration under the fluorescence microscope. Slides were examined at 100x magnification under blue-light excitation using an Olympus epifluorescence microscope.

Table A.1: Raw bacteria counting at day 0 in the background water. S.D. stands for standard deviation.

	Sample							
Counts	C1-1	C1-2	C2-1	C2-2	C3-1	C3-2	C4-2	C4-1
1	18	50	75	132	113	65	62	72
2	57	13	80	47	67	45	78	50
3	77	10	69	35	93	69	48	82
4	72	25	88	62	67	72	55	43
5	12	15	83	52	66	133	52	10
6	88	6	93	67	52	88	67	11
7	52	8	94	40	154	82	43	81
8	43	23	96	29	106	66	38	71
9	43	19	110	41	67	64	48	78
10	49	45	93	6	86	82	72	46
11	86	37	79	7	65	54	76	70
12	83	28	80	46	73	72	38	61
13	53	16	79	50	46	42	20	24
14	61	11	44	47	35	48	46	84
15	34	41	52	51	53	36	38	45
16	42	33	61	37	67	111	61	67
17	61	36	53	32	80	125	63	15
18	81	27	32	39	64	107	46	86
19	71	88	59	52	55	98	59	41
20	59	90	59	35	43	90	47	33
Mean	57.10	31.05	73.95	45.35	72.60	77.45	52.85	53.50
S.D.	21.41	23.53	19.91	25.38	27.57	27.26	14.59	25.33

A.5 ^{234}Th, ^{238}U

There are several manners by which downward export carbon fluxes (or new production) can be measured. Techniques can be divided in two groups: (1) indirect measurements which are based on nutrients (Sanders *et al.*, 2005; Henson *et al.*, 2006b), on oxygen (Jenkins, 1982), on radioisotopes (Buesseler, 2001; Van der Loeff *et al.*, 2006; Morris *et al.*, 2007) and synthesising numerous biological rate processes (Boyd and Newton, 1999). (2) Direct measurements which are provided by sediments traps or drifting sediments traps (Lampitt *et al.*, 2008).

The radioactive short-lived Thorium-234 (^{234}Th, $t_{1/2}$=24,1d) has been used as a tracer of several transport processes and particle cycling in aquatic systems by

different techniques (Van der Loeff *et al.*, 2006). ^{234}Th, is often used to estimate how much POC is exported into the deep ocean (Buesseler *et al.*, 1992; Cochran and Masque, 2003; Van der Loeff *et al.*, 2006); the most widespread application of this radionuclide (Waples *et al.*, 2006). ^{234}Th is a daughter isotope of naturally occurring 238-Uranium (^{238}U, $t_{1/2} = 4{,}47.10^9$y). ^{238}U shows a conservative behaviour in the seawater and is proportional to salinity in well oxygenated environments (Ku *et al.*, 1977; Chen *et al.*, 1986) while ^{234}Th is particle reactive in the water column. As particles associated with ^{234}Th sink through the water column, a radioactive disequilibrium is formed between ^{238}U and ^{234}Th (Figure A.2), which can be used to quantify the rate of carbon export from the surface ocean. This is possible with POC to particulate ^{234}Th activity ratios (Tsunogai and Minagawa, 1976) obtained from large volume samples (e.g. *in situ* pumps: SAPS). The ability of ^{234}Th to estimate carbon export comes from the opposite behaviour of the pair ^{234}Th/^{238}U, respectively non conservative and conservative.

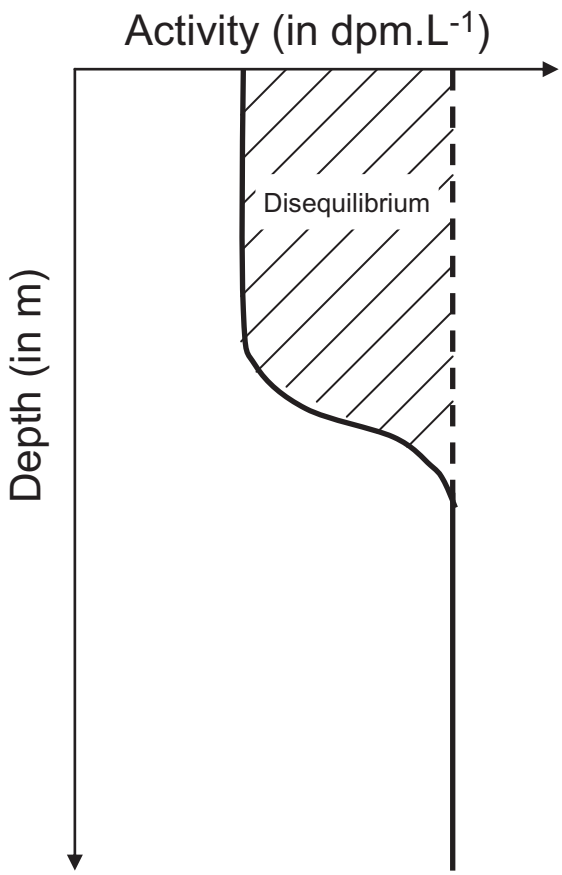

Figure A.2: Schematic cartoon of the disequilibrium observed in the upper ocean between ^{238}U and ^{234}Th. Dashed lines represent the ^{238}U activity and the full line represent the ^{234}Th activity. Hashed areas represent a ^{234}Th removal.

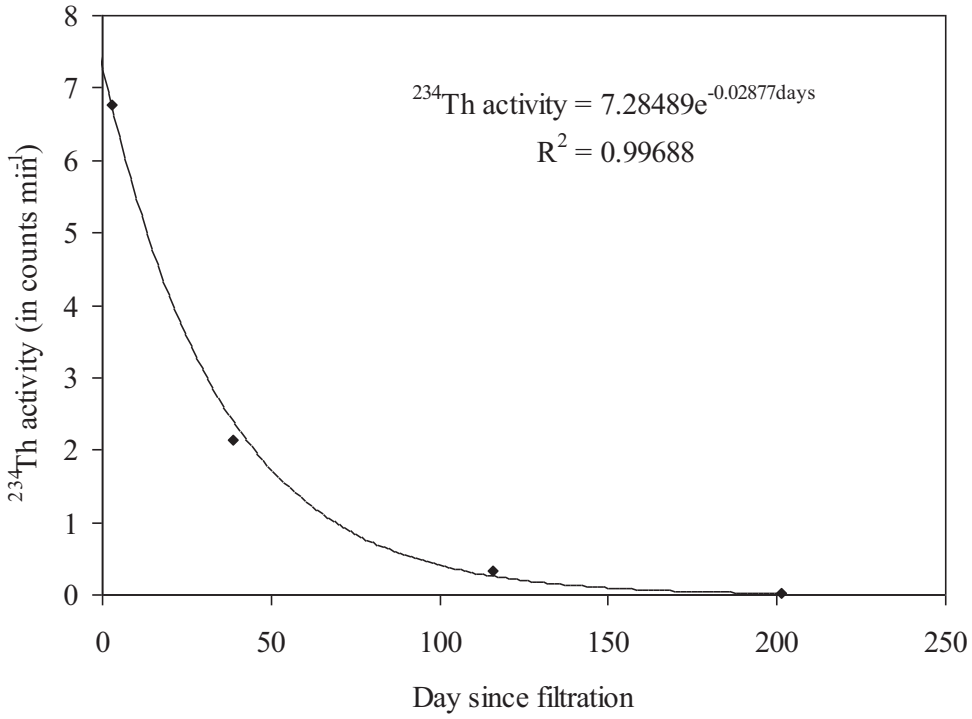

Figure A.3: ^{234}Th β activity decay in a sample from D341. Symbols display background corrected counting vs time. The solid line shows the theoretical decay of ^{234}Th with a decay constant (λ); λ = - 0.02876.

A.6 Large volume technique

The "large volume" technique was used during D341 (chapters 2 and 3). Total ^{234}Th was extracted from water samples using a medium-volume technique based on (Rutgers Van Der Loeff *et al.*, 1997). Three drops of 25% NH_3 and 125 µL of 60 $g.L^{-1}$ $KMnO_4$ were added and mixed, followed by 50 µL of 400 $g.L^{-1}$ $MnCl_2.4H_2O$ to form a MnO_2 precipitate, which scavenges ^{234}Th and other radionuclides while leaving its parent ^{238}U in the dissolved phase. Before adding reagents, samples were rendered alkaline with three drops of NH_3, the MnO_2 precipitate being stable only at alkaline pH. The precipitate was allowed to accumulate and settle for about 8 h before being filtered onto 142-mm diameter polycarbonate (Millipore) 0.8 mm pore size filters. The

extraction efficiency (Van der Loeff *et al.*, 2006) was checked by a second precipitation made with 10 samples with results not considered to be significantly different from 100%.

Filters were dried for 24-48 hours in Petri dishes, folded in a reproducible and consistent way into squares of 18×18mm, wrapped in Mylar foil and then counted for ß activity on a low level beta GM multicounter system (Model RisØ GM-25-5A) for ^{234}Th activity. The first counts were made straight after folding on board the ship. The second counts took place 1 month after the first, and a third and final counting was undertaken after 6 months (>6 ^{234}Th half-lives) to allow background correction. An example of the ^{234}Th decay is presented in Figure A.3 More details of the procedure can be found in Morris *et al.*, (2007). ^{238}U activity (A_U, dpm kg^{-1}) was calculated as A_U = 0.0686 × salinity, based on the average uranium concentration in seawater (of 3.238 ng g^{-1}) normalised to a salinity of 35 (Chen *et al.*, 1986). The uncertainty in the ^{238}U-salinity relationship was estimated by Chen *et al.* (1986) to be 3.3%. The uncertainty over the counting procedure were not higher than 3.1% (approximately 1000 counts). The uncertainties over the entire analytical method was comprised between 6 and 15% of the final ^{234}Th flux.

A.7 Small volume technique and recovery procedure.

The "small volume" technique was used during the D350 and D354 cruises using 4l sample with recovery measured with ICP-MS (Pike *et al.*, 2005). The great advantage of this technique is to reduce the amount of water required. In order to recover the potential loss of precipitate due to this small volume method, a yield monitor of ^{230}Th is added before the precipitation (see below). After background counting ^{229}Th is

added to the sample and the ratio of $^{230}Th/^{229}Th$ to estimate the percentage of precipitate lost during the entire process.

Samples were drained from the CTD rosette bottles into 4l acid cleaned HDPE carboys. 6-7 ml of concentrated HNO_3 were added to samples to reach a pH of 1-2. pH was estimated with pH paper. Then, 25 µl of ^{230}Th (90mBq) was added to each sample with a pre calibrated and dedicated micropipette. Samples were well shaken and left to equilibrate for 6-8 hours. Afterwards, 7-8 ml of NH_4 was added to raise the pH to 8.0-8.1. After being well shaken, the pH was checked to avoid being below pH 8 and fail the precipitation. Once the right pH is obtained, 50 µl of $KMnO_4$ (7.5 mg l^{-1}) and 50 µl of MnCl2 (7.5 mg l^{-1}) were successively added. The precipitate was allowed to form and scavenge the thorium for 6-8 hours. Samples were then filtered onto 25mm QMA (low background filters) with filter holders shown in figure A.4 and dried for 12-24 hours. Filters were counted following similar procedures as described above (thorium large volume technique). The uncertainties over the entire analytical method was comprised between 10 and 38% of the final ^{234}Th flux

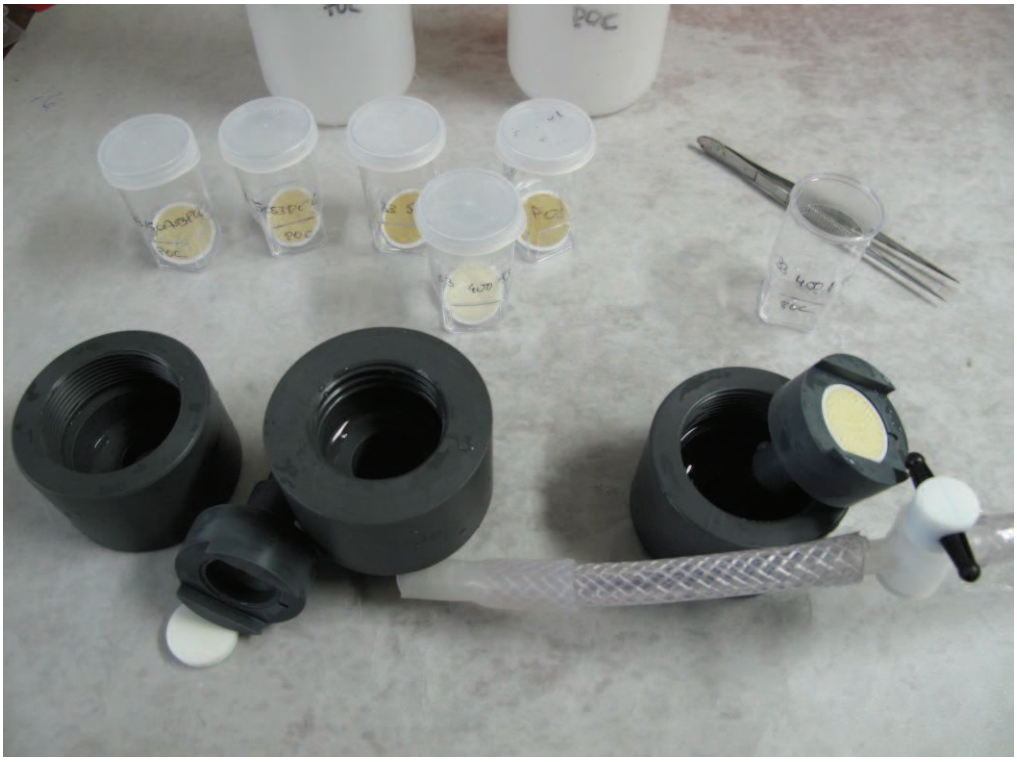

Figure A.4: Filter holders used at sea for the filtration of the thorium small volume technique.

For the recovery work, samples were then dismounted and filters (+ precipitate) dissolved in 50% HNO_3 + 10%H_2O_2. Then, 12.8 pg ^{229}Th was added to each sample, and Th purified on AG 1-X8 anion exchange resin. The purified samples were then redissolved in a 2%HNO_3 matrix suitable for a further analysis of 229/230 ratio by inductively-coupled plasma mass (ICPMS) spectrometry on a Thermo Element II to determine the recovery percentage during precipitation. Mass bias was corrected for using a natural uranium standard (from Physikalisch-Technische Bundesanstalt, Germany) as described in Martin (2011). The laboratory procedures for preparation of ^{229}Th and ^{230}Th spikes are presented in Martin, (2011). The recoveries obtained for D350 and D354 are presented in appendix, tables C.3 and C.4. The uncertainties over the entire analytical method was comprised between 6 and 39% of the final ^{234}Th flux.

A.8 ^{210}Po, ^{210}Pb

Lead-210 ($t_{1/2}$=22.3y) and Polonium-210 ($t_{1/2}$=138,4) are particle reactive radioisotopes in the ^{238}U decay series (Figure A.5). This pair can be used as a tracer of particle cycling in the surface ocean (Cochran and Masqué, 2003). As the ^{234}Th/^{238}U pair, the ^{210}Pb and the ^{210}Po have an opposite behaviour regarding the bindings mechanisms to the particles in the ocean (Verdeny *et al.*, 2008). The ^{210}Pb is adsorbed onto particles surface whereas ^{210}Po is biologically incorporated into the intracellular compartment of some species of phytoplankton and bacteria (Fisher *et al*., 1983; Cherrier *et al*.,1995; La Rock *et al*., 1996). As a result, cells containing ^{210}Po could be assimilated by zooplankton and excreted in sinking particles (faecal pellets).

Thus, when the biological activity is strong, disequilibrium between the ^{210}Pb/^{210}Po pair appears and can be used to estimate the particle export following the ^{234}Th/^{238}U disequilibrium (Figure A.5, see above). The ^{210}Pb/^{210}Po can assess particles carbon export on timescales from several months to a year, constrained by the half-life of ^{210}Po, which is a usefull time scale to estimate the carbon biogeochemical dynamics of mesoscale structures such as eddies (Verdeny *et al*., 2008). The uncertainties over the entire analytical method was comprised between 6 and 39% of the final ^{210}Po flux.

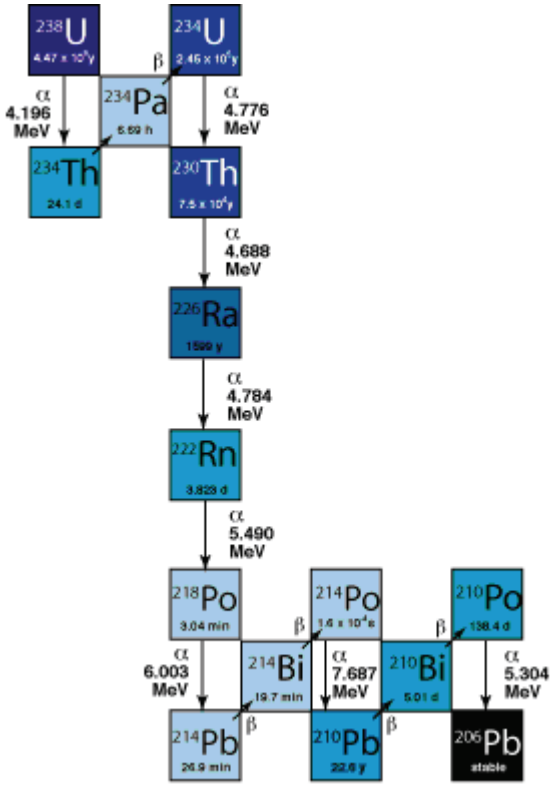

Figure A.5 : ^{238}U decay-series redraw from Bourdon *et al*. (2003). Half-lives and decay energies are given for each isotope (^{234}Th and ^{238}U are located in the top left hand side and ^{210}Po, ^{210}Pb in the bottom right hand side). The blue scale reflects the half-life with darker blues for longer half-lives.

A.9 Technique

Immediately after collection, seawater samples were acidified to pH ~ 2 with HNO_3 to avoid adsorption of ^{210}Po and ^{210}Pb onto the carboy walls, and spiked with ^{209}Po ($T_{1/2}$=102 yr) as an internal tracer for ^{210}Po determination, stable Pb^{2+} to determine ^{210}Pb scavenging and carrier Fe^{3+} (Verdeny *et al.*, 2008). After 8 hours, NH_3 was added until the pH was raised to 8.5 to precipitate $Fe(OH)_3$ which scavenges ^{210}Po and ^{210}Pb. The iron hydroxide was left to settle in 250ml bottles. The radiochemical separation and measurement of ^{210}Po from ^{210}Pb was undertaken in the CITIUS

(Centro de Investigación, Tecnología e Innovación, Sevilla, Spain) laboratory at the Universidad de Sevilla. In brief, iron hydroxide was dissolved in concentrated hydrochloric acid, heated until dried and then finally dissolved in 1M HCl. Ascorbic acid was added to reduce Fe^{3+} to Fe^{2+} and ^{210}Po self-deposited onto a silver disk while gently heating and stirring for at least six hours. ^{210}Po activity was measured in these disks. Afterwards, a second plating on silver was done to remove any traces of Po and only ^{210}Pb remained in the solution. The solution was ^{209}Po-spiked a second time and the samples were stored for at least 6 months to allow ^{210}Po in-growth from ^{210}Pb. ^{210}Po and ^{209}Po were self-deposited onto silver disks and measured. Polonium counting was done using alpha detector PIPS type (Canberra) and ^{210}Po activity calculated. ^{210}Pb activity was inferred from this ^{210}Po concentration after the subsequent decay corrections to the sampling day.

A.10 ^{234}Th, ^{238}U and ^{210}Po, ^{210}Pb export flux models

Export rates of both ^{234}Th and ^{210}Po from the surface ocean were calculated using a one-box model (Coale and Bruland, 1987; Buesseler *et al.*, 1992; Cochran *et al.*, 2000). In a given parcel of water, the total activity of ^{234}Th (^{210}Po) is controlled by several processes such as ingrowth from the father radioisotope ^{238}U (^{210}Pb), radioactive decay, loss or gain on settling particles and physical processes (advection and diffusion). These terms can be summarised as, (Eq.A1)

$$\frac{\partial A_2}{\partial t} = (A_1 - A_2) \cdot \lambda - P + V \qquad \text{(Eq.A1)}$$

A_1 is the total father activity concentration (dpm m^{-3}) for ^{238}U or ^{210}Pb; A_2 is the total ^{234}Th or ^{210}Po activity concentration (dpm m^{-3}); λ is the decay constant of the daughter (d^{-1}); and P is the loss of the daughter due to sinking particles (dpm m^{-3} d^{-1}).

The term *V* includes all physical processes such as advection and diffusion that could potentially supply or remove ^{234}Th (^{210}Po) to or from the system. The effect of upwelling on the thorium balance is significant in regions of high upwelling velocity, such as the equatorial Pacific (Buesseler *et al.*, 1995; Bacon *et al.*, 1996; Dunne and Murray, 1999), where fluxes were 25–35% higher when upwelling was considered (Buesseler *et al.*, 1995), and the north-western Arabian Sea during the Southwest Monsoon (Buesseler, 1998). Horizontal processes affecting the intensity of thorium scavenging are likely to be more important in coastal areas (Buesseler *et al.*, 1995) but could also be strong in regions of mesoscale activity or eastern boundary currents. In general, upwelling in the north and south subtropical gyres is not well developed, so we assume its contribution to the ^{234}Th flux estimates is small. Previous ^{234}Th studies at the same site have also ignored the advection/diffusion term (Thomalla *et al.*, 2006; Lampitt *et al.*, 2008; Thomalla *et al.*, 2008).

However, the effects of advection in ^{210}Po flux calculation are more complex, because the longer half-life of ^{210}Po (138 days) means that measurements are more strongly impacted in areas influenced by lateral advection and the upwelling of deep waters (Buesseler *et al.*, 2008a; Verdeny *et al.*, 2009). That would cause the water mass to carry a signal of export particle scavenging that had happened many kilometers away. Advection effects have been neglected in this case. The coherence of results shown below validate the assumption, however further studies should be done in order to study the limits of this hypothesis.

Assuming steady state condition, $\frac{\partial A_2}{\partial t} = 0$, and no supply of ^{234}Th(^{210}Po) related to physical processes (*V = 0*), the ^{234}Th(^{210}Po) flux (dpm m^{-2} d^{-1}) is calculated through the water column as, (Eq.A2)

$$P = \lambda \sum_{z=0}^{z=h} (A_2 - A_1) \cdot dz \qquad \text{(Eq.A2)}$$

POC, PIC and BSi export estimates use ratios of POC, PIC or BSi to particulate ^{234}Th (POC:Th, PIC:Th, BSi:Th), in µmol dpm^{-1}, (or ratios to Po) multiplied by the ^{234}Th(^{210}Po) flux at each station.

A.11 High volume collection of particulate matter

As mentioned in the previous section, the way the thorium technique operates requires collection of a large quantity of particulate organic matter in order to estimate the ratio between POC, biomineral (or potentially other elements in the particulate phase) to particulate ^{234}Th activity following methods described above. Large quantity of particulate organic matter were collected using Stand Alone Pumping System (SAPS, Challenger Oceanic®). Particles were collected by filtering seawater through 293mm diameter, 53µm (and 1 µm) nylon mesh. SAPS were deployed overboard (see Figure A.6) during 60 to 90 min (corresponding to 1000 to 2500l of filtered water) to allow a sufficient quantity of particle to be sampled.

Figure A.6: SAPS deployment during D354 onboard the R.R.S. *Discovery* with help of Chris Marsay (University of Southampton) and “DD” (NMF).

B. Chapter 3 Supplementary Material

Table B.1: POC:^{234}Th ratio, POC:^{210}Po ratio, ^{234}Th derived POC export flux, ^{210}Po derived POC export flux. Export values using SAPS at 150 m are calculated with the ^{234}Th and ^{210}Po flux integrated at 150 m and export values using SAPS at 50 m are calculated with the ^{234}Th and ^{210}Po flux integrated at 50 m on both size fractions. Propagated analytical error are provided.

SAPS depth and size fraction	Station ID	POC:^{234}Th ratio (µmol dpm^{-1})	POC:^{234}Th ratio error	^{234}Th derived POC flux (mmol m^{-2} d^{-1})	^{234}Th derived POC flux error	POC:^{210}Po ratio (µmol dpm^{-1})	POC:^{210}Po ratio error	^{210}Po derived POC flux (mmol m^{-2} d^{-1})	^{210}Po derived POC flux error
150m	16477	1.34	0.33	2.10	0.44	19.32	1.03	1.06	0.16
53µm	16497	10.00	2.17	7.72	1.64	77.23	9.33	5.09	0.77
	16523	8.51	1.09	11.22	2.38	86.04	10.86	5.08	0.61
	16544	8.51	1.06	17.27	3.66	86.04	10.86	4.74	0.53
	16559	8.51	1.06	11.93	2.53	-	-	-	-
	16583	7.12	1.43	8.49	1.80	61.99	9.13	2.55	0.44
	16592	4.17	3.20	6.75	1.43	36.96	5.09	1.60	0.24
	16619	2.81	0.59	4.21	0.89	51.76	5.89	2.07	0.38
	16640	3.87	1.21	1.70	0.36	80.91	12.51	4.70	0.85
	16659	4.47	1.77	7.49	1.59	33.90	4.54	2.29	0.33
150m	16477	7.43	1.17	11.59	2.46	277.73	15.60	15.25	2.92
1µm	16497	-	-	-	-	-	-	-	-
	16523	3.34	0.53	4.41	0.94	47.77	5.95	2.82	0.41
	16544	3.34	0.53	6.79	1.44	47.77	5.95	2.63	0.36
	16559	3.34	0.53	4.69	0.99	-	-	-	-
	16583	5.70	0.90	6.80	1.44	63.96	9.97	2.63	0.43
	16592	5.25	0.83	8.52	1.81	66.21	8.190	2.87	0.50
	16619	2.76	0.44	4.14	0.88	111.97	17.17	4.48	1.08
	16640	3.79	0.60	1.67	0.35	97.94	14.33	5.69	0.74
	16659	-	-	-	-	-	-	-	-
50m	16477	8.90	1.41	10.41	2.21	47.71	2.51	0.77	0.15
53µm	16497	10.46	1.65	9.07	1.92	74.29	11.13	1.16	0.23
	16523	11.74	1.86	12.30	2.61	112.75	10.34	1.69	0.28
	16544	11.74	1.86	12.30	2.61	112.75	10.34	2.40	0.29
	16559	11.74	1.86	14.83	3.15	-	-	-	-
	16583	4.91	0.78	4.95	1.05	89.50	12.03	0.67	0.22

	16592	4.00	0.63	8.52	1.81	60.35	9.41	0.72	0.20
	16619	2.90	0.46	3.80	0.81	62.48	7.85	0.30	0.12
	16640	5.11	0.81	1.58	0.33	61.96	8.81	0.87	0.16
	16659	4.07	0.64	5.67	1.20	16.22	1.68	0.20	0.03
50m	16477	1.91	0.23	2.23	0.47	100.41	17.14	1.62	0.38
1µm	16497	-	-	-	-	-	-	-	-
	16523	11.47	1.81-	6.81-	1.32-	319.79	38.18	4.80	1.11
	16544	11.47	1.81-	6.81-	1.32-	319.79	38.18	6.81	1.37
	16559					-	-	-	-
	16583	8.19-	1.3-	1.07	0.34	143.68	16.72	1.07	0.35
	16592	6.07	0.96	1.33	0.4	112.56	16.84	1.33	0.39
	16619	-	-	-	-	-	-	-	-
	16640	-	-	-	-	-	-	-	-
	16659	6.76	1.01	2.18	0.36	181.45	17.96	2.19	0.37

Table B.2: PIC:^{234}Th ratio, PIC:^{210}Po ratio, ^{234}Th derived PIC export flux, ^{210}Po derived PIC export flux. Export values using SAPS at 150 m are calculated with the ^{234}Th and ^{210}Po flux integrated at 150 m and export values using SAPS at 50 m are calculated with the ^{234}Th and ^{210}Po flux integrated at 50 m on both size fractions. Propagated analytical error are provided

SAPS depth and size fraction	Station ID	PIC:^{234}Th ratio (µmol dpm^{-1})	PIC:^{234}Th ratio error	^{234}Th derived PIC flux (mmol m^{-2} d^{-1})	^{234}Th derived PIC flux error	PIC:^{210}Po ratio (µmol dpm^{-1})	PIC:^{210}Po ratio error	^{210}Po derived PIC flux (mmol m^{-2} d^{-1})	^{210}Po derived PIC flux error
150m	16477	0.62	0.10	0.96	0.20	8.87	0.47	0.49	0.07
53µm	16497	1.12	0.18	0.86	0.18	8.64	1.04	0.57	0.09
	16523	0.14	0.02	0.19	0.04	1.43	0.18	0.08	0.01
	16544	0.14	0.02	0.29	0.06	1.43	0.18	0.08	0.01
	16559	0.14	0.02	0.20	0.04	-	-	-	-
	16583	0.28	0.04	0.33	0.07	2.41	0.36	0.10	0.02
	16592	0.14	0.02	0.22	0.05	1.22	0.17	0.05	0.01
	16619	0.17	0.03	0.25	0.05	3.08	0.35	0.12	0.02
	16640	0.11	0.02	0.05	0.01	2.35	0.36	0.14	0.02
	16659	0.21	0.03	0.36	0.08	1.62	0.22	0.11	0.02
150m	16477	0.52	0.08	0.81	0.17	19.38	1.09	1.06	0.20
1µm	16497	-	-	-	-	-	-	-	-
	16523	0.12	0.02	0.16	0.03	1.78	0.22	0.11	0.02
	16544	0.12	0.02	0.25	0.05	1.78	0.22	0.10	0.01
	16559	0.12	0.02	0.17	0.04				
	16583	0.09	0.01	0.11	0.02	1.00	0.16	0.04	0.01
	16592	-	-	-	-	-	-	-	-
	16619	0.05	0.01	0.08	0.02	2.20	0.34	0.09	0.02
	16640	0.04	0.01	0.02	0.00	1.12	0.16	0.07	0.01
	16659	0.32	0.03	0.51	0.11	13.44	1.83	0.59	0.09
50m	16477	0.91	0.14	1.06	0.22	4.85	0.25	0.08	0.01
53µm	16497	-	-			-	-	-	-
	16523	0.24	0.04	0.25	0.05	2.30	0.21	0.03	0.01
	16544	0.24	0.04	0.25	0.05	2.30	0.21	0.05	0.01
	16559	0.24	0.04	0.30	0.06	-	-	-	-
	16583	-	-			-	-	-	-
	16592	0.38	0.06	0.81	0.17	5.70	0.89	0.07	0.02
	16619	0.08	0.01	0.11	0.02	1.73	0.22	0.008	0.003
	16640	0.01	0.00	0.30	0.06	0.12	0.02	0.165	0.03

	16659	0.39	0.06	0.54	0.12	1.56	0.16	0.019	0.003

Table B2 (continued)

50m	16477	0.20	0.03	0.23	0.05	10.35	1.77	0.17	0.04
1µm	16497	-	-	-	-	-	-	-	-
	16523	-	-	-	-	-	-	-	-
	16544	0.29	0.05	0.30	0.06	7.95	0.95	0.17	0.03
	16559	0.29	0.05	0.36	0.08				
	16583	-	-	-	-	-	-	-	-
	16592	1.37	0.22	2.92	0.62	25.37	3.80	0.30	0.09
	16619	-	-	-	-	-	-	-	-
	16640	-	-	-	-	-	-	-	-
	16659	0.06	0.01	0.09	0.02	1.66	0.16	0.02	0.003

Table B.3: BSi:^{234}Th ratio, BSi:^{210}Po ratio, ^{234}Th derived BSi export flux, ^{210}Po derived BSi export flux. Export values using SAPS at 150 m are calculated with the ^{234}Th and ^{210}Po flux integrated at 150 m and export values using SAPS at 50 m are calculated with the ^{234}Th and ^{210}Po flux integrated at 50 m on both size fractions. Propagated analytical error are provided

SAPS depth and size fraction	Station ID	BSi:^{234}Th ratio (µmol dpm^{-1})	BSi:^{234}Th ratio error	^{234}Th derived BSi flux (mmol m^{-2} d^{-1})	^{234}Th derived BSi flux error	BSi:^{210}Po ratio (µmol dpm^{-1})	BSi:^{210}Po ratio error	^{210}Po derived BSi flux (mmol m^{-2} d^{-1})	^{210}Po derived BSi flux error
150m	16477	0.023	0.004	0.036	0.008	0.018	0.003	0.018	0.003
53µm	16497	0.046	0.007	0.036	0.008	0.024	0.004	0.024	0.004
	16523	0.038	0.006	0.050	0.011	0.023	0.003	0.023	0.003
	16544	0.038	0.006	0.077	0.016	0.021	0.002	0.021	0.002
	16559	0.038	0.006	0.053	0.011	-	-	-	-
	16583	0.034	0.005	0.041	0.009	0.012	0.002	0.012	0.002
	16592	0.027	0.004	0.043	0.009	0.010	0.002	0.010	0.002
	16619	0.007	0.001	0.011	0.002	0.005	0.001	0.005	0.001
	16640	0.019	0.003	0.009	0.002	0.024	0.004	0.024	0.004
	16659	0.005	0.001	0.008	0.002	0.002	0.000	0.002	0.000
150m	16477	0.044	0.007	0.068	0.014	0.089	0.017	0.089	0.017
1µm	16497	-	-	-	-	-	-	-	-
	16523	0.041	0.007	0.054	0.012	0.035	0.005	0.035	0.005
	16544	0.041	0.007	0.084	0.018	0.032	0.004	0.032	0.004
	16559	0.041	0.007	0.058	0.012				
	16583	0.033	0.005	0.040	0.008	0.015	0.003	0.015	0.003
	16592	-	-	-	-	-	-	-	-
	16619	0.014	0.002	0.021	0.005	0.023	0.006	0.023	0.006
	16640	0.031	0.005	0.014	0.003	0.046	0.006	0.046	0.006
	16659	0.003	0.000	0.004	0.001	0.005	0.001	0.005	0.001
50m	16477	0.087	0.014	0.102	0.022	0.008	0.001	0.008	0.001
53µm	16497	0.023	0.004	0.020	0.004	0.003	0.001	0.003	0.001
	16523	0.008	0.001	0.008	0.002	0.001	0.000	0.001	0.000
	16544	0.008	0.001	0.008	0.002	0.002	0.000	0.002	0.000
	16559	0.008	0.001	0.010	0.002	-	-	-	-
	16583	0.009	0.001	0.009	0.002	0.001	0.000	0.001	0.000
	16592	0.009	0.001	0.020	0.004	0.002	0.000	0.002	0.000
	16619	0.009	0.001	0.012	0.003	0.001	0.000	0.001	0.000
	16640	0.017	0.003	0.005	0.001	0.003	0.001	0.003	0.001

	16659	0.039	0.006	0.055	0.012	0.002	0.000	0.002	0.000

Table B.3 (continued)

50m	16477	0.039	0.006	0.046	0.010	0.033	0.008	0.033	0.008
1μm	16497	-	-	-	-	-	-	-	-
	16523	-	-	-	-	-	-	-	-
	16544	0.012	0.002	0.012	0.003	0.007	0.001	0.007	0.001
	16559	0.012	0.002	0.015	0.003	-	-	-	-
	16583	-	-	-	-	-	-	-	-
	16592	0.010	0.002	0.022	0.005	0.002	0.001	0.002	0.001
	16619	-	-	-	-	-	-	-	-
	16640	-	-	-	-	-	-	-	-
	16659	0.011	0.002	0.015	0.003	0.004	0.001	0.004	0.001

C Chapter 4 Supplementary Material

Table C.1: Locations, cruise names, stations ID , sampling period and reference of the ^{234}Th derived POC and mineral exports data used in this study. *POC and BSi fluxes in Morris, (2008), ** PIC fluxes, unpublished data. Posistive values of latitude means northern hemisphere

Sampling Area	Latitude (ºN)	Longitude (ºE)	Sampling period	Cruise name	Integration depth (m)	Station ID	Reference
Iceland Basin	61.47	-21.04	July-August 2010	D354	150	04	Le Moigne and Villa (unpublished)
Iceland Basin	59.59	-23.37	July-August 2010	D354	140	06	Le Moigne and Villa (unpublished)
Irminger sea	60.00	-34.59	July-August 2010	D354	150	08	Le Moigne and Villa (unpublished)
Irminger sea	59.54	-41.25	July-August 2010	D354	150	10	Le Moigne and Villa (unpublished)
Irminger sea	59.59	-34.59	July-August 2010	D354	150	15	Le Moigne and Villa (unpublished)
Irminger sea	62.59	-35.00	July-August 2010	D354	140	16	Le Moigne and Villa (unpublished)
Irminger sea	62.59	-29.49	July-August 2010	D354	140	18	Le Moigne and Villa (unpublished)
Irminger sea	58.13	-35.07	July-August 2010	D354	150	20	Le Moigne and Villa (unpublished)
Irminger sea	63.49	-35.05	July-August 2010	D354	150	22	Le Moigne and Villa (unpublished)
Irminger sea	63.49	-34.59	July-August 2010	D354	140	24	Le Moigne and Villa (unpublished)
Iceland Basin	62.02	-24.20	July-August 2010	D354	140	27	Le Moigne and Villa (unpublished)
Iceland Basin	61.13	-20.46	July-August 2010	D354	140	28	Le Moigne and Villa (unpublished)
Iceland Basin	61.19	-20.57	July-August 2010	D354	150	33	Le Moigne and Villa (unpublished)
Iceland Basin	60.58	-34.58	April-May 2010	D350	150	02A	Le Moigne and Villa (unpublished)
Iceland Basin	60.01	-34.57	April-May 2010	D350	150	03A	Le Moigne and Villa (unpublished)
Iceland Basin	60.00	-31.58	April-May 2010	D350	160	04A	Le Moigne and Villa (unpublished)
Iceland Basin	59.59	-28.58	April-May 2010	D350	150	05A	Le Moigne and Villa (unpublished)
Iceland Basin	59.56	-26.07	April-May 2010	D350	150	06A	Le Moigne and Villa (unpublished)
Iceland Basin	60.50	-21.45	April-May 2010	D350	150	07A	Le Moigne and Villa (unpublished)
PAP site	48.54	-17.10	July-August 2009	D341	150	16523	Le Moigne et al., (in review)
PAP site	49.07	-16.63	July-August 2009	D341	150	16544	Le Moigne et al., (in review)
PAP site	48.91	-16.07	July-August 2009	D341	150	16559	Le Moigne et al., (in review)
PAP site	48.98	-16.93	July-August 2009	D341	150	16583	Le Moigne et al., (in review)
PAP site	48.81	-16.50	July-August 2009	D341	160	16592	Le Moigne et al., (in review)
PAP site	48.97	-16.42	July-August 2009	D341	170	16619	Le Moigne et al., (in review)
PAP site	48.91	-16.54	July-August 2009	D341	160	16640	Le Moigne et al., (in review)
PAP site	48.78	-16.99	July-August 2009	D341	170	16659	Le Moigne et al., (in review)

Table C.4 (continued)

Iceland Basin	59.59	-19.52	July-August 2008	D321	80	16204	Sanders *et al* (2010)
Iceland Basin	59.42	-20.27	July-August 2008	D321	50	16209	Sanders *et al* (2010)
Iceland Basin	58.52	-19.53	July-August 2008	D321	80	16222	Sanders *et al* (2010)
Iceland Basin	58.51	-20.59	July-August 2008	D321	80	16226	Sanders *et al* (2010)
Iceland Basin	59.59	-20.28	July-August 2008	D321	50	16247	Sanders *et al* (2010)
Iceland Basin	59.11	-19.05	July-August 2008	D321	50	16260	Sanders *et al* (2010)
Iceland Basin	59.12	-19.53	July-August 2008	D321	80	16274	Sanders *et al* (2010)
Iceland Basin	59.40	-18.43	July-August 2008	D321	80	16285	Sanders *et al* (2010)
Iceland Basin	59.17	-19.47	July-August 2008	D321	130	16286	Sanders *et al* (2010)
Atlantic Gyres	-41.04	-41.56	May 2004	AMT-14	101	CTD05	Thomalla *et al* (2008)
Atlantic Gyres	-32.97	-31.01	May 2004	AMT-14	203	CTD14	Thomalla *et al* (2008)
Atlantic Gyres	-24.23	-25.00	May 2004	AMT-14	121	CTD25	Thomalla *et al* (2008)
Atlantic Gyres	-12.28	-25.00	May 2004	AMT-14	128	CTD35	Thomalla *et al* (2008)
Atlantic Gyres	-0.94	-25.00	May 2004	AMT-14	300	CTD43	Thomalla *et al* (2008)
Atlantic Gyres	11.40	-29.37	May 2004	AMT-14	202	CTD52	Thomalla *et al* (2008)
Atlantic Gyres	38.67	-16.39	May 2004	AMT-14	265	CTD79	Thomalla *et al* (2008)
Southern Ocean	-46.04	51.80	Dec 2004-Jan 2005	D285-286	103	M3.2	Morris *et al* (2007), Le Moigne and Planquette (unpublished)
Southern Ocean	-49.00	51.49	Dec 2004-Jan 2005	D285-286	104	M6.1	Morris *et al* (2007), Le Moigne and Planquette (unpublished)
Southern Ocean	-46.05	51.79	Dec 2004-Jan 2005	D285-286	156	M3.3	Morris *et al* (2007), Le Moigne and Planquette (unpublished)
Southern Ocean	-45.50	48.98	Dec 2004-Jan 2005	D285-286	179	M7	Morris *et al* (2007), Le Moigne and Planquette (unpublished)
Southern Ocean	-44.90	49.90	Dec 2004-Jan 2005	D285-286	101	M8E	Morris *et al* (2007), Le Moigne and Planquette (unpublished)
Southern Ocean	-44.80	49.66	Dec 2004-Jan 2005	D285-286	103	M8W	Morris *et al* (2007), Le Moigne and Planquette (unpublished)
Southern Ocean	-46.06	51.78	Dec 2004-Jan 2005	D285-286	184	M3.4	Morris *et al* (2007), Le Moigne and Planquette (unpublished)
Southern Ocean	-45.99	56.15	Dec 2004-Jan 2005	D285-286	203	M5	Morris *et al* (2007), Le Moigne and Planquette (unpublished)
Southern Ocean	-46.06	51.78	Dec 2004-Jan 2005	D285-286	204	M3.5	Morris *et al* (2007), Le Moigne and Planquette (unpublished)
Southern Ocean	-49.00	51.53	Dec 2004-Jan 2005	D285-286	144	M6.2	Morris *et al* (2007), Le Moigne and Planquette (unpublished)
Southern Ocean	-47.80	52.84	Dec 2004-Jan 2005	D285-286	163	M2.2	Morris *et al* (2007), Le Moigne and Planquette (unpublished)
Southern Ocean	-46.03	51.87	Dec 2004-Jan 2005	D285-286	154	M3.7	Morris *et al* (2007), Le Moigne and Planquette (unpublished)

Table C.2: Station groups, corresponding cruises, enclosed stations, sample number and corresponding oceanic provinces according to Longhurst (1998). * North Atlantic Subtropical Gyral Province (East); † North Atlantic Tropical Gyral Province; ‡ Western Tropical Atlantic Province; ∞ South Atlantic Gyral Province.

Station group	Corresponding cruises	Enclosed station codes	Sample number (n)	Longhurst province
PAP (*PA*)	D341	16523; 16544; 16559; 16583; 16592; 16619; 16640; 16659;	8	North Atlantic Drift Province (NADR)
Iceland (*Ice*)	D321, D350, D354	16204; 16209; 16222; 16226; 16247; 16260; 16274; 16285; 16286; 02A; 03A; 04A; 05A; 06A; 07A; 4; 6; 18; 27; 28; 33; ; 8; 10; 15; 16; 20; 22; 24	28	Atlantic Subarctic Province (SARC); Atlantic Arctic Province (ARCT)
Crozex (*Cro*)	D285-D286	M3.2; M6.1; M3.3; M7; M8E; M8W; M3.4; M5; M3.5; M6.2; M2.2; M3.7	11	Subantarctic Province (SANT)
Atlantic gyres (*AG*)	AMT-14	CTD05; CTD14; CTD 25; CTD 35; CTD43; CTD52; CTD79	7	NASE*, NATR†, WTRA‡, SATL∞

Table C.3: Recoveries obtained for D350 samples. Sample I.Ds, depths and stations are indicated. The mean of the recoveries was 0.942 ± 0.034 %, n= 66.

Sample I.D.	Station	Depth (m)	Recovery (%)	Sample I.D.	Station	Depth (m)	Recovery (%)
11	02	500	0.954	66	05	60	0.969
22	02	200	0.950	77	05	53	0.972
33	02	150	0.941	88	05	35	0.944
44	02	100	0.928	99	05	20	0.916
55	02	80	0.921	1010	05	10	1.000
66	02	60	0.958	11	06	105	0.969
77	02	53	0.955	33	06	505	0.900
88	02	35	0.935	44	06	355	0.973
99	02	20	0.923	55	06	215	0.963
1010	02	10	0.928	66	06	155	0.965
11	03	500	0.957	77	06	105	0.982
22	03	200	0.950	88	06	74	0.968
33	03	150	0.900	1010	06	11	0.869
44	03	100	0.931	Eq1	06	1002	0.920
55	03	80	0.929	Eq2	06	1002	0.919
66	03	60	0.893	Eq3	06	1002	0.944
77	03	53	0.926	44	07	100	0.958
88	03	35	0.861	66	07	60	0.969
99	03	20	0.913	77	07	53	0.963
1010	03	10	0.860	88	07	35	0.917
11	04	500	0.970	99	07	20	0.929
22	04	200	0.951	1010	07	10	0.938
33	04	150	0.962	11	08	500	0.950
44	04	100	0.940	22	08	200	1.000
55	04	80	0.926	33	08	150	0.989
66	04	60	0.922	44	08	100	0.954
77	04	53	0.935	55	08	80	0.972
88	04	35	0.899	66	08	60	0.988
99	04	20	0.901	77	08	53	0.980
1010	04	10	0.867	88	08	35	0.915
11	05	500	0.997	99	08	20	0.949
22	05	200	0.970	1010	08	10	0.962
33	05	150	0.997	Mean			0.942
44	05	100	0.977	S.D.			0.034
55	05	80	0.978				

Table C.4: Recoveries obtained for D350 samples. Sample I.Ds, depths and stations are indicated. The mean of the recoveries was 0.906 ± 0.067 %, n= 116.

Sample I.D.	Station	Depth (m)	Recovery (%)	Sample I.D.	Station	Depth (m)	Recovery (%)
22	04	154.5	0.929	22	20	153.8	0.954
33	04	104.0	0.916	33	20	103.9	0.961
44	04	83.6	0.932	44	20	82.8	0.953
55	04	63.5	0.958	55	20	62.4	0.964
66	04	53.3	0.939	66	20	52.4	0.938
77	04	42.9	0.905	77	20	42.3	0.929
88	04	32.9	0.826	88	20	32.6	0.887
99	04	22.8	0.833	99	20	21.8	0.755
1010	04	12.6	0.773	1010	20	12.2	0.869
22	06	154.4	0.949	22	22	153.8	0.947
33	06	104.0	0.953	33	22	105.0	0.939
44	06	83.6	0.949	44	22	84.3	0.954
55	06	63.4	0.900	55	22	64.0	0.954
66	06	53.3	0.933	66	22	53.6	0.954
77	06	43.1	0.806	77	22	43.7	0.951
88	06	32.9	0.840	88	22	33.4	0.925
99	06	12.7	0.743	99	22	23.1	0.921
1010	06	12.7	0.717	1010	22	12.9	0.889
22	08	154.3	0.886	eq1	22	1018.6	0.939
33	08	104.4	0.908	eq2	22	1018.6	0.936
44	08	83.8	0.968	eq3	22	1018.6	0.884
55	08	63.2	0.820	eq4	22	1018.6	0.960
66	08	52.7	0.854	eq5	22	1018.6	0.968
77	08	42.6	0.899	11	24	20.0	0.904
88	08	32.9	0.780	22	24	30.0	0.937
99	08	22.7	0.956	33	24	40.0	0.952
1010	08	12.8	0.900	44	24	50.0	0.940
22	10	154.5	0.985	55	24	75.0	0.937
33	10	104.5	0.999	66	24	100.0	0.945
44	10	83.5	0.962	77	24	200.0	0.939
55	10	63.5	0.970	22	27	155.0	0.925
66	10	53.3	0.963	33	27	104.8	0.942
77	10	43.2	0.936	44	27	84.1	0.935
88	10	32.9	0.843	55	27	63.8	0.931
99	10	22.7	0.901	66	27	53.7	0.860
1010	10	12.3	0.939	77	27	43.5	0.931
55	15	64.7	0.949	88	27	33.7	0.902
66	15	50.5	0.946	99	27	23.4	1.084
77	15	40.2	0.949	1010	27	13.3	0.927
88	15	30.2	0.959	22	28	153.8	0.967
99	15	20.1	0.824	33	28	103.5	0.891
1010	15	9.9	0.975	44	28	83.1	0.949
33	16	105.7	0.967	55	28	62.7	0.949
44	16	84.8	0.970	66	28	52.9	0.952
55	16	54.5	0.948	77	28	42.7	0.952

Table C.4 (continued)

77	16	44.1	0.924	88	28	32.7	0.798
88	16	34.1	0.897	1010	28	12.4	0.784
99	16	23.7	0.923	22	33	152.7	0.972
1010	16	13.6	0.912	33	33	103.0	0.971
22	18	154.3	0.952	44	33	82.5	0.974
33	18	104.2	0.952	55	33	62.1	0.948
44	18	83.6	0.936	66	33	52.2	0.944
55	18	63.3	0.916	77	33	42.0	0.908
66	18	53.2	0.930	88	33	31.8	0.908
77	18	43.1	0.925	99	33	21.8	0.926
88	18	33.1	0.933	1010	33	11.7	0.844
99	18	22.8	0.709	Mean			0.906
1010	18	12.6	0.865	S.D.			0.067

D. Rolling tanks experiments

D.1 Background

The export of particulate organic carbon is composed of a mix of different origin such as dead sinking phytoplankton cells, (aggregated or not) or faecal pellets. This complex mix of biogeochemical material presents great variations from one oceanic area to another. The processes leading to the formation and breakdown of marine particles (also known as marine snow or aggregates) are therefore as critical as the primary production to understand the export flux of carbon in the surface ocean. Marine snow is thus an important component of the marine environment, but because aggregates are extremely hard to collect and easily disrupted by many sampling methods, most studies have described a standing stock characteristic of marine snow (Shanks and Edmondson, 1989). The great attraction of the rolling tanks technique is that its fundamental operation allows studying the dynamic formation of the marine snow as well as the chemical, biological and morphological properties of it. Recently, studies of the chemical, biological and morphological characteristics of natural aggregates have been improved thanks to specifically designed devices such as the marine snow catcher (Lampitt *et al.*, 1993; Riley *et al.*, 2012) or by the use of viscous polyacrylamide gels (McDonnell and Buesseler, 2010) in various sort of sediments traps. Although these recent advances are promising, artificially made aggregates have brought important insights in our understanding of the vertical export of carbon from the upper ocean and more broadly of the biological carbon pump (e.g. Passow and De la Rocha, 2006; Moriceau *et al.*, 2007; De La Rocha *et al.*, 2008; Ploug *et al.*, 2008a; Engel *et al.*, 2009a; Engel *et al.*, 2009b).

D.2 Technical specifications

The roller tables used in this study consisted of a high density plastic frame on which rested four parallel steel bars wrapped with gardening hoses and supported by pillow block style bearings (Figure D.1). The bars were connected to a variable speed motor. The system was long enough to rotate 6 tanks with space reserved at the end of the table for video shooting during the experiments to perform sinking speed measurements (see (Laurenceau, 2011)). Two similar tables were used in order to perform our 12 tanks experiment. The tanks were 4.5 L volume tanks made in totally transparent plexiglass plastic closed with stable rubber corks.

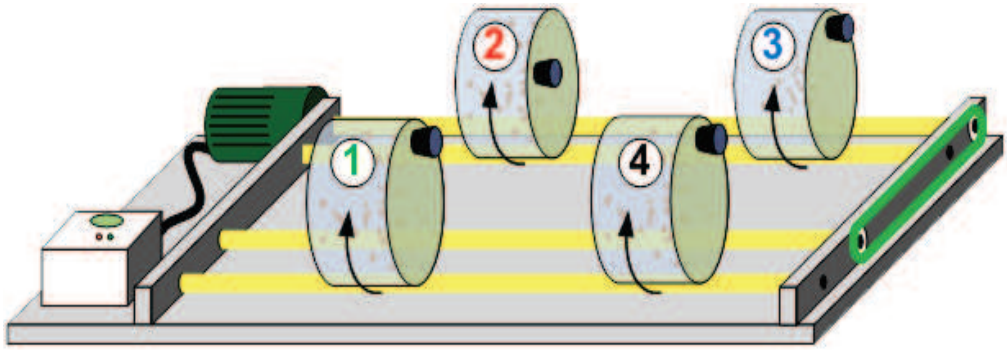

Figure D.1: Plankton cultures and experiment preparation

D.3 Phytoplankton cultures

Two species of diatoms (*Skeletonema marinoi* and *Chaetoceros gracilis*) were used to form aggregates. Phytoplankton was inoculated in sterilized natural seawater at 20°C. The diatoms were grown in F/2 media depleted in nutrient with limiting Si(OH)4 in concentration as following: ($Si(OH)_4$ = 50µM; PO_4^{3-} = 4µM; NO_3^- = 64µM) under 12:12h light:dark cycles. Both cultures were grown separately until they reached

concentrations 1,000,000 cells ml^{-1} and 600,000 cells ml^{-1} for *Skeletonema marinoi* and *Chaetoceros gracilis* respectively.

D.4 Microzooplankton culture

Strain of rotifers specie *Brachionus sp* was provided by the Oceanopolis Brest aquarium facilities. Rotifers were fed with the microalgae *Isochrysis galbana* at 20°C under 12:12h light:dark cycles. The final concentration obtained to inoculate our tanks was containing approximately 60 ind. ml^{-1}. At day 0 before actual inoculation, the inoculation culture was concentrated to a volume of 120 ml by filtering through a 200 µm mesh to remove largest detritus and through a 100 µm mesh to only collect rotifers. Before the experiment was performed, aggregation tests were performed using mix of diatoms cultures. Once aggregates were obtained, rotifers were inoculated to an aggregates containing solution in order to verify their affinity for aggregates as a feeding source thanks to binocular microscope (D.2).

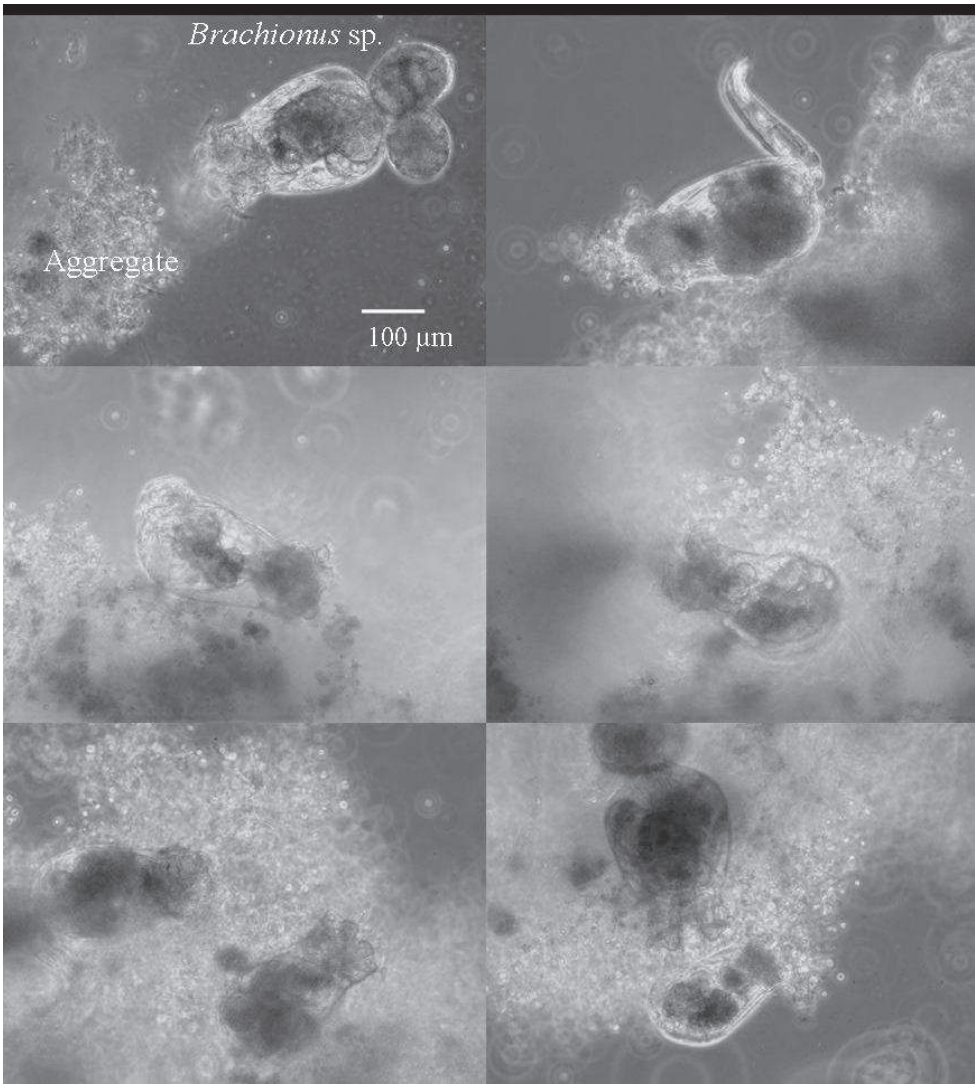

Figure D.2: *Brachionus* sp grazing on aggregates

D.5 Calcite solution preparation

Cretaceous chalk from the cliffs of Rügen, Germany, on the Baltic Sea (De La Rocha et al., 2008), was disaggregated, ground, soaked overnight in bleach and rinsed with deionised distilled water. Particles were suspended in artificial seawater and only those remaining in suspension after several minutes were used in the experiment. Similar chalk solution used in De La Rocha (2008) consisted largely of coccoliths and smaller calcium carbonate debris. Additions of chalk aimed for a final concentration

of 1500 µg l^{-1} in each "with mineral" tank (phytoplankton + mineral tanks and phytoplankton + zooplankton + mineral tanks).

D.6 Preparation of the tanks

On day 0, before inoculation, cultures of *Skeletonema marinoi* and *Chaetoceros gracilis* were mixed in equal proportions in a 20l carboy. Then, in order to increase the volume required to perform the experiment, this preliminary volume of 20l of mix of two species of phytoplankton (*Skeletonema marinoi* and *Chaetoceros gracilis* 50/50) was diluted down to 90l using filtered seawater (0.2µm) from the bay of Brest. The total volume of 110l was homogenized in cylindrical bioreactors. This diluted mix of diatoms cultures was then separated back into four 20l carboys. A solution of calcium carbonate was inoculated in carboys C3 and C4 (Figure D.3). The twelve 4.5l tanks were filled with the homogenized content of the four carboys and the rotifers were added at the very last moment to tanks 2, 6, 10, 4, 8 and 12 before closing. The experiment was conducted in a controlled temperature container (15°C) in the dark, during 8 days.

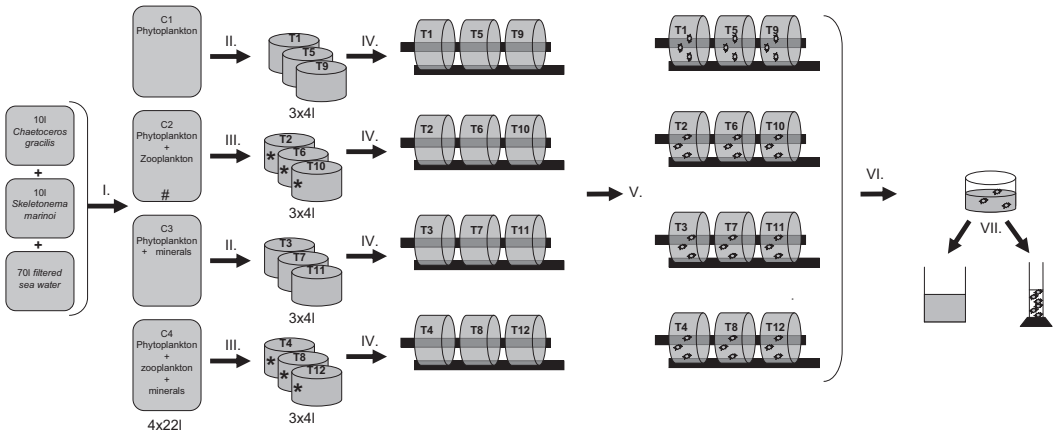

Figure D3: Experimental set up. C: carboy; T: tank.T1, T5, T9 (from C1): « phytoplankton tanks »; T2, T6, T10 (from C2): « zooplankton tanks » ; T3, T7, T11 (from C3) : « mineral tanks » ; T4, T8, T12 (from C4) : « mineral + zooplankton tanks». I. Mixing of cultures with filtered seawater (0.6µm), filling of treatment carboys and addition of calcite solution in C3 and C4. II. Filling of tanks T1, T5, T9, T3, T7 and T11 with solution mix from C1 and C2. III. Filling of tanks T2, T6, T10, T4, T8 and T12 with solution mix from C3 and C4. Rotifers are added in those tanks once filled up. IV.Tanks are placed on the roller tables. V. Aggregation of cultures for 2 days (T1, T2, T3, T4), 4 days (T5, T6, T7, T8) and 8 days (T9, T10, T11, T12) in dark at 15ºC. VI. Sedimentation of aggregates. VII. Removal of aggregates into measuring cylinder for further filtration and sampling of background water for further analysis.

E. Publications and Communications

This work has led to several other publication and presentation that are listed below:

E.1 Publications

- S. A. Henson, R. Sanders, E. Madsen, P. J. Morris, **F. Le Moigne** & Graham D. Quartly. A reduced estimate of the strength of the ocean's biological carbon pump. 2011, *Geophys. Res. Lett.* doi:10.1029/2011GL046735**.**

- J.S. Riley, R. Sanders, C. Marsay, **F. Le Moigne**. Estimates of upper ocean POC fluxes at the Porcupine Abyssal Plain: A novel study using the Marine Snow Catcher. 2012, *Glob. Biog. Cycles*.

- L. Resplandy, A. Martin, **F. Le Moigne**, L. Mémery, M. Lévy, P. Martin, R. Sanders. Impact of dynamical spatial variability on Thorium export estimates. accepted. *Deep Sea Research part I.*

- J. M. Gómez-Guzmán, M. Villa, **F. Le Moigne**, J.M. López-Gutiérrez. AMS measurements of ^{129}I in seawater around Iceland and Irminger Sea. *In review, AMS journal*.

E.2 Presentations

- AGU Chapman conference 2009, Brockenhurst, U.K. *Poster*

- Ocean Sciences 2010, Portland, Oregon, USA. *Poster and Poster as co-author*

- Challenger conference 2010, Southampton, U.K. *Poster*

- COCCOS workshop 2010, Bergen, Norway. *Talk*

- ASLO 2011, San Juan, Puerto Rico, USA. *Talk co author and poster. Awarded as ASLO outstanding student presentation.*

- AMS-12 conference 2011, Wellington, New Zealand. *Poster as co-author*

- Liège Colloquium on Ocean Dynamics, 2011, Liege, Belgium. *Talks as co-author and Poster as co-author.*

- EGU General Assembly 2012, CalMarO special session. Vienna, Austria. *Poster*

References

References

Alldredge, A., 1998. The carbon, nitrogen and mass content of marine snow as a function of aggregate size. Deep-Sea Research I 45 (4-5), 529-541.

Alldredge, A., Gotschalk, C., 1988. The in situ settling behaviour of marine snow. Limnology and Oceanography 33 (3), 339-351.

Alldredge, A.L., Jackson, G.A., 1995. Aggregation in Marine Systems - Preface. Deep-Sea Research Part Ii-Topical Studies in Oceanography 42 (1), 1-7.

Alonso-Gonzalez, I., J., Aristegui, J., Lee, C., Sanchez-Vidal, A., Calafat, A., Fabres, J., Sangra, P., Masque, P., Hernandez-Guerra, A., Benitez-Barrios, V., 2010. Role of slowly settling particles in the ocean carbon cycle. Geophys. Res. Lett. 37.

Alvain, S., Moulin, C., Dandonneau, Y., Breon, F.M., 2005. Remote sensing of phy4567toplankton groups in case 1 waters from global SeaWifs imagery. Deep Sea Research I 52, 1989-2004.

Amiel, D., Cochran, J.K., Hirschberg, D.J., 2002. Th-234/U-238 disequilibrium as an indicator of the seasonal export flux of particulate organic carbon in the North Water. Deep-Sea Research II 49 (22-23), 5191-5209.

Aminot, A., Kerouel, R., 2001. An automated photo-oxidation method for the determination of dissolved organic phosphorus in marine and fresh water. Marine Chemistry 76, 113-126.

Aminot, A., Kerouel, R., 2007. Dosage automatique des nutriments dans les eaux marines. Editions de l'IFREMER ISBN 978-2-7592-0023-8, 188p.

Anderson, L.A., Sarmiento, J.L., 1994. Redfield ratios of remineralization determined by nutrient data analysis. Global Biogeochemical Cycles 8 (1), 65-80.

Antia, A.N., Maaßen, J., Herman, P.,Voß, M., Scholten, J., Groom, S., Miller, P., 2001. Spatial and temporal variability of particle flux at the N.W.European continental margin. Deep-Sea Research II 48, 3083-3106.

Antia, A.N., Suffrian, K., Holste, L., Muller, M.N., Nejstgaard, J.C., Simonelli, P., Carotenuto, Y., Putzeys, S., 2008. Dissolution of coccolithophorid calcite by microzooplankton and copepod grazing. Biogeosciences 5, 1-23.

Armstrong, R.A., Lee, C., Hedges, J.I., Honjo, S., Wakeham, S.G., 2002. A new, mechanistic model for organic carbon fluxes in the ocean based on the quantitative association of POC with ballast minerals. Deep-Sea Research II 49 (1-3), 219-236.

Azam, F., 1998. Microbial control of oceanic carbon flux: The plot thickens. Science 280 (5364), 694-696.

Bacon, M.P., Cochran, J.K., Hirschberg, D., Hammar, T.R., Fleer, A.P., 1996. Export flux of carbon at the equator during the EqPac time-series cruises estimated from ^{234}Th measurements. Deep-Sea Research II 43 (4-6), 1133-1153.

Balch, W.M., Gordon, H.R., Bowler, B.C., Drapeau, D.T., Booth, E.S., 2005. Calcium carbonate measurments in the surface global ocean based on Moderate-Resolution Imaging Spectroradiometer data. Journal of Geophysical Research 110 (C7).

Balzano, S., Statham, P.J., Pancost, R.D., Lloyd, J.R. 1999. Role of microbial populations in the release of reduced iron to the water column from marine aggregates. Aquatic Microbial Ecology, 54, 291-303.

Banse, K., 1990. New views on the degradation and disposition of organic particles as collected by sediment traps in the open sea. Deep-Sea Research I 37 (7A), 1177-1195.

Barlow, R., Mantoura, R., Gough, M., Fileman, T., 1993. Pigment signatures of the phytoplankton composition in the northeastern Atlantic during the 1990 spring bloom. Deep sea Research II 40 (1-2), 459-477.

Behrenfeld, M.J., Falkowski, P.G., 1997. Photosynthetic rates derived from satellite-based chlorophyll concentration. Limnology and Oceanography 42 (1), 1-20.

Benitez-Nelson, C., Buesseler, K.O., Karl, D.M., Andrews, J., 2001. A time-series study of particulate matter export in the North Pacific Subtropical Gyre based on Th-234 : U-238 disequilibrium. Deep-Sea Research Part I-Oceanographic Research Papers 48 (12), 2595-2611.

Bianchi, D., Dunne, J.P., Sarmiento, J.L., Galbraith, E.D., 2012. Data-based estimated of suboxia, denitrification and N_2O prodcution in the ocean, and their sensitivities to dissolved O_2. Global Biogeochemical Cycles. Vol 26, 13PP

Bishop, J.K.B., 1994. Geeting good weight. In: Hurd, D.C., Spencer, D.W. (Eds.), Maine Particles: Analysis and Characterization, Geophysical Monograph 63. American Geophysical Union, Washington, DC, USA, 229-234.

Bishop, J.K.B., Edmond, J.M., Ketten, D.R., Bacon, M.P., Silker, W.B., 1977. The chemistry, biology, and vertical flux of particulate matter from the upper 400 m of the equatorial Atlantic Ocean. Deep-Sea Research 24 (6), 511-548.

Bopp, L., Aumont, O., Cadule, P., Alvain, S., Gehlen, M., 2005. Response of diatoms distribution to global warning and potential implications: A global model study. Geophys. Res. Lett. 32, L19606.

Boyd, P., Newton, P., 1995. Evidence of the Potential Influence of Planktonic Community Structure on the Interannual Variability of Particulate Organic-Carbon Flux. Deep-Sea Research I 42 (5), 619-639.

Boyd, P.W., Newton, P.P., 1999. Does planktonic community structure determine downward particulate organic carbon flux in different oceanic provinces? Deep-Sea Research I 46 (1), 63-91.

Boyd, P.W., Trull, T.W., 2007. Understanding the export of biogenic particles in oceanic waters: Is there consensus? Progress in Oceanography 72 (4), 276-312.

Brew, H.S., Moran, S.B., Lomas, M.W., Burd, A.B., 2009. Plankton community composition, organic carbon and thorium-234 particle size distributions, and particle export in the Sargasso Sea. Journal of Marine Research 67 (6), 845-868.

Brewin, R.J.W., Hardman-Mountford, N.J., Lavender, S.J., Raitos, D.E., Hirata, T., Uitz, J., Devred, E., Bricaud, A., Ciotti, A., Gentili, B., 2011. An intercomparison of bio-optical techniques for detecting dominant phytoplankton size from satellite remote sensing. Remote sensing environment 115, 325-339.

Broecker, W.S., Peng, T.-H., 1982. Tracers in the Sea. Eldigio, New York.

Brown, W.O., Heim, R.R., 1998. National Climate Data Center, Climate Variations Bulletin Volume 10, Number 12, Historical, Climatology Series; Available at http://www.ncdc.noaa.gov/ol/documentlibrary/cvb.html.

Buesseler, K., Ball, L., Andrews, J., Benitez-Nelson, C., Belastock, R., Chai, F., Chao, Y., 1998. Upper ocean export of particulate organic carbon in the Arabian Sea derived from thorium-234. Deep-Sea Research Part II-Topical Studies in Oceanography 45 (10-11), 2461-2487.

Buesseler, K.O., 1998. The decoupling of production and particulate export in the surface ocean. Global Biogeochemical Cycles 12 (2), 297-310.

Buesseler, K.O., 2001. Ocean Biogeochemistry and the Global Carbon Cycle: An Introduction to the U.S. Joint Global Ocean Flux Study. Oceanography 14 (4), 5-17.

Buesseler, K.O., Andrews, J.A., Hartman, M.C., Belastock, R., Chai, F., 1995. Regional estimates of the export flux of particulate organic carbon derived from thorium-234 during the JGOFS EqPac program. Deep-Sea Research II 42 (2-3), 777-804.

Buesseler, K.O., Andrews, J.E., Pike, S.M., Charette, M.A., Goldson, L.E., Brzezinski, M.A., Lance, V.P., 2005. Particle export during the Southern Ocean iron experiment (SOFeX). Limnology and Oceanography 50 (1), 311-327.

Buesseler, K.O., Bacon, M.P., Cochran, J.K., Livingston, H.D., 1992. Carbon and nitrogen export during the JGOFS North Atlantic Bloom Experiment estimated from ^{234}Th:^{238}U disequilibria. Deep-Sea Research I 39 (7-8), 1115-1137.

Buesseler, K.O., Barber, R.T., Dickson, M.L., Hiscock, M.R., Moore, J.K., Sambrotto, R., 2003. The effect of marginal ice-edge dynamics on production and export in the Southern Ocean along 170 degrees W. Deep-Sea Research II 50 (3-4), 579-603.

Buesseler, K.O., Benitez-Nelson, C.R., Moran, S.B., Burd, A., Charette, M., Cochran, J.K., Coppola, L., Fisher, N.S., Fowler, S.W., Gardner, W., Guo, L.D., Gustafsson, O., Lamborg, C., Masque, P., Miquel, J.C., Passow, U., Santschi, P.H., Savoye, N., Stewart, G., Trull, T., 2006. An assessment of particulate organic carbon to thorium-234 ratios in the ocean and their impact on the application of Th-234 as a POC flux proxy. Marine Chemistry 100 (3-4), 213-233.

Buesseler, K.O., Boyd, P.W., 2009. Shedding light on processes that control particle export and flux attenuation in the twilight zone of the open ocean. Limnology and Oceanography 54 (4), 1210-1232.

Buesseler, K.O., Lamborg, C., Cai, P., Escoube, R., Johnson, R., Pike, S., Masque, P., McGillicuddy, D., Verdeny, E., 2008a. Particle fluxes associated with mesoscale eddies in the Sargasso Sea. Deep-Sea Research Part II-Topical Studies in Oceanography 55 (10-13), 1426-1444.

Buesseler, K.O., Lamborg, C.H., Boyd, P.W., Lam, P.J., Trull, T.W., Bidigare, R.R., Bishop, J.K.B., Casciotti, K.L., Dehairs, F., Elskens, M., Honda, M., Karl, D.M., Siegel, D.A., Silver, M.W., Steinberg, D.K., Valdes, J., Van Mooy, B., Wilson, S., 2007. Revisiting carbon flux through the ocean's twilight zone. Science 316 (5824), 567-570.

Buesseler, K.O., Lampitt, R.S., 2008. Introduction to "Understanding the Ocean's biological pump: Results from VERTIGO" - Preface. Deep-Sea Research Part II-Topical Studies in Oceanography 55 (14-15), 1519-1521.

Buesseler, K.O., Pike, S., Maiti, K., Lamborg, C.H., Siegel, D.A., Trull, T.W., 2009. Thorium-234 as a tracer of spatial, temporal and vertical variability in particle flux in the North Pacific. Deep-Sea Research Part I-Oceanographic Research Papers 56 (7), 1143-1167.

Burd, A., Hansell, D.A., Steinberg, D.K., Anderson, T.R., Aristegui, J., Baltar, F., Beaupre, S.B., Buesseler, K.O., Dehairs, F., Jackson, G.A., Kadko, D.C., Koppelman, R.K., Lampitt, R.S., Nagata, T., Reinthaler, T., Robinson, C., Robison, B.H., Tamburini, C., Tanaka, T., 2010. Assessing the apparent imbalance between geochemical and biochemical indicators of meso- and bathypelagic biological activity: What the @$# is wrong with present calculations of carbon budgets? Deep sea Research II 57, 1557-1571.

Burd, A., Jackson, G.A., 2009. Particle aggregation. Annual Review Marine Sciences (1), 65-90.

Burd, A.B., Moran, S.B., Jackson, G.A., 2000. A coupled adsorption-aggregation model of the POC/Th-234 ratio of marine particles. Deep-Sea Research I 47 (1), 103-120.

Cai, P.H., Dai, M.H., Lv, D.W., Chen, W.F., 2006. An improvement in the small-volume technique for determining thorium-234 in seawater. Marine Chemistry 100 (3-4), 282-288.

Caldeira, K., Wickett, M.E., 2003. Anthropogenic carbon and ocean pH. Nature 425 (6956), 365-365.

Caron, D.A., Goldman, J.C., Dennett, M.R., 1988. Experiment demonstration of the role of bacteria and bacterivorous protozoa in plankton nutrient cycles. Hydrobiologia 159, 27-40.

Chavez, F.P., Barber, R.T., 1987. An estimate of new production in the equatorial Pacific. Deep Sea Research I 34 (7), 1229-1243.

Chen, J.H., Edwards, R.L., Wasserburg, G.J., 1986. ^{238}U, ^{234}U and ^{232}Th in seawater. Earth and Planetary Science Letters 80 (3-4), 241-251.

Cherrier, J., Burnett, W.C., Larock, P.A., 1995. Uptake of Polonium and sulfur by bacteria. Geomicrobiology Journal 13 (2), 103-115.

Christian, J.R., Lewis, M.R., Karl, D.M., 1997. Vertical fluxes of carbon, nitrogen, and phosphorus in the North Pacific Subtropical Gyre near Hawaii. Journal of Geophysical Research-Oceans 102 (C7), 15,667-677.

Coale, K.H., Bruland, K.W., 1987. Oceanic stratified euphotic zone as elucidated by ^{234}Th:^{238}U disequilibria. Limnology and Oceanography 32 (1), 189-200.

Cochran, J.K., Buesseler, K.O., Bacon, M.P., Wang, H.W., Hirschberg, D.J., Ball, L., Andrews, J., Crossin, G., Fleer, A., 2000. Short-lived thorium isotopes (Th-234, Th-228) as indicators of POC export and particle cycling in the Ross Sea, Southern Ocean. Deep-Sea Research Part II-Topical Studies in Oceanography 47 (15-16), 3451-3490.

Cochran, J.K., Masque, P., 2003. Short-lived U/Th series radionuclides in the ocean: Tracers for scavenging rates, export fluxes and particle dynamics. Uranium-Series Geochemistry 52, 461-492.

Cochran, J.K., Miquel, J.C., Armstrong, R., Fowler, S.W., Masque, P., Gasser, B., Hirschberg, D., Szlosek, J., Baena, A., Verdeny, E., Stewart, G.M., 2009. Time-series measurements of Th-234 in water column and sediment trap samples from the northwestern Mediterranean Sea. Deep-Sea Research Part II-Topical Studies in Oceanography 56 (18), 1487-1501.

Cochran, J.K., Roberts, K.A., Barnes, C., Achman, D., 1997. Radionuclides as indicators of particle and carbon dynamics on East Greenland Shelf. In: Germain, P., Guarry, J.C., Guegueniat, P., Metivier, H. (Eds.), Radioprotection - Colloques. Proceedings of RADOC 96-97 Radionuclides in the Ocean. Les Éditions de Physique, Cherbourg, pp. 129-136.

Conte, M.H., Ralph, N., Ross, E.H., 2001. Seasonal and interannual variability in deep ocean particle fluxes at the Oceanic Flux Program (OFP)/Bermuda Atlantic Time Series (BATS) site in the western Sargasso Sea near Bermuda. Deep-Sea Research II 48 (8-9), 1471-1505.

Cutter, G.R., Andersson, P., Codispoti, L., Croot, P., Francois, R., Lohan, M.C., Obata, H., Rutgers van der Loeff, M., 2010. Sampling and Sample-handling for GEOTRACES Cruises. 2010 Geotraces Standards and Intercalibration Committee.

De La Rocha, C.L., Nowald, N., Passow, U., 2008. Interactions between diatom aggregates, minerals, particulate organic carbon, and dissolved organic matter: Further implications for the ballast hypothesis. Global Biogeochemical Cycles 22 (4).

De La Rocha, C.L., Passow, U., 2007. Factors influencing the sinking of POC and the efficiency of the biological carbon pump. Deep-Sea Research Part II-Topical Studies in Oceanography 54 (5-7), 639-658.

del Giorgio, P.A., Duarte, C.M., 2002. Respiration in the open ocean. Nature 420, 379-384.

Deuser, W.G., Ross, E.H., Anderson, R.F., 1981. Seasonality in the supply of sediment to the deep Sargasso Sea and implications for the rapid transfer of matter to the deep ocean. Deep Sea Research (28), 495-505.

Dilling, L., Alldredge, A., 2000. Fragmentation of marine snow by swimming macrozooplankton: a new process impacting carbon cycling in the sea. Deep Sea Research I 47, 1227-1245.

Dilling, L., Wilson, J., Steinber, D.K., Alldredge, A.L., 1998. Feeding by the euphausiid *Euphausia pacifia* and the copepod *Calanus pacificus* on marine snow. Marine Ecology Progress Series 170, 189-201.

DiTullio, G.R., Grebmeier, J.M., Arrigo, K.R., Lizotte, M.P., Robinson, D.H., Leventer, A., Barry, J.B., VanWoert, M.L., Dunbar, R.B., 2000. Rapid and early export of *Phaeocystis antarctica* blooms in the Ross Sea, Antarctica. Nature 404 (6778), 595-598.

Ducklow, H.W., Harris, R.P., 1993. Introduction to the JGOFS North-Atlantic bloom experiment. Deep-Sea Research Part Ii-Topical Studies in Oceanography 40 (1-2), 1-8.

Dunne, J.P., Murray, J.W., 1999. Sensitivity of ^{234}Th export to physical processes in the central equatorial Pacific. Deep-Sea Research I 46 (5), 831-854.

Dunne, J.P., Sarmiento, J.L., Gnanadesikan, A., 2007. A synthesis of global particle export from the surface ocean and cycling through the ocean interior and on the seafloor. Global Biogeochemical Cycles 21 (4).

Ejsmont-Karabin, J., 1983. Ecological characteristics of lakes in North-eastern Poland versus their trophic gradient. VIII. Role of nutrient regeneration by planktonic rotifers and crustaceans in 42 lakes. Ekol Pol 31, 411-427.

Engel, A., Abramson, L., Szlosek, J., Zanfei, L., Stewart, G., Hirschberg, D., Lee, C., 2009a. Investigating the effect of ballasting by CaCO3 in Emiliania huxleyi: II. Decomposition of particulate organic matter. Deep-Sea Research Part II-Topical Studies in Oceanography 56 (18), 1408-1419.

Engel, A., Szlosek, J., Abramson, L., Liu, Z.F., Lee, C., 2009b. Investigating the effect of ballasting by CaCO3 in Emiliania huxleyi: I. Formation, settling velocities and physical properties of aggregates. Deep-Sea Research Part II-Topical Studies in Oceanography 56 (18), 1396-1407.

Eppley, R.W., Peterson, B.J., 1979. Particulate organic matter flux and planktonic new production in the deep ocean. Nature 282 (5740), 677-680.

Falkowski, P., Scholes, R.J., Boyle, E., Canadell, J., Canfield, D., Elser, J., Gruber, N., Hibbard, K., Hogberg, P., Linder, S., Mackenzie, F.T., Moore, B., Pedersen, T., Rosenthal, Y., Seitzinger, S., Smetacek, V., Steffen, W., 2000. The global carbon cycle: A test of our knowledge of earth as a system. Science 290 (5490), 291-296.

Falkowski, P.G., Barber, R.T., Smetacek, V., 1998. Biogeochemical controls and feedbacks on ocean primary production. Science 281 (5374), 200-206.

Fischer, G., Karakas, G., 2009. Sinking rates and ballast composition of particles in the Atlantic Ocean: implications for the organic carbon fluxes to the deep ocean. Biogeosciences 6 (1), 85-102.

Fisher, N.S., Burns, K.A., Cherry, R.D., Heyraud, M., 1983. Accumulation and cellular distribution of ^{241}Am, ^{210}Po and ^{210}Pb in two marine algae. Marine Ecology Progress Series 11, 233-237.

Fowler, S.W., Knauer, G.A., 1986. Role of large particles in the transport of elements and organic compounds through the oceanic water column. Progress in Oceanography 16 (3), 147-194.

Francois, R., Honjo, S., Krishfield, R., Manganini, S., 2002. Factors controlling the flux of organic carbon to the bathypelagic zone of the ocean. Global Biogeochemical Cycles 16 (4).

Friedrich, J., van der Loeff, M.M.R., 2002. A two-tracer (Po-210-Th-234) approach to distinguish organic carbon and biogenic silica export flux in the Antarctic Circumpolar Current. Deep-Sea Research I 49 (1), 101-120.

Gardner, W.D., Richardson, M.J., Carlson, C.A., Hansell, D., Mishonov, A.V., 2003. Determining true particulate organic carbon: bottles, pumps and methodologies. Deep-Sea Research II 50 (3-4), 655-674.

Gehlen, M., Beck, L., Calas, G., Flank, A.M., Van Bennekom, A.J., Van Beusekom, J.E.E., 2002. Unraveling the atomic structure of biogenic silica: evidence of the

structural association of Al and Si in diatom frustules. Geochimica Et Cosmochimica Acta 66 (9), 1601-1609.

Geibert, W., Usbeck, R., 2004. Adsorption of thorium and protactinium onto different particle types: Experimental findings. Geochimica Et Cosmochimica Acta 68 (7), 1489-1501.

Goldthwait, S., Yen, J., Brown, J., Alldredge, A., 2004. Quantification of marine snow fragmentation by swimming euphausiids. Limnology and Oceanography 49, 940-952.

Goldthwait, S.A., Carlson, C.A., Henderson, G.K., Alldredge, A.L., 2005. Effects of physical fragmentation on remineralization of marine snow. Marine Ecology Progress Series 305, 59-65.

Gregg, W.W., Casey, N.W., 2007. Modelling coccolithophores in the global oceans. Deep sea Research II 54, 447-477.

Gregg, W.W., Ginoux, P., Schopf, P.S., Casey, N.W., 2003. Phytoplankton and iron: validation of a global three-dimensional ocean biogeochemical model. Deep-Sea Research II 50 (22-26), 3143-3169.

Grossart, H.P., Ploug, H., 2001. Microbial degradation of organic carbon and nitrogen on diatom aggregates. Limnology and Oceanography 46 (2), 267-277.

Guo, L.D., Hung, C.C., Santschi, P.H., Walsh, I.D., 2002. Th-234 scavenging and its relationship to acid polysaccharide abundance in the Gulf of Mexico. Marine Chemistry 78 (2-3), 103-119.

Hamm, C.E., 2002. Interactive aggregation and sedimentation of diatoms and clay-sized lithogenic material. Limnology and Oceanography 47 (6), 1790-1795.

Harris, R.P., 1994. Zooplankton grazing on the coccolithore Emiliania huxleyi and its role in organic carbon flux. Marine Biology 119, 431-439.

Hedges, J.L., Keil, R.G., 1995. Sedimentary organic matter preservation: an assessment and speculative synthesis. Marine Chemistry 49, 81-115.

Heinze, C., 2004. Simulating oceanic CaCO/sub 3/ export production in the greenhouse. Geophysical Research Letters 31 (16), 4 pp.

Heinze, C., Maier-Reimer, E., Winn, K., 1991. Glacial $_pCO_2$ reduction by the world ocean: experiments with the Hamburg carbon cycle model. Paleoceanography 6 (4), 395-430.

Henson, S., Sanders, R., Madsen, E., Morris, P., Le Moigne, F., Quartly, G., 2011. A reduced estimate of the strength of the ocean's bioloical carbon pump. Geophys. Res. Lett. 38 (L046006).

Henson, S.A., Dunne, J.P., Sarmiento, J.L., 2009. Decadal variability in North Atlantic phytoplankton blooms. Journal of Geophysical Research - Part C - Oceans, 114, C04013.

Henson, S.A., Robinson, I., Allen, J.T., Waniek, J.J., 2006a. Effect of meteorological conditions on interannual variability in timing and magnitude of the spring bloom in the Irminger Basin, North Atlantic. Deep-Sea Research Part I-Oceanographic Research Papers 53 (10), 1601-1615.

Henson, S.A., Sanders, R., Holeton, C., Allen, J.T., 2006b. Timing of nutrient depletion, diatom dominance and a lower-boundary estimate of export production for Irminger Basin, North Atlantic. Marine Ecology-Progress Series 313, 73-84.

Henson, S.A., Sanders, R.J., Madsen, E., 2012. Global patterns in efficiency of particulate organic carbon export and transfer to the deep ocean. Global Biogeochemical Cycles 26 (1028), 14.

Heyraud, M., Fowler, S.W., Beasley, T.M., Cherry, R.D., 1976. Polonium-210 in euphausiids: a detailed study. Marine Biology (34), 127-138.

Hofmann, M., Scellnhuber, H. J. 2009. Oceanic acidification affects marine carbon pump and triggers extended marine oxygen holes. PNAS, 106, no 9, 3017-3022

Honda, M., Watanabe, S., 2010. Importance of biogenic opal as ballast of particulate organic carbon (POC) transport and existence of mineral ballast-associated and residual POC in the Western Pacific Subarctic Gyre. Geophys. Res. Lett. 37 (L02605).

Hoppe, H.-G., Kim, S.-J., Gocke, K., 1988. Microbial decomposition in Aquatic Environments: Combined Process of Extracellular Enzyme Activity and Substrate Uptake. Applied and Environmental Microbiology 54, 784-790.

Hull, C.D., Burnett, W.C., 1996. Radiochemistry of Florida phosphogypsum. Journal of Environmental Radioactivity 32 (3), 213-238.

Hung, C.C., Gong, G.C., 2010. POC/Th-234 ratios in particles collected in sediment traps in the northern South China Sea. Estuarine Coastal and Shelf Science 88 (3), 303-310.

Hung, C.C., Gong, G.C., 2011. Biogeochemical Responses in the Southern East China Sea after Typhoons. Oceanography 24 (4), 42-51.

Hung, C.C., Guo, L.D., Roberts, K.A., Santschi, P.H., 2004. Upper ocean carbon flux determined by size-fractionated 234Th data and sediment traps in the Gulf of Mexico. Geochemical Journal, 38 (6), 601-611.

Hung, C.C., Xu, C., Santschi, P.H., Zhang, S.J., Schwehr, K.A., Quigg, A., Guo, L.D., Gong, G.C., Pinckney, J.L., Long, R.A., Wei, C.L., 2010. Comparative evaluation of sediment trap and (234)Th-derived POC fluxes from the upper oligotrophic waters of the Gulf of Mexico and the subtropical northwestern Pacific Ocean. Marine Chemistry 121 (1-4), 132-144.

Irigoien, X., Harris, R.P., Verheye, H.M., Joly, P., Runge, J., Starr, M., Pond, D., Campbell, R., Shreeve, R., Ward, P., Smith, A.N., Dam, H.G., Peterson, W., Tirelli, V., Koski, M., Smith, T., Harbour, D., Davidson, R., 2002. Copepod hatching success in marine ecosystems with high diatom concentrations. Nature 419, 386-388.

Iversen, M.H., Ploug, H., 2010. Ballast minerals and the sinking carbon flux in the ocean: carbon-specific respiration rates and sinking velocity of marine snow aggregates. Biogeosciences 7, 2613-2624.

Jenkins, W.J., 1982. Oxygen Utilization Rates in North-Atlantic Sub-Tropical Gyre and Primary Production in Oligotrophic Systems. Nature 300 (5889), 246-248.

Jickells, T.D., An, Z.S., Andersen, K.K., Baker, A.R., Bergametti, G., Brooks, N., Cao, J.J., Boyd, P.W., Duce, R.A., Hunter, K.A., Kawahata, H., Kubilay, N., laRoche, J., Liss, P.S., Mahowald, N., Prospero, J.M., Ridgwell, A.J., Tegen, I., Torres, R., 2005a. Global iron connections between desert dust, ocean biogeochemistry, and climate. Science 308 (5718), 67-71.

Keeling, C.D., Whorf, T.P., 1997. Atmospheric CO_2 concentrations, Mana Loa Observatory, Hawaii. In: Trends online: a compendium of data on global change. Carbon Dioxide Information Analysis Centre, Oak Ridge National Laboratory, Oak Ridge, TN. Available at http://cdiac.esd.ornl.gov.ftp.ndp00.

Klaas, C., Archer, D.E., 2002. Association of sinking organic matter with various types of mineral ballast in the deep sea: Implications for the rain ratio. Global Biogeochemical Cycles 16 (4).

Koroleff, F., 1969. Direct determination of ammonia in natural water as indophenol blue. Information on Techniques and Methods for the Seawater Analysis.

Ku, T.L., Knauss, K.G., Mathieu, G.G., 1977. Uranium in open ocean: concentration and isotopic composition. Deep-Sea Research 24 (11), 1005-1017.

Kuss, J., Kremling, K., 1999. Spatial variability of particle associated trace elements in near-surface waters of the North Atlantic (30ºN/60ºW to 60ºN/2ºW), derived by large volume sampling. Marine Chemistry 68, 71-86.

Kwon, E.Y., Primeau, F., Sarmiento, J.L., 2009. The impact of remineralization depth on the air-sea carbon balance. Nature Geoscience 2, 630-635.

La Rock, P., Hyun, J.H., Boutelle, S., Burnett, W.C., Hull, C.D., 1996. Bacterial mobilization of polonium. Geochimica Et Cosmochimica Acta (60), 4321-4328.

Lam, P.J., Doney, S.C., Bishop, J.K.B., 2011. The dynamic ocean biological pump: insights from a global compilation of Particulate Organic Carbon, $CaCO_3$ and opal concentrations profiles from the mesopelagic. Global Biogeochemical Cycles, 25, GB3009.

Lambert, C.E., Bishop, J.K.B., Biscaye, P.E., Chesselet, R., 1984. Particulate aluminium, iron and manganese chemistry at the deep Atlantic boundary layer. Earth and Planetary Science Letters 70, 237-248.

Lampitt, R.S., Bett, B.J., Kiriakoulakis, K., Popova, E.E., Ragueneau, O., Vangriesheim, A., Wolff, G.A., 2001. Material supply to the abyssal seafloor in the Northeast Atlantic. Progress in Oceanography 50 (1-4), 27-63.

Lampitt, R.S., Boorman, B., Brown, L., Lucas, M., Salter, I., Sanders, R., Saw, K., Seeyave, S., Thomalla, S.J., Turnewitsch, R., 2008. Particle export from the euphotic zone: Estimates using a novel drifting sediment trap, Th-234 and new production. Deep-Sea Research Part I-Oceanographic Research Papers 55 (11), 1484-1502.

Lampitt, R.S., Hillier, W.R., Challenor, P.G., 1993. Seasonal and diel variation in the open ocean concentrations of marine snow aggregates. Nature 362 (6422), 737-739.

Laurenceau, E., 2011. Influence of biominerals and microzooplankton grazing on formation, degradation and sinking velocity of diatoms aggregates: implications for the ballast hypothesis. Rapport de stage de Master II, Universite de Bretagne Occidentale, Brest, France, 39pp.

Laws, E.A., Falkowski, P.G., Smith, W.O., Ducklow, H., McCarthy, J.J., 2000. Temperature effects on export production in the open ocean. Global Biogeochemical Cycles 14 (4), 1231-1246.

Le Moigne, F., Sanders, R.J., Villa, M., Henson, S.A., in review-a. On the interpretation of size fractionated C/Th ratios for estimating upper ocean carbon export. Journal of Marine Systems.

Le Moigne, F., Villa, M., Sanders, R., Marsay, C., Garcia-Tenorio, R., Henson, S.A., in review-b. Insights from a POC and biominerals Th and Po derived export fluxes study at the Porcupine Abyssal Plain: Implications for the ballast hypothesis. Deep Sea Research I.

Le Quéré, C., Takahashi, T., Buitenhuis, E.T., Rödenbeck, C., Sutherland, S.C., 2010. Impacy of climate change and variability on the global ocean sink of CO_2. Global Biogeochemical Cycles 24, 1-10.

Lee, C., Armstrong, R.A., Cochran, J.K., Engel, A., Fowler, S.W., Goutx, M., Masque, P., Miquel, J.C., Peterson, M., Tamburini, C., Wakeham, S., 2009a. MedFlux: Investigations of particle flux in the Twilight Zone. Deep-Sea Research Part Ii-Topical Studies in Oceanography 56 (18), 1363-1368.

Lee, C., Peterson, M.L., Wakeham, S.G., Armstrong, R.A., Cochran, J.K., Miquel, J.C., Fowler, S.W., Hirschberg, D., Beck, A., Xue, J.H., 2009b. Particulate organic matter and ballast fluxes measured using time-series and settling velocity sediment traps in the northwestern Mediterranean Sea. Deep-Sea Research Part II-Topical Studies in Oceanography 56 (18), 1420-1436.

Lepore, K., Moran, S.B., Burd, A.B., Jackson, G.A., Smith, J.N., Kelly, R.P., Kaberi, H., Stavrakakis, S., Assimakopoulou, G., 2009. Sediment trap and in-situ pump size-fractionated POC/Th-234 ratios in the Mediterranean Sea and Northwest Atlantic: Implications for POC export. Deep-Sea Research Part I Oceanographic Research Papers 56 (4), 599-613.

Liebig, J., 1847. Chemistry in its Application to Agriculture and Physiology. Taylor and Walton, London.

Liu, H., Suzuki, K., Saito, H., 2004. Community structure and dynamics of phytoplankton in the Western Subartic Pacific Ocean: A synthesis. Journal of Oceanography 60, 119-137.

Liu, Z., Cochran, J.K., Lee, C., Gasser, B., Miquel, J.C., Wakeham, S., 2009. Further investigation on why POC concentrations differ in samples collected by Niskin bottle and *in situ* pump. Deep sea Research II (56), 1558-1567.

Liu, Z., Lee, C., 2007. The role of organic matter in the sorption capacity of marine sediments. Marine Chemistry 105, 240-257.

Liu, Z.F., Stewart, G., Cochran, J.K., Lee, C., Armstrong, R.A., Hirschberg, D.J., Gasser, B., Miquel, J.C., 2005. Why do POC concentrations measured using Niskin bottle collections sometimes differ from those using *in-situ* pumps? Deep-Sea Research I 52 (7), 1324-1344.

Logan, B.E., Passow, U., Alldredge, A.L., Grossart, H.P., Simon, M., 1995. Rapid Formation and Sedimentation of Large Aggregates Is Predictable from Coagulation Rates (Half-Lives) of Transparent Exopolymer Particles (Tep). Deep-Sea Research Part Ii-Topical Studies in Oceanography 42 (1), 203-214.

Longhurst, A.R., 1991. Large marine ecosystems - Patterns, processes and yields. Marine Policy 15 (5), 377-378.

Longhurst, A. R., 1998. Ecological geography of the sea. San Diego: Academic press

Lorrain, A., Savoye, N., Chauvaud, L., Paulet, Y.M., Naulet, N., 2003. Decarbonation and preservation method for the analysis of organic C and N contents and stable

isotope ratios of low-carbonated suspended particulate material. Analytica Chimica Acta 491 (2), 125-133.

Lutz, M.J., Caldeira, K., Dunbar, R.B., Behrenfeld, M.J., 2007. Seasonal rhythms of net primary production and particulate organic carbon flux to depth describe the efficiency of the biological carbon pump in the global ocean. Journal of Geophysical Research (112), 26PP.

Maiti, K., Benitez-Nelson, C.R., Buesseler, K., 2010a. Insights into particle formation and remineralization using the short-lived radionuclide, Thorium-234. Geophys. Res. Lett. 37, L15608.

Maiti, K., Buesseler, K., Benitez-Nelson, C.R., Cochran, J.K., Dai, M., Dehairs, F., Masque, P., Miller, L.A., Moran, S.B., Morris, P.J., Miquel, J.C., Peine, F., Planchon, F., Rutgers van der Loeff, M., Santschi, P.H., Turnewitsch, R., Waples, J.T., 2010b. Total and particulate Thorium-234 results from GEOTRACES intercalibration cruises. 2010, Ocean Sciences Meeting, Portland, U.S.A.

Mann, K.H., Lazier, J.R., 2006. Dynamics of Marine Ecosystems. 3rd ed., Blackwell.

Marsay, C., Achterberg, E., Sanders, R., 2011. Mesopelagic depth measurment of POC and biominerals in the North Atlantic, using neutrally buoyant, free drifting dediment traps. ASLO meeting 2011.

Martin, J.H., Knauer, G.A., Karl, D.M., Broenkow, W.W., 1987. Vertex - Carbon Cycling in the Northeast Pacific. Deep-Sea Research Part A 34 (2), 267-285.

Martin, P., 2011. Particle export and flux through the mesopelagic in the high-latitude North and South Atlantic. PhD thesis, University of Southampton.

Martin, P., Lampitt, R., Perry, M.J., Sanders, R., Lee, C., D'asaro, E., 2011. Export and mesopelagic particle flux during a North Atlantic spring diatom bloom. deep sea Research part I 58 (4), 338-349.

Masque, P., Sanchez-Cabeza, J.A., Bruach, J.M., Palacios, E., Canals, M., 2002. Balance and residence times of (210)Pb and (210)Po in surface waters of the northwestern Mediterranean Sea. Continental Shelf Research 22 (15), 2127-2146.

Matthews, K.M., Kim, K.K., Martin, P., 2007. Determination of ^{210}Po in environmental materials: A review of analytical methodology applied radiation and isotopes 65 (3), 267-279.

Mayer, L.M., 1994. Surface area control of organic carbon accumulation in continental shelf sediment. Geochimica Et Cosmochimica Acta 58, 1271-1284.

McDonnell, A., M., P., Buesseler, K., 2010. Variability in the average sinking velocity of marine particles. Limnology and Oceanography 55 (5), 2085-2096.

Mohan, R., Mergulhao, L.P., Guptha, M.V.S., Rajakurnar, A., Thamban, M., AnilKurnar, N., Sudhakar, M., Ravindra, R., 2008. Ecology of coccolithophores in the Indian sector of the Southern Ocean. Marine Micropaleontology 67 (1-2), 30-45.

Monaghan, E.J., Ruttenberg, K.C., 1999. Dissolved organic phosphorus i n the coastal ocean: Reassessment of available methods and seasonal phosphorus profiles from the Eel River Shelf. Limnology and Oceanography, 44, 7, 1702-1714.

Moran, S.B., Moore, R.M., 1992. Kinetics of the removal of dissolved aluminium by diatoms in seawater: A comparison with thorium. Geochimica Et Cosmochimica Acta 56 (9), 3365-3374.

Moriceau, B., Garvey, M., Ragueneau, O., Passow, U., 2007. Evidence for reduced biogenic silica dissolution rates in diatom aggregates. Marine Ecology-Progress Series 333, 129-142.

Moriceau, B., Goutx, M., Guigue, C., Lee, C., Armstrong, R., Duflos, M., Tamburini, C., Charriere, B., Ragueneau, O., 2009. Si-C interactions during degradation of the diatom Skeletonema marinoi. Deep-Sea Research Part II-Topical Studies in Oceanography 56 (18), 1381-1395.

Morris, P.J., 2008. Carbon export from natural iron fertilisation in the Southern Ocean. PhD, University of Southampton, Southampton.

Morris, P.J., Sanders, R., 2011. A carbon budget for a naturally iron fertilised bloom in the Southern Ocean. Global Biogeochemical Cycles. 25, GB3004.

Morris, P.J., Sanders, R., Turnewitsch, R., Thomalla, S., 2007. Th-234-derived particulate organic carbon export from an island-induced phytoplankton bloom in the Southern Ocean. Deep-Sea Research Part II-Topical Studies in Oceanography 54 (18-20), 2208-2232.

Nagata, W.D., 1989. Nitrogen flow through a *Brachionus* / *Chlorella* mass culture system. Hydrobiologia 186/187, 401-408.

Nelson, D.M., Smith, W.O., Muench, R.D., Gordon, L.I., Sullivan, C.W., Husby, D.M., 1989. Particulate matter and nutrient distribution in the ice-edge zone ofthe Weddell sea - Relationship to hydrography during late summer. Deep-Sea Research Part a-Oceanographic Research Papers 36 (2), 191-209.

Painter, S.C., Lucas, M.I., Stinchcombe, M.C., Bibby, T.S., Poulton, A.J., 2010a. Summertime trends in pelagic biogeochemistry at the Porcupine Abyssal Plain study site in the northeast Atlantic. Deep-Sea Research Part II-Topical Studies in Oceanography 57 (15), 1313-1323.

Painter, S.C., Pidcock, R.E., Allen, J.T., 2010b. A mesoscale eddy driving spatial and temporal heterogeneity in the productivity of the euphotic zone of the northeast Atlantic. Deep-Sea Research Part II-Topical Studies in Oceanography 57 (15), 1281-1292.

Pan, X., Sanders, R., Tappin, A.D., Worsfold, P.J., Achterberg, E., 2005. Simultaneous determination of Dissolved Organic Carbon and Total Dissolved Nitrogen on a Coupled High-Temperature Combustion Total Organic Carbon-Nitrogen Chemiluminescence Detection (HTC TOC-NCD) system. J Autom Methods Manag Chem, 240-246.

Parekh, P., Dutkiewicz, S., Follows, M.J., Ito, T., 2006. Atmospheric carbon dioxide in a less dusty world. Geophys. Res. Lett. 33, 2006.

Parkhill, J.P., Maillet, G., Cullen, J.J., 2001. Fluroescence-based maximal quantum yield for PSII as a diagnostic of nutrient stress. Journal Phycolohy 37, 517-529.

Passow, U., 2002. Production of transparent exopolymer particles (TEP) by phyto- and bacterioplankton. Marine Ecology-Progress Series 236, 1-12.

Passow, U., De la Rocha, C.L., 2006. Accumulation of mineral ballast on organic aggregates. Global Biogeochemical Cycles, 20, GB1013.

Passow, U., Engel, A., Ploug, H., 2003. The role of aggregation for the dissolution of diatom frustules. Fems Microbiology Ecology 46 (3), 247-255.

Pike, S.M., Buesseler, K.O., Andrews, J., Savoye, N., 2005. Quantification of Th-234 recovery in small volume sea water samples by inductively coupled plasma-mass spectrometry. Journal of Radioanalytical and Nuclear Chemistry 263 (2), 355-360.

Planquette, H., Fones, G.R., Statham, P.J., Morris, P.J., 2009. Origin of iron and aluminium in large particles (>53 um) in the Crozet region Southern Ocean. Marine Chemistry 115, 31-42.

Ploug, H., 2001. Small-scale oxygen fluxes and remineralization in sinking aggregates. Limnology and Oceanography 46 (7), 1624-1631.

Ploug, H., Grossart, H.P., 2000. Bacterial growth and grazing on diatom aggregates: Respiratory carbon turnover as a function of aggregate size and sinking velocity. Limnology and Oceanography 47 (7), 1467-1475.

Ploug, H., Iversen, M.H., Fischer, G., 2008a. Ballast, sinking velocity, and apparent diffusivity within marine snow and zooplankton fecal pellets: Implications for substrate turnover by attached bacteria. Limnology and Oceanography 53 (5), 1878-1886.

Ploug, H., Iversen, M.H., Koski, M., Buithenhuis, E.T., 2008b. Production, oxygen respiration rates, and sinking velocity of copepods fecal pellets: Direct measurments of ballasting by opal and calcite. Limnology and Oceanography 53, 469-476.

Ploug, H., Jorgensen, B.B., 1999. A net-jet flow system for mass transfer and microsensor studies of sinking aggregates. Marine Ecology Progress Series 176, 279-290.

Pollard, R.T., Salter, I., Sanders, R.J., Lucas, M.I., Moore, C.M., Mills, R.A., Statham, P.J., Allen, J.T., Baker, A.R., Bakker, D.C.E., Charette, M.A., Fielding, S., Fones, G.R., French, M., Hickman, A.E., Holland, R.J., Hughes, J.A., Jickells, T.D., Lampitt, R.S., Morris, P.J., Nedelec, F.H., Nielsdottir, M., Planquette, H., Popova, E.E., Poulton, A.J., Read, J.F., Seeyave, S., Smith, T., Stinchcombe, M., Taylor, S., Thomalla, S., Venables, H.J., Williamson, R., Zubkov, M.V., 2009. Southern Ocean deep-water carbon export enhanced by natural iron fertilization. Nature 457 (7229), 577-U581.

Poulton, A., Charalampopoulou, A., Young, J.R., Tarran, G.A., Lucas, M.I., Quartly, G.D., 2010. Coccolithophore dynamics in non-bloom conditions during late summer in the central Iceland Basin (July-August 2007). Limnology and Oceanography 4 (55), 1601-1613.

Poulton, A.J., Moore, C.M., Seeyave, S., Lucas, M.I., Fielding, S., Ward, P., 2007. Phytoplankton community composition arounf the Crozet Plateau, with emphasis on diatoms and Phaeocystis. Deep sea Research II 54, 2085-2105.

Poulton, A.J., Sanders, R., Holligan, P.M., Stinchcombe, M.C., Adey, T.R., Brown, L., Chamberlain, K., 2006. Phytoplankton mineralization in the tropical and subtropical Atlantic Ocean. Global Biogeochemical Cycles 20 (4).

Ragueneau, O., Treguer, P., Leynaert, A., Anderson, R.F., Brzezinski, M.A., DeMaster, D.J., Dugdale, R.C., Dymond, J., Fischer, G., Francois, R., Heinze, C.,

Maier-Reimer, E., Martin-Jezequel, V., Nelson, D.M., Queguiner, B., 2000. A review of the Si cycle in the modem ocean: recent progress and missing gaps in the application of biogenic opal as a paleoproductivity proxy. Global and Planetary Change 26 (4), 317-365.

Richardson, T.L., Jackson, G.A., 2007. Small phytoplankton and carbon export from the surface ocean. Science 315 (5813), 838-840.

Riebesell, U., 2004. Effects of CO2 enrichment on marine phytoplankton. Journal of Oceanography 60 (4), 719-729.

Riley, J., Sanders, R., Marsay, C., Le Moigne, F., Achterberg, E., Poulton, A., 2012. The relative contribution of fast and slow sinking particles to ocean carbon export. Global Biogeochemical Cycles 26.

Rutgers Van Der Loeff, M.M., Bathmann, U.V., Buesseler, K.O., 1997. Export production measured with the natural tracer Th-234 and sediment traps. Berichte zur Polarforschung 0 (221), 113-115.

Sabine, C.L., Feely, R.A., 2007. Chapter 3 In Greenhouse Gas Sinks, D. Reay, N. Hewitt, J. Grace, and K. Smith (eds.), CABI Publishing, Oxfordshire, UK, 31–49

Sabine, C.L., Feely, R.A., Gruber, N., Key, R.M., Lee, K., Bullister, J.L., Wanninkhof, R., Wong, C.S., Wallace, D.W.R., Tilbrook, B., Millero, F.J., Peng, T.H., Kozyr, A., Ono, T., Rios, A.F., 2004. The oceanic sink for anthropogenic CO2. Science 305 (5682), 367-371.

Salter, I., Lampitt, R.S., Sanders, R., Poulton, A., Kemp, A.E.S., Boorman, B., Saw, K., Pearce, R., 2007. Estimating carbon, silica and diatom export from a naturally

fertilised phytoplankton bloom in the Southern Ocean using PELAGRA: A novel drifting sediment trap. Deep-Sea Research Part II-Topical Studies in Oceanography 54 (18-20), 2233-2259.

Sanders, R., Brown, L., Henson, S., Lucas, M., 2005. New production in the Irminger Basin during 2002. Journal of Marine Systems 55 (3-4), 291-310.

Sanders, R., Morris, P.J., Poulton, A.J., Stinchcombe, M.C., Charalampopoulou, A., Lucas, M.I., Thomalla, S.J., 2010. Does a ballast effect occur in the surface ocean? Geophysical Research Letters 37.

Santschi, P.H., Murray, J.W., Baskaran, M., Benitez-Nelson, C.R., Guo, L.D., Hung, C.C., Lamborg, C., Moran, S.B., Passow, U., Roy-Barman, M., 2006. Thorium speciation in seawater. Marine Chemistry (100), 250-268.

Sarmiento, J.L., Toggweiler, J.R., 1984. A new model for the role of the oceans in determining atmospheric $pCO_{2.}$. Nature 308 (5960), 621-624.

Savoye, N., Benitez-Nelson, C., Burd, A.B., Cochran, J.K., Charette, M., Buesseler, K.O., Jackson, G.A., Roy-Barman, M., Schmidt, S., Elskens, M., 2006. Th-234 sorption and export models in the water column: A review. Marine Chemistry 100 (3-4), 234-249.

Schlitzer, R., 2004. Export production in the equatorial and North Pacific derived from dissolved oxygen, nutrient and carbon data. Journal of Oceanography 60 (1), 53-62.

Shanks, A.L., Edmondson, E.W., 1989. Laboratory-made artificial marine snow: a biological model of the real thing. Marine Biology (101), 463-470.

Shanks, A.L., Trent, J.D., 1980. Marine snow - Sinking tates and potential role in vertical flux. Deep-Sea Research Part a-Oceanographic Research Papers 27 (2), 137-143.

Siegel, D.A., Doney, S.C., Yoder, J.A., 2002. The North Atlantic spring phytoplankton bloom and severdrup's critical depth hypothesis. . Science 296, 730-733.

Smayda, T.J., 1971. Normal and accelerated sinking of phytoplankton in sea. Marine Geology 11 (2), 105-&.

Steinberg, D.K., Van Mooy, B.A.S., Buesseler, K.O., Boyd, P.W., Kobari, T., Karl, D.M., 2008. Bacterial vs. zooplankton control of sinking particle flux in the ocean's twilight zone. Limnology and Oceanography 53 (4), 1327-1338.

Stewart, G., Cochran, J.K., Miquel, J.C., Masque, P., Szlosek, J., Baena, A.M.R.Y., Fowler, S.W., Gasser, B., Hirschberg, D.J., 2007a. Comparing POC export from Th-234/U-238 and Po-210/Pb-210 disequilibria with estimates from sediment traps in the northwest Mediterranean. Deep-Sea Research Part I-Oceanographic Research Papers 54 (9), 1549-1570.

Stewart, G., Cochran, J.K., Xue, J.H., Lee, C., Wakeham, S.G., Armstrong, R.A., Masque, P., Miquel, J.C., 2007b. Exploring the connection between Po-210 and organic matter in the northwestern Mediterranean. Deep-Sea Research Part I-Oceanographic Research Papers 54 (3), 415-427.

Stewart, G., Moran, S.B., Lomas, M.W., Kelly, R.P., 2011. Direct comparison of (210)Po, (234)Th and POC particle-size distributions and export fluxes at the

Bermuda Atlantic Time-series Study (BATS) site. Journal of Environmental Radioactivity 102 (5), 479-489.

Stewart, G.M., Fisher, N.S., 2003a. Bioaccumulation of polonium-210 in marine copepods. Limnology and Oceanography 48 (5), 2011-2019.

Stewart, G.M., Fisher, N.S., 2003b. Experimental studies on the accumulation of polonium-210 by marine phytoplankton. Limnology and Oceanography 48 (3), 1193-1201.

Stewart, G.M., Moran, S.B., Lomas, M.W., 2010. Seasonal POC fluxes at BATS estimated from (210)Po deficits. Deep-Sea Research Part I-Oceanographic Research Papers 57 (1), 113-124.

Stramma, L., Johnson, G.C., Sprintall, J., Mohrholz, V., 2008. Expanding oxygen-minimum zones in the tropical oceans. Science 320 (5876), 655-658.

Szlosek, J., Cochran, J.K., Miquel, J.C., Masque, P., Armstrong, R.A., Fowler, S.W., Gasser, B., Hirschberg, D.J., 2009. Particulate organic carbon-Th relationships in particles separated by settling velocity in the northwest Mediterranean Sea. Deep sea Research II 56, 1519-1532.

Theilacker, G.H., Mc Master, M.F., 1971. Mass culture of the rotifer *Brachionus plicatilis* and it sevaluation as a food larval anchovies. Marine Biology 10, 183-188.

Thomalla, S., Turnewitsch, R., Lucas, M., Poulton, A., 2006. Particulate organic carbon export from the North and South Atlantic gyres: The Th-234/U-238 disequilibrium approach. Deep-Sea Research Part Ii-Topical Studies in Oceanography 53 (14-16), 1629-1648.

Thomalla, S.J., Poulton, A.J., Sanders, R., Turnewitsch, R., Holligan, P.M., Lucas, M.I., 2008. Variable export fluxes and efficiencies for calcite, opal, and organic carbon in the Atlantic Ocean: A ballast effect in action? Global Biogeochemical Cycles 22 (1).

Treguer, P., Pondaven, P., 2000. Global change - Silica control of carbon dioxide. Nature 406 (6794), 358-359.

Trull, T.W., Bray, S.G., Buesseler, K.O., Lamborg, C.H., Manganini, S., Moy, C., Valdes, J., 2008. In situ measurement of mesopelagic particle sinking rates and the control of carbon transfer to the ocean interior during the Vertical Flux in the Global Ocean (VERTIGO) voyages in the North Pacific. Deep-Sea Research Part Ii-Topical Studies in Oceanography 55 (14-15), 1684-1695.

Tsunogai, S., Minagawa, M., 1976. Th-234, Pb-210 AND Po-210 in surface and deep waters of Pacific as tracers of particulate materials. Transactions-American Geophysical Union 57 (4), 255-255.

Turner, J.T., 2002. Zooplankton fecal pellets, marine snow and sinking phytoplankton blooms. Aquatic Microbial Ecology 27 (1), 57-102.

Turnewitsch, R., Springer, B.M., Kiriakoulakis, K., Vilas, J.C., Aristegui, J., Wolff, G., Peine, F., Werk, S., Graf, G., Waniek, J.J., 2007. Determination of particulate organic carbon (POC) in seawater: The relative methodological importance of artificial gains and losses in two glass-fiber-filter-based techniques. Marine Chemistry 105 (3-4), 208-228.

Uitz, J., Claustre, H., Morel, A., Stanford, B.H., 2006. Vertical distribution of phytoplankton communities in open ocean: An assessment based on surface chlorophyll. Journal of Geophysical Research 111.

Van der Loeff, M.R., Sarin, M.M., Baskaran, M., Benitez-Nelson, C., Buesseler, K.O., Charette, M., Dai, M., Gustafsson, O., Masque, P., Morris, P.J., Orlandini, K., Baena, A.R.Y., Savoye, N., Schmidt, S., Turnewitsch, R., Voge, I., Waples, J.T., 2006. A review of present techniques and methodological advances in analyzing Th-234 in aquatic systems. Marine Chemistry 100 (3-4), 190-212.

Venables, H., Pollard, R.T., Popova, E.E., 2007. Physical conditions controlling the developement of a regular phytoplankton bloom north of the Crozet Plateau, Southern Ocean. Deep sea Research II 54 (18-20), 1949-1964.

Verdeny, E., Masque, P., Garcia-Orellana, J., Hanfland, C., Cochran, J.K., Stewart, G.M., 2009. POC export from ocean surface waters by means of Th-234/U-238 and Po-210/Pb-210 disequilibria: A review of the use of two radiotracer pairs. Deep-Sea Research Part II-Topical Studies in Oceanography 56 (18), 1502-1518.

Verdeny, E., Masque, P., Maiti, K., Garcia-Orellana, J., Brauch, J.M., Mahaffey, C., Benitez-Nelson, C.R., 2008. Particle export within cyclonic Hawaiian lee eddies derived from Pb-210-Po-210 disequilibrium. Deep-Sea Research Part II-Topical Studies in Oceanography 55 (10-13), 1461-1472.

Verity, P., Williams, S.C., Hong, Y., 2000. Formation, degradation and mass:volume ratios of detritus derived from decaying phytplankton. Marine Ecology Progress Series 207, 53-68.

Villa, M., de Soto, F., Salvador, M., Le Moigne, F., Giering, S., Sanders, R., Garcia-Tenorio, R., 2011. Analysis of sinking particle speed through the water column using 210Po-210Pb concentration profiles. 3rd GEOTRACES Data-Model Synergy Workshop, Barcelona, España.

Villa, M., Mosqueda, F., Hurtado, S., Mantero, J., Manjon, G., Perianez, R., Vaca, F., Garcia-Tenorio, R., 2009. Contamination and restoration of an estuary affected by phosphogypsum releases. Science of the Total Environment 408 (1), 69-77.

Von Brand, T., Rakestraw, N.W., Zabor, J.W., 1942. Decomposition and regeneration of nitrogenous organic matter in sea water. Biological Bulletin, 273-282.

Waite, A.M., Safi, K.A., Hall, J.A., Nodder, S.D., 2000. Mass sedimentation of picoplankton embedded in organic aggregates. Limnology and Oceanography 45 (1), 87-97.

Wang, H., Jiang, L., Weitz, J.S., 2009. Bacterivorious garzers facilitate organic matter decomposition a stoichiometric modeling approach. Fems Microbiology Ecology 69.

Waples, J.T., Benitez-Nelson, C., Savoye, N., Van der Loeff, M.R., Baskaran, M., Gustafsson, O., 2006. An introduction to the application and future use of Th-234 in aquatic systems. Marine Chemistry 100 (3-4), 166-189.

Wedepohl, K.H., 1995. The composition of the continental crust. Geochimica et Cosmochimica Acta 59 (7), 1217-1232.

Wheeler, P.A., Kirchman, D.L., 1986. Utilization of inorganic and organic nitrogen by bacteria in marine systems. Limnology and Oceanography 31.

Xu, C., Santschi, P.H., Hung, C.C., Zhang, S.J., Schwehr, K.A., Roberts, K.A., Guo, L.D., Gong, G.C., Quigg, A., Long, R.A., Pinckney, J.L., Duan, S.W., Amon, R., Wei, C.L., 2011. Controls of (234)Th removal from the oligotrophic ocean by polyuronic acids and modification by microbial activity. Marine Chemistry 123 (1-4), 111-126.

Yoon, W.B., Rosson, R.A., 1990. Improved method of enumeration of attached bacteria for study of fluctuation in the abundance of attached and free-living bacteria in response to diel variation in seawater turbidity. Applied and Environmental Microbiology 56, 595-600.

Zimmermann-Timm, H., Holst, H., Muller, S., 1998. Seasonal dynamics of aggregates and their typical biocoenosis in the Elbe Estuary. Estuaries 21 (4), 613-621.